



HAL
open science

Nanocelluloses as potential materials for specialty papers

Raphael Bardet

► **To cite this version:**

Raphael Bardet. Nanocelluloses as potential materials for specialty papers. Chemical and Process Engineering. Université de Grenoble, 2014. English. NNT : 2014GRENI091 . tel-01647222

HAL Id: tel-01647222

<https://theses.hal.science/tel-01647222>

Submitted on 24 Nov 2017

HAL is a multi-disciplinary open access archive for the deposit and dissemination of scientific research documents, whether they are published or not. The documents may come from teaching and research institutions in France or abroad, or from public or private research centers.

L'archive ouverte pluridisciplinaire **HAL**, est destinée au dépôt et à la diffusion de documents scientifiques de niveau recherche, publiés ou non, émanant des établissements d'enseignement et de recherche français ou étrangers, des laboratoires publics ou privés.

THÈSE

Pour obtenir le grade de

DOCTEUR DE L'UNIVERSITÉ DE GRENOBLE

Spécialité : **Matériaux, Mécanique, Génie Civile, Electrochimie**

Arrêté ministériel : 7 août 2006

Présentée par

Raphael BARDET

Thèse dirigée par **Julien BRAS**
et codirigée par **Naceur BELGACEM**

préparée au sein du **Laboratoire du Génie des Procédés
Papetiers de l'École Internationale du Papier, de la
Communication Imprimée et des Biomatériaux, UMR CNRS
5518**

dans l'**École Doctorale Mécanique des fluides, Energétique,
Procédés**

NANOCELLULOSES AS POTENTIAL MATERIALS FOR SPECIALTY PAPERS

Thèse confidentielle soutenue à huis-clos le **14 Novembre 2014**
devant le jury composé de :

Dr. Laurent HEUX

Directeur de recherche au CERMAV, Président du jury

Dr. Bernard CATHALA

Directeur de Recherche à l'INRA de Nantes, Rapporteur

Pr. Patrice MANGIN

Professeur à l'Université du Québec à Trois-Rivières, Rapporteur

Pr. Etienne FLEURY

Professeur à l'INSA de LYON, Examineur

Dr. Julien BRAS

Maître de Conférences de Grenoble INP, Directeur de Thèse

Pr Naceur BELGACEM

Professeur de Grenoble INP, Co-directeur de thèse

Jocelyne DUMAS

Responsable R&D à Bolloré Thin Papers, Membre invitée



« Il faut cultiver notre jardin », *Candide ou l'Optimisme*, Voltaire (1759)

A mes grands-parents,

À mes parents,

À mes deux petites sœurs,

Remerciements

Cette thèse (convention CIFRE n°325/2011) *s'inscrit dans le cadre d'une collaboration industrielle* entre les Papeteries du Léman (PDL) et le Laboratoire de Génie des Procédés Papetiers (LGP2). Celle-ci a été financée par les Papeteries du Léman et l'*Agence Nationale de la Recherche Scientifique (ANRT)* et réalisée *au sein de l'équipe MATBIO (Matériaux Biosourcés Multi-échelles)* du LGP2.

Je tiens à remercier :

L'ensemble des membres du jury pour m'avoir fait l'honneur d'évaluer mes travaux à travers leur expertise reconnue dans le domaine des nanocelluloses. Laurent Heux pour avoir accepté de présider ce jury, Patrice Mangin et Bernard Cathala pour avoir accepté d'être rapporteurs de ce travail. La version finale de ce manuscrit a bénéficié de leur lecture très attentive, de leurs commentaires et de leurs critiques constructives.

Mes deux exceptionnels Directeurs de thèse qui représentent pour moi des modèles à travers leur parcours, leur expérience et pour ce *qu'ils apportent* à ceux qui ont la chance de les côtoyer. Naceur pour son recul scientifique, sa sagesse, et sa grande humanité. Julien *pour m'avoir transmis sa méthodologie*, son exigence scientifique, son enthousiasme et enfin pour son amitié. *Merci à tous les deux de m'avoir fait confiance et pour tout ce que vous m'avez apporté professionnellement et personnellement depuis ma première année à PAGORA.*

Le soutien considérable des Papeteries du Léman au cours de ces six dernières années universitaires (2009-2014), *pendant mon école d'ingénieur puis pendant ces trois années de doctorat.* En particulier, Jocelyne Dumas et Philippe Agut pour avoir été *à l'origine de ce projet* de thèse industrielle, ainsi que leur précieuse implication qui a largement contribué à sa valorisation. *L'ensemble de l'équipe r&d* et du laboratoire de PDL pour leur accueil chaleureux et leur disponibilité lors de mes séjours à Thonon, en particulier : Mélanie, Aurélie, Julie, Sophie, Éric, Serge, et Guillaume.

À Thomas, Victor, et Charlène que j'ai encadrés et grâce à qui j'ai beaucoup appris sur les qualités humaines nécessaires à la transmission et à l'encadrement. Merci pour votre implication, votre travail, et surtout pour votre indulgence. Je vous souhaite bon courage dans vos carrières respectives, et notamment à Charlène qui continue l'aventure en doctorat.

À Francine et Stéphane du CMTC pour leur disponibilité et leur expertise en FEG-SEM et en XRD, respectivement. À Cécile *pour m'avoir formé à utiliser la plupart des techniques expérimentales de l'équipe MATBIO et notamment pour l'AFM.* À Bertine pour la partie microscopie et surtout pour sa

bonne humeur. À Franck pour avoir résolu avec la plus grande efficacité tous mes problèmes informatiques pendant ces 3 ans. À Anne-Marie pour avoir géré mes déplacements et pour le reste (elle comprendra). À Jean-Luc pour avoir géré l'impression de ma thèse et pour avoir été un meilleur skipper que moi à Virtual Regatta.

À l'ensemble du personnel du LGP2/PAGORA pour qui j'ai une amitié profonde et que j'ai souvent sollicité pour m'aider pendant les « Raclettes de Noël » et le BBQs des doctorants, notamment Olivier, Mickael, Momo, Philippe, Shu, et Xavier. Merci spécialement à Charlotte pour sa gentillesse et d'avoir accepté de préparer une grande partie de mon pot de thèse. Merci à Stéphane pour ces discussions régulières à propos de nos sorties de ski de randonnée. À Isabelle, Nadège, Evelyne, José, Fred, et Didier, que j'ai connu d'abord timidement comme élève et qui sont devenus des collègues, puis des amis au cours de la thèse.

À tous les thésards du LGP2 pour cette bonne ambiance de travail et pour les moments passés ensembles entre l'apéro du jeudi soir, les BBQs, les tournois de squash, et les raclettes... Aux doctorants qui sont devenus docteurs avant moi et qui m'ont rapidement intégré dans cet univers, spécialement Karim, Bertrand, Lucie, Aurélie, et Elsa. À tous les doctorants du LGP2 qui deviendront bientôt docteurs et aux stagiaires qui sont devenus doctorants. Vous êtes certainement en train de passer les meilleures années de votre vie. À la « Brazilian Team », en particulier à Carolina, Daniele, et Fernando. Au bureau B121 et à Fufu, Arnaud, Seema et Benoît. À Aurore pour avoir été ma « grande sœur » de thèse. À Florian pour avoir été mon « petit frère » de thèse.

À tous ces coéquipiers (réguliers ou éphémères) de ski de randonnées avec qui j'ai fait la trace sur les pentes enneigées de Chamechaude quelques matins avant d'aller au labo...et pendant mes RTTs dans le massif des Ecrins, en particulier dans le secteur du refuge de l'Alpe.

À tous mes amis non thésards qui n'ont jamais vraiment compris à quoi servait ma thèse mais qui sont toujours à mes côtés et ont été les premiers à répondre présents pour assister à ma soutenance.

A Mathilde, la « dame de l'accueil », pour m'avoir soutenu, et épaulé pendant ces six longs derniers mois de rédaction qui n'ont pas toujours été des plus agréables...et pour continuer à me supporter aujourd'hui.

À ma mère et mes deux petites sœurs qui m'ont tant encouragé depuis toutes ces années. À mon père avec qui je partage aujourd'hui la fierté d'une publication commune.

Et pour finir, à toutes celles et ceux que j'ai maladroitement oubliés de remercier mais qui j'en sur me pardonneront cet oubli.

General summary

Scientific contributions (2011-2014)	5
Abbreviations	7
General introduction	11
Chapter 1. Literature Review	21
1. Specialty papers: description and expectation	27
2. Isolation of nanomaterial from Cellulose	33
3. Nanocellulose and their use in paper industry	61
Chapter 2. CNFs as dispersive network for particles	103
1. Different strategies for obtaining high opacity films of CNF with TiO ₂ pigments	109
2. Substitution of nanoclay in high gas barrier films of CNF with cellulose nanocrystals and thermal treatment	127
Chapter 3. Self-assembly of cellulose nanocrystals in film	155
1. Flexibility and color monitoring of CNC iridescent solid films using anionic or neutral polymers	161
2. Physicochemical interactions in fluoro-iridescent CNC films	181
Chapter 4. Nanocellulose as potential material for specialty papers	205
1. Cost-effective approach for limiting TiO ₂ in paper formulation with surface coating based on CNF	211
2. Engineered pigments based on iridescent cellulose nanocrystal films	229
General Conclusion	261
Extended abstract in French	269
Appendices	305
1. Appendix 1 - Patents	305
2. Appendix 2 - Poster in Scientific Meetings	323

Scientific contributions (2011-2014)

Scientific journal

1. Raphael Bardet, Naceur Belgacem, Julien Bras, *Different strategies for obtaining high opacity films of MFC with TiO₂ pigments*, Cellulose 20:3025-3037 (2013).
2. Raphael Bardet, Charlène Reverdy, Ingebjørg Leirset, Kristin Syverud, Naceur Belgacem, Michel Bardet, Julien Bras, *Substitution of nanoclay in high gas barrier films of cellulose nanofibrils with cellulose nanocrystals and thermal treatment*, Cellulose 22:1227-1241 (2015).
3. Raphael Bardet, Naceur Belgacem, Julien Bras, *Flexibility and Color Monitoring of Cellulose Nanocrystal Iridescent Solid Films Using Anionic or Neutral Polymers*, Applied Materials and Interfaces 7:4010-4018 (2015).
4. Raphael Bardet, Cécile Sillard, Naceur Belgacem, Julien Bras, *Physico-chemical interactions in fluoro- iridescent cellulose nanocrystals films*, Cellulose Chemistry and Technology (accepted in September 2014).
5. Raphael Bardet, Francine Roussel, Stéphanee Coindeau Naceur Belgacem, Julien Bras, *Engineered pigments based on iridescent cellulose nanocrystal films*, Carbohydrate Polymers 122:367-375 (2015).

Chapter book

1. Raphael Bardet and Julien Bras, *Cellulose Nanofibers and Their Use in Paper Industry*. In Handbook of Green Materials. pp 207-232 (2014).

Patent

1. Julien Bras, Naceur Belgacem, Raphael Bardet, Philippe Agut, Jocelyne Dumas, *Opacifying layer for a paper medium*, Grenoble INP ; Papeteries du Lemman,. WO 2014033409 A1 (2014).
2. Raphael Bardet, Julien Bras, Naceur Belgacem, Philippe Agut, Jocelyne Dumas, *Method for marking paper*, Grenoble INP ; Papeteries du Lemman, WO 2014118466 A1 (2014).

Oral Communication in Scientific Meetings

1. Raphael Bardet, Naceur Belgacem, Julien Bras, *Opacifying films using a tailored suspension of nanoparticle and cellulose nanofibers*, in: Int. Symp. on Wood, Fibre and Pulping Chemistry”, Vancouver, Canada (2013).
2. Raphael Bardet, Naceur Belgacem, Julien Bras, *Optimization of the formation of Iridescent Solid Films of Nanocrystalline Cellulose*, in: EPNOE International Polysaccharide Conference, Nice, France (2013).
3. Raphael Bardet, Naceur Belgacem, Julien Bras, *Use of CNF within paper industry: a review*, in: BioMatPack: Use of nanopolysaccharides in packaging, Grenoble, France (2013).
4. Raphael Bardet, Naceur Belgacem, Julien Bras, *Use of nanocellulose for functional packaging*, in: Axelera Workshop “Utilisation de cellulose pour l'élaboration de matériaux innovants”, Grenoble, France (2014).

Poster in Scientific Meetings

1. Raphael Bardet, Nathalie Lavoine, Naceur Belgacem, Isabelle Desloges, Julien Bras, *Barrier Properties of Specialty Papers Coated with MFC: Influence of Base Paper and Coat Weight*, in TAPPI International Conference on Nanotechnology, Montreal, Canada (2012).
2. Raphael Bardet; Alhem Romdhane; Victor Perrin; Marc Aurousseau; Naceur Belgacem; Agnes Guillet; Evelyne Mauret; Julien Bras, *Investigation of different post-treatments of cellulose nanocrystals in order to obtain narrowly dispersed rods*, in TAPPI International Conference on Nanotechnology, Stockholm, Sweden Stockholm, Sweden (2013).
3. Raphael Bardet, Coralie Cancé, Irina Horvatic, Naceur Belgacem, Julien Bras, *Structural Colored Films Based on Nanocellulose*, in TAPPI International Conference on Nanotechnology, Vancouver, Canada (2014).

Abbreviations

Materials

CAB	<i>Cellulose acetate butyrate</i>
CNF	<i>Cellulose nanofibrils</i>
CNC	<i>Cellulose nanocrystals</i>
CMC	<i>Carboxymethyl cellulose</i>
CNC-T	<i>TEMPO-oxidized cellulose nanocrystal</i>
CNF-T	<i>TEMPO-oxidized cellulose nanofibril</i>
DSPB	<i>Distyryl biphenyl</i>
GCC	<i>Ground Calcium Carbonate</i>
MCC	<i>Microcrystalline Cellulose</i>
MMT	<i>Montmorillonite</i>
OBA	<i>Optical brightening agent</i>
PAAS	<i>Sodium polyacrylate</i>
PCC	<i>Precipitated Calcium Carbonate</i>
PEG	<i>Polyethylene glycol</i>
PEI	<i>Polyethylenimine</i>
PVOH	<i>Polyvinyl alcohol</i>
SBR	<i>Styrene-butadiene rubber</i>
TEMPO	<i>2,2,6,6-tetramethylpiperidine-1-oxyl</i>
TiO₂	<i>Titanium dioxide</i>
TiOSO₄	<i>Titanyl sulphate</i>

Methods

BSE	<i>Back-scattered electrons</i>
DLS	<i>Dynamic light scattering</i>
EA	<i>Elemental analysis</i>
EDS	<i>Energy-dispersive X-ray spectroscopy</i>
E-SEM	<i>Environmental scanning electron microscope</i>
FE-SEM	<i>Field Emission Scanning Electron Microscope</i>
OM	<i>Optical microscopy</i>
OP	<i>Oxygen permeability</i>
OTR	<i>Oxygen transmission rate</i>
PDI	<i>Polydispersity index</i>
POM	<i>Polarized light microscopy</i>
QCM-D	<i>Quartz Crystal Microbalance with Dissipation Monitoring</i>
TGA	<i>Thermogravimetric analysis</i>
VVTR	<i>Water vapor transmission rate</i>
WVP	<i>Water vapor permeability</i>
XRD	<i>X-ray diffraction</i>
z*	<i>Hydrodynamic size</i>

General introduction

General introduction

Industrial context. Specialty papers are a growing interest to the paper industry\ which looks for alternatives for classic newspapers and printing commodity papers. According to an estimation by CEPI (2013), specialty papers account for 6% of global paper. It includes decor, packaging, printing, filtration, electrical, security, and “others.” In 2013, the global demand for specialty papers was estimated at 24 million tons, and will reach 25 million tons in 2014.(PIRA 2014)

This situation contrasts with the declining sales for graphic papers, as demand for writing and newsprint paper continues to fall due to the rise of electronic media and dematerialization. Even if specialty papers represent only a small percentage of the overall production in term of volume, they represent a higher percentage in terms of revenue. As predicted by PIRA (2014), specialty papers will represent the strongest growth in the emerging markets of the next five years (2014-2019).

Due to their high demand, relative rarity, and complex manufacturing, these papers allow a premium price. For European companies, specialty papers represent a promising reconversion of their industrial facilities and an opportunity for production diversification. Indeed, these product ranges address value-added applications with stable pricing over time.

In comparison to standard paper, specialty papers require additional properties that are different from the commodity market sector. Non-conventional raw-materials and processes can be used to achieve customers' requirements such as hydrophobicity,(Samain et al. 2013) highly electrical conductive,(Hu et al. 2009) antimicrobial,(Rodriguez et al. 2007) grease-resistance,(Vaswani et al. 2005) or anti-counterfeiting (van Renesse 1997).

The bulk, or the paper surface, has to be chemically or physically modified with different surface treatments or converting techniques. Therefore, to achieve new functions in specialty papers, several possibilities have existed for decades, and more recently, nanomaterials have been increasingly employed.

Use of nanomaterials in the papermaking industries. Over the past two decades, nanotechnology is at the forefront of modern scientific research and development in the papermaking technology.(Scott 1996)

In particular, nanomaterials are both used for improving the papermaking making process and for improving end-use or functional properties.(Shen et al. 2010)

For instance, colloidal silica is used as a retention and drainage aid for papermaking. Other mineral nanoparticles can be used in the paper coating to improve paper printability, such as, nano PCC, to develop highly barrier coatings with nanoclay, or antimicrobial paper with silver or zinc oxide nanoparticles.

Nanocellulose as a promising biobased nano-scaled material. While many nanomaterials are based on mineral or petrol-based resources, nanomaterials isolated from biomass like “Nanocellulose” appear to be an emerging, sustainable alternative. In comparison to most of nanomaterials, it is extracted from vegetal biomass, features an attractive combination of promising properties such as being bio-based, biodegradable, and relatively biocompatible. In addition it has a low density (~ 1.6), high stiffness (~ 150 GPa), thermal stability ($\sim 300^\circ\text{C}$), and a high density of hydroxyl groups available for chemical modification.(Dufresne 2012) For all these reasons, researchers are convinced that the isolation of nanocellulose with a high surface area ($> 200\text{m}^2/\text{g}$) and strong bonding ability can improve existing materials (paper, gel, composite), or create new performant materials (aerogel, flexible film).(Charreau et al. 2013) This interest in nanocellulose is highlighted by the strong growth of patents and scientific publications since the year 2008 (**Figure 1**).

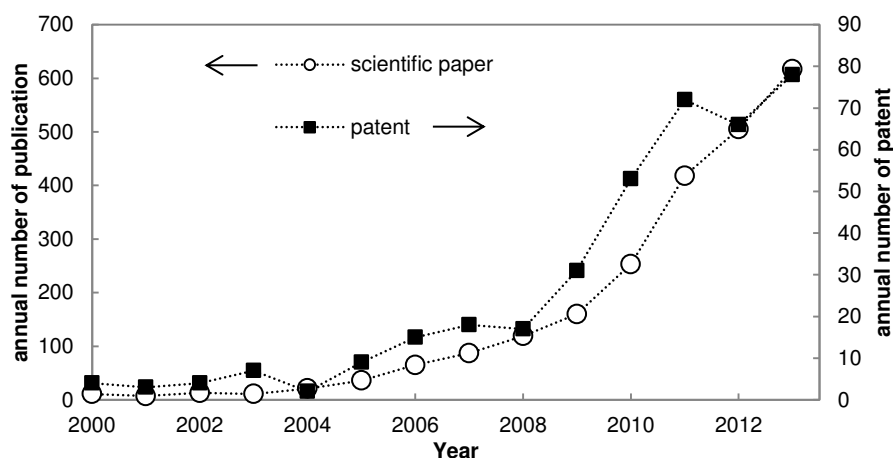


Figure 1- Evolution of the number of patents or publications per year in nanocellulose materials. Extracted from Scifinder September 20014

In addition, nanocellulose is now commercially available with the recent construction of the first Canadian nanocellulose plants in 2011, and creation of new ventures every quarter.(Chauve et al. 2014) Even the nanotoxicology and the risk assessment on nanocellulose are currently under investigation. Preliminary toxicological data confirms that nanocellulose can be considered as non-toxic.(Pitkänen et al. 2014) Finally, nanocellulose was accepted on Canada’s Domestic Substance List (positive list of non-dangerous materials) in early 2012.

Main properties of nanocellulose. As presented in **Figure 2**, different types of nanocellulose are available: Cellulose Nanocrystals (CNCs) and Cellulose Nanofibers (CNFs) which depend on their isolation treatment, either a chemical treatment or high mechanical shearing, respectively.

CNFs are semicrystalline and flexible and consist of aggregates of microfibrils. Their diameter is in the range of 20–60 nm with a length of several micrometers.(Chinga-Carrasco 2011) In contrast, CNCs are rod-like particles with classic dimensions of approximately 5 nm in diameter and 250 nm. Compared to CNF, in which the surface chemistry of cellulose is slightly affected during their isolation, sulfate ester groups are introduced on CNC during the hydrolysis (sulfation).(Habibi et al. 2010)

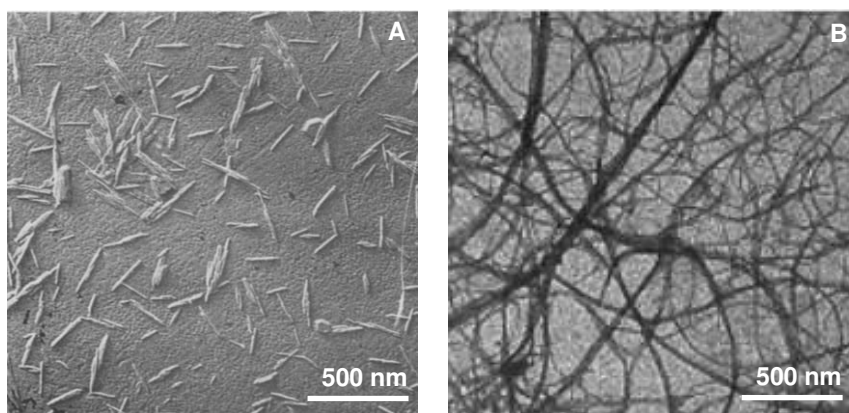


Figure 2 – One of the 1st nanoscale observations in TEM microscopy of nanocellulose: CNC (a) and (b) CNF, (reproduced from (Marchessault et al. 1959) (Dufresne et al. 1998))

It is worth noting there are significant differences between the two nanocellulose families regarding their morphology and surface chemistry, resulting in different properties in suspension and solid states. CNC suspension exhibits birefringence properties from their self-assembly properties.(Gray 1994) One outstanding application is the manufacturing of iridescent materials as patented by Revol et al. (1995).

Oppositely, CNF suspension exhibits gel-like behavior even at low concentrations with shear thinning properties. Because of hydrogen bonds and their flexibility, once dried, CNF form a cohesive and dense entangled network which forms a smooth, strong, and transparent films.(Spence et al. 2010) Films based on CNF also display excellent air, oxygen, and grease barrier properties in dry conditions.(Syverud et al. 2009, Aulin et al. 2010)

The main original feature of this PhD project consists of studying the contribution of both CNC and CNF within specialty papers.

Use of nanomaterials in the papermaking industries. Surprisingly, the use of nanocellulose (essentially CNFs) in paper industry is very recent (less than 10 years) and only a few studies are addressing this theme.

At the beginning of the year 2014, among 2720 scientific papers on nanocellulose, only 40 are directly dedicated to the papermaking industry. In addition, among more than 400 innovations that cover most of the uses and applications of CNFs that have been patented, only one-third concerns the applications in the paper industry. Moreover, more than 20 patents have been granted only in the past three years (during this PhD project).

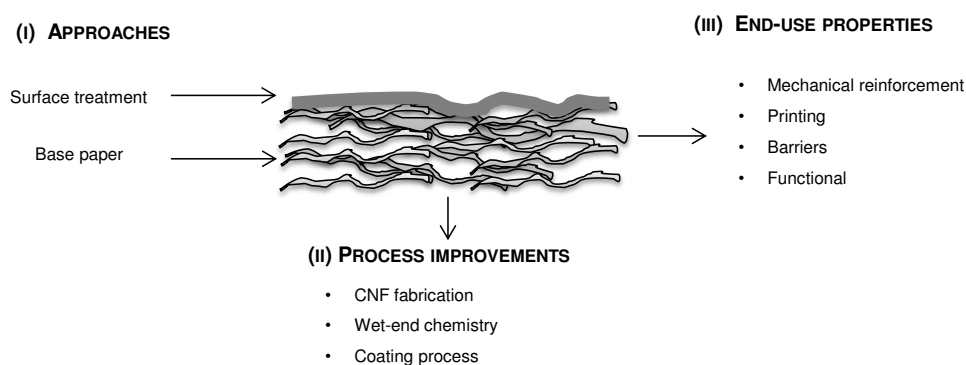


Figure 3 - Approach for utilization of CNF for the paper surface treatment

As shown in **Figure 3**, nanocellulose may succeed in improving the mechanical and barrier properties of paper for various applications like food packaging and printing media. Several studies have been launched on the topic since 2008. For example, a recently completed European project (SUNPAP, 2009-2012), was completely dedicated to the use of CNF within the paper industry. This proves the increasing interest from the nanocellulose community to use nanocellulose in the paper industry. The two different approaches classically proposed in the literature are either bulk addition or surface treatment.

Usually, nanocelluloses appear to be an emerging sustainable alternative to mineral nanomaterials or petrol-based solution for improving the papermaking making process or the end-use properties. To the best of our knowledge, the highest potential seems to lie in the surface treatment.(Bardet et al. 2014)

Outline of the project. For all reasons detailed previously, “Papeteries du Léman” has decided to launch collaboration with LGP2 in 2011 within an industrial PhD framework (CIFRE¹).

The project is entitled “**Nanocelluloses as potential materials for specialty papers**”.

¹ N° 325/2011

The novelty of this PhD project is to validate specificities of CNC and CNF within specialty papers.

The present manuscript is organized in four chapters as shown in **Figure 4**. First, a literature review (**Chapter 1**) introduces the industrial context of the project detailing the specialty papers (i) and nanocellulose (ii). At the crossroad of the two themes, an extended review about the use of nanocellulose in paper industry (iii) is also provided, and an overview of the main challenges of this project is detailed.

The study is then conducted in two steps. First, in **Chapter 2** and **Chapter 3**, the nanocellulose films are considered as model surface layers and their properties are investigated for both families of nanocellulose. Second, the results obtained for model surface layer are implemented at the industrial scale within the papermaking process in the **Chapter 4**

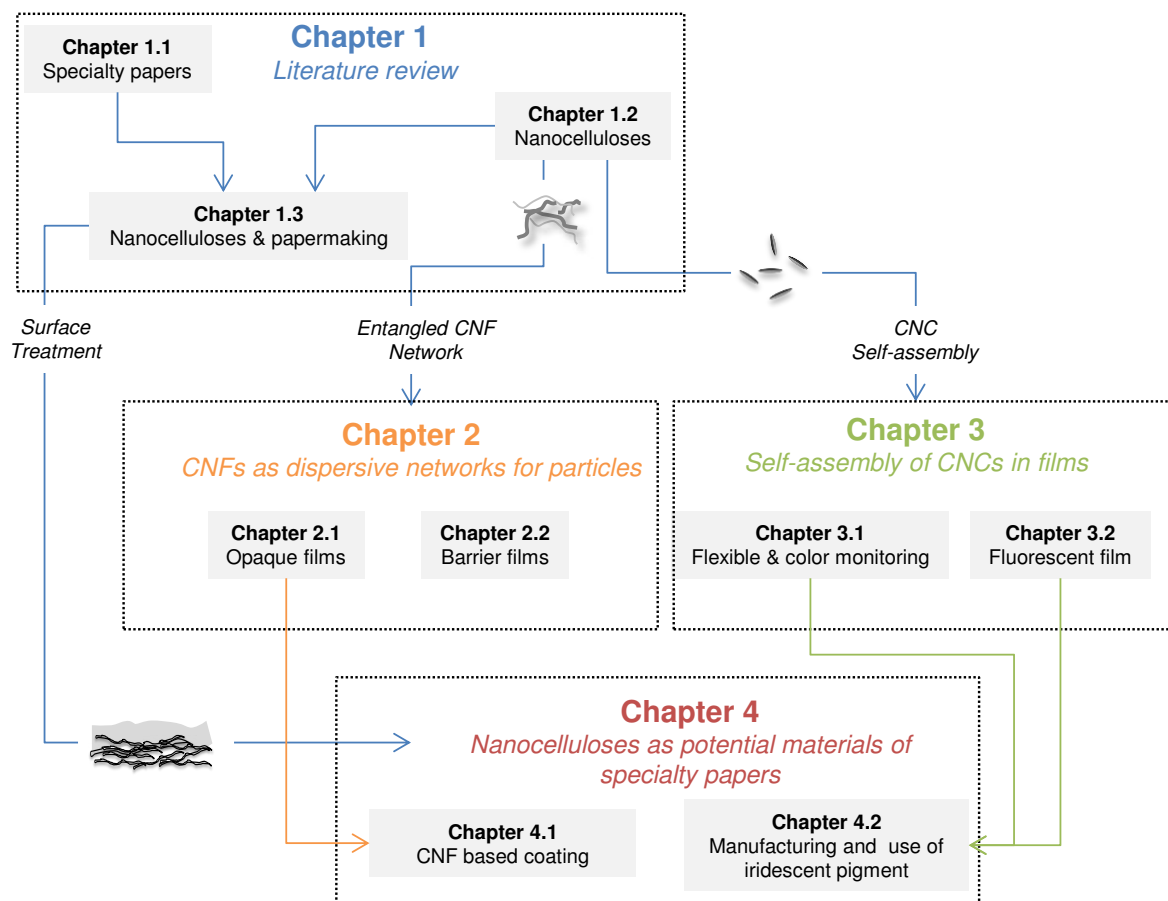


Figure 4 - Schematic view of the manuscript organization

As detailed in **Chapter 1**, CNF forms a cohesive and dense entangled network when dried. This feature will be investigated in **Chapter 2**, in which CNF will be used as dispersive network for particles for (i) replacing existing polymer in thin opaque films or (ii) substituting mineral nanoparticles in barrier materials.

In contrast, CNC and their self-assembly properties allow for the manufacturing of iridescent materials. These specific optical properties will be used to develop flexible iridescent films with tunable color and fluorescent properties in **Chapter 3**.

Secondly, the results obtained for a model surface layer are implemented at the industrial scale within the papermaking process in the **Chapter 4**. From the results obtained in **Chapter 2**, a cost-effective solution for saving opacifying pigment is presented in **Chapter 4.1**. Meanwhile, **Chapter 4.2** presents the manufacturing and use of iridescent pigment within specialty paper for anti-counterfeiting applications. **Figure 5** indicates if sub-chapters deal more with academic scientific understanding or industrial applications. The approach was to cover the entire range.

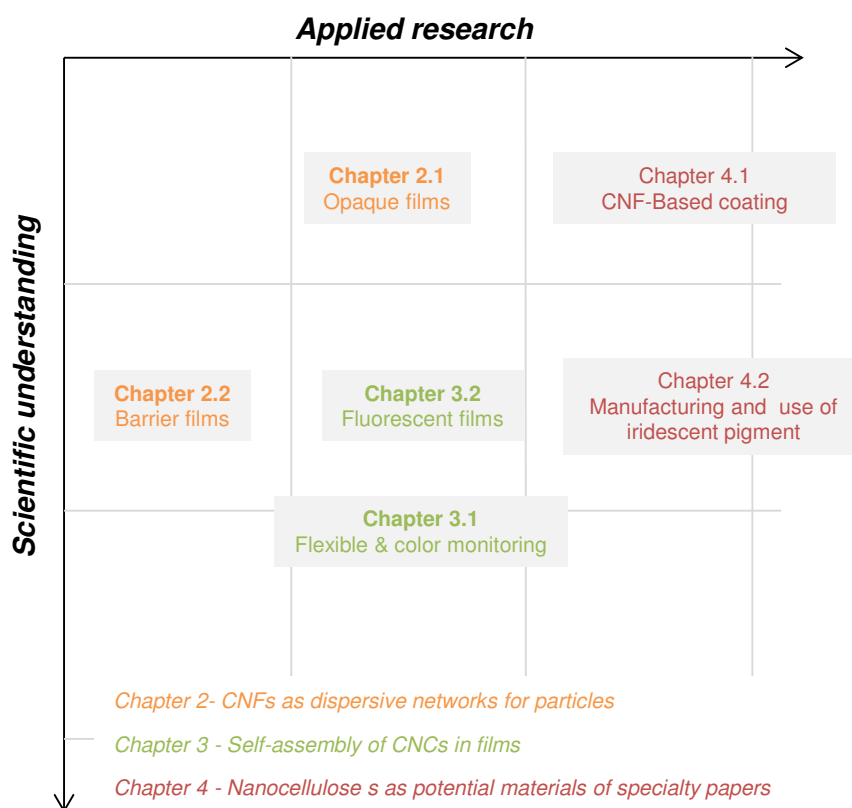


Figure 5 - Schematic Organization of the different chapters of the manuscript regarding the scientific understanding and the applied research

Note that the last part of **Chapter 1** is inspired from a book chapter. **Chapter 2** and **Chapter 3** are mainly based on scientific papers whereas **Chapter 4** is inspired from 2 patent applications and industrial trials conducted during project. To specify or complete the original publications, comments, illustrations, or complementary results may have been added and introductory parts are reduced only highlight the context and the purpose of the study.

References

1. Aulin, Gällstedt, *et al.*, "Oxygen and oil barrier properties of microfibrillated cellulose films and coatings", Cellulose 17(3): 559-574 (2010).
2. Bardet and Bras, "Cellulose Nanofibers and Their Use in Paper Industry", Handbook of Green Materials: 207-232, edited by World Scientific (2014).
3. Cepi, "European Pulp and Paper Industry 2012 - Key Statistics", from <http://www.cepi.org/> (2013).
4. Charreau, L Foresti, *et al.*, "Nanocellulose patents trends: A comprehensive review on patents on cellulose nanocrystals, microfibrillated and bacterial cellulose", Recent patents on nanotechnology 7(1): 56-80 (2013).
5. Chauve and Bras, "Industrial Point of View of Nanocellulose Materials and Their Possible Applications", Handbook of Green Materials: 233-252, edited by World Scientific (2014).
6. Chinga-Carrasco, "Cellulose fibres, nanofibrils and microfibrils: The morphological sequence of MFC components from a plant physiology and fibre technology point of view", Nanoscale Research Letters 6 (2011).
7. Dufresne, "Nanocellulose, From Nature to High Performance Tailored Materials", edited by De Gruyter (2012).
8. Dufresne and Vignon, "Improvement of starch film performances using cellulose microfibrils", Macromolecules 31(8): 2693-2696 (1998).
9. Gray, "Chiral nematic ordering of polysaccharides", Carbohydrate Polymers 25(4): 277-284 (1994).
10. Habibi, Lucia, *et al.*, "Cellulose Nanocrystals: Chemistry, Self-Assembly, and Applications", Chemical Reviews 110(6): 3479-3500 (2010).
11. Hu, Choi, *et al.*, "Highly conductive paper for energy-storage devices", Proceedings of the National Academy of Sciences 106(51): 21490-21494 (2009).
12. Marchessault, Morehead, *et al.*, "Liquid Crystal Systems from Fibrillar Polysaccharides", Nature 184(4686): 632-633 (1959).
13. Pira, "Getting out of the Commodity Trap: 4 steps to success in specialty papers", from <http://downloads.pira-international.com/success-in-specialty-papers-white-paper/> (2014).
14. Pitkänen, Kangas, *et al.*, "Toxicity and Health Issues", Handbook of Green Materials: 181-205, edited by World Scientific (2014).
15. Revol, Godbout, *et al.*, "Solidified liquid crystals of cellulose with optically variable properties", Pulp and Paper Research Institute of Canada, WO9521901A1 (1995).
16. Rodriguez, Battle, *et al.*, "The use of natural essential oils as antimicrobial solutions in paper packaging. Part II", Progress in Organic Coatings 60(1): 33-38 (2007).
17. Samain and Stinga, "Procédé et dispositif de traitement par greffage chromatogénique d'un substrat hydroxyle", WO2013093113A3 (2013).
18. Scott, "Principles of wet end chemistry", edited by Tappi Press Atlanta, Georgia (1996).
19. Shen, Song, *et al.*, "A Review on Use of Fillers in Cellulosic Paper for Functional Applications", Industrial & Engineering Chemistry Research 50(2): 661-666 (2010).

20. Spence, Venditti, *et al.*, "*The effect of chemical composition on microfibrillar cellulose films from wood pulps: Mechanical processing and physical properties*", Bioresource Technology 101(15): 5961-5968 (2010).
21. Syverud and Stenius, "*Strength and barrier properties of MFC films*", Cellulose 16(1): 75-85 (2009).
22. Van Renesse (1997), "*Paper based document security-a review*". European Conference on Security and Detection. London, England.
23. Vaswani, Koskinen, *et al.*, "*Surface modification of paper and cellulose by plasma-assisted deposition of fluorocarbon films*", Surface and Coatings Technology 195(2): 121-129 (2005).

Chapter 1

Literature review

Table of Content

Introduction	25
1 Specialty papers: description and expectation	27
1.1 Paper industry in brief	27
1.2 The papermaking process	29
1.2.1 Stock preparation and the approach flow	30
1.2.1 Paper machine overview	30
1.3 Industry evolution and market expectations	31
2 Isolation of nanomaterial from Cellulose	33
2.1 Overview	33
2.2 The vegetal biomass as the starting material of nanocellulose	34
2.3 Different techniques for the isolation of nanocellulose	37
2.3.1 Isolation of CNC	38
2.3.2 Isolation of CNF	41
2.4 Industrialization of nanocellulose and its potential use	47
2.5 Safety issues and nanotoxicology of nanocellulose	50
2.6 Main features of nanocellulose	52
2.6.1 Nanocellulose assembly as suspension	53
2.6.2 Nanocellulose assembly as films	54
3 Nanocellulose and their use in paper industry	61
3.1 Bulk addition	62
3.1.1 Direct addition of CNF in the pulp suspension	62
3.1.2 Multiply strategy	64
3.1.3 CNF & polyelectrolytes	65
3.2 CNFs and paper surface treatment	69
3.2.1 The surface coating of specialty paper	69
3.2.2 Optical and Printing properties	75
3.2.3 Barrier properties	79
3.3 Conclusions	84
Highlights and next challenges	85
List of Tables	87
List of figures	88
References	90

Chapter 1

Literature review

Introduction

The present chapter aims to set the general background in which this PhD project has evolved during the last three years (2011-2014).

The first part provides a brief historical presentation of paper industry, as well as a recent update on the state of art in paper industry. It ends by giving scientific perspectives and marketing expectations within specialty paper for coming years.

Then, it becomes obvious that among all existing technologies and raw materials to improve or functionalize paper, one of them is indisputably the use of nanocellulose. Moreover, the literature in the field of nanocellulose is exponentially increasing. Therefore, the second part summarizes the different kinds of nanocellulose regarding their isolation processes and their main features. Then, two different uses of nanocellulose as solid films are addressed, i.e. barrier and iridescent films. Because this project focuses on the potential applications' current researches, a review about the industrialization and the potential toxicology concerns is also provided.

Because of the recent interest of nanocellulose in papermaking and in particular for specialty papers, a critical review is also proposed as a last part of this literature survey. This part summarizes the different approaches and potential improvements brought by the use of nanocellulose throughout the paper production protocol. This last section is adapted from a contribution in a recent book chapter. To sum, this chapter identified the main challenges of this project.

1 Specialty papers: description and expectation

1.1 Paper industry in brief

Nowadays, paper is omnipresent in our everyday life in various existing forms: books, newspapers, packagings, paper walls, labels, banknotes and many more. So the paper material widely contributes to the development of the industry, dissemination of knowledge and also distribution of goods or products.(Sonnenfeld 2002) As estimated by FAO in 2012, the annual paper consumption is about 60 kg per person with a substantial difference within regions of the world.(FAO 2014)

For instance, the consumption of paper in the US represents more than 340 kg per person, while developing countries annually consume less than 13 kg of paper. The consumption growth is mostly related to the increase in Gross National Product.

At the present time, while industrialized countries such as the United States, Japan, and the Western European countries have relatively low growth rates, the largest growing potential for paper consumption is in the emerging and BRICS. Therefore, the consumption and production in countries such as China or India have increased over recent years on a large scale. In mature markets such as Europe, Japan, and North America production and consumption have stagnated or even decreased.

As detailed in **Fig 1.1**, they are usually divided into four main categories:

- Writing and printing papers
- Board and packaging
- Tissue paper
- Specialty paper

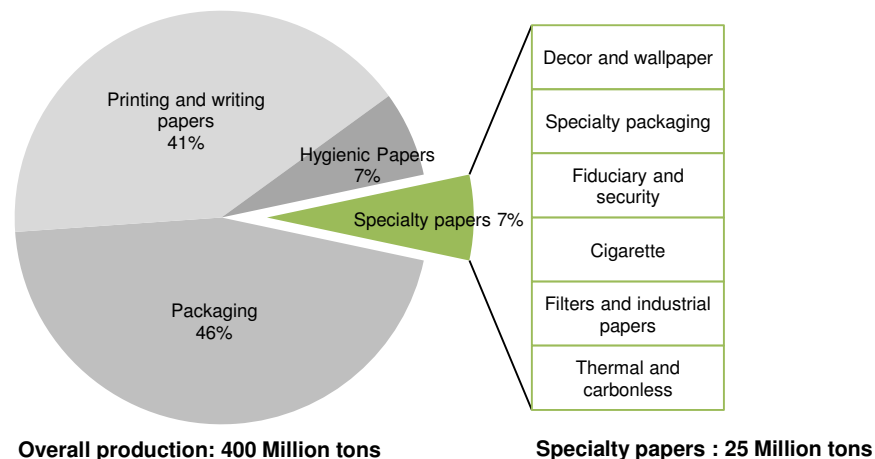


Fig 1.1 - Global paper production share by application. Data collected from (CEPI 2013).

The two first groups of papers are still the most commonly produced with more than 80% of the overall production. Tissue paper production is much more recent, since the first production date started during the year 1950's.

Specialty papers can be defined as all paper grades not dedicated to commodity applications. Generally, they have additional and functional properties. This group of paper covers a wide range of grades of applications such as wallpaper, electro technical papers, cigarette, or thermal papers. All these papers have a common requirement; they must exactly fulfill the defined quality criteria according to the use.

In 2013, the global paper industry represents an annual production about 400 million tons. In comparison, the worldwide plastics production for packaging rose only 290 million tons in same year.(Plastics-Europe 2013)

Owing to The Confederation of European Paper Industries CEPI (2013), this consumption will increase to about 530 million tons in 2020 and 605 million tons in 2030.

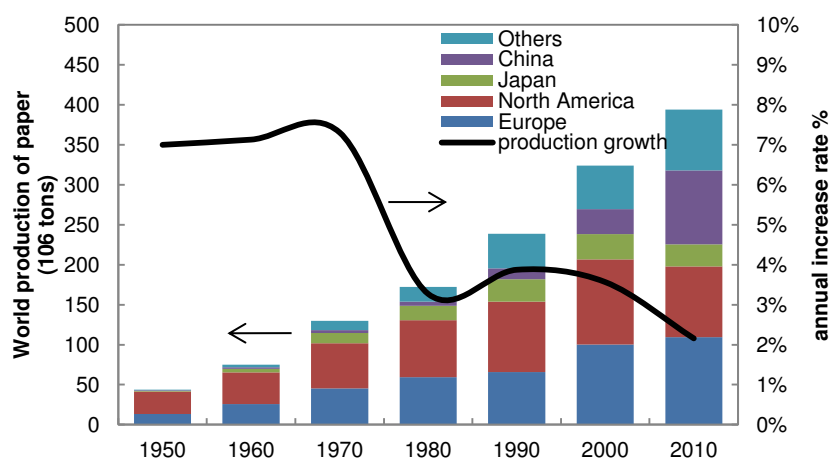


Fig 1.2 - World production of paper for main producer regions since 1950 to 2010

The global market of papers has increased more than nine-fold since the years 1950 and it has still a moderate growing (2% per year) as shown in **Fig 1.2**.

In 2013, Europe, North America, Japan, and China accounted for 80% of the total world production.

However, the production sharing in these regions has varied considerably. The production of paper in China increase more than 18-folds since 1980 and it is now the largest paper producer in the world.

Since the 1980s, Europe has maintained its share of world production, whereas North America has large losses of its share of production.

1.2 The papermaking process

The word "paper" is etymologically derived from “papyrus”, which is the Ancient Greek word for the papyrus plant.

The paper was invented in China in the first century (105 C.E) during the Han Dynasty. In Europe, papermaking started in the 10th Century in the Iberian Peninsula, and slowly spread to Italy and the South of France reaching Germany by the years 1400’s. The rapid expansion of European paper production was enhanced by the invention of the printing press and the beginning of the printing Revolution in the 15th century.(Orsenna 2012)

The first industrial paper machine dates from the 19th century and its spreading occurred in 1900’s with the new energy development coming from hydrokinetics called la “Houille Blanche”. The manufacturing of paper consists of quickly removing the water of a dilute suspension (1-5 g/l) composed of cellulosic fibers, minerals fillers, and additives in order to make a self-standing fibrous material. Hydrogen bonds are created during successive water removal: draining, pressing and evaporating ensure the cohesion of the material, i.e. the paper sheet.

Table 1.1 illustrates the tremendous improvements of the paper manufacturing regarding production speed, width, length and of course its productivity.

Table 1.1 - Overview of papermaking production parameters

	Speed (m/min)	Width (m)	Machine length (m)	Output production
Handsheets (years 1500)	-	1	10	45 kg /day
1 st Fourdrinier machine (years 1900)	300	3	80	240 ton/day
State-of art of paper machine	1500-1700	12	430-600	4500 ton/day

More recently, paper industry has steadily improved its standards according to environmental demands such as water consumption and water effluents, energy consumption, and fiber consumption.(CEPI 2014)

Nowadays, papermaking includes the same process steps as applied for centuries: preparation of the fiber material, web forming, pressing, drying, sizing, and calendaring.

1.2.1 Stock preparation and the approach flow

The papermaking process starts with the delivery of the raw material of the stock components including fibers, fillers, and chemicals additives. Stock preparation is a key process in paper production. Without the suitable furnish, the papermaker cannot produce the desired paper quality. Therefore, the main objective of the stock preparation is to modify the raw materials in such a way that the finished stock suits with the requirements of the paper machine and of the quality required. A stock preparation system consists of several unit processes as summarized in **Table 1.2**:

Table 1.2 - Overview of the main unit operations of the stock preparation

Unit operations	Role	Consistency
disintegration	break down the bleached dried pulp (bales) to a suspension of individual fibers which results in a pumpable suspension	100 g/l
screening cleaning fractionation,	remove undesired interfering solid substances from the suspension, which differ from the fibers in size, shape, and deformability	60 g/l
refining	modify the morphology and surface characteristics of the fibers	60 g/l
mixing a storing	add and dose dyes, fillers and chemicals mix uniformly all the different components	20-60 g/l
Approach flow	supply a continuous suspension flow of a constant consistency, quality, and flow rate at constant pressure to the headbox	20-30

1.2.1 Paper machine overview

Afterwards the diluted furnish additives is sent to the paper machine starting from the headbox and ends with the paper reeling. **Fig 1.3.** below shows the general scheme of a machine used to produce specialty paper¹ such as cigarette or lightweight-coated paper

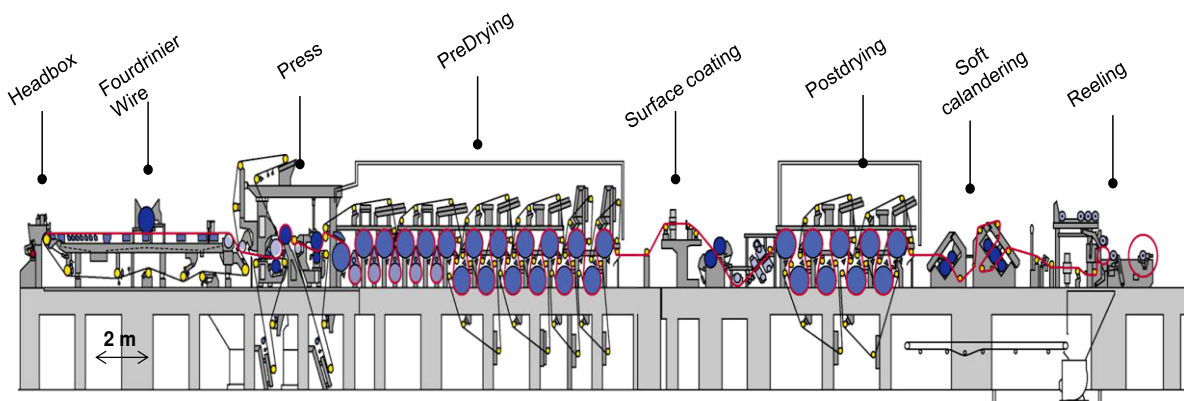


Fig 1.3 - Overview of a specialty paper machine. Adapted from Voith

¹ In this project, a similar paper machine was used for implementing industrial trial at the end of the project

A recent paper machine consists of:

- the headbox distributing the suspension across the machine width onto the wire
- the wire section where the suspension is formed into an endless web by dewatering;
- the press section pressing water out of the web by mechanical means
- the pre-drying section where the residual water is evaporated by heat
- a coating section where coating color is applied to the web
- the post-drying section where the wet coating layer is dried
- the soft calendaring section to smooth the paper surface
- the reeling sections where the paper web is reeled at the reeler at full width

Since its invention, papermaking technologies is constantly adapting their materials to consumer needs. More and more possibilities of on-line treatments such as calendaring, impregnation, surface treatment are now available. In summary, papermaking in Europe is a mature technology, and now more focuses on the optimization of water treatment, energy consumption, and raw materials sustainability.

1.3 Industry evolution and market expectations

The ratio of the worldwide consumption of the different paper grades is still evolving; the specialty and packaging papers have increased graphic paper grades have stagnated, whereas newsprint consumption has declined.

Table 1.3 - Key figures of European Paper industry

Year	Number of machines	Production capacity (10 ⁶ tons)	Employment	Turnover (10 ⁶ €)	Investment (10 ⁶ €)	Added value (10 ⁶ €)
1991	2 182	73 280	411 113	-	-	-
2000	1 858	97 658	279 987	79.3	5.6	24.4
2005	1 725	109 801	246 785	74.5	5.3	17.9
2010	1 393	103 714	194 643	73.9	2.7	16.8
2012	1 335	102 196	185 906	76.0	3.4	15.5
2013	1 300	100 766	183 194	75.0	3.0	15.0

Data collected from (CEPI 2013)

The economic crisis in years 2007 has affected the European paper industry both in term of employment, production capacity, and turnover, as highlighted in **Table 1.3**.

Indeed, the global economy has motivated many companies to perform a close analysis of their paper costs that of course profoundly changed their communication systems. The data released for 2011 indicates a drop in both paper and pulp manufacturing overall, the only area showing growth was tissue and specialty paper.(Skogsindustrierna 2013)

The worst performer was graphic paper, used predominantly in printing, with an overall production nearly lower than 3%. In addition, the shift of newspapers or books from print to digital format is also apparently having an irreversible effect. According to an updated estimation of CEPI (2013), specialty papers account for 6% of the global overall paper. It includes *décor*, packaging, printing, filtration, electrical, security, and 'others'. The global demand for specialty papers is estimated at 24.4 million tons this year 2013, and will reach 25 million tons in 2014.(PIRA 2014)

Its share will only grow as demand for packaging mostly contributing to market growth. This situation contrasts with the declining sales for graphic papers, as demand for writing and newsprint paper continues to fall due to the rise of electronic media and dematerialization. (Ahmadi Achachlouei 2013). Furthermore, in this portfolio even if specialty papers represent only small percentage of the overall production in term of volume, they represent an important percentage in terms of income.

Specialty papers are a growing interest and a promising perspective for the diversification of the paper industry. As predicted by PIRA (2014), specialty papers will represent the strongest growth in the emerging markets of the next five years (2014-2019).

They are more dedicated to value added applications, increased financial performance for the producer, and have stable pricing over time. In addition, due to their high demand, relative rarity, and complex manufacturing, these papers allow a premium price. In comparison to paper, specialty papers require additional properties that are different from the commodity market sector.

To achieve such properties which are unusual for cellulosic materials such as hydrophobicity,(Samain et al. 2013) highly electrical conductive,(Hu et al. 2009) anti-microbial,(Rodriguez et al. 2007) grease-resistance,(Vaswani et al. 2005), and anti-counterfeiting,(van Renesse 1997) specific raw-materials and processes are used. The bulk or the paper surface needs to be chemically or physically modified using different surface treatments or converting techniques, as described in detail final part of this chapter.

Therefore, to achieve new functions in specialty papers, several possibilities exist since decades. However since last five years, a new biobased material is becoming industrially available and sounds very promising for papermaking and in particular for specialty papers. This new material is what is called nanocellulose. This is the main raw material investigated during this PhD project. That is why next chapter will present the basic features of nanocellulose.

2 Isolation of nanomaterial from Cellulose

2.1 Overview

Cellulosic fibers are used to produce paper but not only. Cellulose for industrial use is mainly extracted from wood pulp and cotton. It is considered as the most abundant biopolymer on earth, with about 200 billion tons annually produced by photosynthesis, renewed simply thanks to solar energy, carbon dioxide and water. In addition, only 3% are extracted per year.(Hon 1994, Klemm et al. 2005) This biopolymer can be used in textile or as a reinforcing phase in bio-degradable composites,(Belgacem et al. 2005) or as a wide variety of derivative products(Demirbaş 2001).

In addition, cellulose can be an alternative to fossil-based fuel source and efficiently converted into biofuels from energy crops.(Demirbas 2007)

Lastly, nanomaterials² isolated from cellulose could bring strong economic advantages to the valorization of industrial biomass resources.

Over the past two decades, nanotechnology is at the forefront of modern scientific research and development in commercial products. For instance, the applications include metallic oxide nanoparticles in sunscreen, silver nanoparticles(McIntyre 2012) in food packaging, clothing disinfectants, or households, and carbon nanotubes(Qian et al. 2004) for stain-resistant textiles.

While many nanomaterials are based on fossil-fuel or non-renewable resources and can be suspected or proved nontoxicity issues,(Buzea et al. 2007) nanocellulose have many advantages (Klemm et al. 2009).

It includes:

- low density
- renewable sources, biodegradability, non-food agricultural based economy
- biocompatible
- high specific strength and modulus
- reactive surface which can be used for grafting specific groups

For these reasons, nanocellulose has gained prominence as a nanomaterial. Thus for the last twenty years, the scientific community and the industrial sector have shown a growing interest in the “nanocellulose” study.

² At least one dimension lower than 100 nm

Researchers are convinced that the isolation of nanoparticles with a high surface area ($> 200 \text{ m}^2/\text{g}$) and strong bonding ability can improve existing materials (paper, gel, composite) and create new material (aerogel, flexible film) with improved performance.

As highlighted in **Fig 1.4**, recent developments in the research on cellulosic nanoparticles lead to an increasing and broad literature mainly devoted to isolation, characterization, and uses of nanocellulose.

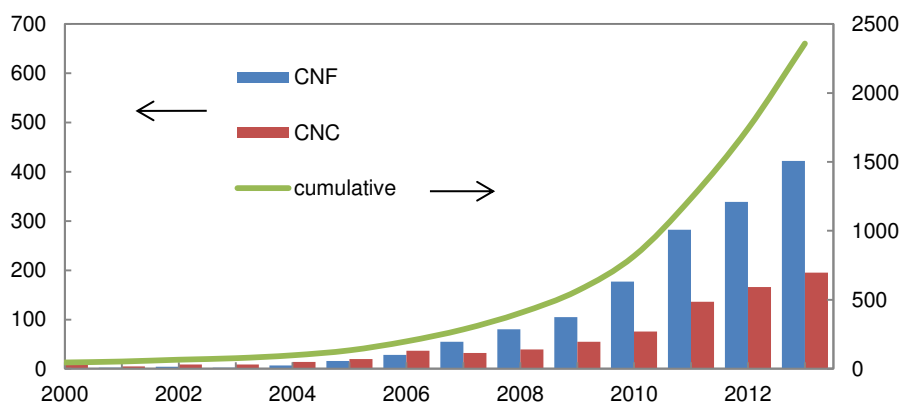


Fig 1.4 - Annual number (histogram) and cumulative number (dotted line) of scientific publication about nanocellulose from 2000 up to now (from SciFinder, Sept. 14)

Even if several names are usually used, two main families³ of nano-sized cellulosic particles are defined: Cellulose Nanocrystals (CNCs) or Cellulose Nanofibrils (CNF)

Such classification only depends on the isolation treatment to which the starting material is subjected, whether a chemical treatment for CNCs or a mechanical disintegration for CNFs. It is clear that the two kinds of nanocellulose have completely different structures, dimensions, and morphologies and consequently, different properties. The different features are detailed in next sections

2.2 The vegetal biomass as the starting material of nanocellulose

Nanocellulose can be isolated from almost all biomasses containing cellulose fibers regardless its origin. It can be extracted from wood (softwood, hardwood), crops and agro-resources, annual plants or marine biomass by several mechanical and chemical treatments (pulp). (Hon 1994)

The main chemical elements of lignocellulosic fibers are cellulose (40-96%), hemicellulose (2-30%), lignin (2-30%) and a smaller proportion of extractives (resin acids, fatty acids, and pectin). (Hon 1994)

³ The specificity of our project is that the two types of nanocellulose will be studied: first MFC as dispersing network and then NCC for producing engineering iridescent pigments

They are generally purified (bleaching) to eliminate non-cellulosic materials such as residual lignin and extractives. (Sjöström 1993) These operations are everyday practiced in pulping industry. Pulping industry annually produces about 300 million tons of bleached cellulose fibers essentially from woods by Kraft or sulphite processes, mainly. (Biermann 1993) The average proportion of these elements as well as the degree of polymerization of cellulose mainly depends on raw materials as summarized in the **Table 1.4**:

Table 1.4 - Chemical composition of some vegetal biomass used for nanocellulose production

	Wood		Annual plants		Agro resources		Marine Biomass	
	Softwood	Hardwood	Cotton	Flax	Bagasse	Straw	Algae	Tunicate
Cellulose	40-44	43-47	95	63-71	40	30		NA
Average DP	6,000 -10,000		15,000	8,000	4,600	4,000	25,000	4,000
Hemicellulose	25-29	25-35	2	12-21	30	50		
Lignin	25-31	16-24	1	2-3	20	15		NA
Extractives	1-5	2-8	0.4	6-13	10	5		

Data collected and summarized from (Sjöström 1993, Han et al. 1997)

As schematized in **Fig 1.5-B**, lignocellulosic fibers can be considered as composites in which cellulose acts as fibers, lignin as a matrix and hemicellulose as interfacial compatibilizing agent.

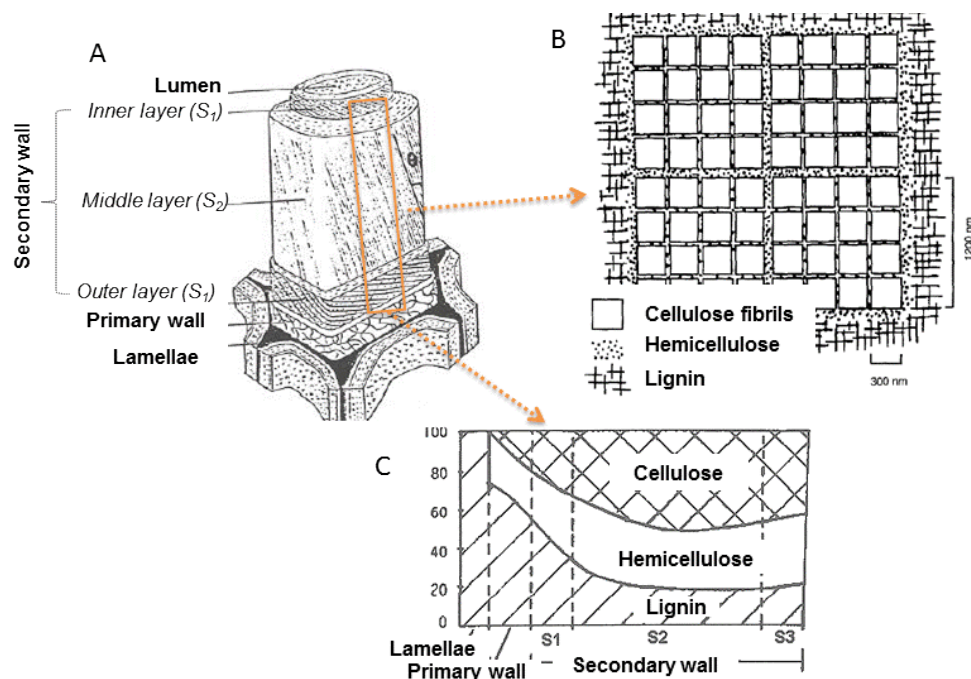


Fig 1.5 - Simplified structure of the cell wall (typical softwood tracheid) (A) and distribution of Cell Wall Components (B) and distribution of chemical components across the fiber wall (C). Adapted from (Hon 1994)

As described in **Fig 1.5-A**, they are made of three structural layers: the lamellae, the primary wall, and the secondary wall. Generally, the secondary wall contains the highest proportion of elementary cellulose fibrils (**Fig 1.5-C**).

The molecular structure of cellulose was revealed in 1930 by Haworth et al. (1930). This is a linear polysaccharide composed of glucose sugar units ($C_6H_{12}O_6$) bonded end-to-end through carbons C_1 and C_4 by $\beta_{1,4}$ glycosidic linkage (**Fig 1.6**). Its repeating unit is constituted by two anhydroglucose units (AGU) namely cellobiose ($C_{12}H_{22}O_{11}$), with a molar mass of 342 g/mol.

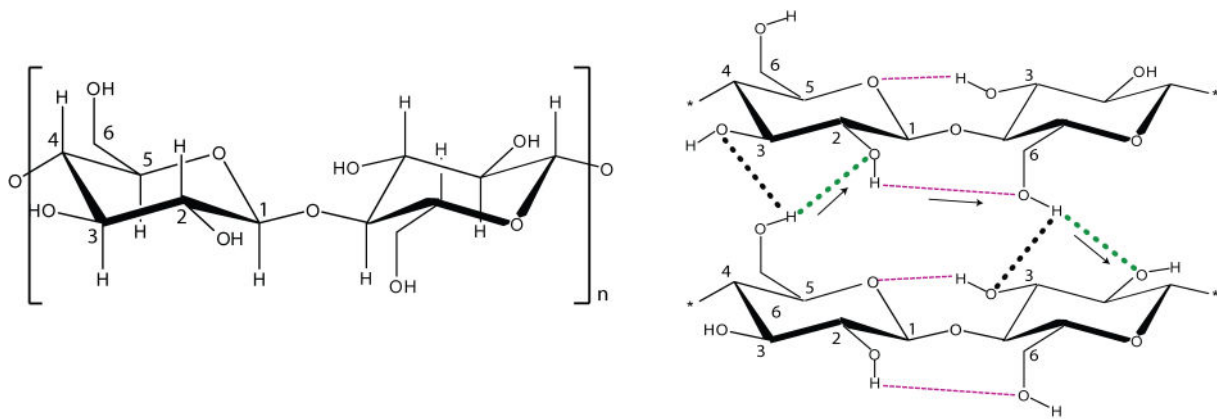


Fig 1.6 - Supra molecular structure of cellulose. Reproduced from (Hon 1994)

The two end-groups of this polymer are not chemically equivalent with a non-reducing end and a reducing end function (aldehyde). The hydroxyl groups on these linear cellulose chains involve strong intra- and inter-molecular hydrogen bonding. The degree of polymerization of these chains ranges from over 10,000 in native wood to few hundred in a bleached Kraft pulp and dissolving pulps.(O'Sullivan 1997)

Cellulose macromolecule is a semi-crystalline polymer with different organization orders throughout the whole structure. There are regions of low order (amorphous regions) and very high crystalline ordered regions. In the ordered regions, cellulose chains are tightly packed together in crystallites, which are stabilized by a strong and very complex intra- and intermolecular hydrogen-bond network.

Four different crystalline allomorphs have been identified. (O'Sullivan 1997, Dinand et al. 2002, Wada et al. 2004). Among them, Cellulose I is the most abundant crystalline polymorphism existing in nature.(Atalla & Vanderhart, 1984)

Cellulose I_α (triclinic) is the predominant form in wood and annual plants, whereas Cellulose I_β (monoclinic) is the predominant form in marine algae and in bacterial cellulose.(Baker, Helbert, Sugiyama & Miles, 1997)

2.3 Different techniques for the isolation of nanocellulose

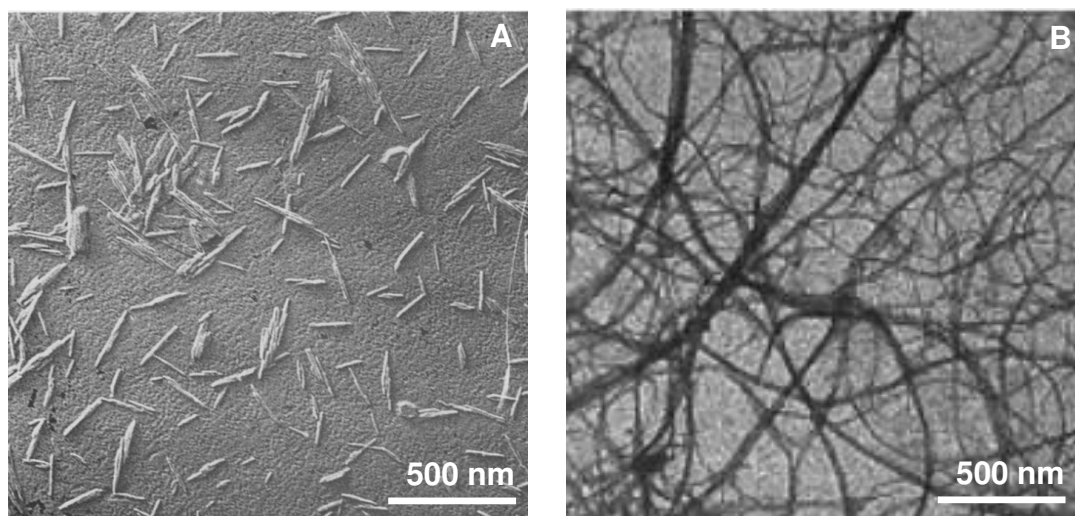


Fig 1.7 – One of the first Nanoscale observation in TEM microscopy of nanocellulose: CNC (A) and (B) CNF. reproduced from (Marchessault et al. 1959) (Dufresne et al. 1998))

First references to the isolation and observation (**Fig 1.7-A**) of Cellulose Nanocrystals (CNCs) were from Ranby (1949). A flow birefringence was firstly observed from the strong hydrolysis with sulfuric acid (H_2SO_4) of mercerized ramie fibers or bacterial cellulose. (Marchessault et al. 1959) Simultaneously, Battista et al. (1956) reported the hydrolysis with hydrochloric acid (HCl) of cellulose fibers which led to the discovery of Microcrystalline Cellulose⁴ (MCC).

One of the first applications of CNC is as a model nanoparticle in the field of liquid crystals system. (Revol et al. 1992) Indeed, a CNC suspension is easier to study than rigid-chain macromolecules such as tobacco mosaic virus. (Bawden et al. 1937)

During the following decades, research groups in Canada (Paprican) and France (Cermav) continued to investigate CNC as liquid crystal system in aqueous, (Gray 1994) and many organic solvents (Heux et al. 2000). In the year 1990s, CNCs were extensively studied for reinforcing composites. (Favier et al. 1995, Helbert et al. 1996, Dufresne et al. 1997)

Since the year 2010, recent investigations not only describe the characterization and production of CNC but also increasingly frequently address its end use in smart applications.

It includes controlling drug release, (Jackson et al. 2011) as an aerogel for insulation, (Heath et al. 2010) as a stimuli-responsive material, (Mendez et al. 2011) pickering emulsions, (Capron et al. 2013) and photonic film (Shopsowitz et al. 2011).

⁴ Nowadays, the annual global market is estimated to more than 100,000 tons and MCC are mainly used in pharmaceuticals and food applications for many uses such as stabilizing, texturing and tableting properties.

In the 1980s, cellulose nanofibrils (CNFs), originally called Microfibrillated Cellulose (MFCs), were discovered by both Herrick and Turbak's research groups. (Turbak et al. 1982, Herrick et al. 1983). A 3 wt % cellulosic fiber suspension was submitted to a high-pressure with a homogenizer (80°C at 8,000 psi). This results in a change of the suspension rheology, which turned into a translucent "gel" (**Fig 1.7-B**). They reported a gel-like behavior of the CNF suspension with thixotropic viscosity properties and excellent stability on storage. (Turbak et al. 1983)

The first applications of CNF suspension were as rheology modifier, (Turbak et al. 1983) and during the last decade in nanocomposites, (Siqueira et al. 2010) flexible films, (Fukuzumi et al. 2008), and aerogels (Kettunen et al. 2011). Since 2012, emerging applications have been found in the field of medical applications, as antimicrobial agents, (Martins et al. 2012) and anti-inflammatory biomaterials (Herranen et al. 2012).

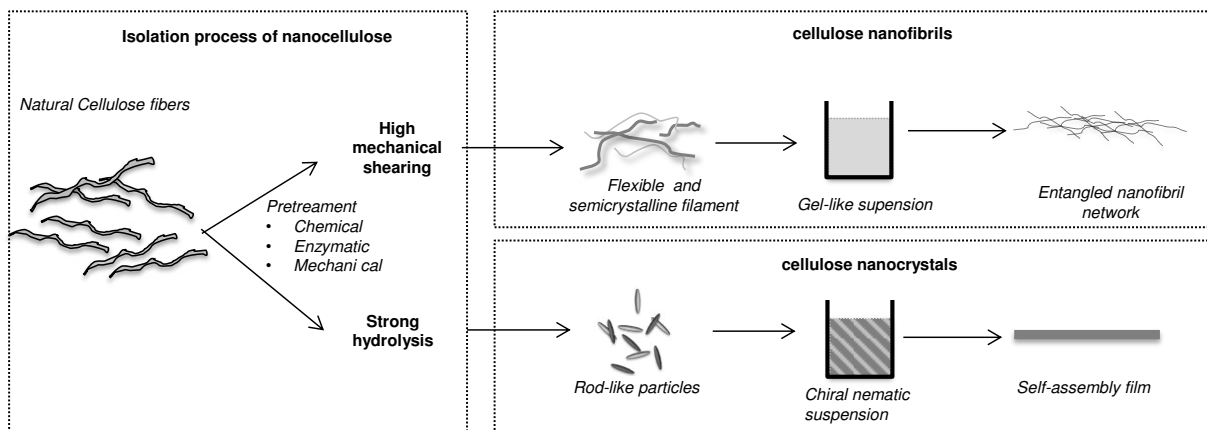


Fig 1.8 - Different routes for the isolation of nanocellulose

As highlighted in **Fig 1.8**, it is important to keep in mind that even if the starting materials of nanocellulose is the same, CNC and CNF must be considered as two different nanomaterial families because of their different crystallinity, flexibility, and aspect ratio.

2.3.1 Isolation of CNC

Techniques to isolate CNCs consist in subjecting the cellulosic material to an acid hydrolysis or oxidation under controlled temperature, agitation, and time, followed by sonication to separate crystals.

The isolation of CNCs originates from the presence of amorphous regions within cellulose microfibrils. Amorphous regions are more accessible to a chemical reaction and so more sensitive to acid attack. CNCs are considered as the smallest building blocks that can be extracted from cellulose microfibrils with a leveling-off hydrolysis.

The optimum chemical conditions reported in the literature are reported in **Table 1.5**.

Table 1.5 - Optimum chemical conditions for isolation of CNC

	Reagent	Reagent to pulp ratio	Cellulose fiber consistency	Time	Temp.	Yield (%)	Ref
Hydrolysis	H ₂ SO ₄	0.06 mol/g	100 g/l	50 min	45-60 °C	38	(Beck et al. 2005)
	HCl	2 mmol/g	29 g/l	360 min	110 °C	85	(Yu et al. 2013)
Oxidation	TEMPO	NaClO :7mmol/g (NaBr: 1.6 mmol/g) (TEMPO :1 mmol/g)	7 g/l	200 min	20 °C	25	(Qin et al. 2011)
	APS	0.1 mol	10 g/l	16 h	60 °	36	(Leung et al. 2011)

2.3.1.1 Acid hydrolysis

The hydronium ions (H₃O⁺) penetrate the cellulose chains in the amorphous domains promoting the hydrolytic cleavage of the glycosidic bonds and finally releasing individual crystallites (**Fig 1.9**).

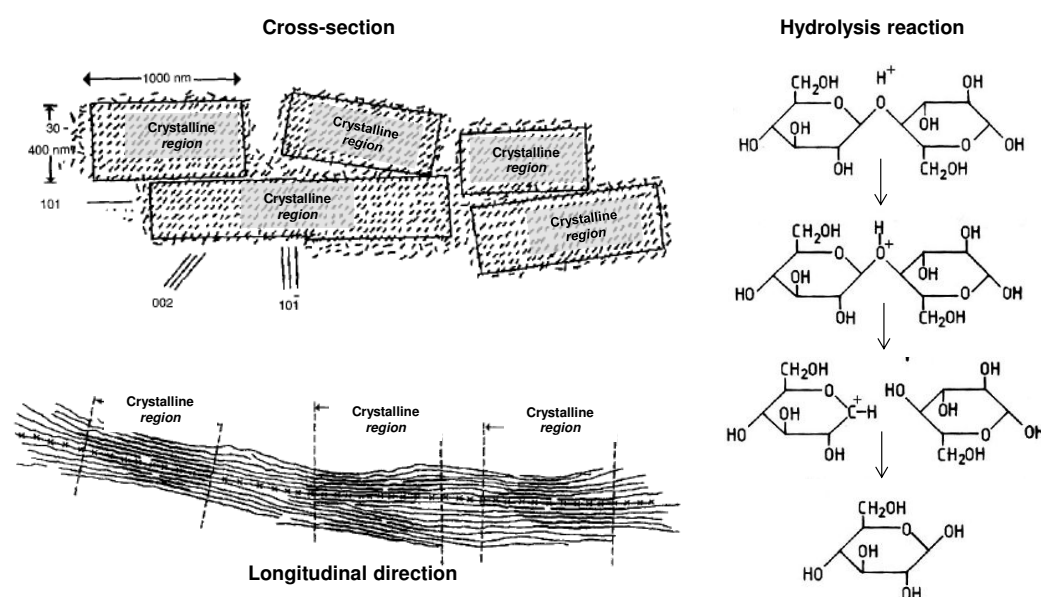


Fig 1.9 - Cross-section(A), transverse (B) representation of a cellulose microfibrils, and predominant hydrolysis mechanism on cellulose adapted from (Hon 1994)

Under controlled acidic conditions, amorphous regions are dissolved in oligomers and glucose sugars whereas crystalline particles are individualized. The hydrolysis must be mild enough to avoid complete hydrolysis of cellulose but enough strong to attack amorphous areas. Precise dimensions of the crystallites depend on several factors, including the source of

cellulose and hydrolysis conditions. However, the source of cellulose is the key parameter. For instance, CNC extracted from marine sources are generally longer (500-1500nm) than those extracted from cotton or wood (100-300nm).(Khandelwal et al. 2013)

Bondeson et al. (2006) proposed an optimization of such hydrolysis parameters by implementing a design of experiments. The goal of the study was to maximize the yield and to obtain an aqueous stable colloid suspension in order to produce large quantity of CNC.

Several mineral and organic acids are used as hydrolyzing agents. Among them, hydrochloric (HCl) and sulfuric acids (H₂SO₄) are mostly used. To a lesser extent, phosphoric,(Camarero Espinosa et al. 2013) hydrobromic,(Sadeghifar et al. 2011) nitric, (Rehman et al. 2014), and maleic acids (Filson et al. 2009) are also used for isolation of CNCs.

The main reason explaining the predominant used of H₂SO₄ for the isolation of CNCs is justified because it gives more stable nanoparticles suspension due to the grafting of negatively surface charged groups. With sulfuric acid, surface charged esters promote dispersion in water and avoid their aggregation.(Araki et al. 1998) Indeed with the use of HCl, CNCs tend to agglomerate due to the hydrogen bonding between crystallites forming micron sized agglomerates which are difficult to disperse.

2.3.1.2 Oxidative methods

Instead of acid hydrolysis treatments, other chemical routes have been proposed in the literature. For instance, oxidative methods can be used to prepare CNC. In this context, TEMPO-mediated reaction is used as a regioselective oxidation of hydroxymethyl groups of polysaccharides (C₆ position).(Montanari et al. 2005)

This leads to the isolation of long uniform nanoparticles with carboxyl groups on the primary carbon of the glucose rings. This treatment is also used as a pretreatment for CNF; in the last case, oxidation parameters are milder to avoid the degradation of amorphous cellulose.

Another method to isolate CNCs is the use of ammonium persulfate (APS) which is investigated by .Leung et al. (2011). When APS is used, it oxidizes the accessible hydroxyl groups and dissolves the amorphous regions of cellulose.(Castro-Guerrero et al. 2014) Morphology of CNCs is close to the one prepared by acid hydrolysis. The main difference is the negative surface charged groups, which are carboxylate groups (COO⁻) instead of sulfate ester groups (SO₃⁻). The main benefit of using the one-step APS oxidation is to avoid the issues of using and recycling concentrated sulfuric acid.(Luong et al. 2011)

Lastly, the isolation with ionic liquids (Man, Muhammad et al. 2011) or enzymatic treatments (Siqueira, Tapin-Lingua et al. 2010) are also proposed in some studies. Nevertheless, in more than 95% of recent scientific papers about CNCs, acid hydrolysis is preferred.

2.3.1.3 Extraction and purification treatment

To end the isolation of CNCs, the treated mixture is extensively diluted to inhibit the reaction. Then, the suspension is submitted to several separations (centrifugation and filtration) and washing steps such as a prolonged dialysis against deionized water follows to remove the remaining reagents and salt residues.

A final centrifuge separation or (micro)filtration steps are often used to remove larger agglomerates (Bai et al. 2009). Lastly, ultrasonic treatment is essential to facilitate dispersion of the crystalline cellulose in the suspension. (Beck et al. 2005)

2.3.2 Isolation of CNF

In comparison with CNCs, CNFs is thicker, relatively porous, and flexible. It consists of several aggregates of cellulose microfibrils. (Svagan et al. 2007) CNFs have a diameter in the range 20–60 nm and are several micrometers long (**Fig 1.10-A**).

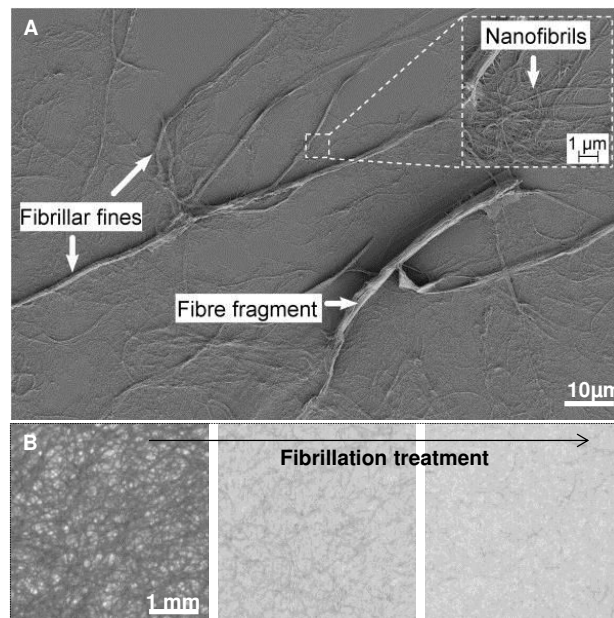


Fig 1.10 - SEM micrograph of CNFs isolated with homogenization treatment(A) showing the different sub-elements remaining after the main mechanical process. Optical micrographs (B) of CNF film with increasing level of homogenization. Adapted from (Chinga-Carrasco 2011)

In the same way than CNCs; CNFs are extracted from any vegetal biomass that contain cellulosic material such as wood fibers,(Syverud et al. 2011) annual plants,(Siqueira et al. 2010) industrial crops,(Siró et al. 2010) or marine algae (Hua et al. 2014).

However, in case of CNFs, the influence of the starting material is much less important than for CNCs. Indeed the main morphological features of CNF depend on the pretreatment and fibrillation processes that are described above.

Chemical wood pulp remains the most suitable source to produce CNF from industrial point of view. Among different grades of pulp, bleached Kraft pulp is often used (Iwamoto et al. 2008), followed by bleached sulfite pulp (Saito et al. 2006). Generally, dried-pulp required more extensive treatment because of the loss of swelling ability and a more compact structure during drying.(Eriksen et al. 2008) In addition, high hemicellulose content in the pulp seems to facilitate the fibrillation process. (Siró et al. 2010).

It is worth to mention that CNFs must be considered as a heterogeneous nanomaterial, as shown in (**Fig 1.10**). Indeed, they consist of a variety of fibers, fiber fragments, fines, and fibrils (**Fig 1.10-A**) and they mainly depend on the level of fibrillation applied to the starting cellulosic materials (**Fig 1.10-B**). Because of this heterogeneity⁵, several grades of CNF are commercially available or produced in different lab facilities.

So, the term CNF still includes a large range of materials with different dimensions and heterogeneity.(Chinga-Carrasco 2011) The characterization of this material is a key challenge, because it makes the comparison easier with other elements reported in several scientific papers and could rationalize the obtained results.

2.3.2.1 Mechanical treatments

As summarized in **Table 1.6**, CNFs can be isolated with different mechanical processes, such as homogenization, microfluidization, fine grinding, ultra-refining, or cryocrushing.

Initially, these technologies were especially dedicated for food applications and they are currently under optimization for the production of CNFs by these suppliers. For instance, microfluidization is a process commonly used in cosmetics, and pharmaceutical industries whereas homogenization is suitable for food industry (milk homogenization) and paint processing (dye and pigment dispersions).

⁵ In our study, we tried to work with a very homogenous CNF suspension with the lowest amount of macroscopic fibers fragments and fines. The same CNF suspension has been used for lab experiments as well as for industrial trials presented in the final chapter.

Table 1.6 - Overview of the technologies used for the CNF production

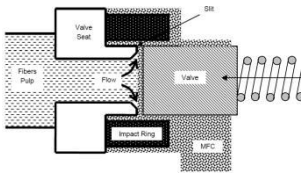
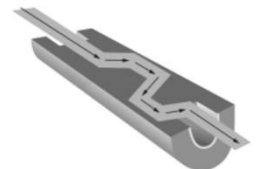
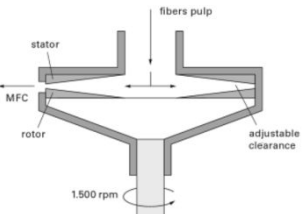
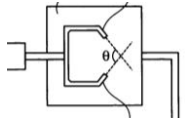
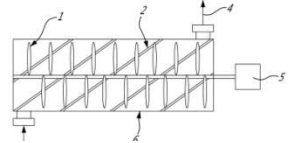
	Scheme	Principle	Standard conditions	Indus. available	Energy MWh/ton	Supplier	Ref
Homogenization		Fiber suspension is subjected to a high pressure homogenizing action into a vessel through a very small nozzle. High velocity and pressure, as well as impact and shear forces on fluid generate shear rates in the stream and decrease the size of fibers to nanoscale particles	10-15 cycles 50 -150 MPa	Yes	9 -70	GEA Process Engineering Inc. Italy	(Siro et al. 2011) (Pääkkö et al. 2007)
Microfluidization		It includes intensifier pump to increase the pressure and interaction chamber to defibrillate the fibers using shear and impact forces against colliding streams and the channel walls	10-30 cycles 2000-3000 bars	Yes	3	Microfluidics Ind., USA	(Taipale et al. 2010) (Iwamoto et al. 2008)
Ultra-fine friction grinding		The pulp slurry passes between a static and a rotating grind stone. The mechanism of fibrillation in grinder is to break down the hydrogen bond and the cell wall structure by shear forces and individualization of pulp to nanoscale fibers	5-60 cycles 1500-3000 rpm	Yes	1.3-3.1	Masuko Sangyo Co. Japan	(Jonoobi et al. 2012)
Aqueous counter collision		Two water jets collide with each other at a high rate, inducing a wet and rapid pulverization of the samples into nanoscale objects dispersed in water.	40-60 cycles 200 MPa	No	-	-	(Kose et al. 2011) (Kondo et al. 2008)
Cryocrushing		Water swollen cellulosic fibers are immersed in liquid nitrogen and subsequently crush by mortar and pestle. Ice crystals exert pressure on the cell wall and lead to the liberation of CNF	Wiley Mill Filtration on a mesh size of 60	no	-	-	(Alemdar et al. 2008) (Chakraborty et al. 2005)

Table 1.6 compares these different technologies. Such processes produce high shear mechanical treatments (pressure/cavitation/shear/impact).

It causes a cleavage along the longitudinal axis of the cell walls, resulting in the liberation of flexible and long cellulose fibrils. Typically, suspension runs through the apparatus several times at a diluted pulp consistency (5-30 g/l). This leads to the extraction of CNFs with diameters between 5 and 30 nm and several microns in length.

A filtration step can be included to remove the larger non-fibrillated and partially fibrillated fractions. (Madani et al. 2011) Until 2007, the main limitations of the development of CNF are mainly associated with the high energy consumption during the fibrillation process. Indeed all mentioned mechanical treatments require high energy consumption.

For instance, the electrical consumption with a homogenizer reaches more than 70,000 kWh for one ton of CNF (as dry). (Eriksen et al. 2008, Spence et al. 2011)

As a comparison, the energy required for refining fibers used for producing specialty papers is about 3,000 kWh/t. (Holik 2006) This explains the number of research and innovation conducted to reduce the high energy consumption for the manufacturing of CNFs.

2.3.2.1 Pretreatments of CNFs

The strong mutual packing of microfibrils within cellulosic fibers makes them difficult to disintegrate because of their natural aggregation. Contrary to the pretreatment for the isolation of CNCs (aiming to obtain the highest purity of cellulose), pretreatments of CNFs are carried out in order to facilitate their mechanical fibrillation. It mainly consists in inhibiting inter-fibrillar bonds without affecting the bulk structure of cellulose. For these reasons, the use of highly water-swollen fibers, previously disintegrated or homogenized, is preferred. With a process point a view, pretreatments are also necessary. Indeed, during the main fibrillation treatment, the feeding and recirculation equipment's (pumps, pipes, and valves) are often clogged with a heterogeneous suspension.

CNF pretreatments are divided into chemical, enzymatic, and refining operations. The three pre-treatments are generally used and can be combined.

Mechanical pretreatment. In order to reduce the average fiber dimensions, suspensions are submitted to a preliminarily mechanical treatment. The mechanical pretreatment are often performed using disk refining, (Nakagaito et al. 2005) PFI milling, (Henriksson et al. 2007) or valley beating (Spence et al. 2011). This enhances the fiber homogenization by increasing the fiber area exposed to mechanical fibrillation. (Nakagaito et al. 2005, Zimmermann et al. 2010)

Enzymatic pretreatment. This pretreatment is widely inspired from the existing enzymatic refining in the paper industry (Noe et al. 1986, Wong et al. 2000).

Since pioneering investigations developed by Henriksson et al. (2007) and Pääkkö et al. (2007), cellulase is now mostly used as pretreatment of CNF. For instance, Pääkkö et al. (2007) achieved an enzymatic hydrolysis treatment combined with mechanical shearing and high pressure homogenization.

Generally, enzymes employed are monocomponent of endoglucanase. They hydrolyze accessible intra-molecular glycoside bonds within cellulose chains, generating oligosaccharides of various lengths and consequently new chain ends (**Fig 1.11**).

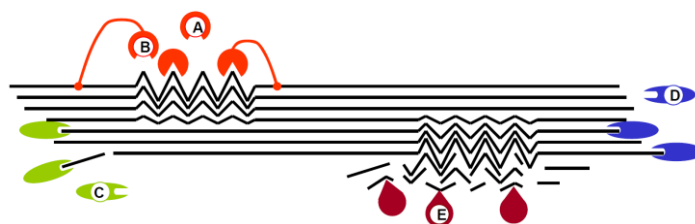


Fig 1.11 - Types of cellulase: (A) endoglucanases without cellulose-binding domain; (B) endoglucanases with cellulose-binding domain; (C) and (D) cellobiohydrolases, and (E) glucosidases. Reproduced from (Köpcke 2008).

Henriksson et al. (2007) tested the pretreatment of sulphite pulp with a solution of endoglucanase Novozym® 476 (Novozym, Denmark) with different enzyme dosage (0.02% to 3% per gram of CNF) before high-pressure homogenization (Henriksson et al. 2007). They found the enzyme-treatment facilitates disintegration, and CNFs have higher average molar mass and larger aspect ratio than CNFs resulting from acidic pretreatment.

Oppositely, exoglucanases (**Fig 1.11**) preferably act on the chain termini to release soluble cellobiose or glucose as major products. They can also be used for the pretreatment of CNF suspensions. (Pääkkö et al. 2007)

To summarize, the enzymatic treatment improved the suspension homogeneity. Depending on the concentration, type of enzyme and reaction time, CNF suspensions features have completely different properties. (Siqueira et al. 2010)

Lastly, with an environmental point of view and compared to most of chemical pretreatments, this presents an obvious advantage regarding its low energy demand and the absence of chemicals needs.

Chemical pretreatment. There are two main chemical pretreatments reported in the literature in order to both facilitate their isolation and to obtain anionic (carboxylated) or cationic CNFs (acetylated or quaternized).

TEMPO-mediated oxidation (**Fig 1.12**) is the most used chemical pretreatment for CNF. (Fukuzumi et al. 2008). In aqueous medium and basic condition (pH around 10), 2,2,6,6-tetramethylpiperidin-1-yl)oxidanyl (TEMPO) molecules catalyzed the conversion of carbohydrate primary alcohols to carboxylate groups in the presence of oxidizing agent such as sodium hypochlorite (NaClO) and sodium bromide (NaBr). (Saito et al. 2007)

Unfortunately, such a treatment causes the cellulose depolymerization and the formation of aldehyde groups (<0.08 mmol/g). Several protocols are now proposed to limit decrease of DP and formation of aldehyde group as recently reviewed by Isogai et al. (2011). Generally, the carboxylate content is about 0.9 to 1.7 mmol/g and the solid recovery ratio is more than 80 wt %.

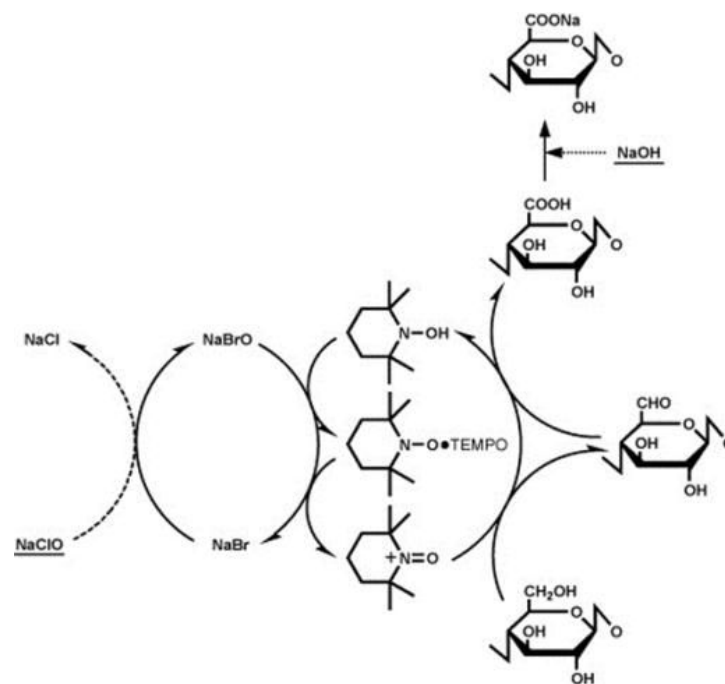


Fig 1.12 - Scheme of the TEMPO-mediated oxidation mechanism on cellulose. Reproduced from (Isogai et al. 2011)

To expand the use of CNFs to non-polar environments, several attempts have been made to decrease the CNFs hydrophilicity, promote fibrillation, improve their dispersion after drying, and increase cationic surface charges. Most common pretreatments are :

- Surface Acetylation with the acetic anhydride reacts with the OH groups on the cellulose. The acetylation of cellulose depends on the accessibility and susceptibility of the OH-groups in the amorphous and crystalline regions within the cellulose polymer chain.(Sassi et al. 1995)
- Surface cationization with quaternization reaction is based on the nucleophilic addition of the alkali-activated hydroxyl groups of cellulose to the epoxy moiety of EPTMAC (2,3-epoxypropyl trimethylammonium chloride).(Wagberg et al. 2008).

2.4 Industrialization⁶ of nanocellulose and its potential use

At the beginning of the 2000s, the beginning of industrialization of nanocellulose was restricted to a couple of companies and research centers, mainly from Scandinavian countries, France and Japan for CNF and North American ones for CNC.

Up to now, the industrialization of nanocellulose remains limited for several issues as summarized in **Table 1.7**.

Table 1.7 - Recap of the main factors limiting industrialization of nanocellulose

Issue	Challenge
Marketing	No clear high added-value application Benefits of using nanocellulose still to be proved in comparison to other existing materials
Manufacturing	No validated technologies for upscaling the production High energy consumption, low recovery of water and chemicals Concentration, drying and dispersion of nanocellulose are still challenging
Standardization and characterization	lack of characterization tools no official standardization
Nanotoxicology	insufficient studies about the evaluation of nontoxicity

However, from the years 2005s several positive factors have promoted the exponential development of a up-and-coming economy based on the production of nanocellulose, as shown by the increasing of patent number presented in **Fig 1.13-A**.

In 2007, many laboratories and research institutes started to produce nanocellulose at pilot-scale (few kilograms/day) for providing sufficient amount of nanocellulose (with reproducible features) in order to investigate new applications areas. Up to now, the main application concerns their process manufacturing and papermaking industry. In a small extent, high added-value applications such as medical, inorganic chemistry, coating, or filtration are also often patented as shown in **Fig 1.13-B**.

⁶ This PhD project is related to industrial expectations of nanocellulose, that is why it was necessary to identify the main major actors

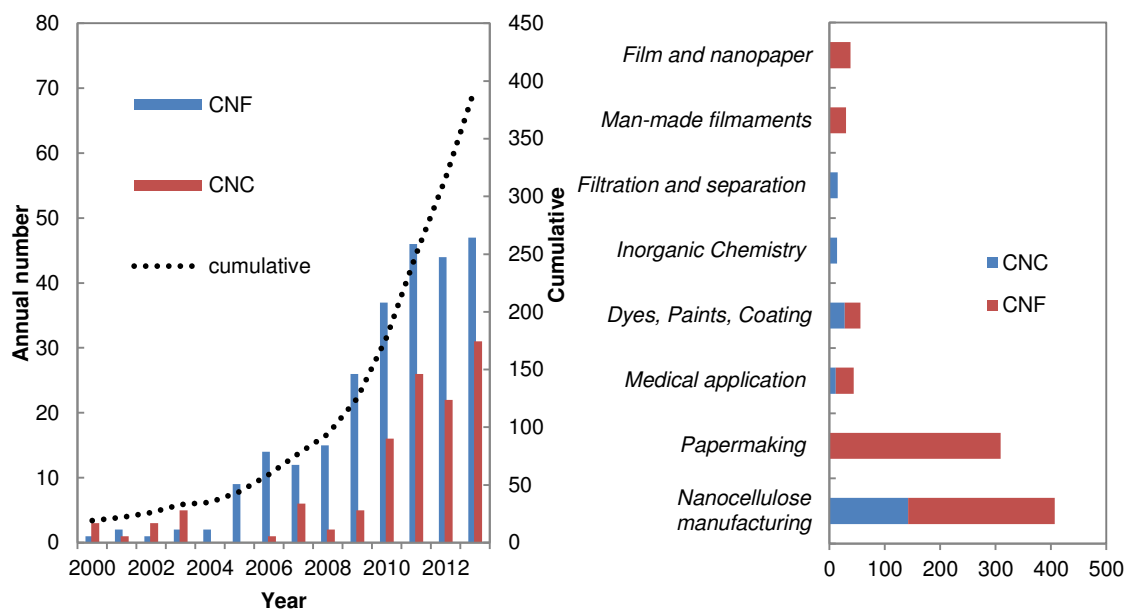


Fig 1.13 - Annual and cumulative number of patent application on nanocellulose (A) and Overview of the main codes used for International Patent Classification (B). Data collected from Espacenet, May 2014

In addition, the scientific community is now organized in view of improving international collaboration, dissemination of scientific results and to put in place the first standardization about nomenclatures, definitions, and characterization techniques.

Indeed, since 2006, a one-week international conference organized by TAPPI association is dedicated to nanocellulose. In addition, since 2010, several national and international projects in partnership with industrials are focused on the scale-up and industrialization of nanocellulose.

Table 1.8 gathers a recap about all manufacturing companies which have the project to produce or which are currently manufacturing nanocellulose⁷. According to a recent estimation from Cowie et al. (2014), the annual demand for nanocellulose will reach about 1.1 to 3.3 million tons for next 5 years. Another estimation provides by Miller (2014) estimates the market to 1.2 million in 2015 in which paper industry market will represent about 1.0 million tons.

As a conclusion, for the pulp and paper industry, the industrialization of nanocellulose may represent a promising reconversion of their industrial facilities and an opportunity for their production diversification, including high-added values products manufacturing.

⁷ It is worth nothing that at the starting of this R&D project (October 2011) less than 10 companies on 29 identified companies produced nanocellulose

Table 1.8 - List of manufacturing companies of nanocellulose

Company information			Production capacity			
Company name	Country	Status	Date	Daily Capacity	Technology	
CNF plant						
EMPA	Switz.		2011	15 kg	Dry powder	
VTT	Fin		2010	15 kg	Susp.(2.0%)	
PFI	Norway	Research center	2013	100 kg	Susp.(2.0%)	
Forest Bioproducts Research Institute	USA		2011	1 ton	Susp. (6.5%)	
FCBA	France		2011	100 kg day	Homogenizer	
Innventia	Sweden					
-BASF/Zelpho	Germany		2013	NA	NA	NA
Nanofilament	Canada	Joint-Venture	2014	NA		High consistency refining
Perf.BioFilaments	Canada		2014	NA	Dry powder Susp (30-50%)	
Daicel	Japan		2000	NA	Susp	TEMPO
JRS	Germany		2011	NA	Susp (10-20%)	Ultra refining
UPM	Sweden		2011	Satellite plant		Fine Grinder
Oji paper	Japan		2008	100		
Norske Skog	Sweden	Private company	2009	Integrated		
Verso Paper	USA		2010	NA		
Nippon paper	Japan		2013	150 kg		
Stora Enso	Swed		2011	100		
Omya	Switz		2012	Satellite plant		Fibrillation with fillers
Imerys	France		2012	Satellite plant		
Borregard	Norway		2010	100		
Cellucomp	UK		2014	-		
Bettulium	Finland	Start-up	2014	-		
Inofib	France		2014	-	Dry	Homogenizer
CNC Plant						
Forest Bioproducts Research Institute's	USA	Research center	2011	10kg	Dry /Susp	Sulfated
FPIInnov.	Canada		2009	5kg	Dry/ Susp	Sulfated
Alberta Innovates	Canada		2011	20kg	Susp.	Sulfated
BioVision	Canada	Start-up	2012	10kg	Susp.	Carboxylated
Melodea	Israel	Start-up	2012	Lab	Susp.	Sulfated
Celluforce Domtar- FPIInnov.	Canada	Joint-Venture	2012	1tons	Dry	Sulfated

2.5 Safety issues and nanotoxicology of nanocellulose

The potential of nanocellulose has been highlighted and is clearly proved. However, for further industrial applications, several concerns about their safety and nanotoxicology must be considered.

According to the World Health Organization (WHO 2012), cellulose fibers, bacterial cellulose (BC) and microcrystalline cellulose (MCC) are considered as a non-toxic substances when used in “normal” quantities. Since the 1980s, MCC is used in the pharmaceutical industry as excipient, (Jivraj et al. 2000) or in food industry as stabilizer,(Okiyama, Motoki et al. 1993) and texture modifier (Okiyama et al. 1993, Gohel et al. 2005).

However in case of cellulose nanoparticles, uncertainties remain because their characteristics are totally different from cellulosic fibers and MCC in term of particle size, shape, surface area, charge, chemical properties, solubility, and degree of agglomeration.

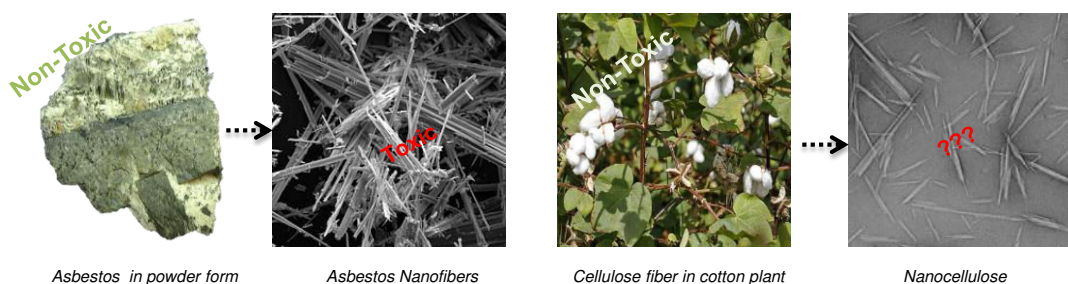


Fig 1.14 - Comparison with need-like shape nanomaterials extracted from mineral or biomass pictures reproduced from (Buzea et al. 2007), (Dufresne 2012)

Moreover, the needle shape morphology of nanocellulose is quite similar to Asbestos nanofibers (Fig 1.14). Since health hazards caused by asbestos used in large quantities in the 1970s,(Buzea et al. 2007) some researchers question whether nanocellulose may also represent a risk because of their morphology which may results in a biopersistent nanomaterial.

Up to now, there are no explicit international guidelines for risk assessment of nanocellulose, their risk evaluation is still under consideration. However, several recent studies tend to confirm the non-toxicity as expected for a biobased material. Indeed, for a long time human beings are in contact with a large quantity of nanoparticles of cellulose present in foods and some consumer’s goods (papers or textiles).

This non-hazardous position is confirmed with CNF because of their tendency to form agglomerates in suspension as well in dry state. Since 2010 with the pioneer work of Kovacs et al. (2010), several investigations are focuses on the safety issues and nanotoxicology of

nanocellulose, as presented in **Table 1.9**. More detailed information about the methodology and extended analyses can be found in this recent book chapter (Pitkänen et al.).

Table 1.9 - Overview of studies that investigate the nanotoxicology risk of nanocellulose

	Purpose and motivations of the study	Type of nanocellulose	Toxicity	Ref
Overview	In vitro and in vivo toxicological assays of nanocellulose		●○○	(Norppa 2012)
	Influence of nanocellulose extracted from various source on different organism, exposure medium and concentration	CNF †	●●○	(de Lima et al. 2012)
Medical	influence of nanostructure on the cytocompatibility of film based on nanocellulose	CNF §,◇	○○○	(Hua et al. 2014)
	Replacement of bacterial cellulose with CNF for regenerative substrate for medicine and wound healing	CNF †,§	○○○	(Alexandrescu et al. 2013)
Production of nanocellulose	Risk assessment during nanocellulose production		○○●	(Rouhiainen et al. 2012)
	Evaluation of exposure risks during friction and spray drying	CNF †,§	○○●	(Vartiainen et al. 2011)
Overview	Ecotoxicological characterization	CNC †	○○●	(Kovacs et al. 2010)
Medical	Scaffolds tissues	CNC ◇	○○○	(Mahmoud et al. 2010)
	Fluorescent Bio imaging		○○○	(Jia et al. 2013)
	Drug delivery and injectable hydrogels	CNC †,◇	○○○	(Dong et al. 2012)
	Hemodialysis		○○●	(Ferraz et al. 2012)
	Biomedical application	CNC †	○○●	(Ni et al. 2012)
Comparison with other nanomaterials	Comparison with carbon nanotubes		○○●	(Clift et al. 2011), (Kümmerer et al. 2011)

Toxicity : ○○○ not proved, ○○● moderated, ●●● confirmed.

Type of nanocellulose : † neat, §modified, ◇fluolabeled

Most of the studies indicate that CNF or CNC can be considered as a non-toxic material. The main reason cited by authors is due to their natural origin and the harmless nature of their bulk forms. Based on the first investigation, CNC was added on the Canada's Domestic Substance List in 2012. However, data sets that are more complete are necessary for the European acceptance with the development of adapted and standardized methods. Therefore, the results are very promising and encourage the investigation concerning the use of nanocellulose for improving properties or adding new functions within specialty papers.

2.6 Main features of nanocellulose

As shown in previous sections, nanomaterials isolated from cellulose are sustainable, biodegradable, and practically non-toxic.

Table 1.10 - Comparison of the main features of CNC and CNF

	CNC	CNF	Ref.	
	Shape	Rod-like	Flexible filament	
Morphology	Building block	Crystallite	Aggregated fibrils	
	Length	200 nm	>1 μ m	
	Thickness	5 nm	25 nm	
	Aspect ratio	25	100	
	Surface area	600 m ² /g	220 m ² /g	(Heath et al. 2010) (Sehaqui et al. 2011)
	Crystallinity index	85	63	(Park et al. 2010)
Chemistry	Degree of polymerization	140-200	230-825	(Battista et al. 1956) (Zimmermann et al. 2010)
	Surface charge	SO ₃ H: 200 μ mol/g	COOH<50 μ mol/g	(Beck et al. 2005)
	Accessibility of OH groups	11 %	25 %	(Siqueira et al. 2008)
	Potential zeta	-31 mV	-10 mV	(Kovacs et al. 2010) (Stenstad et al. 2008)
Thermal-mechanical	Thermal expansion	8.5 ppm/K		(Bergenstr�hle et al. 2007)
	Degradation temperature	220 $^{\circ}$ C	300 $^{\circ}$ C	(Roman et al. 2004) (Sir� et al. 2010)
	Individual Young's		145 GPa	(Iwamoto et al. 2009)

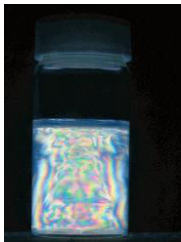
As summarized in **Table 1.10**, they also exhibit interesting properties and in particular, a high strength and stiffness, a low thermal expansion and relatively high degradation temperature and high amount of hydroxyl groups making possible their chemical surface modification. It is worth noting that there are significant differences between the two nanomaterials.

Regarding their morphologies: CNCs are rigid, crystalline whereas CNFs have flexible and relatively porous structure. It causes several differences regarding their aspect ratio, and surface area or even their chemical reactivity. In addition, because of a high density of negatively charged groups, colloidal stability in water suspension is generally better for CNC.

2.6.1 Nanocellulose assembly as suspension

Such properties give different rheological behavior of the ensuing suspensions as well as different properties for dried film based on nanocellulose. The rheological behavior is an important characteristic for several applications. Several studies focus on their rheological properties in order to understand their origin. Furthermore, CNF and CNC suspension display different rheological behavior as summarized below (**Table 1.11**):

Table 1.11 - Comparison of the properties of CNF and CNC suspensions in water

	CNF	CNC
Visual aspect		
		*Observation between cross-polarizers
Behavior	Pseudo-plasticity and shear thinning behavior Viscosity increases with the fibrillation rate and depends on the manufacturing process (Pääkkö et al. 2007) (Iotti et al. 2011) Presence of shear rate-viscosity hysteresis loop	Lyotropic liquid crystals with a four-region rheological behavior: <ul style="list-style-type: none"> • isotropic • iso and anisotropic • anisotropic • gel
Main Origin	-Gel structure consisting of sintered flock -Network formation by temporary hydrogen bonds or VdW interactions (Puisto et al. 2012)	-Rigid rod-like shape (Onsager 1949) -Negative surface charges and colloidal repulsion (Stroobants et al. 1986)

Indeed, after homogenization CNF suspensions have a gel-like behavior even for very low concentration (*i.e.* 2%). Whatever the source and fibrillation used to process the suspension, CNF suspensions display a pseudo plasticity and shear thinning behavior at very low consistency (30g/l). (Pääkkö et al. 2007)

Oppositely, negatively charged CNCs in aqueous suspension (Bercea et al. 2000) or in some organic solvents (Elazzouzi-Hafraoui et al. 2009) display liquid-crystalline behavior due to their self-assembly properties (Gray 1994).

In addition, the viscosity value of the nanocellulose suspension is also commonly used as an indirect-tool to characterize the fibrillation degree of CNF as well as a good indication of dispersion and level of isolation of CNC.

2.6.2 Nanocellulose assembly as films

Nanocellulose suspensions can be converted into solid films⁸ by different processes consisting of removing water mainly by simple evaporation (casting) or by vacuum filtration (paper-like manufacturing). Because of the different intrinsic features of CNF/CNC, the properties and uses of such solid films are completely different as detailed in following sub-sections.

2.6.2.1 Nanopaper based on CNF

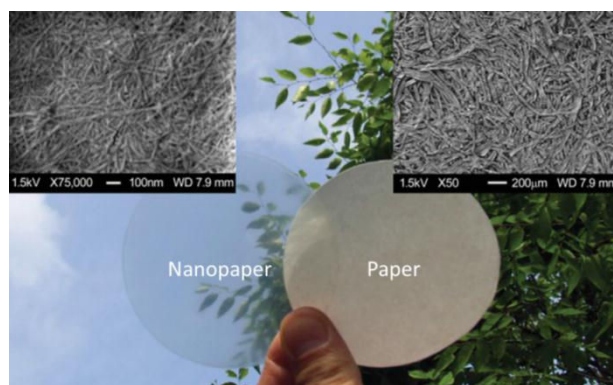


Fig 1.15 - Comparison between a nanopaper and conventional cellulose paper (right) reproduced from (Nogi et al. 2009)

As with a paper sheet prepared from wood pulp fibers, when CNF suspensions are dried, strong inter-fibrillar interactions are formed (**Fig 1.15**). Because of similarity with a handsheet, films based on CNFs are often called “nanopaper” as firstly proposed by Henriksson et al. (2008). However, instead of paper sheets, nanopapers are not easy redispersable in water because of the irreversible aggregation of CNFs during drying.

The first data on the properties of CNF films were presented by Taniguchi et al. (1998). They manufactured a transparent film from CNF suspension and reported the film is 2.5 times stronger than a conventional paper sheet. Generally, CNF films are translucent (or even transparent) and display excellent barrier, flexible and strong mechanical properties as summarized in **Table 1.12**.

Because of hydrogen bonds and their flexibility, once dried, CNFs form a cohesive and dense entangled network that looks like a smooth, strong, flexible, and transparent film

⁸ Instead of manufacturing a transparent, flexible, and dense material, a sponge-like aerogel can be obtained using vacuum drying, freeze-drying, or CO₂ supercritical drying. Such aerogel based on nanocellulose are promising for a number of industrial applications such as functional packaging, catalysis, water and gas filtration. However, such materials were not studied during this project and no more detailed about aerogel would be provided.

(Spence et al. 2010). Films also display excellent air, oxygen, and grease barrier properties in dry conditions. (Syverud et al. 2009, Aulin et al. 2010).

It was not surprising that the film properties are different as a function of type of CNFs (neat, enzymatic, TEMPO-mediated oxidized) as well as the isolation techniques (fine grinding, homogenization, and microfluidization).

Table 1.12 - Recap of the main features of a nanopaper based on CNF.

Properties		Comments
Contexture	Basis weight	17-35 g/m ²
	Thickness	21-33 μm
	Density	0.81-1.2
	Porosity	19-40 %
Optical	Transparent	The transparency is attributed to: <ul style="list-style-type: none"> - absence of agglomerates - high density Large fiber fragments and aggregates of micron size, which can compromise film transparency
	Tensile strength	104-154 MPa
Mechanical	Young's Modulus	15.7-17.5 GPa
	elongation	5.3-8.6 %
		The good mechanical properties are attributed to: <ul style="list-style-type: none"> - high specific area - flexibility - high amount of hydroxyl groups - ability of CNF to form entangled networks
Barrier	Air permeability	9-13 nm/Pa.s
	Oxygen Permeability	17-18.5 ml/m ² .day
	Water vapor Permeability	5-10 x10 ⁻¹¹ (g/m.s.Pa)
		The low gas permeability is attributed to: <ul style="list-style-type: none"> - high crystallinity - dense network and low porosity

Data collected from various sources: (Svagan et al. 2007, Syverud et al. 2009, Aulin et al. 2010)

In addition, the barrier properties of modified CNFs are different from neat CNFs. For most of the chemical treatment, an improvement of barrier properties is often reported. It includes carboxymethylated,(Siro et al. 2011) carboxylated,(Rodionova et al. 2012) and acetylated CNFs (Rodionova et al. 2011).

All these properties are discussed in recent critical review by Lavoine et al. (2012). In addition the combination of CNFs and platelet-like nanoclay improve barrier properties (Liu et al. 2012). It increases the tortuous diffusion pathway and significantly reduces gas permeability even at high humidity.(Wu et al. 2012).

It also provides additional functions to the film such as fire retardancy.(Liu et al. 2013) Those properties have been also widely used to reinforce barrier and mechanical properties of nanocomposites with varying polymer matrixes.(Siró et al. 2010) Lastly, paper properties are also improved (in particular barrier and mechanical properties), as it will further be discussed in a final part of the chapter.

2.6.2.2 Structural films based on CNC

Contrary to CNFs, flexible and low-charged, CNCs, rigid and negatively charged, display self-assembly properties in suspension. Self-assembly property can be preserved with a slow evaporation, resulting in iridescent film. (Revol et al. 1998) **Fig 1.16** gives an example of an iridescent films obtained from the simple evaporation of CNC suspension.

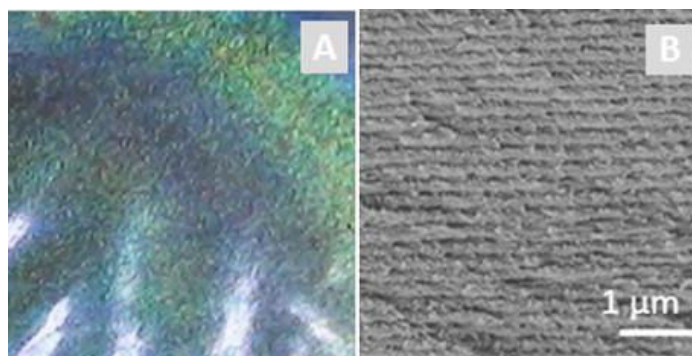


Fig 1.16 - Image of the dry state iridescent CNC film (A) under white light illumination. SEM image of its cross-section multilayer structure (B). Reproduced from (Zhang et al. 2012).

In iridescent films, the (structural) coloration (**Fig 1.16-A**) is only due to the film microstructure (**Fig 1.16-B**). This contrasts with the “standard” coloration generated by pigments, chromophore molecules, and metals. Such compounds absorb or emit light in the visible wavelength. Iridescent property (associated to a color changing with illumination or observation angles) occurs in nature (**Fig 1.17**).

It can be observed in some animals (Kinoshita et al. 2005, Doucet et al. 2009) such as *Figeater beetle*, *Turquoise Emperor butterfly*, or *Satin Bowerbird* but also in some plants (Whitney et al. 2009, Glover et al. 2010, Vignolini et al. 2012) such as *Hibiscus Trionum* flowers, *Tulipa species* or *Pollia Condensata*.

For instance, the shell of *Cotinis Mutabilis* (**Fig 1.17**) display green iridescent properties because of the helicoidally self-orientation of chitin macromolecules. (Kinoshita et al. 2005)

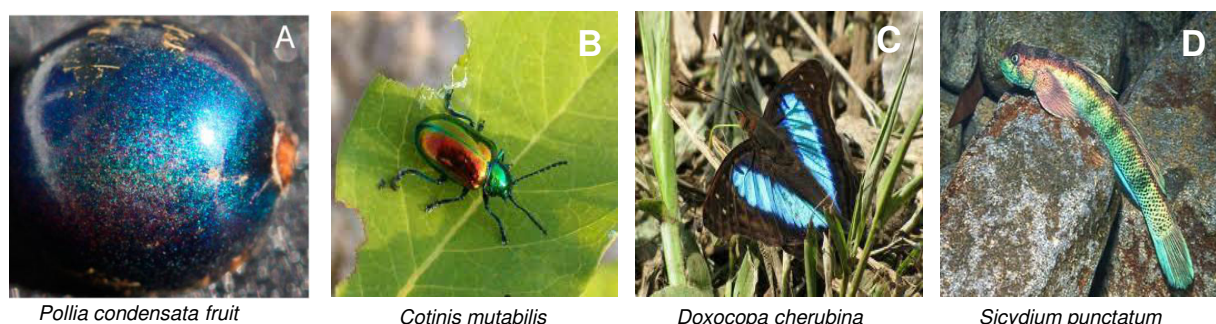


Fig 1.17 - Some examples of iridescent surfaces in nature.

Origin of self-organization of CNC

Iridescent properties of CNC film originate from the property of CNCs to display lyotropic liquid-crystalline⁹ behavior in water, (Revol et al. 1992) and in *a wide variety of organic solvents* (Heux et al. 2000).

At diluted regime, CNCs are in form of stable colloidal particles (**Fig 1.18-A**). When a critical concentration is reached, the suspension is beginning to self-organize in cholesteric structure (**Fig 1.18-B**).

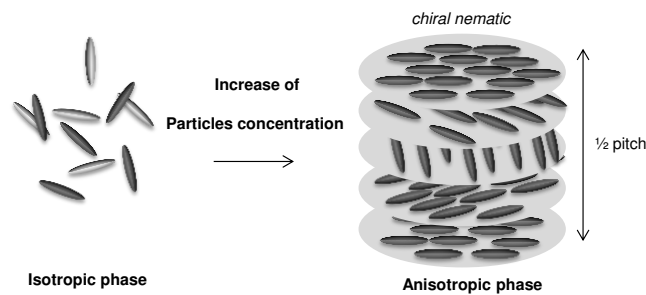


Fig 1.18 - Representation of the orientation of CNC within the isotropic and anisotropic phases

Lyotropic liquid crystals are described as stacked anisotropic layers of stiff particles (or macromolecules) in which the average orientation in each layer rotates along an axis namely “chiral-nematic axis. Initially, such self-organization was reported for cholesterol molecule or cholesterol derivative.(Barois 1996)

In 1951, de Vries (1951) related the characteristic length of pitch with the maximal reflection (λ_{max}) wavelength, the refractive index (n), and the incident observation angle ($\cos \theta$) :

$$\lambda_{max} = n \cdot P \cdot \cos \theta$$

The first macroscopic evidence of a self-organization in CNC suspension goes back to the Marchessault’s work published in 1959 in which a flow birefringence was observed.(Marchessault et al. 1959)

According to Revol et al. (1994), this feature is attributed to their rod-like shape, nanoscale dimension and negative surface charge.Revol et al. (1994) The self-organization is usually characterized by the chiral-nematic pitch (P) which can be measured by polarized optical microscopy (POM) as proposed by Gray (1994)

⁹ Liquid crystal is a matter state that has a behavior of a conventional isotropic liquid and the one of a solid crystal. A liquid crystal may flow like a liquid, but its molecules may be oriented in a crystal-like way. Generally, LCs are divided into two categories: thermotropic and lyotropic. Thermotropic LCs exhibit a phase transition into the liquid-crystal phase as temperature changed. Lyotropic LCs exhibit phase transitions as a function of concentration of macromolecules or nanoparticles

Table 1.13 summarizes the different studies in which a chiral-nematic behavior (birefringence) has been reported for CNC suspension. It highlights that the chiral nematic organization is mostly reported for sulfated CNCs (isolated from cotton) in water suspension. However, chiral-nematic behaviors are also observed in many other solvents, as well as for CNCs isolated by other processes like TEMPO-mediated oxidation, (Saito et al. 2006) APS, (Leung et al. 2011) and phosphoric acid (Leung et al. 2011).

It also appears that negatively charged CNCs always display a better electrostatic repulsion than non-charged CNC. To the best of our knowledge, self-organization properties have never been reported with CNC isolated via HCl hydrolysis. This is explained because the suspension is unstable over time and leading to nanoparticles agglomeration even if strong dispersive energy is applied. (Araki et al. 1998).

Table 1.13 - Overview of CNC that can self-organize in aqueous or solvent medium

Reagent	Source of CNC	Post treatment	Surface Charge	Solvent	Ref
APS	Bacterial Cotton Flax Hemp		COO-	Water	(Leung et al. 2011)
	Bacterial Cellulose			Water	(Hirai et al. 2009, Yun et al. 2010)
				THF	(Yun et al. 2010)
	Tunicate	Sylation		Toluene	(Gousse et al. 2002)
H₂SO₄		Surfactant		Toluene	(Heux et al. 2000)
	Cotton		SO ₃ -	Cyclohexane	(Dong et al. 1997)
				Water	(Viet et al. 2007)
				Formamide	(Viet et al. 2007)
				DMSO	(Viet et al. 2007)
			DMF	(Viet et al. 2007)	
	Hardwood			Cyclohexane	(Elazzouzi-Hafraoui et al. 2009)
	Softwood			Water	(Beck et al. 2005)
H₃PO₄	Cotton		PO ₃ -		(Camarero Espinosa et al. 2013)
HCl	Cotton	sulfation	SO ₃ -		(Araki et al. 2000)
		TEMPO	COO-	Water	(Araki et al. 2000)
TEMPO	Bacterial Cellulose Cotton Softwood Tunicate		COO-		(Saito et al. 2006)

THF: tetrahydrofurane , DMSO: dimethyl sulphoxide, DMF: dimethylformamide

As a conclusion, self-assembly is only observed in stable and non-aggregated dispersions of CNC. Furthermore, the observation of self-assembly can be efficiently used as a “quality control” for the evaluation of the suspension stability.

From chiral nematic-suspension to iridescent solid films.

Revol et al. (1995) were the pioneer to report that the self-organization of oriented CNC may be preserved under simple and undisturbed evaporation. This leads to a smooth and colored iridescent surface (**Fig 1.17**). As key result, colored films are obtained only if the pitch of solid films is approximately the wavelength of visible light. This is the origin of structural coloration within CNC film. (Revol et al. 1998)

Most of the time when transparent non-iridescent films are obtained, the reason is attributed to the absence of structural organization because of aggregated or unstable suspensions. In some case, the structural organization can be preserved but the pitch is outside the wavelength of visible light. This particularity can be due to (i) an over sonication during the suspension leading to a red-shift : reflection in infrared or (ii) an excessive ionic strength of the suspension leading to a blue-shift: reflection in UV. (Abitbol et al. 2014)

Several physical and chemical parameters are reported to influence the coloration of the iridescent of the film due to the angular dependence of the reflected light wavelength.

Table 1.14 - Parameters affecting the coloration of films based on CNC suspension.

	Parameters	Variation range	Film coloration	References
Nanoparticles	↗ Aspect ratio	23-31	Redshift	(Beck et al. 2005)
	↗ Surface charge	0.14-0.68 e/nm ²	Redshift	(Dong et al. 1998)
Suspension	↗ Ionic strength	0-600μM of monovalent salt (NaCl)	Blueshift	(Araki et al. 2001) (Dong et al. 1996)
	↗ Sonication	0-5kJ/g	Redshift	(Beck et al. 2011)
	↗ concentration	0.2- %wt	Blueshift	(Pan et al. 2010)
Drying Evaporation parameters	↗ Contact angle of substrate	20-80°	Blueshift	(Nguyen et al. 2013)
	↗ Evaporation rate	2.5-133μL/h	Redshift	(Pan et al. 2010)
	↗ Temperature	4-70°C 33-72°C	Redshift Blueshift	(Pan et al. 2010) (Beck et al. 2013)

As presented in **Table 1.14**, the structural coloration of films based on CNC is strongly influenced by various factors: their chemical and morphological properties, the suspensions parameters, and the drying parameters. Since these first results, several scientific publications [53], and many conferences [6], and patents [9] were published, which has opened the prospects of new high-valued applications in the fields of security films, printings, and photonic hybrid materials.

3 Nanocellulose and their use in paper industry

This section is adapted from “Raphael Bardet and Julien Bras, Cellulose Nanofibers and Their Use in Paper Industry, In Handbook of Green Materials, pp 207-232 (2014)”

Surprisingly, the use of nanocellulose in paper industry is recent (less than 10 years) and only a few studies are now addressing this theme¹⁰. Based on literature, CNFs may succeed in improving the mechanical and barrier properties of paper for various applications like food packaging and printing media. To note, a recently completed European project (SUNPAP, 2009-2012) was completely dedicated to the use of CNF within the paper industry. This also proves the increasing interest in such applications, demonstrating a growing interest from the nanocellulose community and industry to use nanocellulose in paper industry. At the beginning of the year 2014, among 2720 scientific papers on CNFs, only 40 are directly dedicated to the papermaking industry. In addition, among more than 400 innovations that cover most of the uses and applications of CNFs that have been patented, only one-third concerns the applications in the paper industry. Moreover, more than 20 patents have been granted in the past three years.

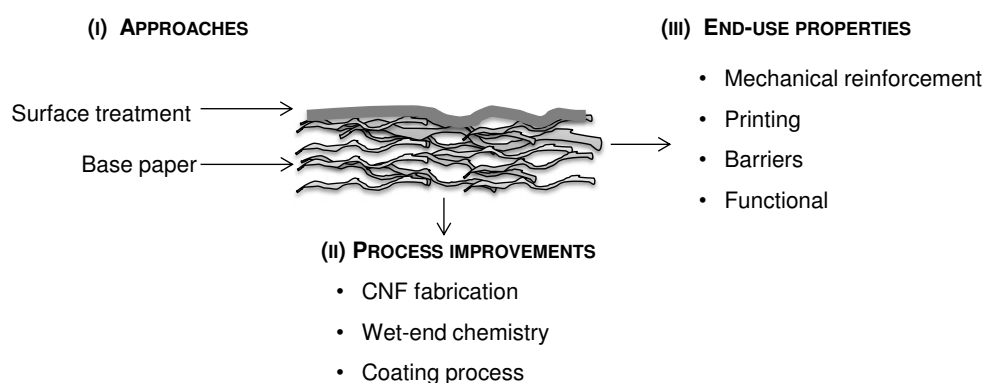


Fig 1.19 - Different uses of nanocellulose in the papermaking industry

This patent portfolio continues to grow considerably, with a strong increase in patent submission since 2007, arising notably from excellent papermaking industries like UPM and Stora Enso. To note, a recently completed European project (SUNPAP) was completely dedicated to the use of CNF within the paper industry. This also proves the increasing interest in such applications, demonstrating a growing interest from the nanocellulose community and industry to use the material in paper industry.

¹⁰ This number was even lower when this project started in 2011

The different approach adopted for realizing several end-use paper applications can be summarized. **Fig 1.19** presents the different strategies and potential improvements brought about by the use of CNF throughout the paper production protocol.

The two approaches will be discussed in the following sections. First, the bulk addition will be reviewed. Subsequently, the contribution of CNF in the surface treatment of paper will be discussed.

3.1 Bulk addition

As described in **Fig 1.20**, the bulk addition of CNFs to the base paper can be divided into four approaches

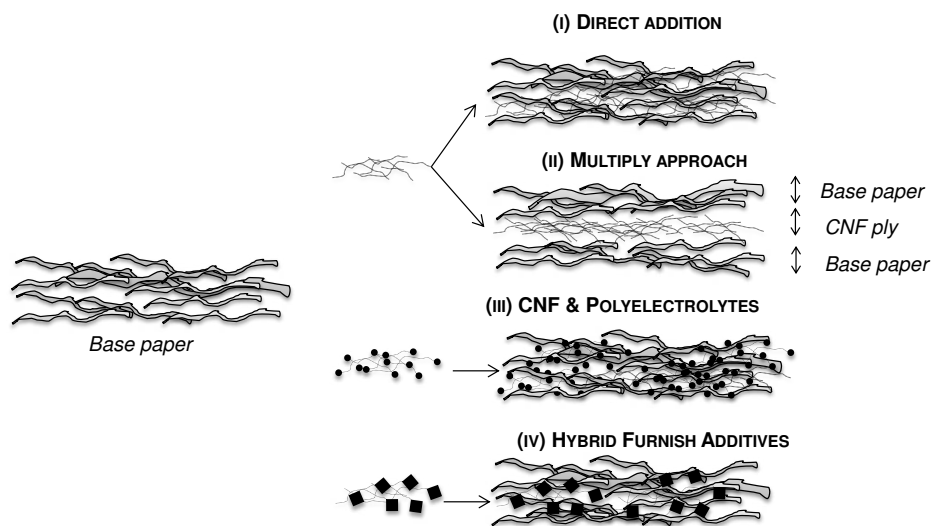


Fig 1.20 - Approaches for the bulk addition of CNFs to the base paper

3.1.1 Direct addition of CNF in the pulp suspension

Early innovations in the year 2000 assess the potential of using of CNFs directly in the base paper.(Matsuda et al. 1996, Koga et al. 1997, Cash et al. 2000)

Initial results were exclusively related to the enhancement of the (dry and wet) mechanical resistance of a paper sheet, and the improvement of the filler retention in the wet-end of the base paper. A part of the initial results has been mainly presented in several international conferences.

It is well known that the strength of the fiber network is enhanced by increasing the number of hydrogen bonds between each fibril or fibers.(Retulainen et al. 1993)

Thus, CNFs with a small size and high surface area and flexibility may naturally increase the strength of the network,(Siró et al. 2010) analogous to what can be achieved by using cellulosic fines.(Taipale 2010)

For instance, 6% (as dry) of CNFs was added into three different pulps for producing 60 g/m² handsheets. (Zou et al. 2007)

In comparison to standard handsheets produced with refined pulp, experimental results showed an increase in the tensile strength (by 26 to 30%) and the water vapor transmission rate (WVTR) as well as an increase in the Cobb value (by 8 to 60%). Similar trends have been confirmed by Bilodeau et al. (2012) and the results have been presented at the *2012 TAPPI International Conference on Nanotechnology*. Hamann (2011) proved the existence of such a positive impact when CNFs were added to unrefined pulp. Moreover, a significant grammage reduction could be achieved by adding CNFs. For instance, a 60 g/m² paper without CNF and a 41 g/m² paper with 10% CNF showed similar tensile strengths.

Torvinen et al. (2011) proposed to increase the filler content in soft-calendared (SC) paper by the addition of a small amount of CNFs (5%, as dry). According to the authors, the filler content could be increased from 30% to 50% without affecting the mechanical properties of the SC papers. This is also expected to save a significant amount of energy during the refining or drying process. (Bilodeau et al. 2012)

The effect of adding different amounts of CNFs on the tensile strength (wet and dry), tear resistance, burst strength, opacity, and porosity of paper sheets was studied by Hassan et al. (2011). Adding CNFs to a bagasse pulp suspension improved the wet and dry tensile strength. The tensile strengths of paper sheets containing CNFs were higher (wet and dry) than that of sheets containing softwood fibers. However, the latter showed higher tear resistance and burst strength.

Different qualities of CNFs are available in the market and clearly, the results will differ depending on the CNF type used. To highlight this issue, Madani et al. (2011) proposed to fractionate a commercial CNF suspension using three different fractionation techniques including gel fractionation, hydrocyclone, and pressure screen. By removing larger particles contained in the CNF suspension, authors compared the impact of adding fractionated and non-fractionated CNFs in paper samples. The results showed improvement in the tensile index (by 25%) by the addition of 10% of CNFs and another additional improvement in the tensile strength (by 10%) by addition of 10% of fractionated CNFs.

It is important to note the difficulty to quantitatively assess different works and scientific publications because the term “CNF” refers to a large range of materials with different chemical natures and morphologies (as explained in other sections).

3.1.2 Multiply strategy

In contrast to the direct introduction of CNFs in the base paper, few scientific publications and patents have focused on using CNF layers embedded in a laminated paper sheet

Morseburg et al. (2009) proposed to use CNFs as a single ply in a paper sheet. The study focused on the interaction between thermomechanical pulp (TMP), CNF, and clay in oriented layered laboratory sheets. Based on an estimation of the overall quality index that considers five variables (roughness, tensile index, strength, z-strength, gloss, and light scattering), they concluded that the best sheet construction was obtained by placing the fillers in the surface layers with the TMP accept fraction and the CNF layer in the center. As a result, the reduction in strength caused by filler addition was counterbalanced by using a CNF layer

A similar approach to obtain a lightweight paperboard with a little or no chemicals, while ensuring retention of the paper's mechanical properties and mitigation of its delamination problem has been patented; in this method, CNF acts as a bonding agent between the different plies of the multilayer board, thus suppressing delamination.

A distinct advantage of this strategy is that the paperboard containing only CNFs as additives can be readily repulped. As an example, CNF suspensions ranging from 0.1 to 2 g/m² (as dry) can be deposited using a spray coating technique between the two plies of the board surface. These materials can be mainly used as food packaging boards. Even though it is proven that CNFs can improve the mechanical properties of the base paper, results should be systematically compared to a different level of highly refined fibers and in terms of end-use quality and global energy consumption. (Kangas et al. 2004)

Moreover, there are several drawbacks of using CNFs in these two strategies. These include :

- a poor retention of CNFs in the fibrous materials
- a relatively higher cost in comparison to other wet and dry strengthening agents commonly used in the wet-end process,
- a negative impact on the drainage properties that directly affect the papermaking process, and more precisely, the drying and pressing sections

For all these reasons, despite the promising laboratory or pilot scale results, commercial use of CNFs by these strategies has been limited.

3.1.3 CNF & polyelectrolytes

Previous sections have showed the limited potential of using solely CNF suspensions because the addition of CNFs will increase the total surface area of the pulp suspension, thus enhancing the water retention by hydrogen bonding within the small capillary interstices of the fibrous network. Hence, the second generation of studies and inventions (with regard to bulk addition) has mainly focused on the combination of CNFs with polyelectrolytes or mineral materials in the view of improving the wet-end process and the final properties, while attempting to reduce the amount of CNFs.

Retention and strengthening agents

There are different types of polyelectrolytes in the wet-end. Most of them are used as strengthening agents, retention and flocculation agents, or as sizing agents. Taipale et al. (2010) focused on the effect of different types of fines and CNFs on the drainage of Kraft pulp suspensions and the paper strength. It was confirmed that a small amount of CNFs (3% as dry) decreases the drainage rate of the pulp suspension while increasing the strength of the paper. In order to compensate this constraint, an optimum dosage of polyelectrolytes (cationic starch (CS) and cationic polyacrylamide (C-PAM)) and process conditions (pH and salt addition) have been found to improve the mechanical resistance without increasing the drainage process.

The effects of CNF addition in combination with CS on the drying shrinkage and the dimensional stability have been investigated by Manninen et al. (2011). The sheets with a basis weight of 60 g/m², containing CNFs ranging from 5 to 20%, were compared to reference sheets containing the same proportion of Kraft fines. Finally, the combined addition of CNFs and CS led to a paper sheet with improved dimensional stability and strength.

A similar strategy has been proposed as a new retention system for the wet-end chemistry. According to this strategy, a cationic polymer (CS) is introduced, then a suspension of CNFs is added, followed by the addition of anionic polymer (carboxymethyl cellulose - CMC). (Axrup et al. 2012) According to the inventors, since CNFs generated many negatively charged “sites” and strongly increased the fiber surface area, this strategy should lead to a better absorption of the cationic polymer and thus increase the strength of the paper.

This opens up the way for a new retention system that involves a protocol that is simpler in comparison with conventional polyelectrolyte systems, bringing about a significant improvement in the mechanical properties of paper with a reduced amount of CNFs.

Sizing agent

For enhancing wet and dry strength of the paper while reducing the amount of polyamidoamine-epichlorohydrin (PAE), Ahola and coworkers Ahola et al. (2008) have investigated the combination of PAE addition with CNF absorption onto pulp fibers using both bilayer and nano-aggregate addition strategies. Experimental results have shown that even if PAE retention is not improved when it is previously adsorbed to CNF, the PAE/CNF bilayer strategy has a dramatic effect on the distribution of PAE leading to strong increases in wet and dry tensile strengths. With the same amount of PAE (0.6% as dry), the wet tensile index of a 60 g/m² paper was better by three times when compared to neat PAE.

To confer hydrophobic character on a fibrous support, Missoum et al. (2013) have carried out a study in which CNFs were chemically modified with a nano-emulsion of alkyl ketene dimmer (AKD). Handsheets of 60 g/m² with increasing ratio (from 5 to 50%) of neat and AKD modified CNFs were produced and then physically and chemically characterized. Consistent with previously mentioned studies, results showed a strong mechanical reinforcement. In comparison to the addition of neat CNF, AKD modified CNFs were majorly beneficial in terms of the sizing effect due to the presence of AKD that induced water absorption equivalent to a standard internal sizing with commercial AKD.

Optical brightening agent

In 2011, Nuopponen et al. (2011) patented a method for improving the dispersion of CNFs and the efficiency of optical brightening agents (OBA). In this patent, inventors suggested the microfibrillation of a blend of the fiber with an anionic OBA. The dispersing effect of the anionic OBA is achieved by inhibiting hydrogen bonding between CNFs. Since the anionic polymer is added before the fibrillating process, both the energy consumption and the amount of chemical additives used like OBA can be reduced.

For all the reasons previously mentioned, the strategy of mixing CNFs with any kind of chemical additives (retention agent, wet and dry strengthening agent, pigments, and dye carriers) represents a promising development because this leads to a drastic increase of many properties of the paper, in addition to aiding the papermaking process and limiting the use of chemicals.

In this case, a very small amount of both CNFs and chemicals are used in comparison to the first strategy that entails directly adding neat CNFs.

3.1.3.1 Hybrid furnish additives: filler/CNF

To the best of our knowledge, the approach of mixing pigments or fillers with CNF suspensions has been little explored. Nonetheless, since 2010, several innovations related to the concept have been patented by:

- key filler suppliers like Omya and Imerys
- world-class paper producers like Stora Enso and UPM

With the current state-of-the-art technologies, there are generally two strategies proposed for the production of a CNF/filler suspension. The first involves fibrillating the cellulose fibers directly with the filler and the second entails adding inorganic materials after the fibrillation. The different strategies of mixing pigments or fillers with CNF suspensions are summarized in **Table 1.15**.

Table 1.15 - Comparison of different patents related to hybrid furnish additive

Process	Type of filler	Filler ratio	Use of additives	Main application	Company	Ref
Premix	Kaolin clay + GCC/PCC	0.5-99.5%	Yes	Bulk and surface coating	IMERYS	(Husband et al. 2010)
Premix	Kaolin clay	75-65 %	No	Functional and barrier coating		(Husband et al. 2012)
Premix	Ultra-fine PCC	33%-66%	No	Paper coatings	OMYA	(Gane et al. 2010)
Premix	All pigments/filler	0.1 % -95 %	Yes	Barrier coating	STORA ENSC	(Heiskanen et al. 2011)
After fibrillation	PCC	5-7.5%	CS	Bulk	UPM	(Laine et al. 2010)

The main advantages of such new CNF production processes include decrease in the energy consumption during fibrillation and/or an increase in the solid content in the suspension by the use of the second strategy. Mostly, such hybrid filler/CNFs have been developed for coating slurry applications.

Other differences can be found in existing patents with regard to the type and dimension of the filler (calcium carbonate, kaolin, clay) and the kind of mechanical treatment used (mixing, fibrillating, homogenization).

Table 1.16 summarizes the different strategies used in the application of CNFs in bulk paper. Some results are very promising, although certain issues are pending and most of the CNF applications are focused on paper surface treatment.

Table 1.16 - Comparison of different uses of CNFs in the bulk paper strategy.

	Type of CNF	Content	Base paper	Objectives and main results	Ref
Direct addition	CNF	1-30%	Tea-bags paper 11 g/m ²	Improve wet & dry resistance	(Koga et al. 1997)◇
	C-CNF	6%	Handsheets 60 g/m ²	Tensile strength : + 26-30% Water absorption : +8%-30% WVTR : +12 %	(Zou et al. 2007) §
	CNF	5%	SC paper	Increasing filler content from 30% to 50%	(Torvinen et al. 2011) §
	CNF	10%	Handsheets 85-90 g/m ²	+160 to180 % in porosity +10 -60% in	(Bilodeau et al. 2012) §
	CNF		Handsheets 60 g/m ²	Strong improvement in tensile and z-strength 5% CNF is comparable to refining pulp to 40 kWh/t	(Hamann 2011) §
	CNF		Handsheets 60 g/m ²	Adding CNF to bagasse pulp improved wet and dry tensile strength	(Hassan et al. 2011) †
	C-CNF F-CNF	0-15%	Handsheets 60 g/m ²	For 10 % of fractionated CNF : +20% Tensile index +170% Strain at break	(Madani et al. 2011) †
Multiply approach	CNF	3-8%	SC handsheets	The best sheet construction is obtained when placing the CNF in the z-center of the paper	(Morseburg et al. 2009) †
	CNF	3-10%	50-250 g/m ² laminate paper	With 10% of CNF : +20-30% Tensile Strength +20-30% Tensile Stiffness	(Ylva Wildlock et al. 2008)◇
	CNF	0.1-2 g/m ²	Multilayer board	Increasing bonds between each ply of a multi-ply board	(Heiskanen et al. 2011)◇
CNF and polyelectrolytes system	CNF/C-PAM CNF/CS	3%	Handsheets 60 g/m ²	Optimum ratio of CNF & polyelectrolytes	(Taipale et al. 2010) †
	CNF/CS	5-20%	Handsheets 60 g/m ²	In comparison to pure CNF, CNF/CS improve the dimensional stability while improving the tensile strength	(Manninen et al. 2011) †
	CNF/CS/ CMC	1-30%		Increase retention of polyelectrolyte Simplify the PEM in the wet-end	(Axrup et al. 2012) †
	CNF/PAE	0.6%	Handsheets 60 g/m ²	Wet tensile index is 3 times better to neat CNF	(Ahola et al. 2008) †
	CNF / AKD	5-50%	Handsheets 60 g/m ²	With 16% of modified CNF : +72% Young's Modulus +51% Breaking length increase	(Missoum et al. 2013)§
CNF/ OBA	30-100%	-	Synergetic dispersion of CNF and OBA	(Nuopponen et al. 2011)◇	

† Scientific publication, § International conference, ◇ Patent. C-CNF : commercial CNF, F-CNF : fractionated CNF, C-PAM : Cationic Polyacrylamide, PAE : Polyamine Amide-Epichlorohydrin, OBA : Optical Brightening Agent, AKD : Alkyl ketene Dimer

3.2 CNFs and paper surface treatment

Most of research studies using CNF in paper are focused on the surface treatment. This section will address the investigation of CNFs for the surface treatment of paper and boards. The section is classified into three portions as described in **Fig 1.21** according to the final end-use of the paper.

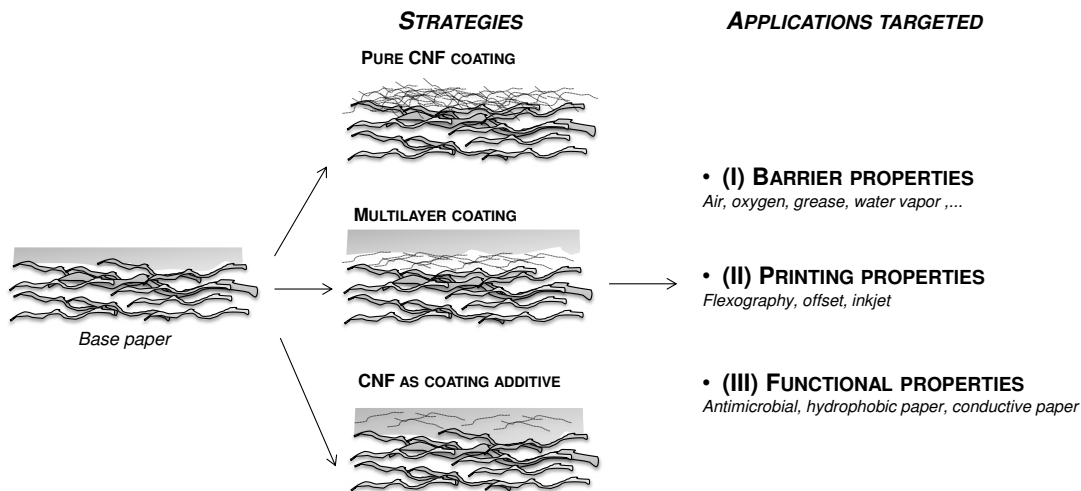


Fig 1.21 - Approach for utilization of CNF for paper surface treatment

Earlier, studies were conducted mainly to investigate the effects of directly coating neat CNFs for barrier or printing applications and other such uses.

Syverud et al. (2009) were the first to use CNFs in paper a few years ago. However, using only neat CNFs has shown its limitations of relatively low improvement, sensitivity to humidity, process issues, and high overall cost.

Hence, most recent studies have focused on developing complex strategies such as the combination of CNFs with different matrices or fillers and multilayer coatings. Each strategy will be discussed in detail separately for each property targeted i.e., barrier, printing, and functional properties. Before that, the next section deals with some basics in the paper surface coating

3.2.1 The surface coating of specialty paper

Usually, the functionalization by coating of a specialty paper operates either directly during their process manufacturing (on-line) or during a separate operation (off-line). A modification of the fibrous structure can be achieved with a thermo-mechanical treatment (calendering) or even chemical modifications by a corona, UV, plasma or chromatografting. (Li et al. 2008, Vernhes et al. 2009, Samain et al. 2013)

With the exception of the surface coating, most of these techniques are achieved off-line. In the next section, only the surface coating of paper will be described. **Fig 1.22** shows the difference between the microstructure of a paper before and after the surface coating.

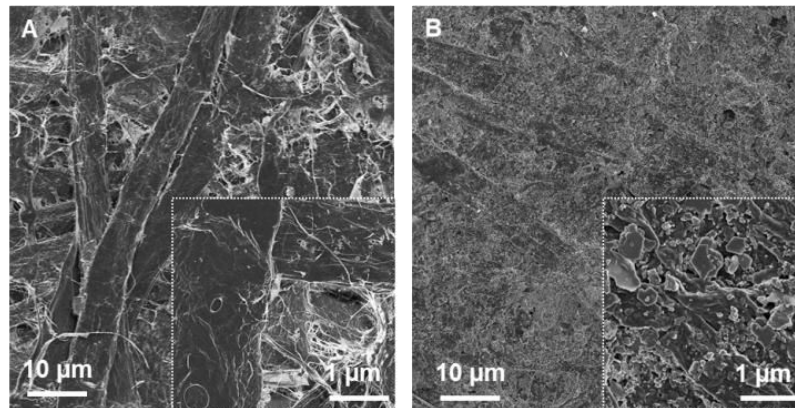


Fig 1.22 - Comparison between an uncoated base paper (A) and a coated paper (B)

The surface coating is equivalent to painting a wall. The painting is distributed with a brush, dried, and smoothed. In case of the paper, rolls or jet applicators replaced the brush and the coating is leveled out with a pneumatic or mechanical system, such as a blade or a metering bar. The moist sheet passes between infrared dryers before being conveyed to high-temperature air floats and drying cylinders. To sum, the coating operation includes the following operations:

- raw material and delivery of coating materials
- coating preparation
- application of the coating color onto the base paper
- metering of the coating
- drying of the coating
- and optionally smoothing of the surface by calendaring

3.2.1.1 The paper coating technologies.

Several technologies are available for the application of the paper coating. They are most or less suitable as a function of the machine configuration (speed and width) and the properties of the base paper. This depends mostly on the end-use properties targeted as well as the quality of the base paper (roughness, brightness, opacity,...). The coating weight varies from a low amount (less than 0.5 g/m²) to a very high amount for printing and writing papers or high quality boards (up to 20 g/m²).

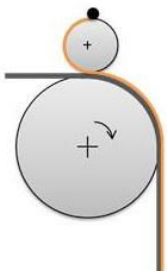
The final paper quality mostly depends on the coating speed and uniformity of the coating layer. The coating processes use different type of composition as a function of end-use

applications and the coating technologies. As described in **Table 1.17**, the coating technology can be separated into two groups by distinguishing contact deposition and non-contact deposition. In most paper companies (about 80% of paper machines), the contact coating technologies are preferred to monitor the amount of deposition.

However, for some specialty papers, the curtain coating (e.g. photographic papers) or the spray coating (e.g. microencapsulated paper) are commonly used. These two non-contact techniques are promising but are not suitable for all coating formulations.

Concerning CNF based coating, only a couple of studies used non-contact techniques. For instance, the deposition of CNF/carbon black mixture by spray coating is proposed for manufacturing highly conductive graphite/carbon fiber/cellulose composite papers (Jabbour et al. 2014) or high barrier packaging using CNF and shellac (Hult et al. 2010).

Table 1.17 - The different coating technologies used in paper industry

	Blade metering	Film Press	Curtain Coating	Spray coating
				
Deposition techniques	the excess coating is removed using a steel blade to control the coat weight	coating is metered on a roll and transfer to the paper surface	free falling coating cast onto a paper surface	Pulverization through a nozzle
Contact	Direct	Direct	Non	Non
Metering	Post	Pre	Pre	Pre
Configuration	1 side	2 side	1 side / multilayer	2 side
Coating weight	2-10	0.5-5	1-15g/m ²	0.5-2
Limitation speed	600-1800	2000	400 m/min	600 m/min
Strength and Weakness	The stress is concentrated over a relatively small area under the tip of the blade, and frequently results in breaks during production,	Universally chosen in installations for the manufacture of lightweight coated of paper	Absence of shear force (non-contact), possible to apply several layers simultaneously	Absence of shear force (non-contact), better coverage in comparison to Film press, snooze clogging when pigments are used
Ref	(Helmer et al. 2005)	(Husband et al. 2005)	(Sugihara 2007)	(Sievänen 2010)

3.2.1.2 The paper Coating formulation

The coating color consists of pigment, binding materials, and other additives to both improve the coating process and end-use properties.

It includes a combination of several pigments (kaolin, calcium carbonate, titanium dioxide), binders (mostly polyvinyl alcohol or latexes such as styrene butadiene), co-binder (e.g., carboxymethylcellulose), and additives (anti-foaming rheology modifier).

Pigments for paper surface coating.

The main component of the paper coating is the mineral pigments (80-90 wt %). Mineral fillers provide numerous benefits like a saving of raw materials costs or for improving the paper end-use properties (such as printability or barrier).

Most common fillers used are calcium carbonate (GCC or PCC), Kaolin, Talc and Titanium dioxide (TiO_2). GCC, PCC and kaolin are used in most of paper coating whereas Talc and TiO_2 are consumed in small quantities for special applications.

They are extracted from natural white minerals, but they can also be engineered by means of calcination, precipitation, or synthesized from petrol-based resources (organic pigment). Their average particle sizes range between 0.3 μm to several 5 μm . Generally, minerals pigments are in the form of powdered solid particles or slurry (dispersion in water). Their different features are summarized in **Table 1.18**

TiO_2 is one of the most efficient pigments regarding its opacifying and covering effects¹¹. However, there are several drawbacks related to the use of TiO_2 regarding its costs (highly expensive and price fluctuation) and its process issues (agglomeration phenomena and highly abrasive).

¹¹ During this PhD project, there is a special focus on opaque lightweight coated paper mainly dedicated to offset lithography as presented in Chapter 2.1 and 4.1. In these specialty papers, high level of printing opacity and brightness are key specifications. In these papers, the amount of TiO_2 is high and contains from 0 to 5% of TiO_2 for industrial catalogues, up to 10% for bible and offset paper and up to 30% in the laminate papers.

Table 1.18 - Overview of mineral pigments used in paper industry

	Kaolin Clay		Talc	Calcium Carbonate		Titanium Dioxide	
Filler	Hydrated	Calcinated	Hydrated	Ground (GCC)	Precipitated (PCC)		
Chemical Formula	Al ₂ O ₃ , 2SiO ₂ , 2H ₂ O		Mg ₃ (Si ₄ O ₁₀)OH ₂	CaCO ₃		TiO ₂	
Crystal structure	Kaolinite structure		Prismatic	Calcite/ Aragonite		Anatase	Rutile
						Tetragonal	
Morphology	Hexagonal Platy (lamellar)	Exfoliated	Leaf-like	Cubic, Prismatic, Rhombohedral	Rhombohedral, scalenohedral, acicular, prismatic, spherical		Spherical spherical
Manufacturing process		Grinding/Air floated/wet process			CaCl ₂ process CaOH process	Sulfate process	Chlorine process
Density	2.58-2.65		2.75-2.78	2.71	2.71-2.92	3.79-3.97	4.23
Average dimension (µm)	0.3-5	0.7-1.5	2.0-9.0	0.8	0.4-2	7-12	7-12
Surface area (m²/g)	9-16	15-25	3-10	2-10	6.0-10	9	9
Binding demand	●○○	●●○	●○○	●●●	●●●	●●○	●●○
Refractive Index	1.57	1.60	1.57	1.56-1.65	1.58-1.63	2.52	2.76
ISO brightness	80-90	90-95	80-85	87-97	96-99		
Abrasion (Moh's hardness)	2-2.5	2.5-3.5	1.0	3-4	4.0-5.0	5-5-6	6.0-6.5
Scattering coefficient	1100-1200	2600-3000		1400-1700	2200-2700		
Main function	Printability / Gloss	Opacity	Smoothness	Brightness	Brightness Opacity		Opacity
Price (€/kg)	0.3	0.5	1.5	0.13	0.3	2.5-2.6	2.7-2.8

Data collected from (Holik 2006) (Mcguffog 2003) (Sangl et al. 2013)

The role of binder.

A waterborne paint has a composition very close to a paper coating because they also include pigments, binders, and additives. The major difference between paints and coating colors is the amount of binders because paints (40-50%) contain much more binders than coating (15-25%).(Hook et al. 2012) Binders are hydro-soluble polymer or latex dispersion, which hold the pigment particles together and bond the coating to the base sheet. They can be either natural (Khwaldia et al. 2010), or synthetic materials (Andersson 2008).

As described in **Fig 1.23**, the role of binders' materials is to bond pigment particles to the surface of the paper (A), to bond pigment particles each other (B), and to fill between particles for reducing the coating porosity voids (C). In addition, binders may also affect the rheological behavior of the coating composition.

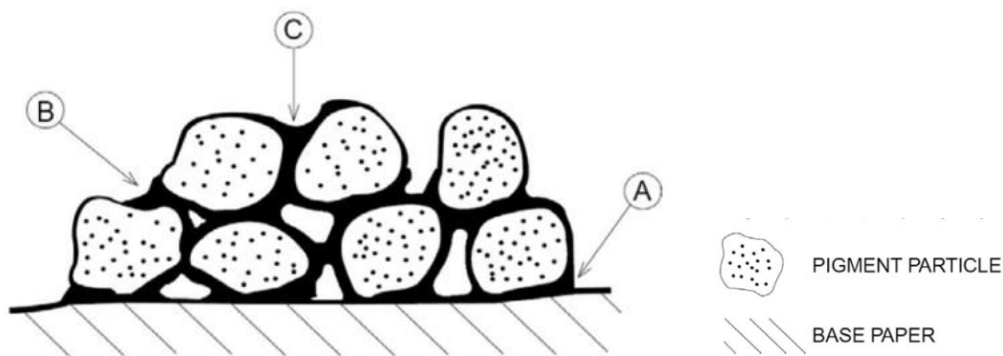


Fig 1.23 - Main functions of binders. Reproduced from (Lehtinen 2000).

With a process consideration, the selection of the binders mainly depends on the viscosity requirement imposed by the coating technology and the drying characteristic. The selection depends also of the specification targeted for the coated paper properties like the smoothness the paper cohesion, the high ink holding or the paper cost.

In addition, each pigment has its own binder demand, and each binder has a different binding strength (**Table 1.18**). Thus, the binder concentration in each coating formulation depends on the type of pigment, binder, the paper technology, and the specification of the paper.

Generally, the binder material¹² is the most expensive component among the paper formulation components of pigment, binder, and substrate. Next sections will address the investigation of CNFs for the surface treatment of paper to improve printing, barrier, and functional properties

¹² In the frame work of this PhD, CNF will be investigated as a biobased alternative to the conventional binders used for the coating formulation of opaque lightweight coated paper.

3.2.2 Optical and Printing properties

Optical properties such as coloration, opacity, brightness, gloss are key features for lightweight papers dedicated to printing applications. It mainly depends on the surface roughness, the light absorbing or light scattering properties of the different components, the shape of the pigments and the coating porosity. (Hubbe et al. 2008)

The benefit of using CNFs for printing applications has recently become the subject of increasing number of studies. In the last years, many conferences have taken place focusing on various works about CNFs as a coating for printing applications. However, only a few of these papers have been published and they will be presented following the three strategies described in **Fig 1.21**.

3.2.2.1 Pure CNF coating

In order to develop high quality printing with synthetic fibrous materials (PVA non-woven sheets), Hamada et al. (2010) have reported the use of CNFs for coating papers dedicated to inkjet and flexographic high quality printing. The nanoporous network of entangled CNFs helps fixing ink pigments at the surface leading to a better print density (increased by 20% for a 3 g/m² CNF layer), as shown in **Fig 1.24**. However, a pure CNF coating does not appear to bring a significant increase in printing properties in comparison to other classical surface treatments such as starch coating.

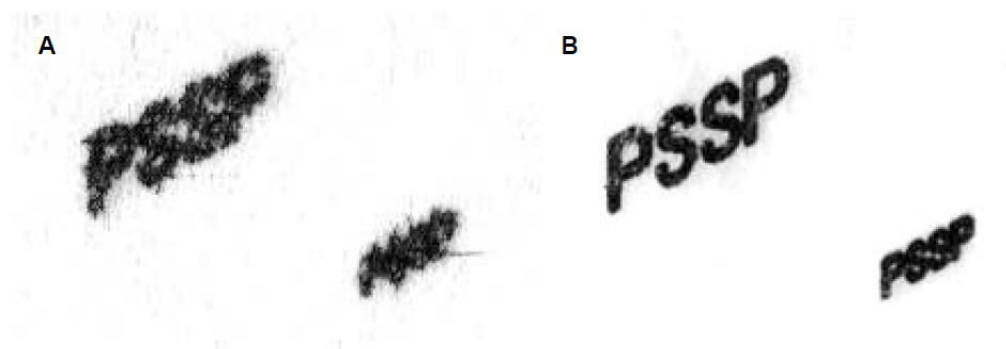


Fig 1.24 - Images of ink-jet printed samples. A: on the uncoated synthetic fiber sheet, B on the 3g/m² CNF coated sheet. Reprinted from (Hamada et al. 2010).

Following this strategy, Luu et al. (2011) proposed to deposit a CNF layer onto a base paper treated with AKD. They aimed to develop an inkjet printing paper with a hydrophobic surface. This should help absorb water-based ink without surface spreading and a hydrophobic base paper for reducing ink penetration and print through. The results showed an

increase of print density for dye-based inks, while no differences were observed for pigmented inks. (Luu et al. 2011)

3.2.2.2 CNFs and polymer blend for printing applications

With a view to reduce the linting and dusting propensity of newspapers, Song et al. (2010) have proposed a surface treatment comprising of anionic starch (A-Starch) and CNFs. A-Starch, CNF, and a 1:1 A-Starch/CNF mixture were coated onto paper with or without chemical additives.

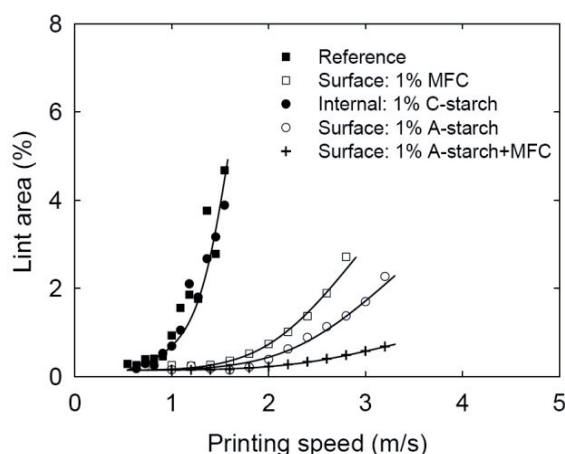


Fig 1.25 - Linting propensity of reference sheets with different chemical treatments at the same addition level. Reprinted from Song et al. (2010)

A synergistic effect was found to exist whilst using a mixture of A-Starch/CNF because A-starch reduces the delamination at higher print speeds. Moreover, the surface treatment was much more efficient than internal treatment for decreasing linting propensity, as shown in **Fig 1.25**. Song et al. (2010) suggested that the use of CNF/starch coating as surface sizing might replace the internal treatment with cationic starch, with the advantage of preserving a good water-based ink absorbability.

A work package of the SUNPAP project has been focused on high-quality Inkjet coating and has been recently presented by Papier et al. (2012). In this study, they used CNFs as coating additives. Very small amounts of CNFs (0.06% as dry) were added to inkjet coating. Experiments were done on a pilot coater at a speed of 300 m/min, which is comparable to an industrial coating machine. However, a visible decrease in gloss has been reported. Nevertheless, some benefits have been noticed because CNF limits migration of ink dyes and cracking level during the drying of the inkjet layer. Authors estimated a potential increase in the production speed by up to 10%.

3.2.2.3 CNF/ hybrid and replacement of synthetic binder

Pajari et al. (2012) presented one other part of the project SUNPAP. This study concerns the replacement of synthetic binders with CNFs in coating dedicated to offset printing papers. Three different types of CNFs were tested in order to replace latexes contained in precoat and topcoat layers. Experiments were carried out on two different types of base papers. They were among the first to report semi-industrial trials of CNF-coated papers calendared at 500 m/min running speed and then printed. This work has taken into account the most important technical and economic parameters for furthering the industrialization of paper. On the negative side, the two main drawbacks of using CNF as a binder in place of oil-based latexes include the decrease of the solid content of coating and decrease of the gloss level. On the positive side, no problem with coating colors containing CNF have been reported, which confirms a new way for replacing commercial latex, which are relatively more expensive.

Hamada et al. (2010) have also looked into the use of CNFs in pigment coating to improve the flexographic printability of a 90 g/m² uncoated paper. Two different approaches were investigated: in the first one, CNFs were used as a pigment and in the other one; CNF replaced the binder in a coating comprising a clay pigment and PVOH binder. The coating formulation with a high amount of CNFs (i.e., CNFs as pigment) was not adapted because some CNFs seemed to penetrate into the base paper. However, the results showed a 25% increase of the print density when CNF replaced the PVOH binder.

CNFs and inorganic particles or pigments can also be mixed for adding printing surface properties. Following a patent previously mentioned (Gane et al. 2011) and with the goal to enhance paper stiffness and surface properties while reducing the overall cost of CNF production, Ridgway et al. (2012) proposed to form an in situ composite obtained by fibrillating cellulose fibers with fine grinder fibers and with the aid of a PCC pigment.

In this study, different coat weights and formulations were tested. These included formulation with or without a latex/PCC precoat covered by three different types of topcoat, a PCC/CNF nanocomposites, a commercial CNF, and a cationic starch surface size. In a 40g/m² base paper coated with latex/PCC precoat (10 g/m²), the hybrid topcoat conferred a bending stiffness of up to 30% more than the same sample coated with the same weight of cationic starch (3 g/m² as dry). Furthermore, the use of the hybrid CNFs rather than pure CNFs was shown to boost the surface smoothness and uniformity. In addition, the use of hybrid CNFs as new filler materials for printing coating have been proposed in many patents, as previously discussed.

For print coating, CNFs are prospective new materials that are renewable and quite easy to recycle. **Fig 1.19** summarizes all results related to the improvements of printing properties with CNF. It is also worth noticing that there are only a couple of scientific papers and mainly conference proceedings. In contrast, barrier properties are more investigated as presented in the next section.

Table 1.19 - Table comparison of different use of CNF in the paper surface treatment for printing applications

	Formulations and Coat weight	CNF ratio	Printing application	Main results	Ref
Pure CNF	CNF 0.5 -3 g/m ²	100%	Flexography Inkjet	For a coated paper with 3g/m ² of CNF : +20 % of the print density in comparison to uncoated paper	(Hamada et al. 2010)†
	CNF/AKD 2-5 g/m ²	99%	Inkjet	+25 % of the print density	(Luu et al. 2011)§
	CNF /Starch 0-5 g/m ²	50%	Offset	Compared to internal treatment with C-starch, the surface treatment is more efficient regarding the linting propensity	(Ankerfors et al. 2009, Song et al. 2010) †◇
CNF and polymer blend	Nanopigment/ PVOH/ CNF	0.06%	Inkjet	Enhance global printing properties Potential for increasing production speed from 5% to 10 %	(Papier et al. 2012)§
	Pigment coating	5 %	Inkjet	Better water resistance and good ink absorption	(Hasunuma et al. 1997)◇
Replacement of synthetic binder	Precoat : MCC 10-30 g/m ² Topcoat: CNF/GCC hybrid	50 % in the Top coat	-	Compared to conventional coating : +30 % in the binding stiffness	(Ridgway et al. 2012)†
	Pigment/CNF			Similar performance than a styrene butadiene latex	(Pajari et al. 2012)§
	Fine Clay/CNF/PVOH 3 g/m ²	5-10%	Flexography	High print density with a small amount of CNF : a 25% increase from the base paper	(Hamada et al. 2010)§

† Scientific publication, § International conference, ◇ Patent. AKD : Alkylketene Dimer, PVA : Polyvinyl Acetate, PVOH : Polyvinyl Alcohol

3.2.3 Barrier properties

Barrier properties against air, water vapor, liquids and gas are expected in case of specialty paper dedicated to packaging applications.

Paper materials display both a good mechanical strength and flexibility for the production of packaging but low barrier properties. Several reviews have already reported the use of bio-based materials and nanoparticles for packaging applications in which barrier properties is one of the key parameters.(Duncan 2011, Johansson et al. 2012)

In addition Lavoine et al. (2012) have published a critical review about the barrier properties and applications of CNFs used in films, nanocomposites, and in paper coating.

3.2.3.1 Pure CNF coating

As previously mentioned, in 2009, Syverud et al. (2009) were among the first to report the preparation of a paper coated with pure CNF. The use of CNFs as a surface layer (0–8% of total basis weight) on a 90 g/m² base paper increased the mechanical strength of the paper sheets significantly and dramatically reduced their air permeability. Authors also investigated the impact of the nature of the CNF and the results showed similar trends when unmodified, anionic, and cationic CNFs were compared. Surprisingly, oxygen transmission rates (OTR) of the films were very low (17 ml/ (m².day)) and a similar trend was observed for the OTR of CNF coated papers.

The strong impact on the reduction of air permeability was later confirmed by Aulin et al. (2010), who coated (coating weight in the range 1–2 g/m²) two different papers, i.e. Kraft paper and greaseproof paper. The air permeability decreased considerably for the two papers and reached less than 1 nm.Pa⁻¹.s⁻¹. They were also the first to investigate the potential of oil barrier properties. They hypothesized that the grease resistance of a CNF layer, because of the reduction of surface porosity induced by the nanoporous network formed by entangled microfibrils, led to an increase in the oil resistance with the CNF coat weight. In addition, they also showed that the use of as-carboxylated CNFs formed a denser coating layer and showed superior air barrier properties when compared to enzymatically pretreated CNFs.(Nygårds 2011)

Pure CNF coating sounds interesting, however due to the low coating weight several coating layers are required. Moreover, such coatings are very sensitive to the moisture humidity. For these reasons, CNF are often combined with other barrier polymer (blend) or deposited as a precoat (multilayer approach).

3.2.3.2 Multilayer approach for barrier applications

Hult et al. (2010) proposed another method to improve the barrier properties of paperboard and paper by the use of CNFs combined with shellac resin. Shellac is a natural resin secreted by lake insects and this resin has been widely used in industrial materials, medicine, and food because of its exceptional properties such as hydrophobicity and nontoxic nature. In their study, two different combinations of CNFs and shellac were tested: a blend of CNFs and shellac and a multilayer system comprising of a CNF precoat layer and a shellac topcoat layer. The air, oxygen, and water vapor barrier properties were measured to quantify the barrier effect brought by the barrier layers. The main contribution of the CNF layer was to ensure good adhesion of the resin layer with the base paper while avoiding penetration into the paper substrate. They found the multilayer coating to be the most efficient because of the sharp drops in the oxygen and water vapor barriers. The barrier properties thus obtained can be classified in the high barrier category for food packaging and could be used for modified atmosphere packaging (MAP).

The use of CNF precoat layers has been also patented, for example, with a view to develop a fiber-based product with barrier properties by a method that is both economical and ecologically benign. Axtrup et al. (2011) (Stora Enso) patented a paper substrate covered with a CNF precoat layer in combination with a polymer topcoat layer deposited by lamination or extrusion coating. As an example, authors mention of a 230 g/m² paperboard precoated with a 1.2 g/m² CNF layer, which was then laminated with a 24 g/m² polyethylene. In comparison to the sample without the CNF precoat, the barrier properties were better with an OTR that was more than 72 times lower.

The different studies on pure CNF coating have helped to identify the main drawbacks of paper directly coated with CNFs. It is generally found that the CNF layer would not cover the paper surface well, and because of the low dry matter of the suspension, it is inconvenient to increase the deposited coat weight.

From an industrial point of view, such a coating is difficult to achieve because in order to deposit onto a substrate of 10 g/m² of CNF, it is more than 300 g of water that has to be evaporated. However, the standard values of dewatering ranges from 10 g/m² to 50 g/m² of evaporated water. For all these reasons, combining CNFs with polymer, filler, or additives is proposed in order to have a complementary synergistic effect.

3.2.3.3 CNF blend for barrier packaging

For developing a barrier packaging board, Guezennec (2012) have proposed to use a PVOH/CNF layer as a barrier coating. A 10 g/m² layer comprising of a 1:20 CNF/PVOH ratio was deposited onto a 182 g/m² baseboard. Regarding the challenges encountered in the coating process, obtaining a PVOH/CNF coating has been found to be more efficient than obtaining a pure PVOH coating. CNFs help the drying of the coating mixture, limiting blister defects and enhancing the paper runnability. With regard to the barrier properties, the water and oxygen barrier properties obtained are close to that of existing oil-based derivatives such as polyamide (PA) or ethylene vinyl alcohol (EVOH), as shown in **Fig 1.26**.

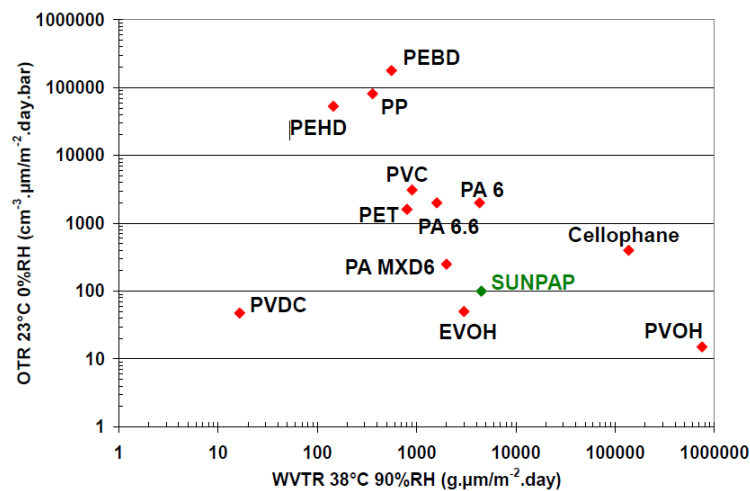


Fig 1.26 - Oxygen vs. water vapor barrier properties of different fossil-based materials and for the PVOH/CNF coating. Reprinted from (Norppa 2012)

There are similar approaches mentioned in the patent literature that focus on the enhancement of barrier properties of paper and board using a blend of polymer and CNF.

In order to reduce WVTR of coated substrates, Heiskanen et al. (2011) (Stora Enso) claimed the use of a coating mixture containing CNF and latex polymers such as polyvinylidene chloride (PVdC) and polyvinyl alcohol (PVOH). In the example given by the inventors, a 15 g/m² CNF-polymer was coated onto a 210 g/m² baseboard and compared to one coated with the same weight of latex. A decrease in WVTR and better grease resistance were observed.

In 2011, a patent describing a barrier coating formulation comprising of CNF, a partially hydrolyzed poly(vinyl acetate) PVA, and a small amount of anionic polymer was also published. (Malmborg et al. 2011) Such combinations of these materials improve the barrier and mechanical properties in comparison to classical barrier coatings.

3.2.3.4 Hybrid barrier coating

In 2011, Berglund et al. (2011) studied nacre-mimicking hybrids comprising of CNF and platelet nanoclay (sodium Montmorillonite, MMT), which can be used as an efficient barrier coating. Besides providing excellent mechanical properties, the coating mixture exhibited high oxygen gas-barrier and fire-retardant properties because of the unique multilayered structure similar to that in natural nacre, as shown in **Fig 1.27**.

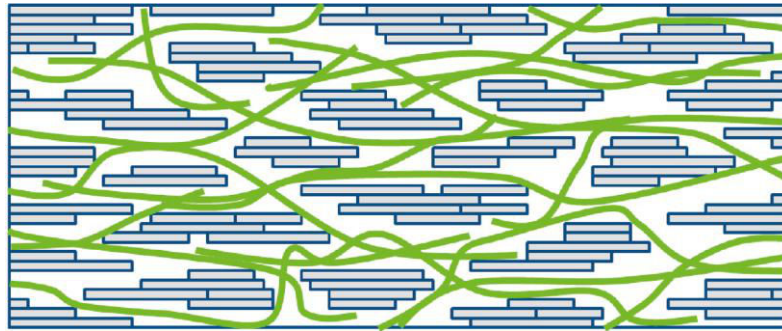


Fig 1.27 - Schematic representation of the structure of the nanopaper cross-sectional surface plane. Reprinted from (Liu et al. 2012)

The hybrid composite could also be improved by adding 10 parts by weight of chitosan. (Liu et al. 2012) These authors also suggested the fabrication of a three-phase clay nanopaper used to form a multilayered nacre-like structure clay nanopaper. In this barrier coating, nanoclay strongly improved the oxygen barrier and thermo stability of the materials.

CNF dramatically improved the mechanical strength and chitosan seemed to decrease moisture swelling. The synergetic effect brought about by the three nacre-mimicking hybrid elements is promising for applications in packaging as films or coatings and as molded laminates. Similar results on CNF films have been recently published by Isogai and coworkers (Wu et al. 2012), which confirmed such high gas barrier systems.¹³

¹³ Based on these previous results, the chapter 2.2 is dedicated to the improvement of barrier properties of CNF films with the aim to substitute nanoclay with CNCs.

Table 1.20 summarizes the main results of the CNF coating strategies and the barrier properties.

Table 1.20 - Comparison of different use of CNF in the paper surface treatment for barrier applications

Approach	Coat weight	Coating composition	Base paper	Targeted Barriers	Ref.
Pure CNF coating	2-8 g/m ²	CNF	Hand sheet 88-82 g/m ²	Air	(Syverud et al. 2009) †
	0-2 g/m ²	CNF CNF-COOH	Greaseproof Kraft	Air Grease	(Aulin et al. 2010) †
	0-6 g/m ²	CNF CNF-COOH	Broad range of office papers 80- 130 g/m ²	Air	(Nygårds 2011) †
CNF and blend	15 g/m ²	CNF/PVOH CNF/PVdC	Baseboard 210 g/m ²	Water vapor Grease	(Heiskanen et al. 2011) †
	10 g/m ²	1:20 CNF/PVOH	Base board 182 g/m ²	Oil Water Water vapor O ₂	(Norppa 2012) §
	-	1:1 CNF/PVA +anionic polymer	Base paper or board	Water vapor O ₂	(Malmberg et al. 2011) †
	-	CNF/Nanoclay CNF/Nanoclay/Chitosan	Base paper or board	O ₂ Fire retardancy	(Liu et al. 2012) † (Liu et al. 2011) † (Berglund et al. 2011) †
	3-20 g/m ²	CNF/Shellac	Base paper 45-65 g/m ²	O ₂ Water vapor	(Hult et al. 2010) †
Multilayer coating	5 g/m ² 23 g/m ²	Precoat :CNF Topcoat :Shellac	Base paper 45-65 g/m ²	O ₂ Water vapor	(Hult et al. 2010) †
	1.2 g/m ² 20 g/m ²	Precoat :CNF Topcoat : polymer (PE)	Base board 230 g/m ²	O ₂	(Axtrup et al. 2011) †

† Scientific publication, § International conference, † Patent. PVOH : Polyvinyl Alcohol, PVdC : Polyvinylidene chloride, PVA : Polyvinyl Acetate, PE : Polyethylene

3.3 Conclusions

This last chapter confirms a recent strong rising interest of both the pulp and paper scientific and industrial communities. The two different strategies proposed in the literature are the bulk addition and the surface treatment.

To the best of our knowledge, the highest potential seems to lie in the surface treatment. Irrespective of the strategies involved, CNFs are more effective once combined with other materials because of synergetic effects in which CNFs play the role of a carrier or binder. CNF would replace existing materials or will be instrumental in the development of new functional materials. For replacing petrol-based materials (strengthening agent, latex, etc.), the commercial cost of CNFs must be at least equivalent to or lower than the price of such materials. In order to conclude and summarize the potential uses of CNFs in the paper industry, a SWOT (strengths/weaknesses/opportunities/threats) analysis is presented in **Table 1.21**.

Table 1.21 - SWOT analysis of the use of nanocellulose within the paper industry

Strengths	Weaknesses
<ol style="list-style-type: none"> 1. Valuable contribution in many areas : mechanical, barriers, printing, and functional properties 2. High potential <ul style="list-style-type: none"> • When combined with other materials. • When used as a surface treatment 3. May replace existing petrol-based materials 4. Positive impact on the product LCA 5. Starting material is relative cheap, available all around the world, renewable, and biodegradable 	<ol style="list-style-type: none"> 1. Rheological behavior and low dry matter of CNF gel may lock the industrial development 2. Current CNF process is not adapted for industrial scale-up <ul style="list-style-type: none"> • Energy intensive • Non-continuous operation 3. Lack of standardization and quality control
Opportunities	Threats
<ol style="list-style-type: none"> 1. Production of CNFs using an optimization of papermaking process and specific know-how of paper industry 2. Development of new functional properties for obtaining value-added papers 3. Additional market : selling dried commercial CNFs to other industries 	<ol style="list-style-type: none"> 1. High pressure on cellulose material can increase the purchase price of cellulosic pulps 2. CNF Patent portfolio can limit the broad use of CNF

Since papermaking is an online process, the development of new production equipment or the upgrading of existing equipment (homogenizer, microfluidizer, fine grinder, etc.) and the standardization and development of quality procedure are exigently required. CNFs will be produced in situ by paper producers with the additional benefit being the emphasis on the life-cycle assessment (LCA) of the final product.

Another prospect is to use CNFs in non-paper industries such as cosmetics, composites, etc., in which the raw material prices are not the major parameters. Indeed, it is clear that the pulp and paper industries are the best for producing CNFs because of their knowledge and their existing production facilities. The contents of the table well conclude this chapter, providing the strengths and weaknesses of applying CNFs in the paper industry.

Highlights and next challenges

Highlights of the literature review. This **Chapter 1** introduces the general context of the PhD project, which concerns industrial applications of nanocellulose within specialty papers. In comparison to a standard paper, specialty papers require complex manufacturing processes and additional properties. Non-conventional raw materials and technologies are used to achieve customers' requirements.

Among them, nanotechnology is at the forefront of development in the papermaking technology. Nanomaterials are both used for enhancing the papermaking making process and for improving the end-use or functional properties.

While many nanomaterials are mineral-based or petrol-based resources, nanomaterials isolated from the biomass namely “Nanocellulose” appear to be a sustainable emerging alternative. Nanocellulose features an attractive combination of promising properties such as being bio-based, biodegradable, and biocompatible. In addition, they also have a low density (~1.6), high stiffness (~150 GPa), thermal stability (~300°C), and high density of hydroxyl groups available for chemical modification.

Since the year 2008, the strong growth of patents and scientific publications highlights the interest in nanocellulose. In addition, with the recent construction of the first Canadian nanocellulose plants in 2011, nanocellulose is now commercially available. Even nanotoxicology and risk assessment on nanocellulose are currently under investigation, and preliminary toxicological data indicated that nanocellulose could be considered as non-toxic. For all these reasons, nanocellulose could improve existing materials (paper, gel, composite) and create new materials (aerogel, flexible film, iridescent film).

Indeed, nanocellulose already succeeds, during the last 5 years, in improving the mechanical and barrier properties of paper for various applications like food packaging and printing media. In these cases, nanocellulose is introduced either as furnish additives in the base paper or as coating additives during the surface treatment. Based on the updated literature review (proposed in this chapter), it seems the highest potential seems to lies in the surface treatment. Using iridescence of cellulose nanocrystals self-organization might also be an interesting way of assessing additional functions to specialty papers.

Next challenges. The main original feature of this project is to study the contribution of both CNC and CNF for application within specialty papers. The study is conducted in two phases. First, the properties of nanocellulose films, considered as model surface layer, are investigated for the both families of nanocellulose in the **Chapter 2** and **Chapter 3**.

Indeed, as detailed in the literature review, CNF suspension exhibit gel-like behavior at even low concentration with a shear thinning properties. Because of hydrogen bonds and their flexibility, once dried, CNF form a cohesive and dense entangled network. This feature will be investigated in **Chapter 2** in which CNF will be used as dispersive network for particles with a view of (i) replacing existing polymer in thin opaque films or (ii) substituting mineral nanoparticles in barrier materials. In contrast, it was also stated in **Chapter 1** that CNC suspension exhibit outstanding iridescent properties from their self-assembly properties. This specific optical property will be used to develop flexible iridescent film with tunable color and fluorescent properties.

Secondly, the results obtained for model surface layer are implementing at the industrial scale within the papermaking process in the **Chapter 4**. Innovative strategies (patented during this PhD), pilot scale and industrial trials are presented. From the results obtained in **Chapter 2**, a cost-effective solution for saving opacifying pigment in thin papers is presented. Concerning findings from **Chapter 3**, the manufacturing of iridescent pigment is presented and their use in industrial application for anti-counterfeiting is proposed.

List of Tables

Table 1.1 - Overview of papermaking production parameters	29
Table 1.2 - Overview of the main unit operations of the stock preparation	30
Table 1.3 - Key figures of European Paper industry	31
Table 1.4 - Chemical composition of some vegetal biomass used for nanocellulose production	35
Table 1.5 - Optimum chemical conditions for isolation of CNC.....	39
Table 1.6 - Overview of the technologies used for the CNF production.....	43
Table 1.7 - Recap of the main factors limiting industrialization of nanocellulose	47
Table 1.8 - List of manufacturing companies of nanocellulose.....	49
Table 1.9 - Overview of studies that investigate the nanotoxicology risk of nanocellulose.....	51
Table 1.10 - Comparison of the main features of CNC and CNF	52
Table 1.11 - Comparison of the properties of CNF and CNC suspensions in water	53
Table 1.12 - Recap of the main features of a nanopaper based on CNF.....	55
Table 1.13 - Overview of CNC that can self-organize in aqueous or solvent medium	58
Table 1.14 - Parameters affecting the coloration of films based on CNC suspension.....	59
Table 1.15 - Comparison of different patents related to hybrid furnish additive.....	67
Table 1.16 - Comparison of different uses of CNFs in the bulk paper strategy.	68
Table 1.17 - The different coating technologies used in paper industry.....	71
Table 1.18 - Overview of mineral pigments used in paper industry.....	73
Table 1.19 - Table comparison of different use of CNF in the paper surface treatment for printing applications	78
Table 1.20 - Comparison of different use of CNF in the paper surface treatment for barrier applications ...	83
Table 1.21 - SWOT analysis of the use of nanocellulose within the paper industry	84

List of figures

Fig 1.1 - Global paper production share by application. Data collected from (CEPI 2013).	28
Fig 1.2 - World production of paper for main producer regions since 1950 to 2010	28
Fig 1.3 - Overview of a specialty paper machine. Adapted from Voith	30
Fig 1.4 - Annual number (histogram) and cumulative number (dotted line) of scientific publication about nanocellulose from 2000 up to now (from SciFinder, Sept. 14)	34
Fig 1.5 - Simplified structure of the cell wall (typical softwood tracheid) (A) and distribution of Cell Wall Components (B) and distribution of chemical components across the fiber wall (C). Adapted from (Hon 1994)	35
Fig 1.6 - Supra molecular structure of cellulose. Reproduced from (Hon 1994)	36
Fig 1.7 – One of the first Nanoscale observation in TEM microscopy of nanocellulose: CNC (A) and (B) CNF. reproduced from (Marchessault et al. 1959) (Dufresne et al. 1998))	37
Fig 1.8 - Different routes for the isolation of nanocellulose	38
Fig 1.9 - Cross-section(A), transverse (B) representation of a cellulose microfibrils, and predominant hydrolysis mechanism on cellulose adapted from (Hon 1994)	39
Fig 1.10 - SEM micrograph of CNFs isolated with homogenization treatment(A) showing the different sub-elements remaining after the main mechanical process. Optical micrographs (B) of CNF film with increasing level of homogenization. Adapted from (Chinga-Carrasco 2011)	41
Fig 1.11 - Types of cellulase: (A) endoglucanases without cellulose-binding domain; (B) endoglucanases with cellulose-binding domain; (C) and (D) cellobiohydrolases, and (E) glucosidases. Reproduced from (Köpecke 2008).	45
Fig 1.12 - Scheme of the TEMPO-mediated oxidation mechanism on cellulose. Reproduced from (Isogai et al. 2011)	46
Fig 1.13 - Annual and cumulative number of patent application on nanocellulose (A) and Overview of the main codes used for International Patent Classification (B). Data collected from Espacenet, May 2014	48
Fig 1.14 - Comparison with need-like shape nanomaterials extracted from mineral or biomass pictures reproduced from (Buzea et al. 2007), (Dufresne 2012)	50
Fig 1.15 - Comparison between a nanopaper and conventional cellulose paper (right) reproduced from (Nogi et al. 2009)	54
Fig 1.16 - Image of the dry state iridescent CNC film (A) under white light illumination. SEM image of its cross-section multilayer structure (B).Reproduced from (Zhang et al. 2012).	56
Fig 1.17 - Some examples of iridescent surfaces in nature.	56
Fig 1.18 - Representation of the orientation of CNC within the isotropic and anisotropic phases	57
Fig 1.19 - Different uses of nanocellulose in the papermaking industry	61
Fig 1.20 - Approaches for the bulk addition of CNFs to the base paper	62
Fig 1.21 - Approach for utilization of CNF for paper surface treatment	69
Fig 1.22 - Comparison between an uncoated base paper (A) and a coated paper (B)	70

Fig 1.23 - Main functions of binders. Reproduced from (Lehtinen 2000). 74

Fig 1.24 - Images of ink-jet printed samples. A: on the uncoated synthetic fiber sheet, B on the 3g/m² CNF coated sheet. Reprinted from (Hamada et al. 2010). 75

Fig 1.25 - Linting propensity of reference sheets with different chemical treatments at the same addition level. Reprinted from Song et al. (2010)..... 76

Fig 1.26 - Oxygen vs. water vapor barrier properties of different fossil-based materials and for the PVOH/CNF coating. Reprinted from (Norppa 2012)..... 81

Fig 1.27 - Schematic representation of the structure of the nanopaper cross-sectional surface plane. Reprinted from (Liu et al. 2012) 82

References

1. Abitbol and Cranston, "Chiral Nematic Self-Assembly of Cellulose Nanocrystals in Suspensions and Solid Films", *Handbook of Green Materials*: 37-56, edited by World Scientific (2014).
2. Ahmadi Achachlouei, "*Environmental Impacts of Electronic Media: A Comparison of a Magazine's Tablet and Print Editions*", PhD Thesis, KTH Royal Institute of Technology, Sweden (2013).
3. Ahola, Österberg, et al., "Cellulose nanofibrils—adsorption with poly(amideamine) epichlorohydrin studied by QCM-D and application as a paper strength additive", *Cellulose* 15(2): 303-314 (2008).
4. Alemdar and Sain, "Isolation and characterization of nanofibers from agricultural residues—Wheat straw and soy hulls", *Bioresource Technology* 99(6): 1664-1671 (2008).
5. Alexandrescu, Syverud, et al., "Cytotoxicity tests of cellulose nanofibril-based structures", *Cellulose* 20(4): 1765-1775 (2013).
6. Andersson, "New ways to enhance the functionality of paperboard by surface treatment—a review", *Packaging Technology and Science* 21(6): 339-373 (2008).
7. Ankerfors, Lindstroem, et al., "Composition for coating of printing paper", STFI - Packforsk, WO2009123560A1 (2009).
8. Araki and Kuga, "Effect of Trace Electrolyte on Liquid Crystal Type of Cellulose Microcrystals", *Langmuir* 17(15): 4493-4496 (2001).
9. Araki, Wada, et al., "Flow properties of microcrystalline cellulose suspension prepared by acid treatment of native cellulose", *Colloids and Surfaces a-Physicochemical and Engineering Aspects* 142(1): 75-82 (1998).
10. Araki, Wada, et al., "Birefringent Glassy Phase of a Cellulose Microcrystal Suspension", *Langmuir* 16(6): 2413-2415 (2000).
11. Aulin, Gällstedt, et al., "Oxygen and oil barrier properties of microfibrillated cellulose films and coatings", *Cellulose* 17(3): 559-574 (2010).
12. Axrup, Heiskanen, et al., "Paper or paperboard product and a process for production of a paper or paperboard product", Stora Enso, WO2012039668A1 (2012).
13. Axrup, Heiskanen, et al., "A paper or paperboard substrate having barrier properties, a process for production of the substrate and a food or liquid package formed of the substrate", Stora Enso, WO2011078770A1 (2011).
14. Bai, Holbery, et al., "A technique for production of nanocrystalline cellulose with a narrow size distribution", *Cellulose* 16(3): 455-465 (2009).
15. Barois (1996), "Cristaux liquides", *Techniques de l'ingénieur*.
16. Battista, Coppick, et al., "Level-Off Degree of Polymerization", *Industrial & Engineering Chemistry* 48(2): 333-335 (1956).
17. Bawden and Pirie, "The isolation and some properties of liquid crystalline substances from solanaceous plants infected with three strains of tobacco mosaic virus", *Proceedings of the Royal Society of London. Series B, Biological Sciences* 123(832): 274-320 (1937).
18. Beck, Bouchard, et al., "Controlling the Reflection Wavelength of Iridescent Solid Films of Nanocrystalline Cellulose", *Biomacromolecules* 12(1): 167-172 (2011).

19. Beck, Bouchard, et al., "Controlled production of patterns in iridescent solid films of cellulose nanocrystals", Cellulose 20(3): 1401-1411 (2013).
20. Beck, Roman, et al., "Effect of Reaction Conditions on the Properties and Behavior of Wood Cellulose Nanocrystal Suspensions", Biomacromolecules 6(2): 1048-1054 (2005).
21. Belgacem and Gandini, "The surface modification of cellulose fibres for use as reinforcing elements in composite materials", Composite Interfaces 12(1-2): 41-75 (2005).
22. Bercea and Navard, "Shear Dynamics of Aqueous Suspensions of Cellulose Whiskers", Macromolecules 33(16): 6011-6016 (2000).
23. Berglund and Liu, "Strong nanopaper with high oxygen barrier properties, comprising nanocomposites of microfibrillated cellulose nanofibers and layered clay and manufacture and use thereof", KTH Holding AB, WO2011059398A1 (2011).
24. Biermann, "Essentials of pulping and papermaking", edited by Academic press (1993).
25. Bilodeau and Bousfield, "Potential applications of nanofibrillated cellulose in printing and writing papers", presented at TAPPI International Conference on Nanotechnology, Montreal, Canada (2012).
26. Bondeson, Mathew, et al., "Optimization of the isolation of nanocrystals from microcrystalline cellulose by acid hydrolysis", Cellulose 13(2): 171-180 (2006).
27. Buzea, Pacheco, et al., "Nanomaterials and nanoparticles: sources and toxicity", Biointerphases 2(4): MR17-MR71 (2007).
28. Camarero Espinosa, Kuhnt, et al., "Isolation of thermally stable cellulose nanocrystals by phosphoric acid hydrolysis", Biomacromolecules (2013).
29. Camarero Espinosa, Kuhnt, et al., "Isolation of thermally stable cellulose nanocrystals by phosphoric acid hydrolysis", Biomacromolecules 14(4): 1223-1230 (2013).
30. Capron and Cathala, "Surfactant-Free High Internal Phase Emulsions Stabilized by Cellulose Nanocrystals", Biomacromolecules 14(2): 291-296 (2013).
31. Cash, Chan, et al., "Derivatized microfibrillar polysaccharides, their formation and use in dispersions", Hercules, WO2000047628A2 (2000).
32. Castro-Guerrero and Gray, "Chiral nematic phase formation by aqueous suspensions of cellulose nanocrystals prepared by oxidation with ammonium persulfate", Cellulose: 1-11 (2014).
33. Ceperi, "European Pulp and Paper Industry 2012 - Key Statistics", from <http://www.cepi.org/> (2013).
34. Ceperi, "CEPI Sustainability Report 2013", from <http://www.cepi.org> (2014).
35. Chakraborty, Sain, et al., "Cellulose microfibrils: a novel method of preparation using high shear refining and cryocrushing", Holzforschung 59(1): 102-107 (2005).
36. Chinga-Carrasco, "Cellulose fibres, nanofibrils and microfibrils: The morphological sequence of MFC components from a plant physiology and fibre technology point of view", Nanoscale Research Letters 6 (2011).
37. Clift, Foster, et al., "Investigating the interaction of cellulose nanofibers derived from cotton with a sophisticated 3D human lung cell coculture", Biomacromolecules 12(10): 3666-3673 (2011).
38. Cowie, Bilek, et al., "Market projections of cellulose nanomaterial-enabled products—Part 2: Volume estimates", Tappi Journal 13(6) (2014).

39. De Lima, Feitosa, et al., "Evaluation of the genotoxicity of cellulose nanofibers", International journal of nanomedicine 7: 3555 (2012).
40. De Vries, "Rotatory power and other optical properties of certain liquid crystals", Acta Crystallographica 4(3): 219-226 (1951).
41. Demirbas, "Progress and recent trends in biofuels", Progress in energy and combustion science 33(1): 1-18 (2007).
42. Demirbaş, "Biomass resource facilities and biomass conversion processing for fuels and chemicals", Energy conversion and Management 42(11): 1357-1378 (2001).
43. Dinand, Vignon, et al., "Mercerization of primary wall cellulose and its implication for the conversion of cellulose I→ cellulose II", Cellulose 9(1): 7-18 (2002).
44. Dong and Gray, "Effect of Counterions on Ordered Phase Formation in Suspensions of Charged Rodlike Cellulose Crystallites", Langmuir 13(8): 2404-2409 (1997).
45. Dong, Hiranu, et al., "Cytotoxicity and cellular uptake of cellulose nanocrystals", Nano Life 2(03) (2012).
46. Dong, Kimura, et al., "Effects of Ionic Strength on the Isotropic–Chiral Nematic Phase Transition of Suspensions of Cellulose Crystallites", Langmuir 12(8): 2076-2082 (1996).
47. Dong, Revol, et al., "Effect of microcrystallite preparation conditions on the formation of colloid crystals of cellulose", Cellulose 5(1): 19-32 (1998).
48. Doucet and Meadows, "Iridescence: a functional perspective", Journal of The Royal Society Interface 6(Suppl 2): S115-S132 (2009).
49. Dufresne, "Nanocellulose, From Nature to High Performance Tailored Materials", edited by De Gruyter (2012).
50. Dufresne, Cavaillé, et al., "Thermoplastic nanocomposites filled with wheat straw cellulose whiskers. Part II: effect of processing and modeling", Polymer composites 18(2): 198-210 (1997).
51. Dufresne and Vignon, "Improvement of starch film performances using cellulose microfibrils", Macromolecules 31(8): 2693-2696 (1998).
52. Duncan, "Applications of nanotechnology in food packaging and food safety: Barrier materials, antimicrobials and sensors", Journal of Colloid and Interface Science 363(1): 1-24 (2011).
53. Elazzouzi-Hafraoui, Putaux, et al., "Self-assembling and Chiral Nematic Properties of Organophilic Cellulose Nanocrystals", The Journal of Physical Chemistry B 113(32): 11069-11075 (2009).
54. Eriksen, Syverud, et al., "The use of microfibrillated cellulose produced from kraft pulp as strength enhancer in TMP paper", Nordic Pulp & Paper Research Journal 23(3): 299-304 (2008).
55. Fao, "Pulp and paper capacities, 2011–2016", from <http://www.fao.org/> (2014).
56. Favier, Canova, et al., "Nanocomposite materials from latex and cellulose whiskers", Polymers for Advanced Technologies 6(5): 351-355 (1995).
57. Ferraz, Strømme, et al., "In vitro and in vivo toxicity of rinsed and aged nanocellulose–polypyrrole composites", Journal of Biomedical Materials Research Part A 100A(8): 2128-2138 (2012).
58. Filson and Dawson-Andoh, "Sono-chemical preparation of cellulose nanocrystals from lignocellulose derived materials", Bioresource Technology 100(7): 2259-2264 (2009).

59. Fukuzumi, Saito, et al., "Transparent and High Gas Barrier Films of Cellulose Nanofibers Prepared by TEMPO-Mediated Oxidation", Biomacromolecules 10(1): 162-165 (2008).
60. Gane, Schenker, et al., "Process for production of nano-fibrillar cellulose gel composites for wide variety of applications", Omya, EP2386683A1 (2011).
61. Gane, Schoelkopf, et al., "Process for the production of nano-fibrillar cellulose suspensions", Omya, WO2010112519A1 (2010).
62. Glover and Whitney, "Structural colour and iridescence in plants: the poorly studied relations of pigment colour", Annals of Botany 105(4): 505-511 (2010).
63. Gohel and Jogani, "A review of co-processed directly compressible excipients", J Pharm Pharm Sci 8(1): 76-93 (2005).
64. Gousse, Chanzy, et al., "Stable suspensions of partially silylated cellulose whiskers dispersed in organic solvents", Polymer 43(9): 2645-2651 (2002).
65. Gray, "Chiral nematic ordering of polysaccharides", Carbohydrate Polymers 25(4): 277-284 (1994).
66. Guezennec, "Développement de nouveaux matériaux d'emballage à partir de micro-et nano-fibrilles de cellulose", PhD Thesis, Université de Grenoble (2012).
67. Hamada, Beckvermit, et al., "Nanofibrillated Cellulose with Fine Clay as a Coating Agent to Improve Print Quality", presented at PaperCon 2010 Conference, Atlanta, USA (2010).
68. Hamada and Bousfield, "Nanofibrillated cellulose as a coating agent to improve print quality of synthetic fiber sheets", Tappi Journal 9: 25-29 (2010).
69. Hamann, "Wet-End Applications of NFC", presented at SUNPAP Workshop, Espoo, Finland (2011).
70. Han and Rowell, "Chemical composition of fibers", Paper composites from agro-based resources: 83-134 (1997).
71. Hassan, Hassan, et al., "Improving bagasse pulp paper sheet properties with microfibrillated cellulose isolated from xylanase-treated bagasse", Wood and Fiber Science 43(1): 76-82 (2011).
72. Hasunuma and Nishikata, "Ink-jet recording sheet containing cellulose", Panatsuku, JP09020067A (1997).
73. Haworth, Hirst, et al., "The Existence of the Cellobiose Residue in Cellulose", Nature 126: 438 (1930).
74. Heath and Thielemans, "Cellulose nanowhisker aerogels", Green Chemistry 12(8): 1448-1453 (2010).
75. Heiskanen, Axrup, et al., "Process for the production of a paper or board product and a paper or board produced according to the process", Stora Enso, WO2011056135A1 (2011).
76. Heiskanen and Backfolk, "A process for the production of a composition comprising fibrillated cellulose and a composition", Stora Enso, WO2011141877A1 (2011).
77. Heiskanen, Backfolk, et al., "Coated substrate with reduced water vapor transmission, comprising a cellulose fiber substrate coated with a polymer latex containing cellulose microfibrils and manufacture thereof and a package therefrom and a dispersion coating therefor", Stora Enso Oyj, Finland . WO2011056130A1 (2011).
78. Helbert, Cavaille, et al., "Thermoplastic nanocomposites filled with wheat straw cellulose whiskers. Part I: processing and mechanical behavior", Polymer composites 17(4): 604-611 (1996).

79. Helmer, Karppinen, et al., "Curtain vs. blade coating: Experience in board application", Paper technology 46(6): 37-42 (2005).
80. Henriksson, Berglund, et al., "Cellulose nanopaper structures of high toughness", Biomacromolecules 9(6): 1579-1585 (2008).
81. Henriksson, Henriksson, et al., "An environmentally friendly method for enzyme-assisted preparation of microfibrillated cellulose (MFC) nanofibers", European Polymer Journal 43(8): 3434-3441 (2007).
82. Herranen and Lohman, "Anti-inflammatory effect of microfibrillated cellulose for treatment of skin disorders", UPM-Kymmene, WO2012107648A1 (2012).
83. Herrick, Casebier, et al., "Microfibrillated cellulose: morphology and accessibility", Journal of applied polymer science 37: 797-813 (1983).
84. Heux, Chauve, et al., "Nonflocculating and Chiral-Nematic Self-ordering of Cellulose Microcrystals Suspensions in Nonpolar Solvents", Langmuir 16(21): 8210-8212 (2000).
85. Hirai, Inui, et al., "Phase Separation Behavior in Aqueous Suspensions of Bacterial Cellulose Nanocrystals Prepared by Sulfuric Acid Treatment", Langmuir 25(1): 497-502 (2009).
86. Holik, "Handbook of paper and board", edited by John Wiley & Sons (2006).
87. Hon, "Cellulose: a random walk along its historical path", Cellulose 1(1): 1-25 (1994).
88. Hook, Moretti, et al., "Building bridges: binder-pigment composites enhance opacity of emulsion paints", Eur. Coat. J.: 29-33 (2012).
89. Hu, Choi, et al., "Highly conductive paper for energy-storage devices", Proceedings of the National Academy of Sciences 106(51): 21490-21494 (2009).
90. Hua, Carlsson, et al., "Translational study between structure and biological response of nanocellulose from wood and green algae", Rsc Advances 4(6): 2892-2903 (2014).
91. Hubbe, Pawlak, et al., "*Paper's appearance: A review*", BioResources 3(2): 627-665 (2008).
92. Hult, Iotti, et al., "Efficient approach to high barrier packaging using microfibrillar cellulose and shellac", Cellulose 17(3): 575-586 (2010).
93. Husband and Hiorns, "The Trend towards Low Impact Coating of Paper and Board", presented at The 6th European Coating Symposium proceeding(2005).
94. Husband, Svending, et al., "Filled and coated paper comprising microfibrillated cellulose and inorganic particulate material", Imerys Minerals Limited, UK . WO2012066308A2 (2012).
95. Husband, Svending, et al., "Paper filler composition", Imerys Minerals Limited, WO2010131016A2 (2010).
96. Iotti, Gregersen, et al., "Rheological Studies of Microfibrillar Cellulose Water Dispersions", Journal of Polymers and the Environment 19(1): 137-145 (2011).
97. Isogai, Saito, et al., "TEMPO-oxidized cellulose nanofibers", Nanoscale 3(1): 71-85 (2011).
98. Iwamoto, Abe, et al., "The Effect of Hemicelluloses on Wood Pulp Nanofibrillation and Nanofiber Network Characteristics", Biomacromolecules 9(3): 1022-1026 (2008).
99. Iwamoto, Kai, et al., "Elastic Modulus of Single Cellulose Microfibrils from Tunicate Measured by Atomic Force Microscopy", Biomacromolecules 10(9): 2571-2576 (2009).

100. Jabbour, Chaussy, et al., "Method for preparing flexible self-supported electrodes", Grenoble INP, EP2764566A1 (2014).
101. Jackson, Letchford, et al., "The use of nanocrystalline cellulose for the binding and controlled release of drugs", International journal of nanomedicine 6(1): 321-330 (2011).
102. Jia, Li, et al., "Effect of microcrystal cellulose and cellulose whisker on biocompatibility of cellulose-based electrospun scaffolds", Cellulose 20(4): 1911-1923 (2013).
103. Jivraj, Martini, et al., "An overview of the different excipients useful for the direct compression of tablets", Pharmaceutical science & technology today 3(2): 58-63 (2000).
104. Johansson, Bras, et al., "Renewable fibers and bio-based materials for packaging applications - A review of recent developments", Bioresources 7(2): 2506-2552 (2012).
105. Jonoobi, Mathew, et al., "Producing low-cost cellulose nanofiber from sludge as new source of raw materials", Industrial Crops and Products 40(0): 232-238 (2012).
106. Kangas, Pohler, et al., "Development of the mechanical pulp fibre surface as a function of refining energy", Journal of Pulp and Paper Science 30(11): 298-306 (2004).
107. Kettunen, Silvennoinen, et al., "Photoswitchable Superabsorbency Based on Nanocellulose Aerogels", Advanced Functional Materials 21(3): 510-517 (2011).
108. Khandelwal and Windle, "Self-assembly of bacterial and tunicate cellulose nanowhiskers", Polymer 54(19): 5199-5206 (2013).
109. Khwaldia, Arab-Tehrany, et al., "Biopolymer coatings on paper packaging materials", Comprehensive Reviews in food science and food safety 9(1): 82-91 (2010).
110. Kinoshita and Yoshioka, "Structural Colors in Nature: The Role of Regularity and Irregularity in the Structure", ChemPhysChem 6(8): 1442-1459 (2005).
111. Klemm, Heublein, et al., "Cellulose: Fascinating Biopolymer and Sustainable Raw Material", ChemInform 36(36): no-no (2005).
112. Klemm, Schumann, et al., "Nanocellulose Materials – Different Cellulose, Different Functionality", Macromolecular Symposia 280(1): 60-71 (2009).
113. Koga and Hattori, "Nonwood pulp-based paper containing microfibrillated cellulose for tea bags", Oji Paper Co., Ltd., Japan . JP09195194A (1997).
114. Kondo, Morita, et al., "Wet pulverizing of polysaccharides", Shin-Etsu Chemical Co, US 7357339 (2008).
115. Köpcke, "Improvement on cellulose accessibility and reactivity of different wood pulps", (2008).
116. Kose, Mitani, et al., "“Nanocellulose” As a Single Nanofiber Prepared from Pellicle Secreted by *Gluconacetobacter xylinus* Using Aqueous Counter Collision", Biomacromolecules 12(3): 716-720 (2011).
117. Kovacs, Naish, et al., "An ecotoxicological characterization of nanocrystalline cellulose (NCC)", Nanotoxicology 4(3): 255-270 (2010).
118. Kümmerer, Menz, et al., "Biodegradability of organic nanoparticles in the aqueous environment", Chemosphere 82(10): 1387-1392 (2011).

- 119.Laine, Oesterberg, et al., "Method for producing furnish and paper by treatment with cationic polyelectrolyte and nanofibrillated cellulose", Upm-Kymmene Corporation, WO2010125247A2 (2010).
- 120.Lavoine, Desloges, et al., "Microfibrillated cellulose - Its barrier properties and applications in cellulosic materials: A review", Carbohydrate Polymers 90(2): 735-764 (2012).
- 121.Lavoine, Desloges, et al., "Microfibrillated cellulose – Its barrier properties and applications in cellulosic materials: A review", Carbohydrate Polymers 90(2): 735-764 (2012).
- 122.Lehtinen, "Book 11: Pigment coating and surface sizing of paper", edited by Fapet Oy (2000).
- 123.Leung, Hrapovic, et al., "Characteristics and Properties of Carboxylated Cellulose Nanocrystals Prepared from a Novel One-Step Procedure", Small 7(3): 302-305 (2011).
- 124.Li, Tian, et al., "Paper-Based Microfluidic Devices by Plasma Treatment", Analytical Chemistry 80(23): 9131-9134 (2008).
- 125.Liu and Berglund, "Clay nanopaper composites of nacre-like structure based on montmorillonite and cellulose nanofibers—Improvements due to chitosan addition", Carbohydrate Polymers 87(1): 53-60 (2012).
- 126.Liu and Berglund, "Fire-retardant and ductile clay nanopaper biocomposites based on montmorillonite in matrix of cellulose nanofibers and carboxymethyl cellulose", European Polymer Journal 49(4): 940-949 (2013).
- 127.Liu, Walther, et al., "Clay Nanopaper with Tough Cellulose Nanofiber Matrix for Fire Retardancy and Gas Barrier Functions", Biomacromolecules 12(3): 633-641 (2011).
- 128.Luong, Male, et al., "Cellulose nanocrystals from renewable biomass", National Research Council of Canada, EP2513149A1 (2011).
- 129.Luu, Bousfield, et al., "Application of Nano-Fibrillated Cellulose as a Paper Surface Treatment for Inkjet Printing", presented at TAPPI PaperCon Conference, Atlanta, USA (2011).
- 130.Madani, Kiiskinen, et al., "Fractionation of microfibrillated cellulose and its effects on tensile index and elongation of paper", Nordic Pulp & Paper Research Journal 26(3): 306-311 (2011).
- 131.Mahmoud, Mena, et al., "Effect of surface charge on the cellular uptake and cytotoxicity of fluorescent labeled cellulose nanocrystals", ACS Applied Materials & Interfaces 2(10): 2924-2932 (2010).
- 132.Malmborg, Heijnesson-Hulten, et al., "Cellulosic barrier composition comprising anionic polymer for self-supporting films or coatings over permeable paper substrates", Akzo Nobel Chemicals International B.V., Neth. . WO2011147823A1 (2011).
- 133.Manninen, Kajanto, et al., "The effect of microfibrillated cellulose addition on drying shrinkage and dimensional stability of wood-free paper", Nord. Pulp Pap. Res. J. 26: 297-305 (2011).
- 134.Marchessault, Morehead, et al., "Liquid Crystal Systems from Fibrillar Polysaccharides", Nature 184(4686): 632-633 (1959).
- 135.Martins, Freire, et al., "Electrostatic assembly of Ag nanoparticles onto nanofibrillated cellulose for antibacterial paper products", Cellulose 19(4): 1425-1436 (2012).
- 136.Matsuda and Ueno, "Manufacture of powder-containing paper", Tokushu Seishi Kk, Japan . JP08081896A1 (1996).
- 137.McGuffog, "Microvoid calcined clay for improved opacity: A new type of calcined clay for the coatings market", European coatings journal(4): 143-147 (2003).

138. McIntyre, "Common nano-materials and their use in real world applications", Science progress 95(1) (2012).
139. Mendez, Annamalai, et al., "Bioinspired Mechanically Adaptive Polymer Nanocomposites with Water-Activated Shape-Memory Effect", Macromolecules 44(17): 6827-6835 (2011).
140. Miller, "Nanocellulose: Technology Applications, and Markets", presented at TAPPI International Conference on Nanotechnology, Vancouver, Canada (2014).
141. Missoum, Martoia, et al., "Effect of chemically modified nanofibrillated cellulose addition on the properties of fiber-based materials", Industrial Crops and Products 48(0): 98-105 (2013).
142. Montanari, Roumani, et al., "Topochemistry of Carboxylated Cellulose Nanocrystals Resulting from TEMPO-Mediated Oxidation", Macromolecules 38(5): 1665-1671 (2005).
143. Morseburg and Chinga-Carrasco, "Assessing the combined benefits of clay and nanofibrillated cellulose in layered TMP-based sheets", Cellulose 16(5): 795-806 (2009).
144. Nakagaito and Yano, "Novel high-strength biocomposites based on microfibrillated cellulose having nano-order-unit web-like network structure", Applied Physics a-Materials Science & Processing 80(1): 155-159 (2005).
145. Nguyen, Hamad, et al., "Tuning the iridescence of chiral nematic cellulose nanocrystals and mesoporous silica films by substrate variation", Chem. Commun. 49(96): 11296-11298 (2013).
146. Ni, Zeng, et al., "Cellulose nanowhiskers: Preparation, characterization and cytotoxicity evaluation", Bio-medical materials and engineering 22(1): 121-127 (2012).
147. Noe, Chevalier, et al., "Action of xylanases on chemical pulp fibers part II: Enzymatic beating", Journal of wood chemistry and technology 6(2): 167-184 (1986).
148. Norppa, "Nanofibrillated cellulose: results of in vitro and in vivo toxicological assays", presented at SUNPAP Final Conference, Milan, Italia (2012).
149. Nuopponen, Paeivaelaeninen, et al., "Method for manufacturing nanofibrillated cellulose pulp for use in paper products and nanofibrillated cellulose composites", UPM-Kymmene Corporation, Finland . WO2011064441A1 (2011).
150. Nygård, "Nanocellulose in pigment coatings: Aspects of barrier properties and printability in offset", PhD Thesis, Linköping University (2011).
151. O'sullivan, "Cellulose: the structure slowly unravels", Cellulose 4(3): 173-207 (1997).
152. Okiyama, Motoki, et al., "Bacterial cellulose IV. Application to processed foods", Food hydrocolloids 6(6): 503-511 (1993).
153. Onsager, "THE EFFECTS OF SHAPE ON THE INTERACTION OF COLLOIDAL PARTICLES", Annals of the New York Academy of Sciences 51(4): 627-659 (1949).
154. Orsenna, "Sur la route du papier: petit précis de mondialisation III", edited by Stock (2012).
155. Pääkkö, Ankerfors, et al., "Enzymatic Hydrolysis Combined with Mechanical Shearing and High-Pressure Homogenization for Nanoscale Cellulose Fibrils and Strong Gels", Biomacromolecules 8(6): 1934-1941 (2007).
156. Pajari, Rautkoski, et al., "Replacement of synthetic binders with nanofibrillated cellulose in board coating : pilot scale studies", presented at TAPPI International Conference on Nanotechnology, Canada, Montreal (2012).

157. Pan, Hamad, et al., "Parameters Affecting the Chiral Nematic Phase of Nanocrystalline Cellulose Films", *Macromolecules* 43(8): 3851-3858 (2010).
158. Papier and Gericke, "Nanofibrillated Cellulose in High-quality Inkjet Coating", presented at SUNPAP Final Conference, Milan, Italia (2012).
159. Park, Baker, et al., "Cellulose crystallinity index: measurement techniques and their impact on interpreting cellulase performance", *Biotechnology for Biofuels* 3(1): 1-10 (2010).
160. Pira, "Getting out of the Commodity Trap: 4 steps to success in specialty papers", from <http://downloads.pira-international.com/success-in-specialty-papers-white-paper/> (2014).
161. Pitkänen, Kangas, et al., "Toxicity and Health Issues", *Handbook of Green Materials*: 181-205, edited by World Scientific (2014).
162. Plastics-Europe, "Plastics – the Facts 2013 ", from www.plasticseurope.org (2013).
163. Puisto, Illa, et al., "Modeling the rheology of nanocellulose suspensions", *Nordic Pulp and Paper Research Journal* 27(2): 277 (2012).
164. Qian and Hinestroza, "Application of nanotechnology for high performance textiles", *Journal of textile and apparel, technology and management* 4(1): 1-7 (2004).
165. Qin, Tong, et al., "Preparation of ultrasonic-assisted high carboxylate content cellulose nanocrystals by TEMPO oxidation", *Bioresources* 6(2): 1136-1146 (2011).
166. Ranby, "Aqueous colloidal solutions of cellulose micelles", *Acta Chem. Scand. (1947-1973)* 3: 649-650 (1949).
167. Rehman, Miranda, et al., "Cellulose and Nanocellulose from Maize Straw: An Insight on the Crystal Properties", *Journal of Polymers and the Environment* 22(2): 252-259 (2014).
168. Retulainen, Nieminen, et al., "Enhancing strength properties of Kraft and CTMP fiber networks", *Appita Journal* 46(1): 33-38 (1993).
169. Revol, Bradford, et al., "Helicoidal self-ordering of cellulose microfibrils in aqueous suspension", *International Journal of Biological Macromolecules* 14(3): 170-172 (1992).
170. Revol, Godbout, et al., "Chiral nematic suspensions of cellulose crystallites; phase separation and magnetic field orientation", *Liquid Crystals* 16(1): 127-134 (1994).
171. Revol, Godbout, et al., "Solidified liquid crystals of cellulose with optically variable properties", *Pulp and Paper Research Institute of Canada*, WO9521901A1 (1995).
172. Revol, J.-F., et al., "Solid self-assembled films of cellulose with chiral nematic order and optically variable properties", *Tappi Journal* 24(5) (1998).
173. Ridgway and Gane, "Constructing NFC-pigment composite surface treatment for enhanced paper stiffness and surface properties", *Cellulose* 19(2): 547-560 (2012).
174. Rodionova, Lenes, et al., "Surface chemical modification of microfibrillated cellulose: improvement of barrier properties for packaging applications", *Cellulose* 18(1): 127-134 (2011).
175. Rodionova, Saito, et al., "Mechanical and oxygen barrier properties of films prepared from fibrillated dispersions of TEMPO-oxidized Norway spruce and Eucalyptus pulps", *Cellulose*: 1-7 (2012).
176. Rodriguez, Battle, et al., "The use of natural essential oils as antimicrobial solutions in paper packaging. Part II", *Progress in Organic Coatings* 60(1): 33-38 (2007).

177. Roman and Winter, "Effect of Sulfate Groups from Sulfuric Acid Hydrolysis on the Thermal Degradation Behavior of Bacterial Cellulose", *Biomacromolecules* 5(5): 1671-1677 (2004).
178. Rouhiainen, Väänänen, et al., "Risk assessment of nanofibrillated cellulose in occupational settings", presented at SUNPAP Final Conference, Milan, Italia (2012).
179. Sadeghifar, Filpponen, et al., "Production of cellulose nanocrystals using hydrobromic acid and click reactions on their surface", *Journal of Materials Science* 46(22): 7344-7355 (2011).
180. Saito, Kimura, et al., "Cellulose Nanofibers Prepared by TEMPO-Mediated Oxidation of Native Cellulose", *Biomacromolecules* 8(8): 2485-2491 (2007).
181. Saito, Nishiyama, et al., "Homogeneous Suspensions of Individualized Microfibrils from TEMPO-Catalyzed Oxidation of Native Cellulose", *Biomacromolecules* 7(6): 1687-1691 (2006).
182. Samain and Stinga, "Procédé et dispositif de traitement par greffage chromatogénique d'un substrat hydroxyle", WO2013093113A3 (2013).
183. Sangl, Auhorn, et al., "Surface Sizing and Coating", *Handbook of Paper and Board*: 745-784, edited by Wiley-VCH Verlag GmbH & Co. KGaA (2013).
184. Sassi and Chanzy, "Ultrastructural aspects of the acetylation of cellulose", *Cellulose* 2(2): 111-127 (1995).
185. Shopsowitz, Hamad, et al., "Flexible and Iridescent Chiral Nematic Mesoporous Organosilica Films", *Journal of the American Chemical Society* 134(2): 867-870 (2011).
186. Sievänen, "Suitability of foam coating on application of thin liquid films", (2010).
187. Siqueira, Bras, et al., "Cellulosic Bionanocomposites: A Review of Preparation, Properties and Applications", *Polymers* 2(4): 728-765 (2010).
188. Siqueira, Bras, et al., "Luffa cylindrica as a lignocellulosic source of fiber, microfibrillated cellulose, and cellulose nanocrystals", *Bioresources* 5(2): 727-740 (2010).
189. Siró and Plackett, "Microfibrillated cellulose and new nanocomposite materials: a review", *Cellulose* 17(3): 459-494 (2010).
190. Siro, Plackett, et al., "Highly Transparent Films from Carboxymethylated Microfibrillated Cellulose: The Effect of Multiple Homogenization Steps on Key Properties", *Journal of Applied Polymer Science* 119(5): 2652-2660 (2011).
191. Sjöström, "Wood chemistry: fundamentals and applications", edited by Gulf Professional Publishing (1993).
192. Skogsindustrierna, "The worlds consumption of paper in 2012", from http://www.forestindustries.se/documentation/statistics_ppt_files/international/the-worlds-consumption-of-paper (2013).
193. Song, Ankerfors, et al., "Reduction of the linting and dusting propensity of newspaper using starch and microfibrillated cellulose", *Nord. Pulp Pap. Res. J.* 25: 495-504 (2010).
194. Sonnenfeld, "Social Movements and Ecological Modernization: The Transformation of Pulp and Paper Manufacturing", *Development and Change* 33(1): 1-27 (2002).
195. Spence, Venditti, et al., "The effect of chemical composition on microfibrillar cellulose films from wood pulps: Mechanical processing and physical properties", *Bioresource Technology* 101(15): 5961-5968 (2010).

196. Spence, Venditti, et al., "A comparative study of energy consumption and physical properties of microfibrillated cellulose produced by different processing methods", Cellulose 18(4): 1097-1111 (2011).
197. Stenstad, Andresen, et al., "Chemical surface modifications of microfibrillated cellulose", Cellulose 15(1): 35-45 (2008).
198. Stroobants, Lekkerkerker, et al., "Effect of electrostatic interaction on the liquid crystal phase transition in solutions of rodlike polyelectrolytes", Macromolecules 19(8): 2232-2238 (1986).
199. Sugihara, "Comparison of the Surface and Print Quality of Curtain and Blade Coated Papers", from <https://www.wmich.edu/pci/faculty/Publication/fleming/Volume%203-%20%20Paper%2016.pdf> (2007).
200. Svagan, Azizi Samir, et al., "Biomimetic Polysaccharide Nanocomposites of High Cellulose Content and High Toughness", Biomacromolecules 8(8): 2556-2563 (2007).
201. Syverud, Chinga-Carrasco, et al., "A comparative study of Eucalyptus and Pinus radiata pulp fibres as raw materials for production of cellulose nanofibrils", Carbohydrate Polymers 84(3): 1033-1038 (2011).
202. Syverud and Stenius, "Strength and barrier properties of MFC films", Cellulose 16(1): 75-85 (2009).
203. Taipale, "Interactions of Microfibrillated Cellulose and Cellulosic Fines with Cationic Polyelectrolytes", Doctoral dissertation, Aalto University (2010).
204. Taipale, Osterberg, et al., "Effect of microfibrillated cellulose and fines on the drainage of kraft pulp suspension and paper strength", Cellulose (Dordrecht, Neth.) 17(Copyright (C) 2012 American Chemical Society (ACS). All Rights Reserved.): 1005-1020 (2010).
205. Taipale, Österberg, et al., "Effect of microfibrillated cellulose and fines on the drainage of kraft pulp suspension and paper strength", Cellulose 17(5): 1005-1020 (2010).
206. Taniguchi and Okamura, "New films produced from microfibrillated natural fibres", Polymer International 47(3): 291-294 (1998).
207. Torvinen, Helin, et al., "Nano fibrillated cellulose as a strength additive in filler-rich SC paper", presented at 2011 TAPPI International Conference on Nanotechnology for Renewable Materials, Arlington, USA (2011).
208. Turbak, Snyder, et al., "Food products containing microfibrillated cellulose", International Telephone And Telegraph Corporation, US4341807 (1982).
209. Turbak, Snyder, et al., "Microfibrillated cellulose, a new cellulose product: properties, uses, and commercial potential", Journal of applied polymer science 37: 815-827 (1983).
210. Van Renesse (1997), "Paper based document security-a review". European Conference on Security and Detection. London, England.
211. Vartiainen, Pöhler, et al., "Health and environmental safety aspects of friction grinding and spray drying of microfibrillated cellulose", Cellulose 18(3): 775-786 (2011).
212. Vaswani, Koskinen, et al., "Surface modification of paper and cellulose by plasma-assisted deposition of fluorocarbon films", Surface and Coatings Technology 195(2): 121-129 (2005).
213. Vernhes, Bloch, et al., "Effect of calendering on paper surface micro-structure: A multi-scale analysis", Journal of Materials Processing Technology 209(11): 5204-5210 (2009).

214. Viet, Beck-Candanedo, et al., "Dispersion of cellulose nanocrystals in polar organic solvents", Cellulose 14(2): 109-113 (2007).
215. Vignolini, Rudall, et al., "Pointillist structural color in Pollia fruit", Proceedings of the National Academy of Sciences 109(39): 15712-15715 (2012).
216. Wada, Heux, et al., "Polymorphism of cellulose I family: reinvestigation of cellulose IVI", Biomacromolecules 5(4): 1385-1391 (2004).
217. Wagberg, Decher, et al., "The build-up of polyelectrolyte multilayers of microfibrillated cellulose and cationic polyelectrolytes", Langmuir 24(3): 784-795 (2008).
218. Whitney, Kolle, et al., "Floral Iridescence, Produced by Diffractive Optics, Acts As a Cue for Animal Pollinators", Science 323(5910): 130-133 (2009).
219. Who, "Safety Evaluation of Certain Food Additives and Contaminants", edited by WHO (2012).
220. Wong, Richardson, et al., "Enzymatic treatment of mechanical pulp fibers for improving papermaking properties", Biotechnology progress 16(6): 1025-1029 (2000).
221. Wu, Saito, et al., "Ultrastrong and High Gas-Barrier Nanocellulose/Clay-Layered Composites", Biomacromolecules 13(6): 1927-1932 (2012).
222. Ylva Wildlock, Anette Monica, et al., "Method of producing a paper product", Akzo Nobel, WO2008076056A1 (2008).
223. Yu, Qin, et al., "Facile extraction of thermally stable cellulose nanocrystals with a high yield of 93% through hydrochloric acid hydrolysis under hydrothermal conditions", J. Mater. Chem. A 1(12): 3938-3944 (2013).
224. Yun, Cho, et al., "Flow-Induced Liquid Crystalline Solutions Prepared from Aspect Ratio-Controlled Bacterial Cellulose Nanowhiskers", Molecular Crystals and Liquid Crystals 519(1): 141-148 (2010).
225. Zhang, Chodavarapu, et al., "Structured color humidity indicator from reversible pitch tuning in self-assembled nanocrystalline cellulose films", Sensors and Actuators B: Chemical(0) (2012).
226. Zimmermann, Bordeanu, et al., "Properties of nanofibrillated cellulose from different raw materials and its reinforcement potential", Carbohydrate Polymers 79(4): 1086-1093 (2010).
227. Zou and Hsieh, "Microfibrillated Cellulose for papermaking", presented at 2007 International Conference on Nanotechnology for the Forest Products Industry, Knoxville, USA (2007).

Chapter 2

**Cellulose nanofibrils as
dispersive network for
particles**

Table of contents

Introduction	107
1 Different strategies for obtaining high opacity films of Cellulose Nanofibrils with TiO₂ pigments.....	109
Abstract	109
1.1 Introduction	110
1.2 Experimental section	112
1.2.1 Materials	112
1.2.2 Methods.....	112
1.3 Results and discussion.....	115
1.3.1 Nanoparticle characterization: CNF and TiO ₂	115
1.3.2 Dispersion of TiO ₂ into CNF hybrid films.....	115
1.3.3 Comparison of CNF with other biobased polymer	117
1.3.4 Comparison of the different strategies for mixing TiO ₂	119
1.3.5 Comparison of the final properties of films	121
1.4 Conclusion and perspectives	125
2 Substitution of nanoclay in high gas barrier films of cellulose nanofibrils with cellulose nanocrystals and thermal treatment	127
Abstract	127
2.1 Introduction	128
2.2 Experimental section	130
2.2.1 Materials	130
2.2.2 Methods.....	131
2.3 Results and discussion.....	135
2.3.1 Nanocellulose characterization	135
2.3.2 Properties of neat and TEMPO-oxidized CNF films.....	137
2.3.3 Improvement of barrier properties of CNF film with nanofillers	138
2.3.4 Thermal treatment of CNF films.....	142
2.4 Conclusion and perspectives	146
Concluding remarks.....	147
List of Tables.....	149
List of figures	149
References	151

Chapter 2

Cellulose nanofibrils as dispersive network for particles

Introduction

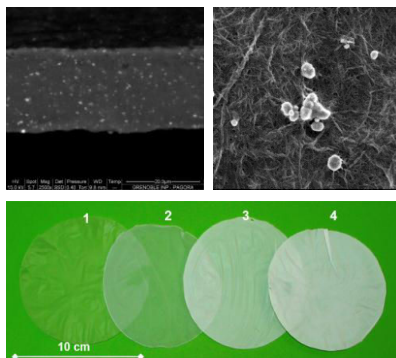
As detailed in the literature review (*Chapter 1*), CNF suspension exhibits gel-like behavior at even low concentrations (2%) with shear thinning properties. Because of hydrogen bonds and their flexibility, once dried, CNF forms a cohesive, dense, entangled network. This feature is investigated in *Chapter 2*, in which CNF will be used as an entangled nanofibril network for (i) replacing existing polymer in thin opaque films or (ii) substituting mineral nanoparticles in barrier materials.

In *Chapter 2.1*, three approaches for manufacturing thin opaque film based on TiO₂ dispersed in a CNF suspension are discussed. They consist of (i) a blend of CNF and TiO₂, (ii) a pre-mix in which TiO₂ particles are used to enhance the fibrillation of CNF, and (iii) a sol-gel process in which TiO₂ particles were directly generated onto the surface of CNF.

The present work proposes, for the first time, the development of the optimal conditions of preparing highly opaque films made of CNF and titanium oxide. The prepared materials have been evaluated in terms of opacity and mechanical resistance, and compared with other biobased matrices. From an industrial point of view, these strategies aim to create sustainable opaque specialty papers with an optimized amount of TiO₂. This is achieved by using CNF without a chemical dispersant, and is also a cost-effective measure

As compared to *Chapter 2.1*, *Chapter 2.2* is focused on the improvement of barrier properties of CNF films. To do so, neat or oxidized CNF was used as a matrix to create an entangled nanoporous network. Then, the CNF matrix was loaded with two different nanofillers: a nanoclay considered as a reference, i.e. mineral Montmorillonite (MMT) and biobased nanoparticles, i.e. oxidized CNC (CNC-T). The main features of the nanoparticles used in the study are reported. For the various films, barrier, optical and mechanical properties were investigated. Finally, a thermal treatment on dried films was proposed in order to reduce the water sensitivity of the films. The purpose of this study was to consider their application as a biobased barrier coating (without nanoclay) for packaging applications.

1 Different strategies for obtaining high opacity films of Cellulose Nanofibrils with TiO₂ pigments



This section is adapted from “Raphael Bardet, Naceur Belgacem, Julien Bras, Different strategies for obtaining high opacity films of MFC with TiO₂ pigments, Cellulose 20:3025-3037 (2013)”.

Abstract

The present study examines the production and characterization of opaque solid films made with cellulose nanofibrils (CNF) suspension and titanium dioxide (TiO₂) nanoparticles. Three different strategies were investigated: a blend of (i) CNF and TiO₂, (ii) a premix in which TiO₂ particles are used to favor the fibrillation step of CNF and (iii) a sol-gel process in which TiO₂ particles were directly generated onto the surface of CNF. The different process parameters have been optimized both for the production of CNF and for the sol-gel reaction. Gel suspensions containing different ratios of TiO₂ were morphologically and chemically characterized. In order to characterize the size and the nature of the particles, Diffraction Laser Scattering (DLS), Atomic Force Microscopy (AFM) were used while thermo Gravimetric Analysis (TGA) and X-Ray Diffraction (XRD) were used to investigate the degradation of CNF for all the three strategies. To highlight the level of dispersion of TiO₂ within the CNF network, Scanning Electron Microscopy (SEM) in BSE mode coupled with an adapted image treatment have been employed. Finally, the transparence and the mechanical properties of solid films were measured by UV spectrophotometry and tensile tests, respectively. Very good TiO₂ dispersion and high opacity CNF films have been achieved with a very low amount of TiO₂. Thus, the best approach that takes into account the easiest process for making the hybrids and leading to the high level of opacity with the lowest ratio of TiO₂ is the premix fibrillation.

Keywords: Cellulose nanofibrils, Hybrid nanomaterials, Titanium dioxide; Film opacity,

1.1 Introduction

The main properties of CNF are their intrinsic outstanding mechanical properties (4-15 GPa), high specific surface area (220 m²/g) and their high surface density of hydroxyl group (**Table 1.10**). For these reasons and thanks to hydrogen bonds that explain why a gel-like suspension is achieved at a very low concentration in water, once dried, CNF are entangled with each other to form an entanglement nanoporous network that looks like a solid, usually, transparent film (**Table 1.12**).

In some applications like food, packaging, the opacity is required to ensure light protection of the product and limit food spoilage. In this context, biobased packaging is expected to be a key candidate in such applications, which motivated us to undertake a study aiming at manufacturing of high opacity hybrid film.

As mentioned in the **Table 1.18**, among all the industrially used pigments, Titanium Dioxide (TiO₂) is one of the most efficient regarding its opacifying and covering effects (Nelson and Deng 2008). However, when TiO₂ particles are not well dispersed and agglomerated in any matrix, their light scattering zones overlap and reduce their opacifying effect. With the increasing interest about environmental concerns and due to the rising price of this geolocalized raw material, new solutions are expecting using biobased materials and limiting TiO₂ quantity.

To the best of our knowledge, the process of obtaining a mineral filler/CNF hybrid film has been studied very little and most studies were mainly devoted to barrier and mechanical properties using different biomimetic approaches such as nacles (Nypelö *et al.* 2011, Liu and Berglund 2012, Ridgway and Gane 2012, Wu *et al.* 2012). Since the beginning of the current decade, several innovations related to this concept have been patented by the filler suppliers or paper producers as summarized in **Table 1.15**. Initially, patents have been mainly developed in order to overcome the drawback of gel-like CNF suspension at a low solid content (Iotti *et al.* 2011, Saarikoski *et al.* 2012). This could cause several constrains regarding the process production and application (during mixing, pumping, and coating steps) and commercialization (cost efficiency). None of these studies have focused on the development high opacity CNF films.

Indeed, to the best of our knowledge, there is no reference in the literature dealing in which a combination of TiO₂ filler and CNF to produce opaque films. However, Schütz *et al.* (2012) have recently proposed to produce a hybrids composed of CNF and ex-situ anatase

TiO₂ in order to investigate a potential use for transparent coatings with a good abrasion resistance and photocatalytic UV activity. Schütz *et al.* (2012)

For the production of a CNF/filler hybrid suspension, several strategies can be tested. The first one consists of fibrillating the cellulose fibers directly with abrasive fillers, (Gane *et al.* 2010, Husband *et al.* 2010), whereas the second deals with adding the inorganic materials after the fibrillation. (Laine *et al.* 2010, Berglund and Liu 2011)

Another approach exists taking into account that cellulosic fibers can act as efficient hydrophilic substrates for the nucleation and growth of inorganic particles in aqueous medium. (Barata *et al.* 2005, Vilela *et al.* 2010)

In a similar way, Marques *et al.* (2006) have investigated the way of *in situ* generation of TiO₂ in the presence of the cellulose fibers. However, this innovative strategy has never been adapted to CNF.

The present work proposes, for the first time, the determination of the optimal conditions of preparing highly opaque films made of CNF and titanium oxide. Three strategies have been tested and compared: (i) a blend of CNF and TiO₂, (ii) a premix in which TiO₂ particles are used as a fibrillation aid of CNF and (iii) a sol-gel process in which TiO₂ were directly generated onto the CNF surface. The prepared materials have been evaluated in terms of opacity and mechanical resistance and compared with other biobased matrices.

1.2 Experimental section

1.2.1 Materials

Titanium Dioxide (TiO₂) powders are two commercial grades with two different polymorphisms, a rutile TiO₂ (Tiona©, Millennium Chemicals, England) and an anatase TiO₂ (Ti-Pure®RPS Vantage®, Dupont, USA). Their average diameter D₅₀ measured by laser granulometry (1190 Particle Size Analyzer®, Cilas, France) are D₅₀=0.37±0.07 μm and 0.40±0.05 μm for rutile and anatase, respectively. Hydrated Titanium (IV) Oxysulphate (Sigma-Aldrich, France) was used as precursor for the sol-gel reaction. Commercial organic binders used were potato starch (Perfectafilm®, Avebe, Holland), sodium carboxymethylcellulose (Blanose® Cellulose Gum, Ashland, USA) and Polyvinyl alcohol (Mowiol® 28-99, Kuraray, Japan). Potato starch, CMC and PVOH were cooked and stored according to the supplier recommendations. Deionized water was used in all experiments.

1.2.2 Methods

CNF production. CNF was prepared from a dried commercial sulphite softwood-dissolving pulp (Domsjö Cellulose Plus®, Domsjö, Sweden) using disintegration, enzymatic pretreatment and fine grinding treatment. First, the pulp suspension (10% w:w) was beaten in a PFI mill until 60 000 revolutions. The resulting suspensions were incubated during 2h at 50°C and buffered with sodium acetate/acetic acid at a pH=5. The enzyme used was a monocomponent endoglucanase (Celluclast 1.5L®, Sigma-Aldrich, France) with an enzymatic activity of 700 ECU/g. Finally, the mixtures were diluted with deionized water to a 2.5 wt % consistency, and then passed through an ultra-fine grinder (Supermasscolloider MKCA6-2®, MASUKO SANGYO CO, LTD, Japan). The suspensions were passed 60 times between a static and a rotating silicon carbides grindstones (MKG-C/46#, MASUKO SANGYO CO, LTD, Japan) with a gap corresponding to the 0-motion point and at a rotating speed of 1500 rpm. At the end of the production, a small quantity of Chloroform (0.01 wt %) was added to the suspension to prevent microbial growth during storage at 4 °C.

Preparation of CNF & TiO₂ hybrid suspensions. The blend of hybrid CNF (approach 1) was prepared by mixing with a homogenizer (UltraTurrax T8®, IKA, France) abrasive TiO₂ particles with the CNF suspension at 10 000 rpm for 5 minutes. The dry content of the suspension thus obtained was adjusted to 2.5 wt %. The protocol of the premix (approach 2) was adapted from the initial protocol for CNF. Thus, TiO₂ powder was added before the suspension fibrillation with the ultra-fine grinder. The consistency of the obtained suspension was adjusted to 2.5 wt % and ground under the same operation parameters. The sol-gel reaction (approach 3) was performed in CNF suspension in order to generate 20 wt % of TiO₂ particles onto the CNF surface. The sol-gel reaction was carried out in a 5L glass flask, where 67.1 g of precursor (Titanium Oxysulphate) was dissolved with 3000 g of the never-dried CNF suspension. The amount of the precursor was set at 0.74 g per gram of dried CNF. The mixture was heated at 50°C under constant mechanical stirring at 500 rpm for 100 minutes. Then, the hybrid suspension was washed following at least three successive centrifugations at 400 Rotation Centrifugal Force and 10°C for 10 minutes, in order to remove the residual sulfuric acid and the precursor. The dry content of the suspension thus obtained were adjusted to 2.5 wt %

Nanoparticle characterization. Individual nanoparticles were imaged using Atomic Force Microscope, AFM, (Nanoscope III®, Veeco, Canada). All samples were previously diluted at 10⁻⁴ wt % and a drop of 0.2 ml was deposited onto freshly cleaved Mica substrates and dried overnight under room conditions. Each sample was characterized in tapping mode with a silicon cantilever (OTESPA®, Bruker, USA) at four different locations and two different scanning areas: 10x10 μm² and 3x3 μm². Both topographical and phase images were captured and images were subjected to 1st order polynomial flattening to reduce the effects of bowing and tilt. Dynamic Light Scattering (DLS) was used to measure the size of in situ nanoparticles (Vasco® I, Corduan Technologies, France). All the samples were previously diluted in DI water at 10⁻² wt %. The analysis mode is the cumulative method and two parameters were taken into account, namely: the average size (z*) and the polydispersity index (PDI). For each sample, 10 acquisitions were performed and each measurement was replicated 3 times.

Hybrid films characterization. Before characterization, the films were conditioned in a constant temperature and humidity chamber kept at 25°C with 50% of relative humidity, for at least 48 h. E-SEM (Environmental Scanning Electron Microscope) in backscattered electron mode (BSE) was used (Quanta 200©, FEI, Japan). Pictures were then treated using image treatment software (ImageJ©, NIMH, USA). The films were previously conditioned and coated with gold/palladium and observed using an applied tension of 15 kV. The cross-section pictures were obtained by a cryofracture of dried hybrid films with liquid nitrogen. The thicknesses of the films were determined from the cross-section pictures of E-SEM micrographs. For each film, 12 measurements were performed at four different locations whereas the basis weight was evaluated using ISO-536:1995 standard. The film density was calculated by dividing the basis weight by the film thickness. Film transparency was estimated with a UV spectrophotometer (UV 1800®, Shimadzu, Japan). The absorption of the solid film has been measured at a wavelength of 550 nm that corresponds to the maximum wavelength absorption peak of TiO₂. For each sample, 3 different measurements and 10 scans have been recorded. The mechanical properties of the films were measured using universal testing machine (Model 4465®, Instron Engineering Corporation, US). The evaluation of the Young's modulus, tensile strength and the elongation were established following the ISO-1924-2:2008 standard. For each film, six specimens with a 15 mm in width and 50 mm in length have been submitted to a 20 mm/min constant speed of elongation. All mechanical tests have been repeated 6 times for each sample. FE-SEM (Field-Emission Scanning Electron Microscope) was used to observe the nanostructure of the surface of hybrid films (Ultra 55 ©, Zeiss, Germany). The films were covered with carbon tape and coated with a 2 nm layer of gold/palladium to ensure the conductivity of all samples. The accelerating voltage (EHT) was 3 kV for a working distance of 6.4 mm. The thermal degradation of cellulosic samples was monitored by TGA (thermo-gravimetric analyzer-STA 6000®, Perkin Elmer Instruments, England). The weight loss and heat flow curves were recorded for a 30 mg sub-sample at a heating rate of 10 C/min in the temperature range of 30–950 C under oxidizing atmosphere (air). For TG analysis, the experiment have been duplicated and averaged. The X-ray diffraction (XRD) patterns were measured for hybrid films with X-ray diffractometer (PANanalytical®, X'Pert PRO MPD). The operating conditions for the refractometer were Cu,K α radiation (1.5418 Å), 2 θ Bragg angle between 5 and 60°, step size of 0.067°, and a counting time of 90s. The cellulose crystallinity index (CI) was evaluated using empirical method developed by Segal and coworkers (Segal *et al.* 1959). For each XRD patterns, the experiments have been duplicated and then averaged.

1.3 Results and discussion

1.3.1 Nanoparticle characterization: CNF and TiO₂

After refining, enzymatic pretreatment and fine grinding process, cellulose nanofibrils (CNF) gel suspensions were achieved. The characterization of this material is a key challenge because it makes easy the comparison with other elements reported in several scientific papers and could rationalize the obtained results (both mechanical and optical). Indeed the term CNF still includes a large range of materials with different dimensions and heterogeneity as reported by Klemm *et al.* (2009).

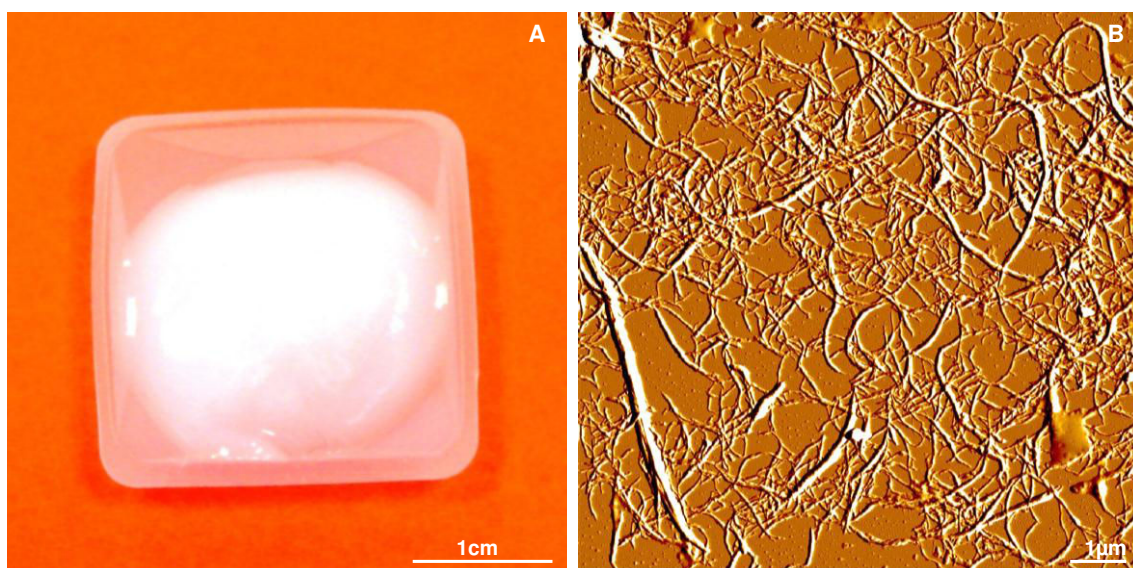


Fig 2.1 - Characterization of the CNF. Picture A corresponds to the gel-like suspension of CNF at 2.5% of consistency whereas Picture B corresponds to the same suspension observed through AFM at a scanning area of $10 \times 10 \mu\text{m}^2$ in TAPPING mode (Amplitude error)

The uniformity and homogeneity of CNF has been visually checked thanks to gel like structure of the suspension (**Fig 2.1-A**) indicating the absence of microscopic cellulosic fibers. In our case, the diameter dimension has been calculated from the average CNF thickness of AFM pictures (**Fig 2.1-B**) and a value of $45 \pm 15 \text{nm}$ was obtained, which is in agreement with recently available literature (Lavoine *et al.* 2012).

1.3.2 Dispersion of TiO₂ into CNF hybrid films

The main target of this study is to obtain opaque films with the lowest amount of opacifying mineral particles. As shown in **Fig 2.2**, it has been found that, when TiO₂ particles are simply mixed with a CNF suspension (approach 1), the solid film thus obtained presents a very low transparency in comparison to the same film obtained without TiO₂ that can be assimilated as a homogenous and transparent film.

It is assumed that the difference in opacity of two films is mainly due to the well-known difference of refractive index (RI) between TiO_2 (RI=2.55-2.73) and cellulose (RI=1.53).

The opacifying effect is proportional to the difference between the refractive index of the pigment and the medium in which it is dispersed. That is one of the reasons that explain the TiO_2 opacity.

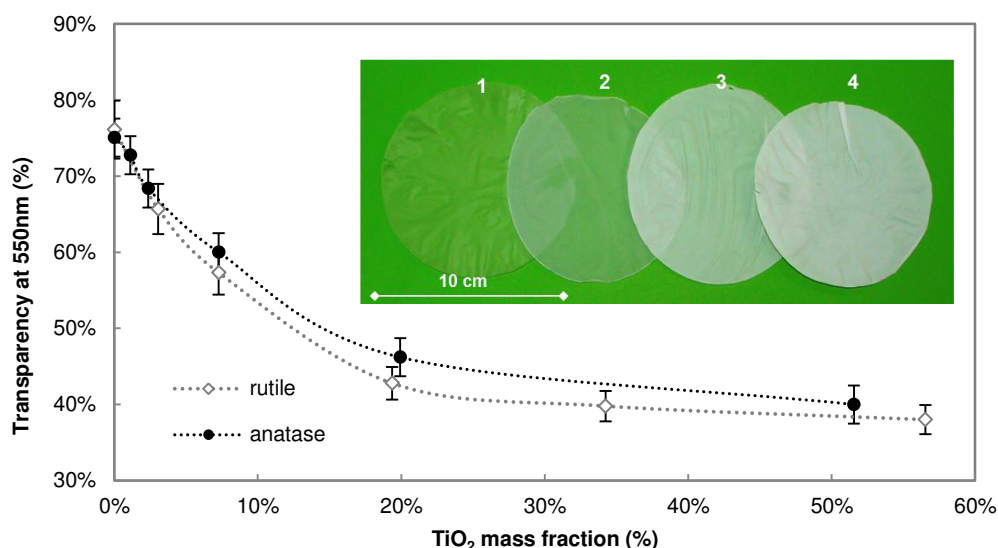


Fig 2.2 - Transparency of a 30g/m² CNF solid film as a function of the volume ratio of TiO_2 . Comparison between rutile (◇) and anatase (●) polymorphs. Pictures 1 to 4 corresponds to CNF films with an increasing amount of rutile TiO_2 (0%, 2%, 7% and 20%)

In order to establish the best range of TiO_2 for producing CNF hybrid films, the influence of the polymorphism type and the amount of TiO_2 on the film transparency has been performed, as presented in **Fig 2.2**. As expected, the transparency of film strongly decreases with the amount TiO_2 . However, the absorbance reaches a plateau value at a volume fraction of 20% of TiO_2 (41% w:w). Beyond 20%, TiO_2 particles are agglomerated and crowded which limits their light scattering properties.

In our experiments, a slight difference has been found between rutile and anatase starting from a 5 wt % content. This may come from a difference in mean diameter and refractive indices, i.e., 2.55 and 2.73, for anatase and rutile, respectively. Nevertheless, it assumed the difference could be considered negligible in this study due to the method used for the evaluation of the transparency. This is why, anatase particles have been chosen for the rest of this study because the sol-gel reaction generates only this polymorphic form (Kolen'ko *et al.* 2003). Moreover, such a solution is cost-effective.

The grey level contrast in E-SEM BSE (Back Scattering Electron) mode of cross-section of hybrid film (**Fig 2.3**) shows the chemical difference between the CNF network (organic) and TiO₂ particles (mineral).

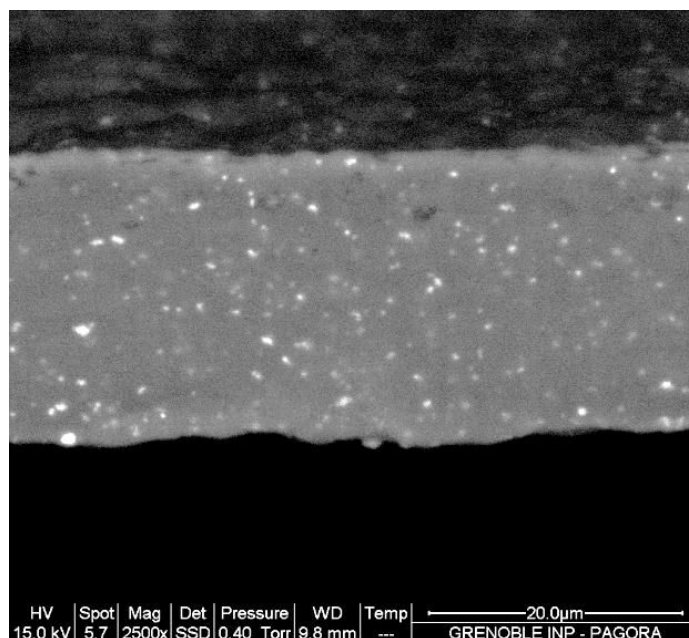


Fig 2.3 - E-SEM (BSE mode) of cross-sectional pictures of a CNF hybrid film (10% of TiO₂)

This highlights the excellent dispersion of mineral particles in the whole thickness of the film. It can be observed that TiO₂ particles are well distributed without sedimentation or agglomeration within the thickness of solid film. The absence of sedimentation and the excellent distribution of TiO₂ particles can be explained by the CNF gel-like structure when the suspensions are produced and their ability to form a nanoporous network that is able to well-disperse small particles such as those of TiO₂. Thus, these micrographs establish that mineral particles can be easily dispersed in a CNF medium to form an opaque solid film.

1.3.3 Comparison of CNF with other biobased polymer

To confirm the benefit of using CNF as a potential matrix for opaque film, the mechanical and optical properties have been compared to other classical matrix used in opacity applications such as PVOH, CMC and starch. The main results are reported in **Table 2.1**.

The mechanical resistance is generally higher for CNF whatever the ratio of TiO₂. By comparing the specific Young's modulus (by dividing E by the film density), CNF films are systematically stronger than those prepared from CMC (+6 to 20%) and PVOH (+19 to 36%) whereas films made of starch are 3 to 4 times weaker than those made of CNF. The results obtained for pure films are really close to the values given in the literature, i.e., Young

Modulus for CNF of about 15-20 MPa (Syverud and Stenius 2009, Plackett *et al.* 2010, Siro *et al.* 2011). Some differences between the values found in the literature could originate from the protocols used for producing CNF and for CNF solid films making and characterization

Table 2.1 - Main features of opaque films made with different matrices with 0, 20 and 50 % TiO₂.

Matrix	Ratio of TiO ₂ (wt %)	Density		Strain at break (%)		Force at break (kN/m)		Specific E Modulus (GPa)		Transparency (%)	
PVA	0	1.3	(0.1)	7.30	(0.20)	2.90	(0.03)	9.0	(0.7)	93.9	(1.3)
CMC		1.6	(0.3)	2.30	(0.07)	2.60	(0.05)	9.2	(1.3)	91.0	(1.2)
Starch		1.2	(0.0)	2.50	(0.03)	1.20	(0.05)	2.7	(0.4)	96.4	(0.8)
CNF		1.0	(0.2)	4.50	(0.03)	3.60	(0.06)	12.3	(1.0)	76.1	(1.2)
PVA	20	1.4	(0.1)	5.20	(0.19)	0.60	(0.10)	2.6	(0.5)	56.4	(0.5)
CMC		1.7	(0.2)	1.65	(0.06)	0.80	(0.10)	2.6	(0.1)	72.9	(0.5)
Starch		1.3	(0.2)	1.30	(0.15)	0.20	(0.00)	1.3	(0.0)	53.9	(1.5)
CNF		1.2	(0.2)	3.00	(0.10)	0.60	(0.05)	5.2	(0.0)	38.7	(0.3)
PVA	50	1.8	(0.1)	2.87	(0.10)	0.10	(0.01)	1.5	(0.8)	38.4	(0.7)
CMC		2.0	(0.3)	2.30	(0.22)	0.10	(0.03)	3.4	(0.3)	57.7	(2.3)
Starch		1.7	(0.3)								
CNF		1.6	(0.1)	2.30	(0.22)	0.20	(0.03)	3.6	(0.3)	30.8	(1.5)

Values into brackets refer to standard deviation

As expected, for high ratio of mineral particles (50% of TiO₂), a significant reduction for all mechanical properties is observed, because the introduction of TiO₂ particles create too many weak points in the film and limits hydrogen bonds. Such a phenomenon is more pronounced in the case of the force at break, which is divided by 10 when 50% TiO₂ is added. Such a dramatic decrease is because CNF films are nano-porous films contrary to other common polymer matrices.

Concerning the films transparency, which is the key parameters of this study, i.e., it was found that films made of CNF are systematically more opaque than the other ones. Only films filled with 20% of TiO₂, were highly opaque and a sharp drop (from 76% to 39%) of the transparency was measured, whereas for PVA-, CMC- and starch-based-films made with the same percentage of TiO₂, the transparency is still high. Moreover, even when increasing the amount of TiO₂ (up to 50%), the obtained films did not reach a similar low transparency. In other words, for producing opaque films with the same optical properties, 60 % of TiO₂ can be saved if PVA or CMC is replaced by CNF.

Such a feature is of high importance from industrial point of view, since such films would contain a lower quantity of TiO_2 and display at least the same the mechanical properties. Alternatively, a weight reduction of the film can be also envisaged. This confirms the impact of the nanofibril networks which enhances the good dispersion of TiO_2 .

1.3.4 Comparison of the different strategies for mixing TiO_2 with nanocellulose

Another target of this study was to check the influence of different strategies of producing CNF- TiO_2 films. As shown previously, CNF hybrid films promote the opacifying effect of TiO_2 and offering very good mechanical. However, with a process consideration and for further commercial application such as for packaging films or coating, the mixing process of TiO_2 must be optimized.

Fig 2.4 presents the three different approaches studied: (i) the blend of CNF and TiO_2 , (ii) the premix in which TiO_2 particles are used to favor the fibrillation step of CNF, and (iii) the sol-gel process in which TiO_2 were *in situ* generated onto the surface of CNF. As described in the experimental section, the blend and the premix strategies are similar regarding the production process

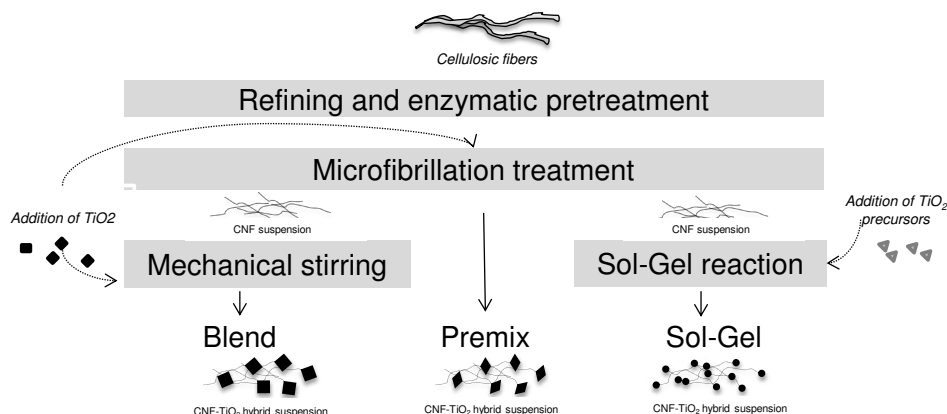


Fig 2.4 - Schematic representation of the 3 strategies used for CNF- TiO_2 hybrid films

However, the main benefit of premixing the suspension with abrasive fine particles is decreasing the number of treatment cycles thus leading to significant energy consumption saving. Indeed, the high abrasiveness of TiO_2 promotes the cellulosic fiber (micro)-fibrillation treatment. This is in agreement with a recent patent using similar concept for limiting energy consumption but using calcium carbonate as abrasive particles. (Gane *et al.* 2011)

In our case, only 15 recirculation cycles were needed compared to the 60 recirculations needed for the production of neat CNF. This also highlights a new benefit of using a fine grinder instead of other conventional technologies, such as homogenizer or microfluidizer (Spence *et al.* 2011) for the production of CNF. Indeed, the addition of such abrasives

particles is only possible by using mechanical disintegration and not adapted to machines based on high-shearing principle.

Concerning the sol-gel reaction (approach 3), following Marques and coworkers study, in which a TiO_2 /cellulose fibers hybrid have been prepared in acidic medium (Marques *et al.* 2006). Thus, the hydrothermal conditions have been adapted for CNF for two main reasons: the final ratio of TiO_2 is too high according to the optimal ratios previously established and reported in the experimental section. In addition, the accessibility of nanocellulose should clearly differ from macroscopic cellulose fibers mainly due to its high surface area.

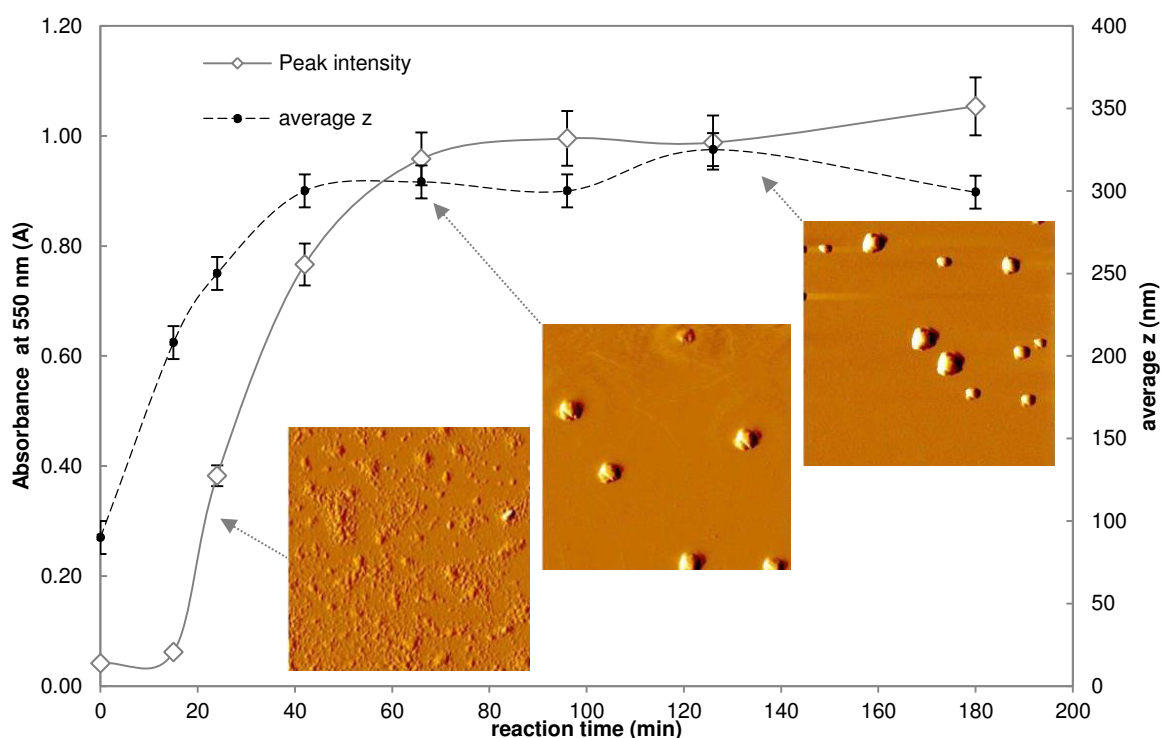


Fig 2.5 - Peak intensity (\diamond) and average z (\bullet) as a function of the sol-gel reaction time. Pictures correspond to the AFM scan imaging in tapping mode (amplitude error, $3 \times 3 \mu\text{m}^2$,) at three reaction times (3, 66 and 126 minutes respectively)

Fig 2.5 highlights the nucleation and growth steps of TiO_2 , as a function of the reaction time and in the absence of cellulosic substrates. As expected, the average diameter of TiO_2 particles significantly increases with increasing the reaction time for the first 40-50 minutes of reaction. Then, the particles size reaches a plateau value at around 300 nm. A similar trend was also found considering the peak intensity at 550 nm, which corresponds to maximum absorption wavelength of TiO_2 . AFM images (**Fig 2.5**) at 3 different reaction times (3, 60 and 120 minutes) also confirm the *in situ* production TiO_2 . This also gives an idea of the generated TiO_2 particles morphology that are in fact clustered particles. In order to prevent the hydrolysis of cellulose during the sol-gel reaction, the shortest reaction time has been chosen

while ensuring an optimum particles size for the light scattering (about 300 nm). For these reasons, a reaction time of 100 minutes (instead of 270 minutes) and a reaction temperature of 50°C (instead of 70°C) have been selected. To reduce the hydrolysis of cellulose, sulphuric acid have been also removed from the initial protocol. Proofs of the sol-gel reaction has been achieved by TGA, XRD and UV-visible characterization that will be detailed later.

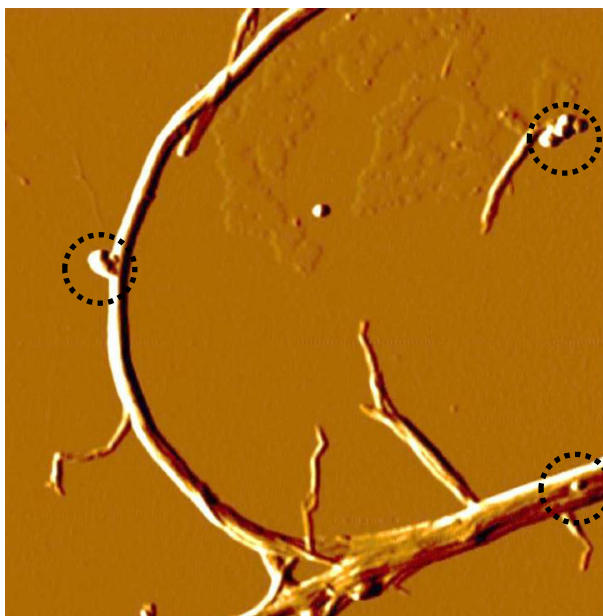


Fig 2.6 - AFM image of individualized CNF in which in-situ TiO_2 (dotted circle) have been generated through the sol-gel reaction at a scanning area of $3 \times 3 \mu\text{m}^2$ in TAPPING mode (amplitude error)

An AFM picture of TiO_2 particles generated onto CNF is presented in **Fig 2.6**. Actually, the sol-gel process is still the most complicated to carry out because it requires several production steps: the production of nanocellulose, the sol-gel reaction in acid medium and finally a neutralization step. However, one of the main benefits of this strategy is the possibility to tune the size of generated TiO_2 particles.

1.3.5 Comparison of the final properties of CNF- TiO_2 films made with different strategies

After having briefly discussed about the production process of CNF hybrid suspension, the end-use properties of the different hybrid films have been compared in terms of mechanical resistance and optical properties. As shown in FE-SEM micrographs of hybrid films, *ex-situ* TiO_2 particles (approach 1 and 2) are trapped into the nanoporous network of entangled CNF (**Fig 2.7-A and B**). *In-situ* TiO_2 particles (approach 3) are well dispersed with spherical shape and in this case, they are considered to be physically adsorbed at the surface of CNF (**Fig 2.7C**).

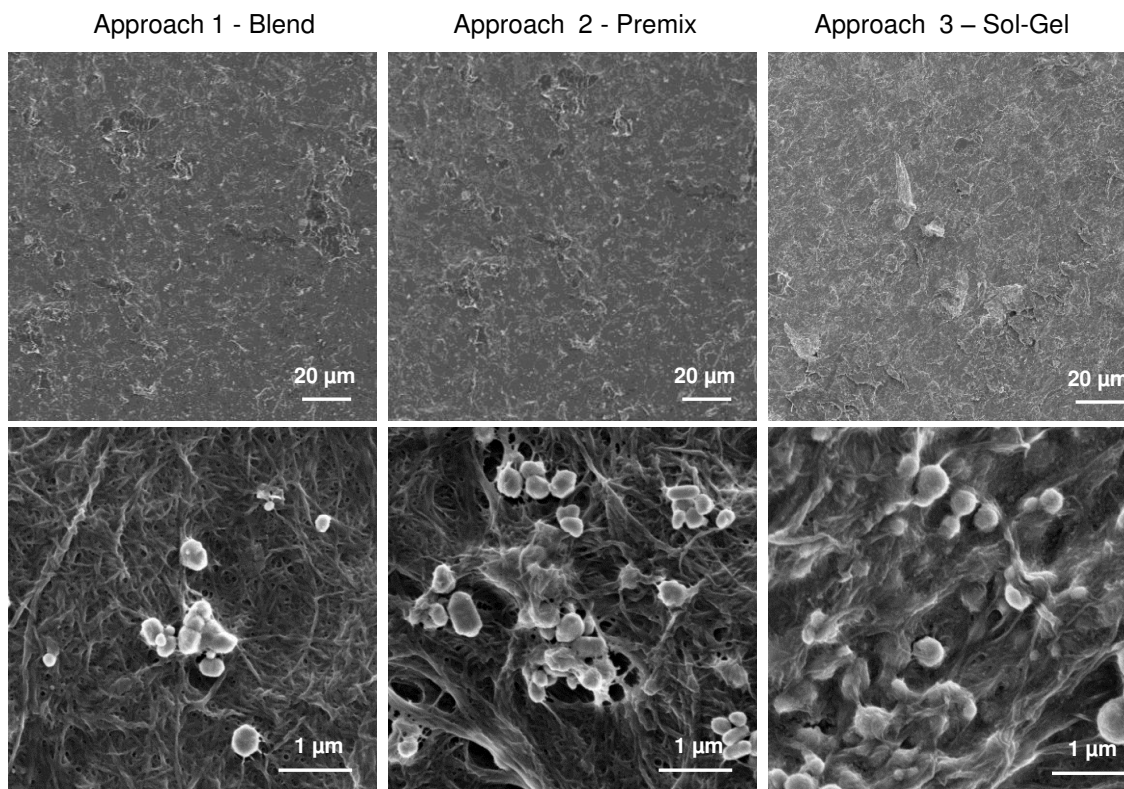


Fig 2.7 - FE-SEM pictures of hybrid films at two magnification level (Up: $\times 10\,000$ and Down: $\times 20\,000$). Comparison between the surface of blend, premix and hybrid films

This confirms that CNF can act as nucleation sites for TiO_2 particles during the sol-gel reaction. The average diameter of individual TiO_2 observed by FE-SEM particles is about 290 ± 10 nm, $225 \text{ nm} \pm 15$ nm and 325 ± 130 nm for blend, premix and sol-gel hybrid films, respectively. High shearing and abrasiveness of ceramic plate of the fine grinding may have led to a reduction of TiO_2 particle size during the fibrillation step (approach 2). Concerning CNF, the average width of CNF used for blend approach is $46 \text{ nm} \pm 11$ nm as already shown by AFM imaging.

Once the sol-gel reaction is performed, the width (30 ± 5 nm) decreases due to acidic conditions. However, these values are still in the nano-range, contrary to those detected in the premix CNF. Indeed, due to a lower number of recirculation cycles (15 instead of 60), the presence of some microscopic fibers bigger than 100 nm were detected. Both mean diameter and standard deviation with a width of 180 ± 90 nm were increased.

The difference between CNF sizes would be taken into account for mechanical and optical properties analysis. Mechanical and optical properties are reported in **Table 2.2**.

Table 2.2 - Main features of hybrid CNF films.

Approach	blend	premix	hybrid
Ratio of TiO ₂ (%)	17.4 (0.3)	17.2 (0.5)	17.5 (0.8)
Density	1.2 (0.2)	1.1 (0.1)	1.5 (0.1)
Strain at break (%)	3.0 (0.3)	3.0 (0.3)	0.5 (0.3)
Force at break (kN/m)	0.6 (0.1)	0.8 (0.02)	0.1 (0.02)
Specific Young Modulus (GPa)	5.2 (0.1)	5.5 (1.3)	1.5 (0.4)
Transparency at 557 nm (%)	38.7 (0.1)	40.3 (0.5)	55 (0.4)

Values into brackets refer to standard deviation

The blend and premix hybrid films have similar properties whereas significant decreases are found for hybrid films both in terms of mechanical properties (-60%) and transparency (-40%). Such results point out that there is a slight chemical degradation of cellulose during the sol-gel reaction giving rise to the weakening of the films properties. In addition, the lowest opacity obtained through sol-gel process can be explained by two main reasons.

As mentioned above, to prevent the degradation of cellulose, the reaction time of the sol-gel reaction have been shortened. So the reaction seems to be uncompleted (some TiO₂ precursors remains) and the generated anatase TiO₂ are not fully crystallized. In addition, a higher density of the sol-gel films (+20%) have been measured which is directly related to a reduction of the internal porosity which affects the opacity of the film.

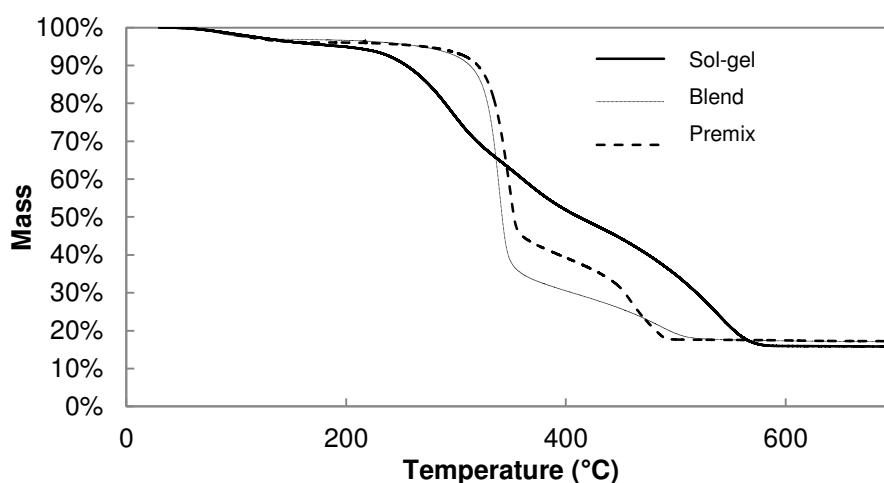


Fig 2.8 - TG curves for hybrid films (TiO₂ 20% w:w) for a 30mg sub-sample at a heating rate of 10 C/min in oxidizing atmosphere in the temperature range of 30–950°C. Comparison between blend, premix and sol-gel strategies

As shown in **Fig 2.8**, TG (thermo-gravimetric) curves highlight the degradation of the cellulose due to the sol-gel reaction. This pyrolysis degradation starts at 238°C for hybrid films whereas it starts over 300°C for blend and premix counterparts. The trend of the curve obtained for blend and premix hybrid film is similar to that obtained with neat CNF (not presented) which indicates there is no chemical modification of cellulose. The analysis of derived TGs (not presented) gives a slower rate of the pyrolysis process for the sol-gel approach. These results confirm that the sol-gel reaction in acid medium tend to cause a partial hydrolysis of CNF, which explains the weakening of sol-gel film in comparison to blend and premix homologues. Over 600°C, the residual mass is between 17 to 18 %. This value can be associated as the inorganic part present in the hybrid films, i.e. the ratio of anatase TiO₂.

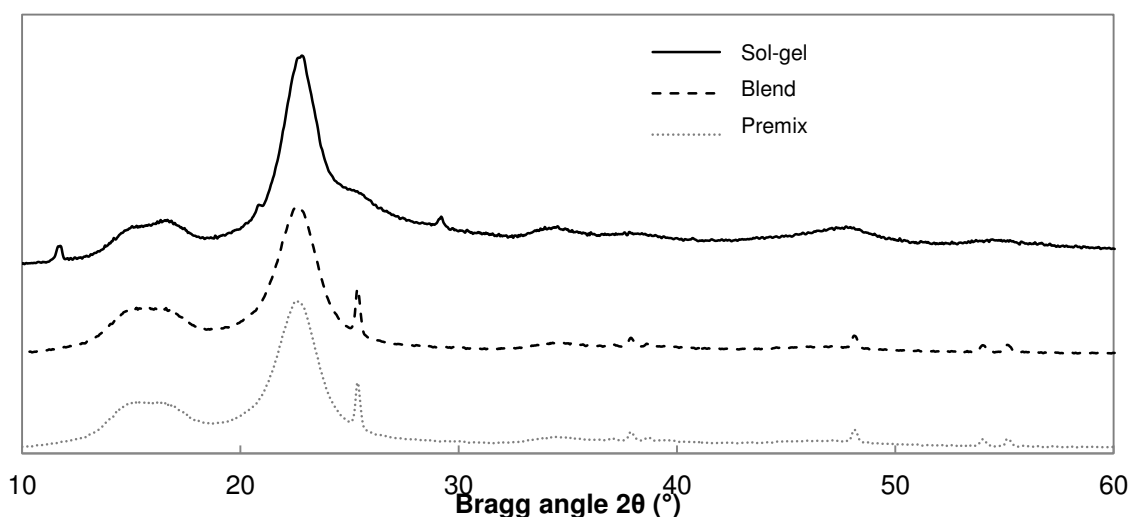


Fig 2.9 - XRD patterns of anatase TiO₂/CNF films. Comparison between blend, premix and hybrid strategies

The XRD patterns of hybrid films presented in **Fig 2.9** are strictly the same for premix and blend approaches indicating that there is no modification or rearrangement of cellulose structure in the presence of *ex-situ* TiO₂, whatever the strategies. Fine peaks are observed at 25.3° (1,0,1), 37.0° (0,0,4), 47.5° (2,0,0), 53.3° (105) and 54.4° (2,1,1) which confirms the presence of highly crystallized anatase TiO₂. The pattern of sol-gel hybrid film is different with anatase broader and smaller peaks of TiO₂. In addition, new peaks can be identified at 11.5°, 15.8°, 20.7° and 29.3°, this peaks are the signature of hydrated Titanium(IV) Oxysulphate used as the precursor, thus confirming that residual amount of the precursors is present in the final film. Residues of precursor and low crystallization of TiO₂ during the reaction explain the highest transparency of the solid film made by *in-situ* TiO₂ route, in comparison to the *ex situ* TiO₂ approach, in which the titanium oxide particles are well-

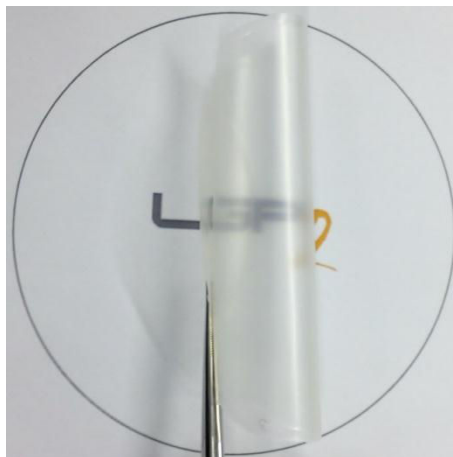
crystallized during the calcination treatment. According to XRD pattern, The CI (crystallinity index) of cellulose is 82.0 and 81.6% for premix and blend hybrid films, respectively. For sol-gel films, the CI of cellulose is close to 86.0%. The higher crystallinity index confirms the hydrolysis of the amorphous part of the cellulose during the sol-gel, as already detected by TG analysis. Among the three strategies studied to produce an opaque CNF film, premixing solid and abrasive particles with the cellulose fibers (approach 2) is the most promising by considering the end-use properties and the process for manufacturing these hybrid films.

1.4 Conclusion and perspectives

One target of this study was to obtain opaque solid film using TiO₂ particles dispersed in CNF network. This was very successful because a very small amount of TiO₂ (starting from 5%) is needed to achieve high opacity film. Based on the gel-like properties of CNF suspensions and the ability of CNF to form a well entangled nanoporous network, spherical shape nanoparticles could be trapped and physically dispersed within the thickness of the CNF films. Moreover, such nanocellulose network is even better than continuous films with TiO₂ and classic matrices, concerning the opacity and the mechanical properties of the ensuing materials.. Three innovative strategies for mixing TiO₂ and CNF have been proposed and compared for the first time. The blend (approach 1) and the premix (approach 2) give the best results regarding both mechanical and optical properties. The premix can be considered as the best solution regarding the process manufacturing.

Even if, the sol-gel reaction (approach 3) permits to tune the size of TiO₂ particles and favor their physical adsorption, this also leads to a partial hydrolysis of cellulose. The thus obtained hybrid films are not suitable to prepare opaque materials. However, other perspectives can be investigated due to the excellent homogeneity and dispersion of semi-crystalline anatase TiO₂. This study proposes different solutions for obtaining highly opaque hybrid CNF films and opens up the prospect to a new generation of opaque films for light barrier packaging or printed electronics.

2 Substitution of nanoclay in high gas barrier films of cellulose nanofibrils with cellulose nanocrystals and thermal treatment



This section is adapted from "Raphael Bardet, Charlène Reverdy, Ingebjørg Leirset, Kristin Syverud, Naceur Belgacem, Michel Bardet, Julien Bras, Substitution of nanoclay in high gas barrier films of cellulose nanofibrils with cellulose nanocrystals and thermal treatment, Cellulose 22:1227-1241 (2015)"

Abstract

The aim of this study is to design a nanocellulose-based barrier film. For this purpose, cellulose nanofibrils (CNF) are used as a film matrix to create an entangled nanoporous network that is filled with two different nanofillers: nanoclay (reference), i.e. the mineral montmorillonite (MMT) and the bio-based TEMPO-oxidized cellulose nanocrystal (CNC-T), to produce different types of nanocelluloses and their main physical and chemical features were assessed. As expected, films based on neat CNFs exhibit good mechanical performance and excellent barrier properties at low moisture content. The introduction of 32.5 wt% of either nanofiller results in a significant improvement of barrier properties at high moisture content. Finally, thermal treatment of a dried CNF/CNC-T film results in a decrease of the oxygen permeability even at high moisture content (>70 %). This is mainly attributed to the hornification of nanocellulose. A key result of this study is that the oxygen permeability of an all-nanocellulose film in 85 % relative humidity (RH), is similar to CNF film with mineral nanoclay (MMT), i.e. 2.1 instead of 1.7 $\text{cm}^3 \cdot \mu\text{m} \cdot \text{m}^{-2} \cdot \text{day}^{-1} \cdot \text{kPa}^{-1}$, respectively.

Keywords: cellulose nanofibril; barrier propertie; cellulose nanocrystal; montmorillonite; thermal treatment; nanoclay

2.1 Introduction

Nowadays, the demand for flexible, strong, transparent and high barrier films for high value-added packaging applications in food, medicine, or electronics is increasing. Petroleum-based polymers such as polyethylene (PE), polypropylene (PP) and Ethylene vinyl alcohol (EVOH) are extensively used (alone or in multilayer strategies) due to their simple processing and low manufacturing costs. In addition, they display suitable properties for flexible packaging such as a low oxygen permeability (OP) as well as mechanical strength and flexibility. The main drawbacks of such polymers are their dependence on fossil fuel and their lack of recyclability (due to multilayer structure) and/or their poor biodegradability. This may represent a serious global environmental problem for future generations. Increasing focus on bio-based polymer materials is then expected. (Johansson *et al.* 2012)

As already mentioned in **Chapter 1 (Table 1.12)**, because of numerous hydrogen bonds and their intrinsic flexibility, once dried, CNFs form a cohesive and dense entangled network that looks like smooth, strong, and transparent films. (Spence *et al.* 2010) Films based on CNF also display excellent air, oxygen, and grease barrier properties in dry conditions (Syverud and Stenius 2009). However, these cellulose-based films have high water affinity and due to this, their OP increase dramatically at relative humidity higher than 70% (Österberg *et al.* 2013). Moisture sensitivity of CNF films can be counterbalanced by different approaches, either by adding filler or by chemical modification. On the one hand, the nanocellulose functionalization will substitute highly hydrophilic surface groups of the cellulose with more hydrophobic groups. In comparison to neat CNF films, carboxymetylated (Minelli *et al.* 2010, Plackett *et al.* 2010), or acetylated (Tingaut *et al.* 2009, Rodionova *et al.* 2011) CNF films impart better gas barrier properties at high moisture content. The main drawbacks of such chemical modification are related to their procedure. They usually require high temperature, solvent-based system, or even a combination of successive filtrations and solvent exchanges.

A simpler approach is to improve the barrier performance of biopolymers by adding inert fillers. The combination of CNF and platelet-like crystalline nanoclay causes an increase of the tortuous diffusion pathway for permeating molecules and the gas permeability can significantly be reduced even at high humidity. (Sehaqui *et al.* 2010, Liu and Berglund 2012, Wu *et al.* 2012) In addition, nanoclay can also provide additional functions to the film such as fire retardancy as proposed by Liu and Berglund (2013). This approach is also considered as a biomimetic solution based on nacre structures.

More recently, Österberg *et al.* (2013) introduced an emerging method based on the hot-pressing of CNF films produced at large scale. This method consists in using elevated pressure (1800 Pa) in combination with heat (100°C) and results in a CNF film with excellent barriers for oxygen gas and grease was reported by. At a relative humidity below 65%, oxygen permeability reported for neat CNF films was below $0.6 \text{ cm}^3 \cdot \mu\text{m}/(\text{m}^2 \cdot \text{day} \cdot \text{kPa})$, and no grease penetrated the film. Lastly, the combination of cationized CNF with silicate nanoclay using a high-shear homogenization followed by pressure filtration and vacuum hot-pressing has extensively studied by Ho *et al.* (2012).

To the best of our knowledge, the use of nanoclay is still the state-of-the-art solution in term of enhancement of barrier properties for hydrophilic biobased polymers at high moisture content. However, one issue regarding the use of nanoclay, is that these combined materials loose sustainability and biodegradability properties that characterize of neat CNF films. The nanoclay-to-CNF ratio is generally ranging from 30-89 wt %, (Berglund and Liu 2011, Aulin *et al.* 2012, Liu and Berglund 2013) making such materials more mineral-based than renewable and bio-based.

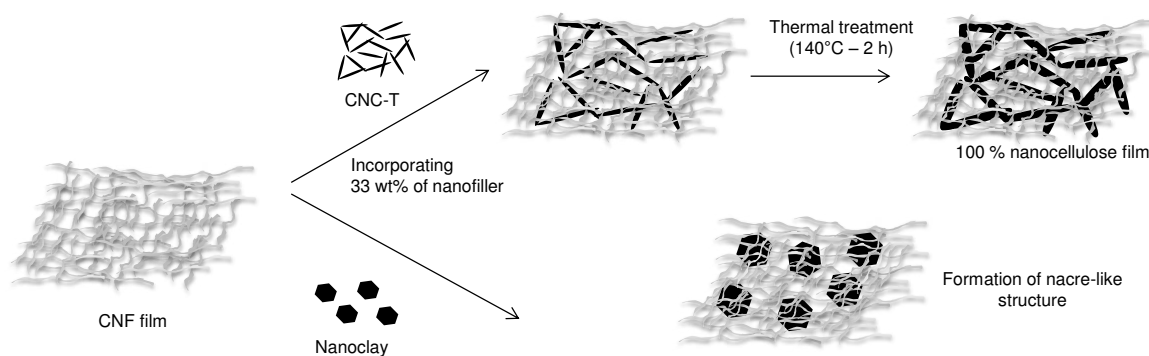


Fig 2.10 - Graphical abstract of the study

The aim of this study is to design a 100 % biobased and transparent film with high barrier that still is efficient at high humidity. To do so, neat or oxidized CNF is used as matrix to create an entangled nanoporous network. Moreover, the CNF matrix is filled with two different nanoparticles: nanoclay (reference), i.e. mineral Montmorillonite, MMT) and biobased nanoparticles, i.e. TEMPO-oxidized CNC (CNC-T) as illustrated in **Fig 2.10**. The main features of nanoparticles used in the study are reported. For the different films, barrier, optical and mechanical properties are investigated. Finally, a thermal treatment on dried films is also proposed in a view to reduce their water sensitivity.

2.2 Experimental section

2.2.1 Materials

The CNFs were produced in pilot scale (CTP, France). CNF was isolated from a sulphite-based softwood-dissolving pulp (Cellulose Plus®, Domsjö, Sweden) using refining and enzymatic pretreatments, followed by homogenization according to a protocol developed in the SUNPAP project (Ariete NS3075, GEA Niro Soavi, Italy). A pre-refining stage was carried out using a pilot refiner system to obtain a slightly refined pulp with a drainage index ~ 25 °SR. An enzymatic treatment was then applied to the pre-refined pulp at 5 % (by weight) consistency, with a commercial cellulase (FibreCare R Novozymes, Denmark), at a concentration of about $1 \text{ mL}\cdot\text{kg}^{-1}$. The pulp was incubated for 1 h at 50 °C. A second refining stage was performed on the enzymatically pretreated pulp at 5 % (by weight) consistency using the same pilot refiner system used for the pre-refining step. Five passes through the homogenizer (one at 1000 bar and four at 1450 bar) working at a maximum flow rate of about $1000 \text{ L}\cdot\text{h}^{-1}$ were successively performed to produce a homogenous gel-like CNF suspension at 2 % (by weight) consistency.

Commercial nanocrystalline cellulose (CNC) was purchased from Celluforce (Canada) as a dry powder; it had been isolated from wood pulp by sulfuric acid hydrolysis. After being diluted to 2.0 % by weight, the CNC suspension was homogenized using a 200-Watts sonication probe (Sonifier® S-250A, Branson, USA), operating at a dispersion energy of $1 \text{ kJ}\cdot\text{g}^{-1}$. The nanoclay used in the experiments, MMT (Cloisite Na⁺, Southern Clay Products, USA), is a natural Na-MMT with a cation exchange capacity of 92 mequiv/100 g and specific gravity of $2.86 \text{ g}\cdot\text{cm}^{-3}$, as reported by the supplier.

Nanoclay dispersion was prepared by dispersing 10 g of the clay in 1 L of deionized water under vigorous stirring and sonication ($1 \text{ kJ}\cdot\text{g}^{-1}$) before use. 2,2,6,6-tetramethylpiperidin-1-oxyl (TEMPO, used as a catalyst), sodium bromide (NaBr), a 12 % sodium hypochlorite (NaClO) solution, and other chemicals such as NaCl, NaOH, NaCl, etc. were of laboratory grade (Sigma-Aldrich, USA) and were used without further purification. Deionized water was used in all experiments.

2.2.2 Methods

TEMPO-mediated oxidation of nanocellulose

TEMPO-mediated oxidation was carried out as a post-treatment of nanocellulose, adapted from a protocol proposed by Saito *et al.* (2007). The same oxidation parameters (ratio of reactants, reaction time, and purification procedure) were used for both CNF and CNC. Nanocellulose (10 g) was suspended in water (1000 mL) containing TEMPO (0.1 mmol per gram of nanocellulose) and NaBr (2.5 mmol per gram of nanocellulose) under vigorous stirring. The 12 wt% NaClO solution was adjusted to pH 10 by addition of 0.1 M NaCl solution. TEMPO-mediated oxidation was initiated by adding the NaClO solution (12 mmol per gram of nanocellulose). The reaction was conducted at room temperature by stirring at 500 rpm. The pH was maintained at 10 by adding 0.5 M NaOH using a pH-stat until no NaOH consumption was observed. The reaction was inhibited by the addition of 1 mL of methanol and the pH of the reaction mixture was gradually lowered to 7 by addition of 0.1 M HCl solution. Then oxidized nanocellulose was diluted 3 times in deionized water and then was extensively dialyzed (Spectra/Por® 4, SpectrumLabs, USA) over 7 days against a large excess of deionized water. Finally, the nanocellulose suspensions were concentrated by centrifugation (Sigma 6-16K Centrifuge, Sigma, UK) at $10000 \times g$ for 10 min and redispersed in deionized water at 2.0 wt.%.

Preparation of CNF films reinforced with nanofiller

All-cellulose films were prepared as follows: CNF suspensions were mixed with neat or TEMPO-modified CNC (used as nanofillers) and were homogenized (UltraTurrax T8®, IKA, France) at 10000 rpm for 5 min. As references, control samples were prepared by substituting CNC with MMT following the same procedure and nanofiller ratio. The nanofiller (CNC or MMT) to CNF ratio was set at 32.5 wt%. Finally, 12 mL of the homogenized suspension was diluted in 30 mL of deionized water and was casted in a smooth aluminum plate (6-cm diameter) and left to dry for 3 days at 23 °C with 50 % RH. For each series, films with a basis weight of about $45 \text{ g}\cdot\text{m}^{-2}$ were obtained and stored under these conditions until analysis.

Thermal treatment of CNF film

Cross-linking and hornification were carried out by over-drying the CNF films in a highly ventilated thermostated oven (ED 53 binder, Binder, Germany) for 2 h at 140 °C. To avoid shrinkage, the films were placed between two heavy metal rings.

Characterization of nanoparticles

Morphological analysis. Individual nanoparticles were imaged using an atomic force microscope (AFM, Nanoscope III®, Veeco, Canada). All the samples were diluted to 10⁻⁴ wt% and a drop of 0.2-mL volume was deposited onto freshly cleaved mica substrates and were dried overnight under room conditions. Each sample was characterized in the tapping mode with a Si cantilever (OTESPA®, Bruker, USA) at four different locations and over two different scanning areas: 10 × 10 μm² and 3 × 3 μm². Both topographical and phase images were captured and were subjected to first-order polynomial flattening to reduce the effects of bowing and tilt. Only the most representative images are presented in this study; however, morphological dimensions were obtained as an average of at least 50 individual nanoparticles with a minimum three different images.

Surface chemistry analysis. The surface charge was determined through a conductometric titration (CT) of 100 mL of nanocellulose suspension (1 g in the dried state) with 250 mL of a 0.1 M HCl solution for 10 min. The suspension was then extensively dialyzed (Spectra/Por® 4, SpectrumLabs, USA) for 7 days against a large excess of deionized water. Afterwards, the conductivity of the suspension was adjusted to 700 μS·cm⁻¹ by adding 0.1 M NaCl solution and then titrated with a 10 mM NaOH solution with 0.1 mL increments until all the charged groups have been neutralized. Each titration has been repeated thrice.

The electrophoretic mobility of nanoparticles was measured using a zeta potential analyzer (Zeta 2000, Malvern, UK). Dispersions were diluted to ~ 0.05 wt% in deionized water in the presence of NaCl solution to maintain a constant ionic strength of 500 μS·cm⁻¹. The reported zeta potential corresponds to the average value of three independent measurements.

Characterization of films

Before characterization, the films were conditioned in a humidity chamber maintained at 25°C with 50 % RH, for at least 48 h.

Structural properties. The thermal degradation of samples was monitored by thermogravimetric analysis (TGA-STA 6000®, Perkin Elmer Instruments, England). The mass-loss and heat-flow curves were recorded for a 30 mg sub-sample at a heating rate of 10 °C·min⁻¹ in the temperature range of 30–950 °C under oxidizing atmosphere (air). The experiments have been duplicated and then averaged. The X-ray diffraction (XRD) patterns were recorded with an X-ray diffractometer (PANanalytical®, X'Pert PRO MPD). The operating conditions were Cu-Kα radiation (λ = 1.54 Å), Bragg angle (2θ) of 5–60°, a step-size of 0.067°, and a counting time of 90 s. The cellulose crystallinity index was evaluated

using an empirical method developed by Segal *et al.* (1959). For each XRD pattern, the experiments have been duplicated and their results averaged.

Field-emission scanning electron microscopy (FE-SEM) was used to observe the nanostructure (cross-section and surface) of a nanopaper (Ultra 55 ©, Zeiss, Germany). The samples were covered with carbon tape and coated with a 2-nm thick layer of Au/Pd to render them conductive. The accelerating voltage (EHT) was 3 kV for a working distance of 6.4 mm. Thicknesses of the films were determined from their cross-sections as shown in the FE-SEM micrographs. For each film, six measurements were made at three different locations whereas the basis weight was evaluated using ISO-536:1995 standard. The film-density was estimated by dividing the basis weight with the film-thickness.

NMR experiments. The samples were gently ground prior to measurements to ensure to ensure their homogeneity. All 1D NMR experiments were carried out at room temperature with a BRUKER AVANCE DSX 500 MHz spectrometer, operating at a ^1H frequency of 500.13 MHz (^{13}C frequency of 125.7 MHz). 1D ^{13}C spectra were acquired with a 4 mm Bruker CPMAS probe-head, using the combination of cross-polarization (CP), magic-angle spinning (MAS) of the sample, and high-power proton decoupling methods. The MAS speed was set to 12000 Hz. ^1H radio-frequency field strengths of 70 kHz and 87 kHz were used for proton pulses (90 °-pulse duration of 2.8 μs) and proton dipolar decoupling, respectively. The ^{13}C radio-frequency field strength was set to match the Hartman-Hahn condition during CP. For each spectrum, 12000 transients were accumulated with a CP contact time of 2 ms and a recycle delay of 5 s. The chemical shift values were calibrated indirectly with the carbonyl signal of glycine set at 176.03 ppm relative to tetramethylsilane (TMS). ^1H NMR spectra were recorded using the same probe with direct proton excitations. The MAS speed was set at 12000 Hz and 16 transients were accumulated.

Barrier properties. OP was monitored at 23 °C and 20, 50, 65, 85 and 90 % RH by using the equal-pressure method and a coulometric analyzer (OX-TRAN® Model 1/50, Mocon, USA), according to the ASTM F1927–07 standard. The samples were conditioned for 24 h at room temperature. The specific exchange surface was 5.0 cm², and the oxygen content of the test gas was 21 %. The assessments were run until stable values were obtained. The experiments were carried out in duplicate.

Water Vapor Permeability (WVP) of the films was estimated by a gravimetric method according to the ISO 12572:2001 standard. It involved measuring the weight-uptake of 10 g of anhydrous CaCl₂ in a metal cup covered by the sample films and sealed by beeswax. The specific exchange surface was 78.5 cm². For controlling the environmental conditions, the

cups were placed in a conditioned room at 23 °C and 50 % RH. The water vapor weight gain through the film was monitored as a function of time over 7 days (at least 2 measurements a day). Water vapor weight gain was calculated as the total cell weight gain minus the gain through the sealing. All the tests were duplicated and WVP values of each film were calculated as follows:

$$WVP(g/m.s.Pa) = \frac{\Delta m \times e}{A \times \Delta t \times \Delta P} \quad (1)$$

Δm (g) is the mass increase, A is the area of the film ($78.5 \times 10^{-3} \text{ m}^2$), and Δt is the exposure time in the chamber. The thickness of the film is e and ΔP (1430 Pa) is the partial pressure difference of water vapor across the film specimen corresponding to 50 % RH at 25 °C.

Grease resistance was evaluated according to the modified TAPPI T-507 standard. First, commercial sunflower oil was colored with Sudan II red dye. The colored oil was generously applied onto a butter paper. Then, films ($4 \times 2 \text{ cm}^2$) were placed between an unsaturated and an oil-soaked butter paper. The whole stack (unsaturated butter paper, nanopaper, oil-soaked paper) was covered between two aluminum foils, pressed with a 300 g weight and kept in oven at 60 C for 4 h. Then, the assembly was removed and the stain absorbers on the unsaturated butter paper were examined. For each absorber the area and the number of stained spots, if any, were determined. Results are shown as the average of three samples.

Mechanical and optical properties. The mechanical properties of the films were measured using a universal testing machine (Model 4465®, Instron Engineering Corporation, US) equipped with 100 N load cells. The methods of evaluation of the Young's modulus, tensile strength, and the elongation were adapted from the ISO-1924-2:2008 standard. Specimens of length 40 mm and width 8 mm were subjected to a constant speed of elongation of $4 \text{ mm} \cdot \text{min}^{-1}$. All the mechanical tests were repeated 6 times for each sample. Transparency of the films were estimated with a UV spectrophotometer (UV 1800®, Shimadzu, Japan). The transmittance was measured over a wavelength range of 200–800 nm, by placing the films vertically in special sample holders. For each sample, 3 different measurements and in each measurement 10 scans were recorded.

2.3 Results and discussion

2.3.1 Nanocellulose characterization and influence of TEMPO-mediated oxidation of nanocellulose

Before investigating the properties of films, the chemical and mechanical features of the different nanoparticles used were determined and summarized in **This study** includes both types of nanocellulose, CNF and CNC, before and after TEMPO-oxidized treatment (CNF-T and CNC-T), as well the reference MMT.

Table 2.3. This study includes both types of nanocellulose, CNF and CNC, before and after TEMPO-oxidized treatment (CNF-T and CNC-T), as well the reference MMT.

Table 2.3 - Physical and chemical properties of nanocellulose and nanoclay used in the study

Properties	Nanocellulose				Nanoclay		
	Neat		oxidized		MMT		
	CNF	CNC	CNF-T	CNC-T			
Morphology	Shape	<i>fibrillar</i>		<i>rod-like</i>		<i>platelet-like</i>	
	Length ^a (nm)	652 (292)	174 (83)	532 (145)	173 (55)	532 (125)	
	Thickness ^a (nm)	14 (5)	8 (3)	8 (3)	6 (3)	3 (1)	
	Aspect ratio	47 (27)	22 (13)	67 (31)	29 (17)	177 (72)	
Chemical	Crystallinity Index ^b (%)	77 (1)	86 (1)	81 (1)	85 (1)	-	-
	Surface charge ^c (μmol/g)	101 (13)	159 (26)	1563 (42)	727 (105)	943	
	Zeta potential ^d (mV)	-18 (3)	-30 (2)	-47 (2)	-44 (3)	-40 (1)	
Thermal	Temperature of thermal degradation ^e (°C)	289 (13)	241 (7)	223 (13)	223 (5)	305 (5)	

Values measured from AFM^a, XRD^b, CT^c. Conductivity^d adjusted to 500 μS/cm by the addition of NaCl solution. Temperature^e corresponding to a 10% mass loss from TGA.

Value in brackets refers to the standard deviation. Fig 2.11-A

CNF has a fibrillar structure with average length above 600 nm (**Fig 2.11-A**). The gel-like structure of the suspension indicating a low amount of macroscopic cellulosic fibers, which is common in fibril suspensions as reported by Chinga-Carrasco (2011), along with the uniformity and homogeneity of CNF were confirmed by optical microscopy (not presented). In contrast, CNCs are rod-like (**Fig 2.11-B**) with average dimensions of the nanocrystals being 8-nm thick and 174-nm long. MMT has a platelet-like morphology with a lower thickness of ~ 1-2 nm (**Fig 2.11-E**). As estimated by AFM analysis, the lateral dimension of the platelets varies from 10 nm to 500 nm, resulting in an average aspect ratio of about 180. The zeta potential of CNC is highly negative because of the high surface charge density of

sulfate ester groups (Araki *et al.* 1999), whereas CNF has a moderate negative charge due to the presence of carboxyl groups in residual hemicellulose groups (Iwamoto *et al.* 2008).

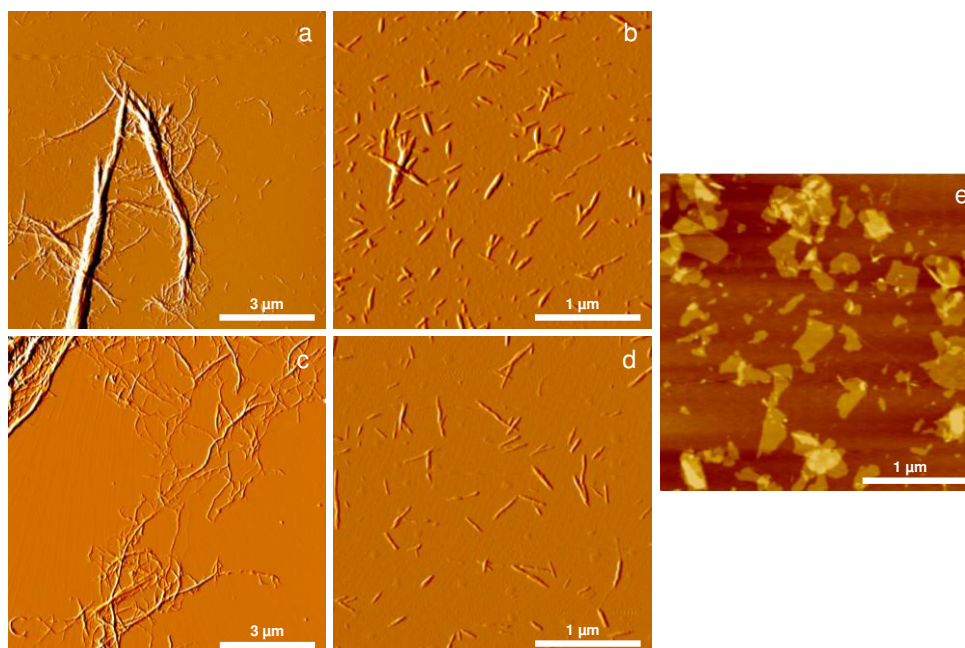


Fig 2.11 - AFM images showing individualized nanoparticles: CNF(a) and CNC (b), after TEMPO-mediated oxidation, CNF-T (c) and CNC-T (d). Sample (e) corresponds to nanoclay (MMT).

The TEMPO-mediated oxidation of nanocellulose is detected by the increase of zeta potential values from -18.3 to -46.5 mV for CNF and from -30.2 to -44.3 mV for CNC. In addition, oxidation of the nanocellulose was also confirmed by the NMR experiments (**Fig 2.18.B**) a new signal appears at δ 174.7 ppm, assigned to carboxyl groups formed during regioselective TEMPO-oxidation of cellulose as shown by Montanari *et al.* (2005). Even if it is assumed that TEMPO-oxidation is only surface modification, the bulk structure of CNF seems to be affected, according to the increase of the crystallinity index from 77 to 82 % and the size reduction of CNF-T (**Fig 2.11-C**). This can be attributed to chemical depolymerization and partial solubilization of cellulose and hemicellulose oligomers during post-oxidation. (Shinoda *et al.* 2012). In contrast, the main amorphous part of CNC-T was dissolved during its chemical isolation with sulfuric acid. The morphology of the nanoparticles is affected only slightly by the oxidative post-treatment as shown in **Fig 2.11-D** and consistent with previous results reported by Habibi *et al.* (2006).

As shown by Fukuzumi *et al.* (2010), TEMPO-oxidation has a negative impact on the onset of temperature degradation; in the present study it decreased from 289 to 223 °C for CNF and from 241 to 223°C for CNC. In spite of these slight changes, it is worth noting that relatively similar structures and morphologies are obtained after oxidation. Mainly the larger

number of carboxylic moieties (hence the increased charge) contributes to possible variations of barrier properties.

2.3.2 Properties of neat and TEMPO-oxidized CNF films

In this section, the end-use properties of neat and TEMPO-oxidized films were compared (Table 2.4) to investigate which matrix (CNF or CNF-T) is the most suitable for manufacturing flexible barrier films.

Table 2.4 - Mechanical, barrier, and optical properties of CNF films

	Properties	CNF		CNF-T	
Contexture	Basis weight (g/m ²)	41	(2)	43	(3)
	Thickness (μm)	40	(5)	36	(4)
	Density (g/cm ³)	1.00	(0.05)	1.28	(0.51)
	Porosity (%)	33	(3)	15	(1)
Mechanical properties	Specific Young's modulus (GPa)	7.5	(0.9)	10.2	(2.5)
	Elongation at break (%)	2.9	(1.0)	2.1	(0.5)
	Tensile strength (Mpa)	91	(13)	138	(27)
Barrier permeability 23 °C and 50%RH	Oxygen permeability (cm ³ ·μm/m ² ·day·bar)	0.9	(0.2)	1.2	(0.1)
	Water Vapor permeability (g/m.s.Pa) × 10 ¹³	3.8	(0.3)	9.2	(0.3)
	Grease permeability (mm ² /cm ²)	Very low grease permeability (below the detection limit)			
Optical	Transmittance at 557nm (%)	74	(4)	87	(3)

Value in brackets refers to the standard deviation

TEMPO-oxidation affects the mechanical properties as shown with an increase in both the Specific Young's modulus (+ 36 %) and tensile strength (+ 51 %). Consistent with recent results reported by Österberg et al. (2013) and Ho et al. (2012), both films exhibit excellent barrier properties: their grease permeabilities are almost zero and OP at low moisture content (50 %) is about 1 cm³·μm·m⁻²·day⁻¹·kPa⁻¹.

Such barrier properties are thought to be linked to the relatively high crystallinity and the dense networks held together by the strong hydrogen bonds between the fibrils that are produced during the film formation. (Syverud and Stenius 2009) Similar improvement was observed when a 0.4-μm thin layer of TEMPO-oxidized CNF is coated onto a 25-μm thick PLA film. The OP decreased from 746 to about 1 mL·m⁻²·day⁻¹·Pa⁻¹ (Fukuzumi et al. 2008). However, most barrier properties were evaluated at relatively low moisture content, i.e.

typically in the 0–50 % RH range. When such properties were investigated at > 50 % RH, the CNF films displayed an accelerated water uptake due to partial replacement of CNF–CNF hydrogen bonds with CNF–water hydrogen bonds, as proposed by Aulin et al. (2010).

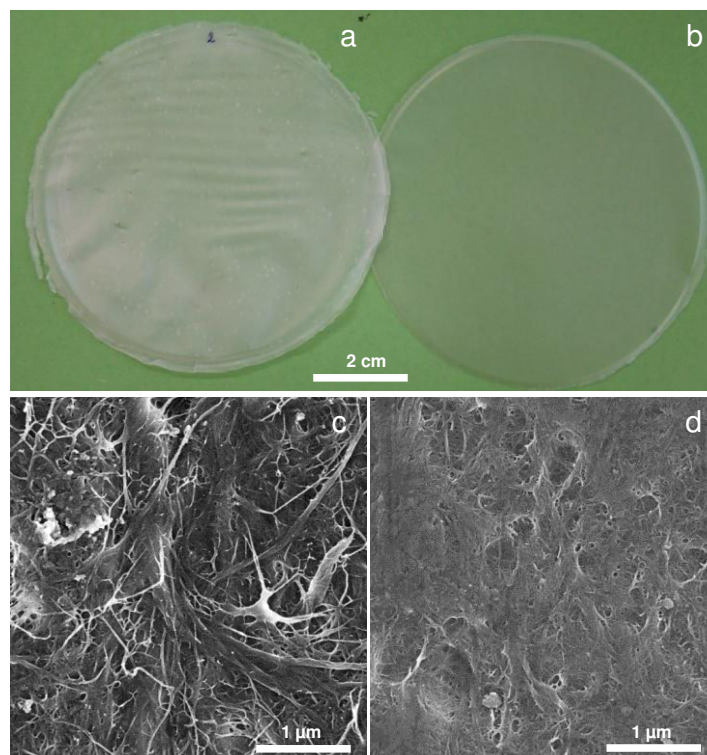


Fig 2.12 - Photographs and FE-SEM images of surfaces of a neat CNF film (a, c), and a TEMPO-oxidized CNF film (b,d)

Lastly, the negative impact of the oxidation on the barrier properties is greater at higher RH. WVP of CNF is more than 3 times lower than CNF-T films, due to the strong hydrophilic nature of carboxylic group. Hence, CNF films were used as reference matrix for the rest of the study.

2.3.3 Improvement of barrier properties of CNF film with nanofillers

Two types of nanofillers (exfoliated MMT or CNC-T), 32.5 % by weight, were combined with CNF suspension to improve barrier properties of CNF films in humid environment (**Fig 2.10**). The film properties are summarized in **Table 2.5**.

Previous studies shown a positive impact of MMT, but to the best of our knowledge, there are no reports on studies on an all-cellulose solution with CNF and CNC-T. Such colloidal suspensions are well-homogenized because of their colloidal dimensions, anionic charge, and the dispersion procedure (see experimental section).

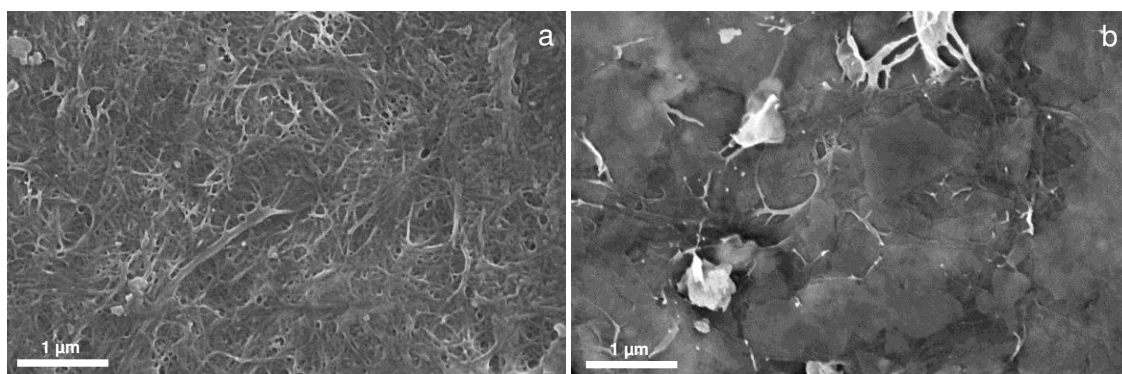


Fig 2.13 - FE-SEM images of surfaces of a CNF film reinforced with 32.5 wt % of CNC-T (a), and MMT (b)

The films were prepared by casting and free water evaporation of the suspensions, following the same procedure used in the previous section. In comparison to the neat CNF film (**Fig 2.12-C**), FE-SEM analyses revealed the incorporation of CNC-T in the nanoporous fibrils network (**Fig 2.13-C**). This is in contrast with the surface structure of films reinforced with MMT, which is smoother and shows the MMT to be well-dispersed on the surface and entangled in the CNF networks (**Fig 2.13-B**).

Table 2.5 - Mechanical, barrier and optical properties of CNF film reinforced with 32.5 wt% of CNC-T or MMT.

	Properties	Neat CNF		with CNC		with MMT	
Contexture	Type of nanofiller			CNC-T		MMT	
	Nanofiller ratio (wt%)	-		32.5		32.5	
	Density (g/cm ³)	1.00	(0.05)	1.28	(0.07)	1.25	(0.1)
	Porosity (%)	33	(4)	19	(1)	30	(2)
Mechanical	Specific Young's modulus (GPa)	7.5	(1)	10.1	(1.4)	7.8	(1)
	Elongation at break (%)	2.9	(1)	2.8	(0.7)	2.8	(1)
	Tensile strength (Mpa)	91	(16)	115	(8)	80	(4)
Barrier permeability 23°C and 50%RH	Oxygen permeability (cm ³ *μm/m ² .day.bar)	0.9	(0.2)	1.0	(0.1)	1.0	(0.1)
	Water Vapor permeability (g/m.s.Pa) x 10 ¹³	3.8	(0)	2.78	(0.17)	1.9	(1)
	Grease permeability (mm ² /cm ²)	Very low grease permeability (below the detection limit)					
Optical	Transmittance at 557nm (%)	74	(4)	80	(2)	65	(6)

Value in brackets refers to the standard deviation

The incorporation of nanofillers increases the density of the films from $1.0 \text{ g}\cdot\text{cm}^{-3}$ to about $1.2 \text{ g}\cdot\text{cm}^{-3}$. In the case of MMT, the higher density is mainly due to its specific gravity of nanoclay being higher (2.86) than that of the nanocellulose (1.50). However in the case of CNC-T, their incorporation results in real densification of materials with a significant decrease of air-porosity from 33 % to 19 %. This can be explained by the formation of hydrogen bonds between surface carboxyl groups of CNC-T and hydroxyl groups of CNF and, because CNC-T may have a tendency to fill the porous entangled network created by CNF. Such assumption must be confirmed by mercury-intrusion porosimetry analysis.

This leads to changes in the macroscopic scale as revealed by optical and mechanical properties. An increase of the transparency (74 % to 80 %) is measured for CNF/CNC-T films whereas films based on MMT are less transparent (65 %).

The incorporation of CNC-T in the CNF network has a positive impact on mechanical properties as well, as reflected by an increase in tensile strength and specific Young's modulus by 26 % and 35 %, respectively. Several studies reported a synergistic effect in the case of CNF/MMT films, which results in an improvement of mechanical properties (Aulin *et al.* 2012, Ho *et al.* 2012, Wu *et al.* 2012), however, in our case no such improvements were revealed, suggesting a partial exfoliation of MMT.

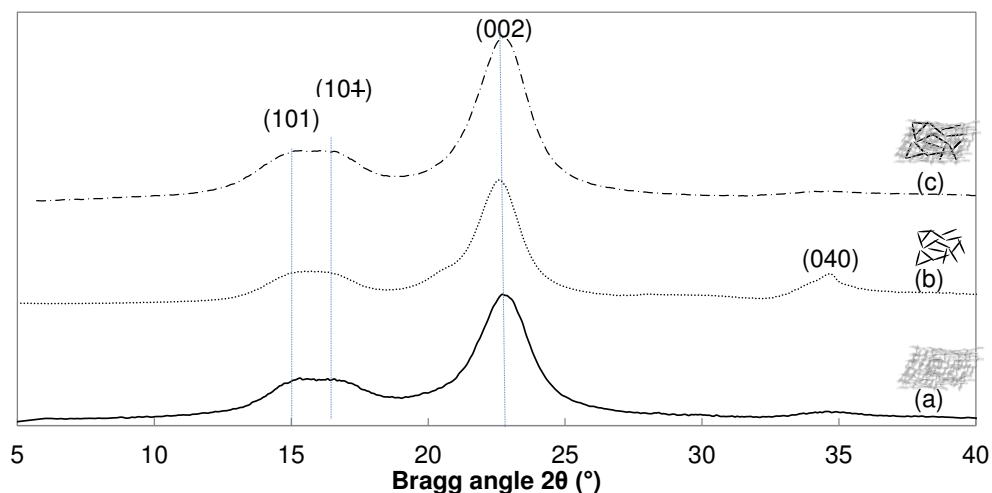


Fig 2.14 - XRD patterns of neat CNF film (a), freeze-dried CNC-T (b), and CNF/CNC-T film (c)

XRD patterns (**Fig 2.14**) of nanocellulose samples have the same characteristics as native cellulose (semi-crystalline cellulose I β) with broad peaks at $15.1, 16.8^\circ$ and 22.8° characteristic of (101), (101), and (002) lattice planes, respectively. For freeze-dried CNC-T samples, a more intense peak characteristic of lattice plane (040) is identified at 33.3° . This peak can only be attributed to the sample preparation because CNC-T sample (**Fig 2.14-B**) was freeze-dried whereas CNF and CNF/CNC-T samples were not (**Fig 2.14-A and C**).

Since the crystallinity index of CNC-T (85 %) is higher than that of CNF (78 %), the incorporation of CNC-T within CNF suspension results in an increase of the overall crystallinity of the CNF/CNC-T film (81 %).

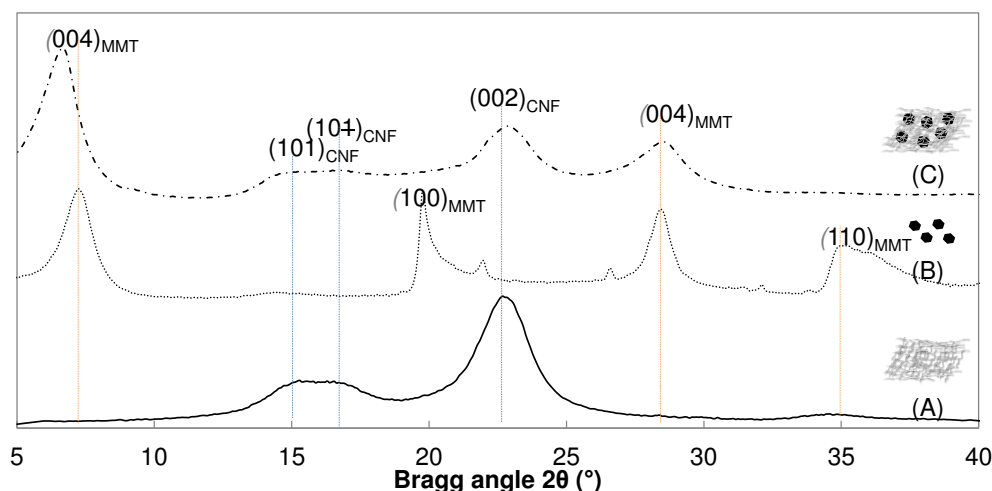


Fig 2.15 - XRD patterns of neat CNF film (a), freeze-dried MMT (b), and CNF/MMT film (c)

XRD spectrum of the CNF/MMT film (**Fig 2.15-C**) displays the characteristics of both, the CNF with the broad peaks at 15.1°, 16.8° and 22.8° and the MMT component with intense peaks at 6.7° and 28.6° corresponding to the (001) and (004) lattices planes of MMT. However, the broad peak (001) at 7.3° for the freeze-dried MMT sample shifts to a lower angle in the CNF/MMT films. This is explained by an increase of the interlayer distance (partial exfoliation) because of intercalation of microfibrils, as explained by Wu *et al.* (2012). Lastly, the (100) and (110) lateral lattice planes of MMT (**Fig 2.15-B**) are not detected in CNF/MMT films (**Fig 2.15-C**) This suggests that the platelet-like MMTs are horizontally stacked within the film structure as shown in (**Fig 2.13-B**).

The incorporation of either nanofiller has no negative impact on grease barrier properties (**Table 2.5**). A slight improvement in WVP is observed with CNC-T, in spite of the higher water-vapor-sensitivity of CNC-T. This might be due to the slight increase of density. For the CNF/MMT films, both the increased density and the low water-sensitivity explains the decrease of average WVP by 2. However, it is noteworthy that the standard deviation is very high, proving the heterogeneity of MMT distribution but it may also be due to possible defects in the film, favoring capillarity migration of water vapor.

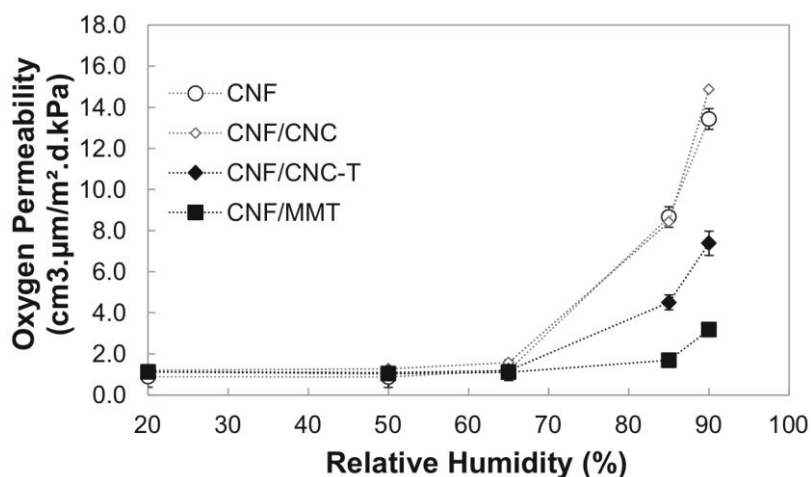


Fig 2.16 – Oxygen permeability as a function of relative humidity for 45 g m^{-2} films based on neat CNF (○), and reinforced with 32.5 wt% of CNC (◇), CNC-T (◆) or MMT (◻)

Fig 2.16 detailed the OP of different CNF films through a large range of humidity rate. There is almost no influence of nanofillers below 50–65 % RH. In case of MMT, the incorporation of these plateletshaped particles generates a tortuous path that significantly reduces gas-permeability at high humidity (**Fig 2.16**). Such findings are in accordance with similar results obtained for CNF/MMT materials (Wu *et al.* 2012), although the authors did not present gas barrier properties at high RH (> 50 %).

The positive impact of CNC-T on barrier properties is unexpected (**Fig 2.16**), since the oxidized CNF is expected to be more hydrophilic than neat CNF and the addition of 32.5 wt% of unmodified CNC does not lower the OP. The improvement of barrier properties for CNF/CNC-T can be attributed to the increase of density and crystallinity even though a moderate increases were measured. A possible explanation is that the water molecules tend to be chemically absorbed by osmosis and remain in the film, without permeating the film structure.

It is important to note that CNF/MMT films exhibit better moisture-resistant properties compared to CNF/CNC-T films. However, it is the first time that CNC-T nanofiller has been reported to enhance the oxygen-permeability of neat CNF films.

2.3.4 Thermal treatment of CNF films

In order to overcome the moisture-sensitivity of nanocellulose-based films (CNF or CNF/CNC-T films), they were subjected to a thermal treatment (140 °C, 2 h). The original idea is to increase the hornification of nanofibrils (irreversible H-bonding upon drying, also called thermal annealing for other polymers with a high amount of hydroxyl groups) as well as their cross-linking with the CNC-T nanofiller. Cross-linking is a well-known reaction to

reduce moisture-sensitivity in hydrophilic polysaccharides by using polycarboxylic acids, as proposed by Yang *et al.* (1997). This reaction occurs on heating and starts at temperatures around 140 °C when water from esterification is eliminated, driving the reaction forward (Le Chatelier's principle). In our study, similar reaction temperatures and reaction time have been used. The main difference in the present study is that highly crystalline solid nanoparticles (i.e. CNC-T) are used instead of common cross-linking molecules such as citric acid (Reddy and Yang 2010) or poly(acrylic acid) (Spoljaric *et al.* 2013).

In order to overcome the moisture-sensitivity of nanocellulose-based films (CNF or CNF/CNC-T films), they were subjected to a thermal treatment (140 °C, 2 h). The original idea is to increase the hornification of nanofibrils (irreversible H-bonding upon drying, also called thermal annealing for other polymers with a high amount of hydroxyl groups) as well as their cross-linking with the CNC-T nanofiller. Cross-linking is a well-known reaction to reduce moisture-sensitivity in hydrophilic polysaccharides by using polycarboxylic acids, as proposed by Yang *et al.* (1997). This reaction occurs on heating and starts at temperatures around 140 °C when water from esterification is eliminated, driving the reaction forward (Le Chatelier's principle). In our study, similar reaction temperatures and reaction time have been used. The main difference in the present study is that highly crystalline solid nanoparticles (i.e. CNC-T) are used instead of common cross-linking molecules such as citric acid (Reddy and Yang 2010) or poly(acrylic acid) (Spoljaric *et al.* 2013).

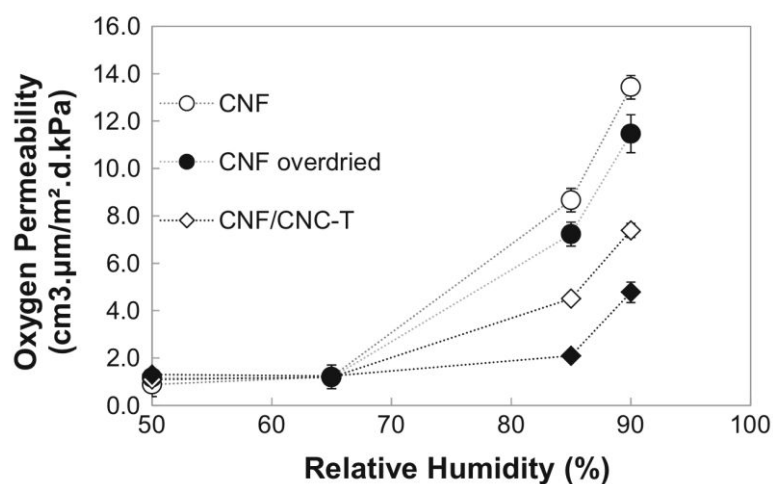


Fig 2.17 – Oxygen-permeability as a function of relative humidity for 45 g m⁻² films based on neat CNF (○) and overdried (●), reinforced with 32.5 wt% of CNC-T (◇) and overdried (◆)

As presented in **Fig 2.17**, the thermal treatment was successful because it has a positive impact on oxygen barrier properties at high moisture contents (85 or 90 % RH). When

compared to a neat CNF film, oxygen-permeability is about 3 times lower. Thus, the OP at 85 % RH is almost equal to CNF/MMT films (2.1 instead of $1.7 \text{ cm}^3 \cdot \mu\text{m} \cdot \text{m}^{-2} \cdot \text{day}^{-1} \cdot \text{kPa}^{-1}$).

Such results are also confirmed by a recent study proposed by Sharma *et al.* (2014), in which a similar thermal treatment is used to enhance the barrier properties of neat CNF films. They reported the OP and WVP to decrease by 25-fold and 2-fold, respectively, after treatment at $175 \text{ }^\circ\text{C}$ for 3 h. The reduction in permeability was attributed to an increase in crystallinity, a reduction in the interfibril space or porosity, and an increase in hydrophobicity due to hornification.

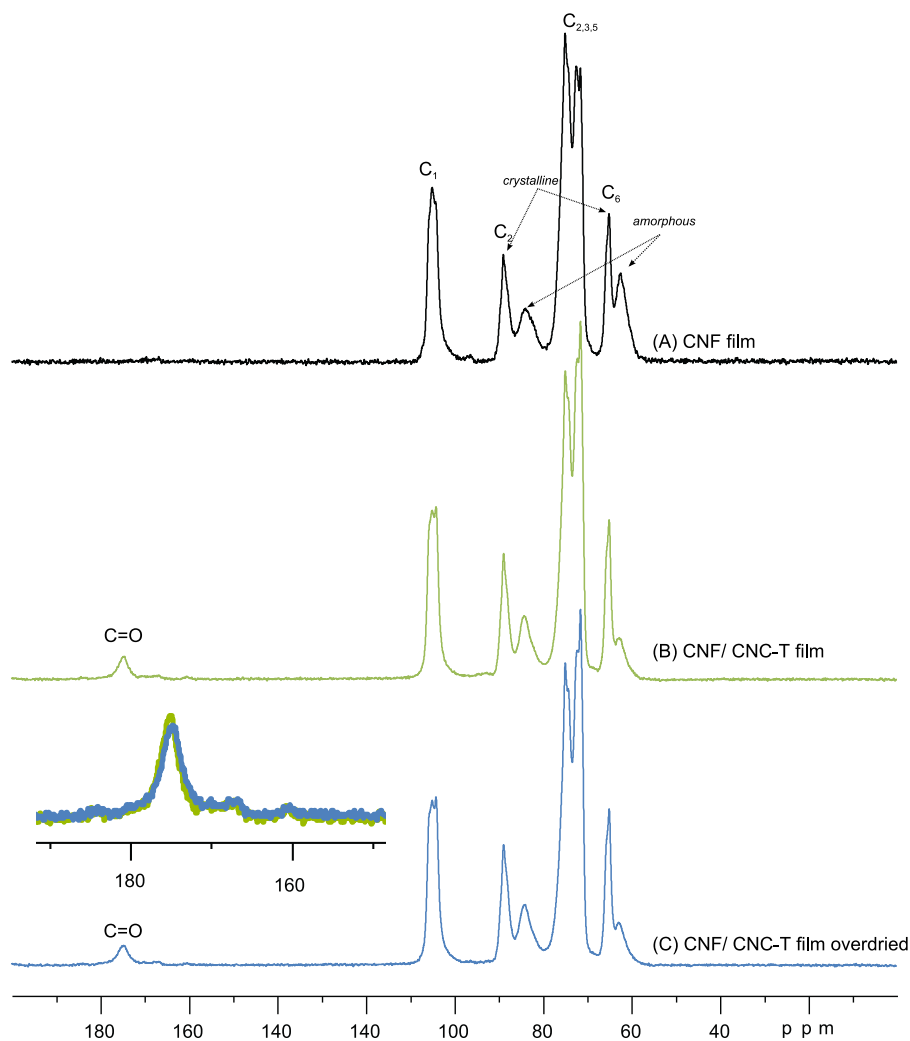


Fig 2.18 - CP-MAS Carbon-13 NMR spectra of nanocellulose films: neat CNF (A), CNF/CNC-T (B), and CNF/CNC-T overried (C) films. The spectral region corresponding to the $\text{C}=\text{O}$ signals (190–150 ppm) has been multiplied by a factor 5.

Fig 2.18 shows a typical high resolution ^{13}C NMR acquired under CPMAS condition of CNF and of the CNF/CNC-T films. For the spectrum of neat CNF films, the typical signals of cellulose were assigned to C_1 (δ 105 ppm), C_4 in crystalline forms (δ 89 ppm), C_4 in

amorphous forms (δ 84 ppm), C₂/C₃/C₅ (δ 75 and δ 72 ppm), C₆ in crystalline forms (δ 65 ppm), and C₆ in amorphous forms (δ 63 ppm). These assignments are based on previous studies (Atalla and VanderHart 1999, Montanari *et al.* 2005). The complex signal centered at 110 ppm assigned to C1 of celluloses is used for intensity normalization and to compare each spectrum. Very interestingly, the spectrum of CNF/CNC-T film is similar to the CNC film with two main differences. In comparison to the neat CNF film, the signal at δ 63 ppm of C₆ in amorphous forms presents a smaller intensity.

Secondly, a new signal appears at δ 175 ppm and is assigned to carboxyl groups formed during the oxidation of CNCs. No significant changes are observed for the other signals. The ¹³C NMR spectra (**Fig 2.18**) of both CNF/CNC-T without or with thermal treatment are strictly identical (no changes in the intensity of peaks or in the chemical shifts) although they exhibit different barrier properties (**Fig 2.17**). This feature clearly demonstrates that the thermal treatment of dried CNF/CNC-T films does not lead to formation of new covalent bonds. In addition, ¹H NMR spectra (not presented) shows that the total number of protons decreases significantly on thermal treatment, which can be interpreted as loss of water.

Based on both ¹³C and ¹H NMR spectra, there is no evidence that the carboxyl groups of CNC-T cross-link with the hydroxyl groups of CNF (or other CNC-T) during prolonged heating, since no change is observed for the signal at δ 174.8 ppm, neither in the signal shape nor in its intensity.

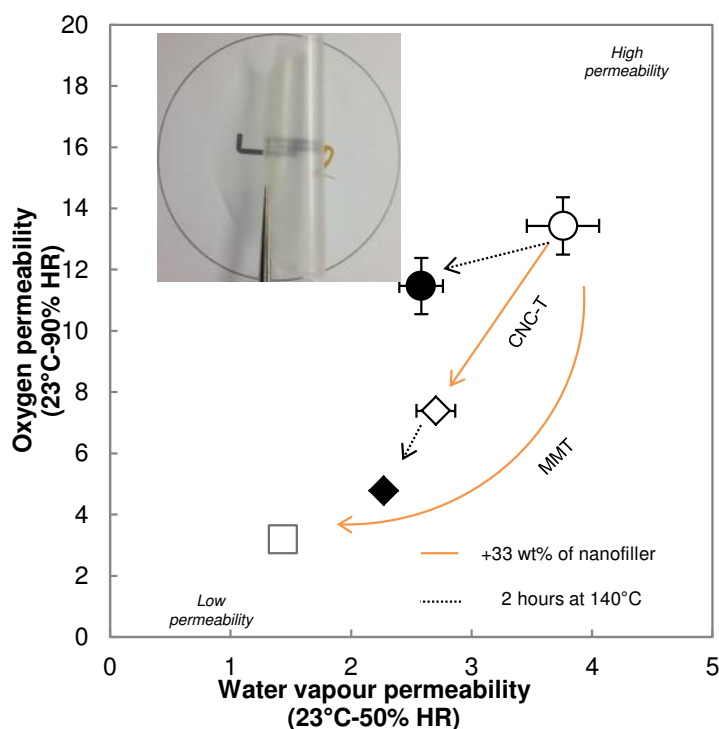


Fig 2.19 - WVP versus oxygen-permeability for different CNF films

Based on such results, it seems that the thermal treatment (i.e. 2 h at 140 °C) on a dried film only promotes H-bonding between the surface hydroxyl groups of CNF, creating a more cohesive network than for a film obtained by simple evaporation. **Fig 2.19** summarizes all the results obtained and proves the positive impact of CNC-T nanofiller in combination with dried CNF films submitted to a thermal treatment.

2.4 Conclusion and perspectives

The aim of this study was to design a transparent barrier film based only on nanocellulose with the same properties as films reinforced with nanoclay (i.e sodium montmorillonite, MMT). Films based on neat or oxidized CNFs exhibited good mechanical properties and excellent barrier properties to air and grease at low moisture content (< 50 % RH). However, they do not display good moisture-barrier properties, which is a prerequisite for packaging applications. To improve their performance, CNC-T or MMT were introduced as nanofillers. This resulted in increased density as well as increased crystallinity, which led to improved barrier properties. The CNF/MMT films are less moisture-sensitive. The main advantages of incorporating CNC-T nanofiller is an increase in mechanical properties as well as transparency of the CNF films. In addition, the films obtained are 100 % cellulose-based.

The last section was dedicated to bring about an additional improvement with thermal treatment (i.e. 2 h at 140 °C). It promotes H-bonding between the surface hydroxyl groups of the nanocellulose, creating a more cohesive network than for a film obtained by simple evaporation. This treatment has a strong impact on the oxygen-barrier properties at high moisture content (85 or 90 % RH).

Thus, the OP at 85 % RH is about the same as that of a CNF film with 32.5 wt% of MMT (2.1 instead of 1.7 $\text{cm}^3 \cdot \mu\text{m} \cdot \text{m}^{-2} \cdot \text{day}^{-1} \cdot \text{kPa}^{-1}$). This work paves the way for future studies or application of nanocellulose in high gas-barrier films or surface coatings for packaging.

Concluding remarks

In the present chapter, CNF films were considered as a model surface layer and two specific features were investigated. CNF were used as dispersive network for particles in a to (i) replace existing polymer in thin opaque films or (ii) as a substitute for mineral nanoparticles in barrier materials.

One target of the *Chapter 2.1* was to obtain an opaque solid film using TiO₂ particles dispersed in a CNF network. This was very successful because only a very small amount of TiO₂ (starting from 5 wt%) is needed to achieve high opacity film. From fundamental point of view, CNF forms a well-entangled nanofiber network in which spherical shape particles could be trapped and physically dispersed within the thickness of the CNF films. Such a nanocellulose network is an improvement compared continuous films with TiO₂ and classic matrices, in regards to the opacity and the mechanical properties of the ensuing materials. This study proposes different solutions for obtaining highly opaque hybrid CNF films and opens up the prospect for a new generation of opaque films or layers for specialty papers, but also light barrier packaging or printed electronics.

The aim of *Chapter 2.2* was to design a transparent and barrier film only based on all-nanocellulose with the same properties as films reinforced with nanoclay (i.e sodium Montmorillonite, MMT). To improve barrier properties of CNF film, oxidized CNCs were introduced as a nanofiller. This leads to a significant improving of barrier properties at high moisture content. The films obtained are 100% cellulose based. Lastly, all-nanocellulose films were submitted to a thermal treatment (i.e. 2 hours at 140°C). This treatment has a strong impact in oxygen barrier properties at high moisture content. As a key result, the oxygen permeability is about the same to CNF reinforced with MMT. This work paves the way for future studies for the application of all-cellulose barrier films or surface coatings.

Results obtained for the CNF model films demonstrate the potential of CNF for replacing conventional binder for two different applications, i.e. opaque and thin barrier materials. The results are promising since these properties are highly regarded in specialty papers. *Chapter 4* will focus on the first property (i.e. opacity). Indeed the CNF-based surface coating will be implemented at the industrial scale as a means of developing an innovative and cost effective solution for opaque lightweight paper dedicated to the offset lithography as shown in *Chapter 4.1*. Before the industrial application presentation, another type of nanocellulose, i.e. cellulose nanocrystals, will be studied in detailed in the next chapter for their iridescent properties.

List of Tables

Table 2.1 - Main features of opaque films made with different matrices with 0, 20 and 50 % TiO ₂	118
Table 2.2 - Main features of hybrid CNF films.....	123
Table 2.3 - Physical and chemical properties of nanocellulose and nanoclay used in the study.....	135
Table 2.4 - Mechanical, barrier, and optical properties of CNF films.....	137
Table 2.5 - Properties of CNF film reinforced with 32.5 wt% of CNC-T or MMT.....	139

List of figures

Fig 2.1 - Characterization of the CNF. Picture A corresponds to the gel-like suspension of CNF at 2.5% of consistency whereas Picture B corresponds to the same suspension observed through AFM at a scanning area of 10x10μm ² in TAPPING mode (Amplitude error).....	115
Fig 2.2 - Transparency of a 30g/m ² CNF solid film as a function of the volume ratio of TiO ₂ . Comparison between rutile (◇) and anatase (●) polymorphs. Pictures 1 to 4 corresponds to CNF films with an increasing amount of rutile TiO ₂ (0%, 2%, 7% and 20%).....	116
Fig 2.3 - E-SEM (BSE mode) of cross-sectional pictures of a CNF hybrid film (10% of TiO ₂).....	117
Fig 2.4 - Schematic representation of the 3 strategies used for CNF-TiO ₂ hybrid films.....	119
Fig 2.5 - Peak intensity (◇) and average z (●) as a function of the sol-gel reaction time. Pictures correspond to the AFM scan imaging in tapping mode (amplitude error, 3x3μm ² ,) at three reaction times (3, 66 and 126 minutes respectively).....	120
Fig 2.6 - AFM image of individualized CNF in which in-situ TiO ₂ (dotted circle) have been generated through the sol-gel reaction at a scanning area of 3x3μm ² in TAPPING mode (amplitude error).....	121
Fig 2.7 - FE-SEM pictures of hybrid films at two magnification level (Up:x10 000 and Down:x20 000). Comparison between the surface of blend, premix and hybrid films.....	122
Fig 2.8 - TG curves for hybrid films (TiO ₂ 20% w:w) for a 30mg sub-sample at a heating rate of 10 C/min in oxidizing atmosphere in the temperature range of 30–950°C. Comparison between blend, premix and sol-gel strategies.....	123
Fig 2.9 - XRD patterns of anatase TiO ₂ /CNF films. Comparison between blend, premix and hybrid strategies.....	124
Fig 2.10 - Graphical abstract of the study.....	129
Fig 2.11 - AFM images showing individualized nanoparticles: CNF(a) and CNC (b), after TEMPO-mediated oxidation, CNF-T (c) and CNC-T (d). Sample (e) corresponds to nanoclay (MMT).....	136
Fig 2.12 - Photographs and FE-SEM images of surfaces of a neat CNF film (a, c), and a TEMPO-oxidized CNF film (b,d).....	138
Fig 2.13 - FE-SEM images of surfaces of a CNF film reinforced with 32.5 wt % of CNC-T (a), and MMT (b).....	139
Fig 2.14 - XRD patterns of neat CNF film (a), freeze-dried CNC-T (b), and CNF/CNC-T film (c).....	140

Fig 2.15 - XRD patterns of neat CNF film (a), freeze-dried MMT (b), and CNF/MMT film (c)..... 141

Fig 2.16 – Oxygen permeability as a function of relative humidity for 45 g m⁻² films based on neat CNF (○), and reinforced with 32.5 wt% of CNC (◇), CNC-T (◆) or MMT (□) 142

Fig 2.17 – Oxygen-permeability as a function of relative humidity for 45 g m⁻² films based on neat CNF (○) and overdried (●), reinforced with 32.5 wt% of CNC-T (◇) and overdried (◆)..... 143

Fig 2.18 - CP-MAS Carbon-13 NMR spectra of nanocellulose films: neat CNF (A), CNF/CNC-T (B), and CNF/CNC-T overdried (C)films. The spectral region corresponding to the C=O signals (190–150 ppm) has been multiplied by a factor 5. 144

Fig 2.19 - WVP versus oxygen-permeability for different CNF films 145

References

1. Araki, Wada, et al., "Influence of surface charge on viscosity behavior of cellulose microcrystal suspension", Journal of Wood Science 45(3): 258-261 (1999).
2. Atalla and Vanderhart, "The role of solid state ¹³C NMR spectroscopy in studies of the nature of native celluloses", Solid State Nuclear Magnetic Resonance 15(1): 1-19 (1999).
3. Aulin, Gällstedt, et al., "Oxygen and oil barrier properties of microfibrillated cellulose films and coatings", Cellulose 17(3): 559-574 (2010).
4. Aulin, Salazar-Alvarez, et al., "High strength, flexible and transparent nanofibrillated cellulose–nanoclay biohybrid films with tunable oxygen and water vapor permeability", Nanoscale 4(20): 6622-6628 (2012).
5. Barata, Neves, et al., "Growth of BiVO₄ particles in cellulosic fibres by in situ reaction", Dyes and Pigments 65(2): 125-127 (2005).
6. Berglund and Liu, "Strong nanopaper with high oxygen barrier properties, comprising nanocomposites of microfibrillated cellulose nanofibers and layered clay and manufacture and use thereof", KTH Holding AB, WO2011059398A1 (2011).
7. Chinga-Carrasco, "Cellulose fibres, nanofibrils and microfibrils: The morphological sequence of MFC components from a plant physiology and fibre technology point of view", Nanoscale Research Letters 6 (2011).
8. Fukuzumi, Saito, et al., "Transparent and High Gas Barrier Films of Cellulose Nanofibers Prepared by TEMPO-Mediated Oxidation", Biomacromolecules 10(1): 162-165 (2008).
9. Fukuzumi, Saito, et al., "Thermal stabilization of TEMPO-oxidized cellulose", Polymer Degradation and Stability 95(9): 1502-1508 (2010).
10. Gane, Schenker, et al., "Process for production of nano-fibrillar cellulose gel composites for wide variety of applications", Omya, EP2386683A1 (2011).
11. Gane, Schoelkopf, et al., "Process for the production of nano-fibrillar cellulose suspensions", Omya, WO2010112519A1 (2010).
12. Habibi, Chanzy, et al., "TEMPO-mediated surface oxidation of cellulose whiskers", Cellulose 13(6): 679-687 (2006).
13. Husband, Svending, et al., "Paper filler composition", Imerys Minerals Limited, WO2010131016A2 (2010).
14. Iotti, Gregersen, et al., "Rheological Studies of Microfibrillar Cellulose Water Dispersions", Journal of Polymers and the Environment 19(1): 137-145 (2011).
15. Iwamoto, Abe, et al., "The Effect of Hemicelluloses on Wood Pulp Nanofibrillation and Nanofiber Network Characteristics", Biomacromolecules 9(3): 1022-1026 (2008).
16. Johansson, Bras, et al., "Renewable fibers and bio-based materials for packaging applications - A review of recent developments", Bioresources 7(2): 2506-2552 (2012).
17. Klemm, Schumann, et al., "Nanocellulose Materials – Different Cellulose, Different Functionality", Macromolecular Symposia 280(1): 60-71 (2009).
18. Kolen'ko, Burukhin, et al., "Synthesis of nanocrystalline TiO₂ powders from aqueous TiOSO₄ solutions under hydrothermal conditions", Materials Letters 57(5-6): 1124-1129 (2003).

19. Laine, Oesterberg, et al., "Method for producing furnish and paper by treatment with cationic polyelectrolyte and nanofibrillated cellulose", Upm-Kymmene Corporation, WO2010125247A2 (2010).
20. Lavoine, Desloges, et al., "Microfibrillated cellulose – Its barrier properties and applications in cellulosic materials: A review", *Carbohydrate Polymers* 90(2): 735-764 (2012).
21. Liu and Berglund, "Clay nanopaper composites of nacre-like structure based on montmorillonite and cellulose nanofibers—Improvements due to chitosan addition", *Carbohydrate Polymers* 87(1): 53-60 (2012).
22. Liu and Berglund, "Fire-retardant and ductile clay nanopaper biocomposites based on montmorillonite in matrix of cellulose nanofibers and carboxymethyl cellulose", *European Polymer Journal* 49(4): 940-949 (2013).
23. Liu, Walther, et al., "Clay Nanopaper with Tough Cellulose Nanofiber Matrix for Fire Retardancy and Gas Barrier Functions", *Biomacromolecules* 12(3): 633-641 (2011).
24. Marques, Trindade, et al., "Titanium dioxide/cellulose nanocomposites prepared by a controlled hydrolysis method", 66(7-8): 7 (2006).
25. Minelli, Baschetti, et al., "Investigation of mass transport properties of microfibrillated cellulose (MFC) films", *Journal of Membrane Science* 358(1-2): 67-75 (2010).
26. Mohanty, Misra, et al., "Sustainable Bio-Composites from Renewable Resources: Opportunities and Challenges in the Green Materials World", *Journal of Polymers and the Environment* 10(1-2): 19-26 (2002).
27. Montanari, Roumani, et al., "Topochemistry of Carboxylated Cellulose Nanocrystals Resulting from TEMPO-Mediated Oxidation", *Macromolecules* 38(5): 1665-1671 (2005).
28. Nelson and Deng, "Enhanced light scattering from hollow polycrystalline TiO₂ particles in a cellulose matrix", *Langmuir* 24(3): 975-982 (2008).
29. Nypelö, Österberg, et al., "Tailoring Surface Properties of Paper Using Nanosized Precipitated Calcium Carbonate Particles", *ACS Applied Materials & Interfaces* 3(9): 3725-3731 (2011).
30. Plackett, Anturi, et al., "Physical Properties and Morphology of Films Prepared from Microfibrillated Cellulose and Microfibrillated Cellulose in Combination with Amylopectin", *Journal of Applied Polymer Science* 117(6): 3601-3609 (2010).
31. Reddy and Yang, "Citric acid cross-linking of starch films", *Food Chemistry* 118(3): 702-711 (2010).
32. Ridgway and Gane, "Constructing NFC-pigment composite surface treatment for enhanced paper stiffness and surface properties", *Cellulose* 19(2): 547-560 (2012).
33. Rodionova, Lenes, et al., "Surface chemical modification of microfibrillated cellulose: improvement of barrier properties for packaging applications", *Cellulose* 18(1): 127-134 (2011).
34. Saarikoski, Saarinen, et al., "Flocculated flow of microfibrillated cellulose water suspensions: an imaging approach for characterisation of rheological behaviour", *Cellulose* 19(3): 647-659 (2012).
35. Schütz, Sort, et al., "Hard and Transparent Films Formed by Nanocellulose–TiO₂ Nanoparticle Hybrids", *PLoS ONE* 7(10): e45828 (2012).
36. Segal, Creely, et al., "An empirical method for estimating the degree of crystallinity of native cellulose using the x-ray diffractometer", *Text. Res. J.* 29: 786-794 (1959).
37. Sehaqui, Liu, et al., "Fast preparation procedure for large, flat cellulose and cellulose/inorganic nanopaper structures", *Biomacromolecules* 11(9): 2195-2198 (2010).

38. Shinoda, Saito, et al., "Relationship between length and degree of polymerization of TEMPO-oxidized cellulose nanofibrils", Biomacromolecules 13(3): 842-849 (2012).
39. Siro, Plackett, et al., "Highly Transparent Films from Carboxymethylated Microfibrillated Cellulose: The Effect of Multiple Homogenization Steps on Key Properties", Journal of Applied Polymer Science 119(5): 2652-2660 (2011).
40. Spence, Venditti, et al., "Water vapor barrier properties of coated and filled microfibrillated cellulose composite films", BioResources: 4370-4388 (2011).
41. Spoljaric, Salminen, et al., "Crosslinked nanofibrillated cellulose: poly (acrylic acid) nanocomposite films; enhanced mechanical performance in aqueous environments", Cellulose 20(6): 2991-3005 (2013).
42. Syverud and Stenius, "Strength and barrier properties of MFC films", Cellulose 16(1): 75-85 (2009).
43. Tang, Kumar, et al., "Recent Advances in Biopolymers and Biopolymer-Based Nanocomposites for Food Packaging Materials", Critical Reviews in Food Science and Nutrition 52(5): 426-442 (2011).
44. Tingaut, Zimmermann, et al., "Synthesis and Characterization of Bionanocomposites with Tunable Properties from Poly(lactic acid) and Acetylated Microfibrillated Cellulose", Biomacromolecules 11(2): 454-464 (2009).
45. Vilela, Freire, et al., "Synthesis and characterization of new CaCO₃/cellulose nanocomposites prepared by controlled hydrolysis of dimethylcarbonate", Carbohydrate Polymers 79(4): 1150-1156 (2010).
46. Wu, Saito, et al., "Ultrastrong and High Gas-Barrier Nanocellulose/Clay-Layered Composites", Biomacromolecules 13(6): 1927-1932 (2012).
47. Yang, Wang, et al., "Ester crosslinking of cotton fabric by polymeric carboxylic acids and citric acid", Textile Research Journal 67(5): 334-342 (1997).

Chapter 3

Self-assembly of cellulose nanocrystals in film

Table of contents

Introduction	159
1 Flexibility and color monitoring of CNC iridescent solid films using anionic or neutral polymers.....	161
Abstract	161
1.1 Introduction	162
1.2 Experimental section	164
1.2.1 Materials	164
1.2.2 Methods.....	164
1.3 Results and discussion.....	167
1.3.1 Self-assembly property of CNC in suspension	167
1.3.2 Interactions of water-soluble polymers with the CNC suspension	168
1.3.3 Adsorption phenomena of the water-soluble polymer with CNC	170
1.3.4 Adsorption phenomena of the water-soluble polymer with CNC	172
1.3.5 Tuning of iridescent solid film coloration.....	173
1.4 Conclusion and perspectives	179
2 Self-assembly of CNC with fluorescent agent in iridescent films	181
Abstract	181
2.1 Introduction	182
2.2 Experimental section	184
2.2.1 Materials	184
2.2.2 Methods.....	184
2.3 Results and discussion.....	187
2.3.1 Nanocellulose characterization and photophysical properties of DSBP...	187
2.3.2 Interactions between CNC particles and DSBP solution	188
2.3.3 Adsorption phenomena of DSPB with CNC	190
2.3.4 Efficiency of DSPB sorption on CNCs.....	192
2.3.5 Formation of fluorescent and iridescent film based on CNCs.....	194
2.4 Conclusions & perspectives	195
Concluding remarks.....	197
List of Tables.....	199
List of figures	199
References	201

Chapter 3

Self-assembly of cellulose nanocrystals in film

Introduction

It was also stated in **Chapter 1** that contrary to CNF suspension, a CNC suspension exhibits outstanding iridescent properties because of their self-assembly properties. This specific optical property will be used to develop a flexible, iridescent film with tunable color and fluorescent properties. While iridescent films based on CNCs are now widely reported in the literature, the two studies presented here address various enhancements in regards to (i) improving the film flexibility, (ii) controlling the coloration, and (iii) incorporating fluorescent properties.

In **Chapter 3.1**, two different water-soluble polymers are used. An anionic polymer, i.e. sodium polyacrylate (PAAS), is used to modulate the film coloration and, a neutral polymer, i.e. polyethylene glycol (PEG), is used to improve the iridescent film's flexibility.

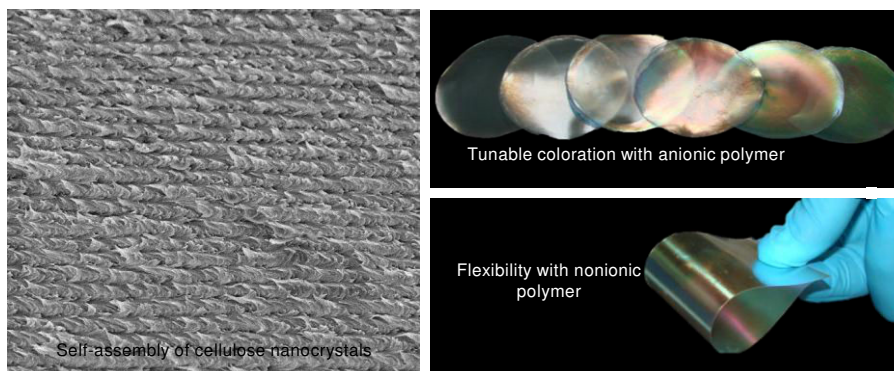
In **Chapter 3.2**, a fluorescent molecule, i.e. distyrylbiphenyl sodium sulphonate (DSBP) is studied to develop a film with iridescent properties under natural light and fluorescent when observed with UV illumination. The sub-chapters are organized as follows: (i) the characterization of commercial CNC, as well as the investigation of the CNC self-assembly property in suspension, (ii) the physical-chemical interaction of the additive with CNCs, and (iii) end-use properties of iridescent film (mechanical, thermal, and optical)

It should be pointed out that the choice of these different additives was motivated by a couple of considerations. Because of their chemical nature and low molecular weight, they do not inhibit CNC self-organization. In addition, their different roles as plasticizers, dispersants, and fluorescent agents are already proven in other material. Lastly, industrial partners commonly use these materials.

Another point to mention is that to facilitate the industrialization within the project, CNCs used in this study came from commercially available sources, either the University of Maine (USA) or Celluforce (Canada). To the best of our knowledge, none of the scientific papers dealing with the self-assembly of CNC in films have used such type of commercial CNCs. In this project, the use of iridescent materials is anticipated for use in designing anti-counterfeiting papers.

1 Flexibility and color monitoring of cellulose nanocrystal iridescent solid films using anionic or neutral polymers

This section is adapted from “Raphael Bardet, Victor Perrin, Naceur Belgacem, Julien Bras, Flexibility and color monitoring of cellulose nanocrystals iridescent solid films thanks to anionic or neutral polymers, Applied Materials and Interfaces (submitted in september 2014)”.



Abstract

One property of sulfated cellulose nanocrystals (CNCs) is their ability to self-assemble from a concentrated suspension under specific drying conditions into an iridescent film. Such colored films are very brittle, which makes them difficult to handle or integrate within an industrial process. The goal of this study is (i) to produce flexible films using neutral polyethylene glycol (PEG) and (ii) to modulate their coloration using an anionic polyacrylate (PAAS). The first part is dedicated to studying the physicochemical interactions of the two polymers with CNCs using techniques such as zeta potential measurements, dynamic light scattering (DLS), quartz crystal microbalance (QCM) and atomic force microscopy (AFM). Iridescent solid films were then produced and characterized using scanning electron microscopy (SEM) and UV-visible spectroscopy. The mechanical and thermal properties of films incorporating CNC were measured to evaluate improvements in flexibility. The addition of 10 wt % of PEG makes these films much more flexible (with a doubling of the elongation), with the coloration being preserved and the temperature of degradation increasing by almost 35°C. Up to 160 $\mu\text{mol/gCNC}$ PAAS can be added to tune the coloration of the CNC films by producing a narrower, stronger coloration in the visible spectrum (higher absorption) with a well-pronounced fingerprint texture.

Keywords: Cellulose nanocrystals, structural color, flexible iridescent films; polymer additives

1.1 Introduction

In contrast to common pigment coloration, some surfaces appear colored only because of the interaction between light and their microstructure. This is known as structural coloration, and iridescence associated with this phenomenon is a major field of investigation (Kinoshita *et al.* 2008). Progress in engineering nanostructures has enabled the mimicry of nature for applications within many fields, such as display technologies, painting, printing, textiles and cosmetics (Parker and Townley 2007, Moon *et al.* 2011).

Since 2010, the use of biobased nanomaterials for the design of photonic nanostructures has become a promising prospect in the field of optical encryption technology. Cellulose nanocrystal (CNC) is one of the most promising biobased nanomaterials, as exhibited by growing interest at the industrial scale following the recent construction of the first CNC processing plants in 2011 and the growth of the patent portfolio since 2008 (Charreau *et al.* 2013).

This study will focus only on the self-organization properties of CNC. Due to the well-known property of CNCs to display liquid-crystalline behavior in water, one outstanding application is the manufacturing of iridescent materials as stated in the **Chapter 1**. As a reminder, several physical and chemical parameters are reported to influence the coloration of the iridescence of the film (**Table 1.14**).

To the best of our knowledge, the most efficient parameters for tuning the film coloration are the addition of monovalent salts and sonication as reported by Beck *et al.* (2011). However, over sonication or the addition of an excess of salt can irreversibly inhibit the self-organization, resulting in a loss of coloration. Another outstanding issue is that iridescent films based on only CNC are usually very brittle and difficult to handle. However, only a couple of studies have tried to overcome this drawback. Polyvinyl alcohol (PVA) and styrene-butadiene (SB) latex have been used to improve the CNC film flexibility without affecting the iridescence as patented by Zou *et al.* (2010). More recently, the incorporation of cellulose nanofibrils within the CNC suspension has also been reported to improve film flexibility. (Xiong *et al.* 2014) In this case, it seems that the iridescent properties of films are inhibited with cellulose nanofibrils addition.

One approach that can address these two issues is to use water-soluble polymers or surfactants to interact with the CNC self-assembly process. In most cases, this promotes the suspension gelation of the CNC suspension; so no chiral nematic order was reported. (Boluk *et al.* 2012, Dorris and Gray 2012, Hu *et al.* 2014)

The use of an anionic polymer for this purpose has never been investigated. Recently, the addition of polyols to the CNC dispersion has been proposed as a means of plasticizing the CNC film,(Kelly *et al.* 2013) thus eliminating cracking and modifying the coloration of the iridescent films through a redshift (Mu and Gray 2014).

This study investigates the influence of anionic and neutral water-soluble polymers on the self-assembly properties of CNC in both suspensions and solid films. An anionic polymer, sodium polyacrylate (PAAS), was used to modulate the film's coloration, and a neutral polymer, polyethylene glycol (PEG), was used to improve the film's flexibility. These polymers were selected because they do not cause flocculation of the CNC suspension. The first part of the study determines the main features of CNCs and their self-assembly properties in suspension, and the second part investigates the added polymers' physical and chemical interactions with CNC in suspension.

1.2 Experimental section

1.2.1 Materials

The starting material for producing iridescent solid films is a commercial Cellulose Nanocrystal (CNC) suspension used as received (without dialysis). It was purchased from the UMaine Process Development Center (University of Maine, USA) that was extracted from wood pulp using sulfuric acid hydrolysis. The dry matter of the CNC suspension was 6.5 wt %, as measured using a moisture analyzer (MA35, Sartorius, Germany). The anionic sodium polyacrylate (PAAS) is a commercial dispersant agent (TOPSPERCE® GXN, Coatex, France). According to the supplier, the molecular weight (Mw) of the dispersant is 5000 g/mol and the pH is 7.5. The sample is of commercial grade, and so it will have some impurities as received. Polyethylene glycol (PEG) with a molecular weight of 200 g/mol and polyethylenimine (PEI) with a molecular weight of 1300 g/mol were delivered by Sigma-Aldrich (USA). Deionized water (5 μ S/cm) was used in all experiments.

1.2.2 Methods

CNC dispersion and solid film formation

To obtain a homogeneous and well-dispersed suspension, the 6.5 wt % CNC suspension was exposed to a dispersive energy of 5 kJ/g_{CNC} using a 200 watt sonication probe (Sonifier® S-250A, Branson, USA). The CNC suspension and 100 μ M polymer solutions were mixed with a homogenizer (Ultraturrax T8®, IKA, France) for 3 minutes at room temperature.

CNC suspensions (with or without PEG and PAAS) were cast into a smooth aluminum plate (6 cm in diameter) and left to dry for 3 days under ambient conditions (50% RH, 23°C). For each series, 4 dry freestanding films of 100 g/m² were obtained and stored under these conditions until analysis.

Rheological and self-assembly characterizations of CNC suspensions

The rheological behavior of the suspensions was investigated using a controlled-stress rheometer (Physica MCR 301, Anton Paar Physica, Austria) with a cone/plate spindle (ref. n°: CC 50) used at a 1 s⁻¹ constant shear rate with a 1 mm gap via a Peltier system. Flow curves were recorded at 20°C for 500 s until flow stabilization, and the viscosity was calculated using the average of the last 30 seconds. Each measurement was taken in triplicate and averaged.

Interactions of the water-soluble polymer with the CNC suspension

Samples were prepared from CNC suspensions diluted to approximately 0.5 wt % in deionized water or 100 μM polymer solutions (PAAS, PEG, PEI).

The electrophoretic mobility of CNC was measured using a zeta potential analyzer (Zeta2000, Malvern Instruments, USA). The reported electrophoretic mobility (U_e and zeta potential) was determined from an average of 10 measurements. A few drops of 1mM NaCl solution was added to maintain the conductivity of the suspension ($500 \mu\text{S}\cdot\text{cm}^{-1}$).

Dynamic light scattering (DLS) was used to measure the size of the nanoparticles (Vasco® I, Corduan Technologies, France). The cumulative method was used and two parameters were taken into account, the hydrodynamic diameter (z^*) and the polydispersity index (PDI). For each sample, each measurement was replicated 3 times. NaCl solution was added to maintain the conductivity of the suspension ($500 \mu\text{S}\cdot\text{cm}^{-1}$).

Sorption measurements were taken using a quartz crystal microbalance with dissipation (QCM-D). This instrument (Q-Sense® E1, Biolin Scientific, Sweden) measures the resonance frequency of the oscillation of a quartz crystal for its fundamental frequency (5 MHz) and selected overtones (15, 25, 35, 45, 55 and 75 MHz). Only the seventh overtone was used in the data evaluation since it provides both an appropriate measurement sensitivity and a very stable and reproducible measurements as compared to lower overtones.

The adsorbed mass (ng/nm^2) was estimated from the frequency change (Δf) using the Sauerbrey equation. Adsorption curves were calculated from the process as carried out onto 100 nm gold-coated quartz crystals (QSX301, Biolin Scientific, Sweden).

All measurements were performed under a constant flow rate (100 $\mu\text{l}/\text{min}$) and temperature (23°C). Before performing analyses, gold surfaces were cleaned with a “piranha” solution (30% of $\text{H}_2\text{O}_2/\text{NH}_3$ 1:3, by weight) for 20 minutes at 70°C, rinsed with deionized water, and then submitted to an UV/ozone treatment (ProCleaner™, Bioforce, USA) for 20 minutes.

Prior to processing, a 100 μM cationic polyethylenimine solution (PEI, Sigma Aldrich) was adsorbed onto the clean gold surfaces to facilitate the irreversible adsorption and bonding of CNCs to the crystal sensor. In the beginning of each experiment, deionized water was passed through the chamber until a stable baseline ($\Delta f < 0.05/\text{min}$) was achieved for 5-20 minutes.

Solid film formation.

CNC suspensions (at 5.3 wt % with or without PEG and PAAS) were cast (5 ml per film) into a smooth aluminum plate (6 cm in diameter) and left to dry for 3 days under ambient and controlled conditions (50% RH, 23°C). For each series, 4 dry free-standing films of 100 g/m² were obtained and stored under these conditions until analysis.

Film characterization. The structural coloration of the films was analyzed using UV-visible spectroscopy (UV 1800, Shimadzu, Japan). The absorption intensity of the solid film was recorded within the wavelength range of 200 to 1100 nm with a normal incidence. For each film, three different measurements and ten scans were recorded and averaged.

Mechanical properties were measured using a universal testing machine (Model 4465®, Instron Engineering Corporation, US). Young's modulus, the tensile strength and the elongation rate were established following the ISO-1924-2:2008 standard. For each series, six samples of 15 mm in width and 50 mm in length were submitted to a 10 mm/min constant rate of elongation. The thermal degradation of the samples was monitored using TGA (thermogravimetric analyzer, STA 6000®, PerkinElmer Instruments, England). The mass loss was recorded for a 30 mg subsample upon a heating rate of 10°C/min in the temperature range of 30–950°C under an oxidizing atmosphere (air). The analyses were duplicated and averaged.

FE-SEM (Field-emission scanning electron microscope) was used to observe the film microstructure (Ultra 55 ©, Zeiss, Germany). Samples were glued onto a specific holder and coated with a 2 nm layer of gold/palladium to ensure the conductivity of all samples. The accelerating voltage (EHT) was 3 kV for a working distance of 6.4 mm.

1.3 Results and discussion

1.3.1 Self-assembly property of CNC in suspension

Before proceeding to the film formation, the physical and chemical properties of the commercial cellulose nanocrystal (CNC) suspension were determined as summarized in **Table 3.1**.

Table 3.1 - Physical and chemical properties of the CNC used in the study

Properties	Techniques	Value	Standard deviation	
Morphology	Length (nm)	205	(83)	
	Thickness (nm)	5	(3)	
	Aspect ratio	41	(14)	
	Crystallinity Index (%)	XRD	86	(2)
Chemical	Sulfur content ($\mu\text{mol/g}_{\text{CNC}}$)	EA	372	(16)
Physicochemical	Surface charge density (e/nm^2)	calculation based on both AFM and EA	0.56	(0.02)

CNCs have a rod-like shape and their average dimensions are 5 nm thick by 205 nm long. Such a morphology is in accordance with previous studies for CNCs extracted with similar hydrolysis conditions (wood pulp and sulfuric acid). (Habibi *et al.* 2010) The XRD pattern (not presented) is typical of the crystalline polymorph of neat cellulose I (native cellulose). The major crystalline peak (002) occurs at 22.84° , and the associated crystallinity index (CI) is 88%. The sulfur content estimated via ICP-AES elemental analysis is $370 \mu\text{mol/g}_{\text{CNC}}$. The surface charge density is approximately $0.56 \text{ e}/\text{nm}^2$, as calculated using both AFM and EA. By comparison, values between $0.16\text{-}0.66 \text{ e}/\text{nm}^2$ were previously reported for CNCs having self-assembly properties. (Dong *et al.* 1998, Beck *et al.* 2005) Therefore, according to these preliminary characterizations, it should be possible to obtain colored films from this pilot-scale production of CNCs.

As mentioned in the introduction, it is essential to determine the critical anisotropic concentration C_A^* for which the suspension is completely anisotropic. (Shafiei-Sabet *et al.* 2012) For this purpose, rheological analyses as a function of the CNC concentration were combined with polarized optical microscopy (POM), as illustrated in **Fig 3.1**.

A well-dispersed, CNC suspension of 13 wt % concentration was prepared by centrifugation ($10,000g$, 10 min, 10°C). Other concentrations were prepared with successive dilutions to a minimum of 0.5 wt % using DI water and sonicated at $5 \text{ kJ/g}_{\text{CNC}}$.

The minimal concentration in which an anisotropic texture was observed was approximately 2.5 wt % (**Fig 3.1-A**). Below this concentration, the suspension was isotropic, with CNC randomly dispersed in the aqueous medium. At 5.3 wt %, the CNC suspension was predominantly anisotropic, and fingerprint textures were observed on the whole POM micrograph (**Fig 3.1-B**).

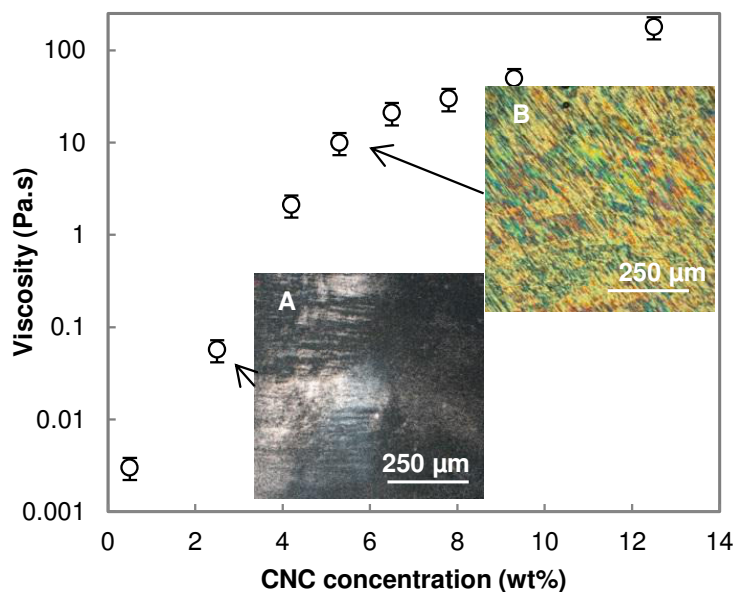


Fig 3.1 - Viscosity as a function of the CNC concentration (25°C with a shear of 1/s) with the corresponding micrographs between crossed polarizers (A: 2.5 wt % and B: 5.3%)

The value of C_A^* reported here is in accordance with a more extensive study in which authors reported a value of 6.5 wt % obtained with the study of phase separation of CNC isolated from cotton filter with a surface charge density of 0.35 e/nm^2 . (Ureña-Benavides *et al.* 2011) 5.3 wt % has been considered as the optimum concentration for casting CNC suspensions to manufacture iridescent solid films considering both the suspension is predominantly anisotropic and not too viscous to obtain a good film by evaporation.

1.3.2 Interactions of water-soluble polymers with the CNC suspension

Before discussing the manufacturing of iridescent CNC films, this section focuses on the interactions of anionic or neutral polymers with CNC in suspension. Two polymers have been investigated, an anionic dispersant, i.e. sodium polyacrylate (PAAS), to tune the coloration of the iridescent CNC film and a neutral plasticizer, i.e. polyethylene glycol (PEG), to improve film flexibility. In addition, a classic cationic polymer, polyethylenimine (PEI), was also tested to understand the interactions that favor deposition onto CNCs, as measured by QCM-D. It is assumed that a colloidal dispersion is stabilized via either electrostatic repulsion or steric stabilization with adsorbed or grafted polymers. (Hu *et al.* 2014)

One advantage of CNC stabilized via steric stabilization is that the colloidal state is less sensitive to the presence of monovalent salt.(Araki *et al.* 2000) In the other cases, physicochemical interactions are critical to iridescence because the self-assembly of CNCs is extremely sensitive to the electrochemical equilibrium.(Araki and Kuga 2001) The *zeta* potential can be used as a measurement of the electrostatic repulsive forces, which can provide information on the stability of the colloidal system, and indirectly on the self-organization of CNCs in suspension. A value smaller than ± 15 mV is considered to indicate the onset of particle agglomeration. Values greater than ± 30 mV generally mean that there is sufficient mutual repulsion, which results in colloidal stability.(Mirhosseini *et al.* 2008)

Table 3.2 compares the hydrodynamic and electrokinetic parameters of CNCs dispersed in deionized water with ionic (PAAS) and non-ionic (PEG) polymers. The zeta potential of CNCs dispersed in deionized water is highly negative (-44.5 mV) due to the high surface charge density of the sulfate half-ester groups.

Table 3.2 - Electrokinetic potential, hydrodynamic size and colloidal behavior of a 0.5% CNC suspension dispersed in water and 100 μ M water-soluble polymer solutions

	CNC dispersed in				
	DI water	PAAS	PEG	PEI	
Hydrodynamic properties^a	z^* (nm)	105 (5)	120 (10)	122 (10)	856 (8)
	PDI	0.20 (0.05)	0.18 (0.05)	0.22 (0.08)	0.75 (0.22)
Electrokinetic potential^b	$p\zeta$ (mV)	-44.8 (1.2)	-45.3 (0.8)	-32.3 (1.0)	+15.0 (1.1)
	Ue (V)	-3.5 (0.07)	-3.5 (0.2)	-3.22 (0.09)	1.18 (0.09)
Colloidal behavior^c	Birefringent	Birefringent	Birefringent	No	

Obtained via DLS^a and zeta potential^b analyses. Observation between cross polar after stirring^c. Values in brackets refer to the standard deviations.

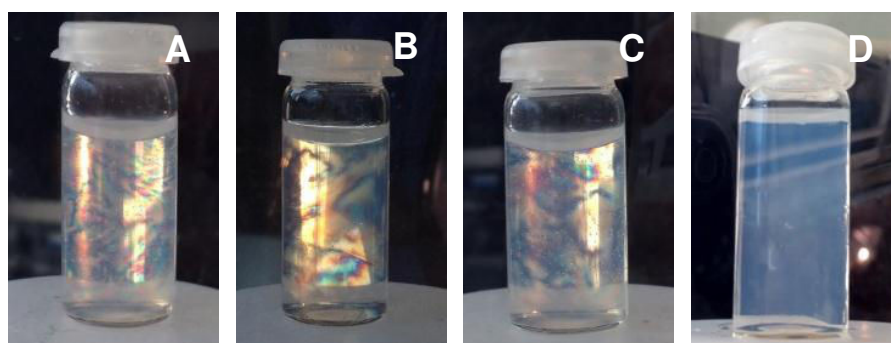


Fig 3.2 - Crossed polarizers observation of 0.5wt % CNC dispersed in water (A) and in 100 μ M polymers solutions of PAAS (B), PEG (C), and PEI (D)

In the presence of anionic polymers such as PAAS, the surface charge remains highly negative (-45.3 mV) and the hydrodynamic diameter is unmodified. Upon the addition of a neutral polymer like PEG, the mobility decreases (-32.3 mV) because of polymer absorption.

It also influences the hydrodynamic diameter (z^*), which increases from 105 to 122 nm. As for CNC dispersed in DI water, intense birefringence patterns are observed for CNC dispersed in PAAS and PEG solutions (**Fig 3.2 A, B, and C**). This confirms the absence of agglomeration, as well as the preservation of the self-assembly properties of CNC in suspension. In contrast, in the case of dispersion in a cationic PEI solution, the flow birefringence completely disappeared (**Fig 3.2.D**) and the zeta potential shifted from -44.5 mV to +15.0 mV. This confirms an ionic interaction between the negative sulfate half-ester groups of CNCs and the positive amino groups of PEI. This also led to the formation of particle flocculation, as proven via DLS measurement ($z^*=856$ nm). This last experiment was conducted only to evaluate the absorption phenomena because PEI was only used for the functionalization of the gold-coated mica plate for QCM experiments and CNC deposition.

1.3.3 Adsorption phenomena of the water-soluble polymer with CNC

The adsorption phenomena were evaluated using a quartz crystal microbalance (QCM) (Figure 2) in combination with AFM analysis (**Fig 3.3**).

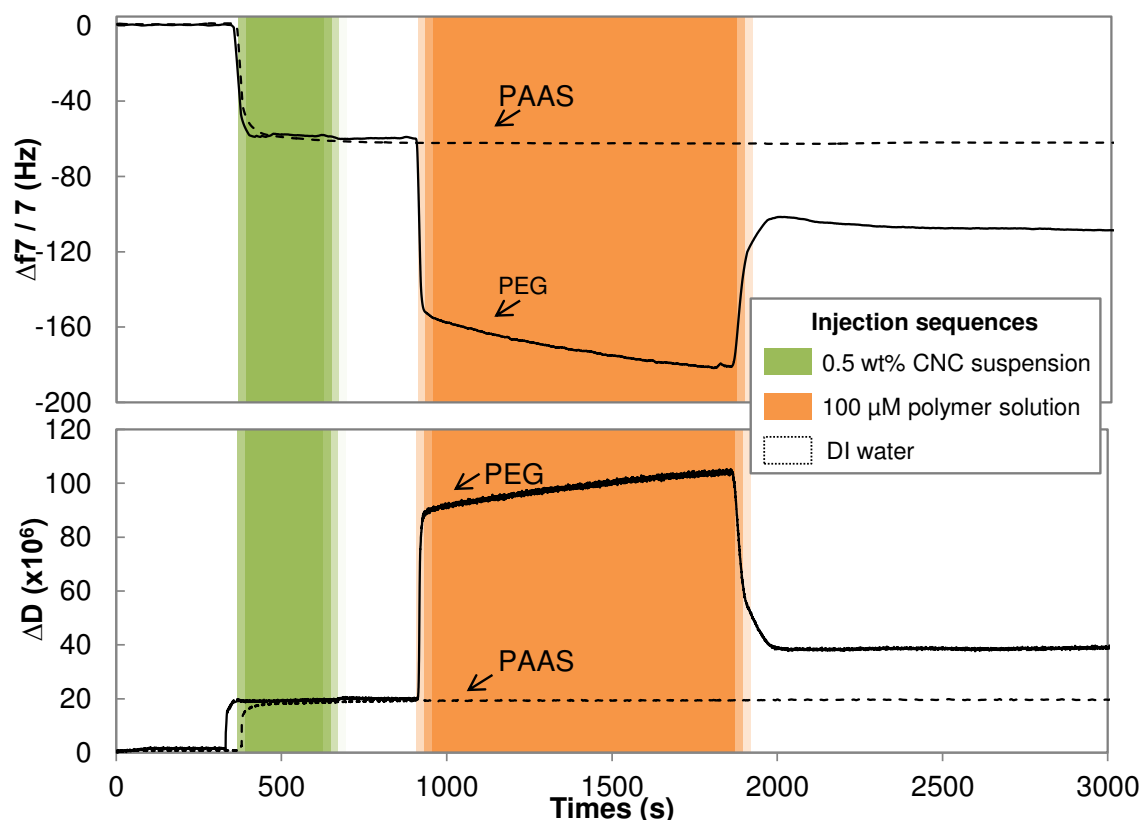


Fig 3.3 - QCM-D studies (7th overtone) of CNC and polymer (PAAS and PEG) adsorption on a PEI-modified gold surface. The 1st injection corresponds to the 0.5 wt % CNC suspension (green area) whereas the 2nd one injection corresponds to of the 100 μ M polymer solutions (orange area). Uncolored sections correspond to the rinsing stage with DI water.

As a preliminary investigation, it was verified that the adsorbed CNC layer was thick enough to avoid a positively charged substrate effect with PEI. Based on the frequency drop ($\Delta f \sim -57$ Hz) and the Sauerbrey equation, the average adsorbed weight of CNC onto the substrate was approximately 1180 ng/cm^2 , corresponding to a CNC layer of approximately 7 nm, assuming the density of CNCs is 1.53. This confirms that the adsorbed CNC layer is thick enough to avoid possible interactions with the cationically charged sensor (PEI layer).

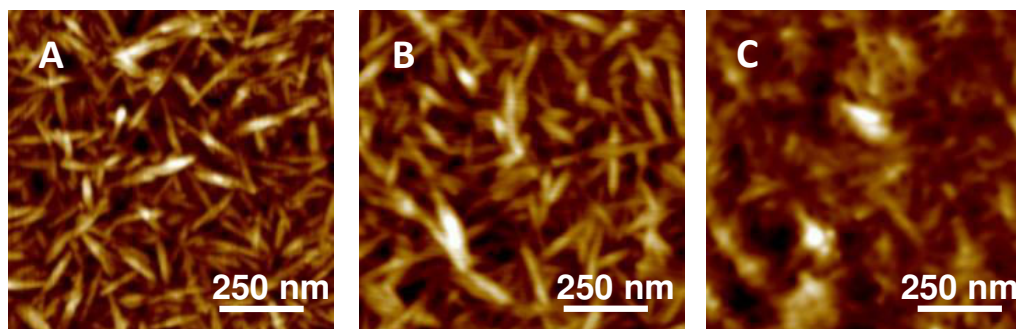


Fig 3.4 - AFM pictures (height sensor) corresponding to the air-dried substrate analysis of QCM experiments: after injection of CNC and rinsing (A), after injection of PAAS and rinsing (B), after injection of PEG and rinsing (C).

AFM analyses were carried out on the air-dried substrate surface after CNC adsorption and rinsing with DI water (**Fig 3.4-A**). These AFM pictures emphasize that the CNC adsorbed layer displays good surface coverage with a random orientation of rods. The CNC layer can also form a three-dimensional network with a larger exposed surface area. The adsorbed CNC cannot be considered as a continuous layer, as can films formed by classical polymers with a high film-forming ability. Hence, for further calculation of the amount of adsorbed polymers on the CNC substrate, it is necessary to take into consideration the specific surface topography of the CNC layer as proposed for CNFs by Ahola *et al.* (2008). From AFM calculations carried out on three scanning areas of $9 \mu\text{m}^2$, the developed surface area of the CNC layer is approximately $16 \pm 2 \mu\text{m}^2$. This means that for an adsorption study using QCM, a sensor of 1 cm^2 must be considered to have a surface area of 1.8 cm^2 . Based on the heterogeneity of the CNC substrate, the amount of adsorbed polymer should be considered only semi quantitative.

When PAAS is injected, no adsorption ($\Delta f < -0.5$ Hz) was detected using QCM. That makes sense because PAAS as anionic surfactant has no tendency to adsorb onto negatively charged CNCs. Furthermore, there is no difference between AFM images before and after the injection of PAAS (**Fig 3.4-A and B**), confirming the absence of adsorption of PAAS onto CNC, suggesting depletion stabilization.

On the other hand, QCM measurements upon the adsorption of PEG show a large frequency drop ($\Delta f \sim -121$ Hz), suggesting the occurrence of physical sorption. For this polymer, nonionic interactions (hydrogen bonds) between CNCs and PEG may be the cause of the sorption phenomena. Just after the injection of PEG solution, an important desorption ($\Delta f \sim +79$ Hz) is observed during rinsing with DI water.

This confirms that CNC surfaces are saturated with the adsorbed polymer, suggesting steric stabilization. The adsorbed amount of PEG on CNC surface ($\Delta f \sim -40$ Hz, i.e. 830 ng/cm²) is equivalent to that reported by Hu *et al.* (2014) for hydroxypropyl guar (HPG) on similar surfaces. Using the average CNC dimensions (5 nm × 5 nm × 205 nm), the specific surface area is calculated to be 250 m²/g, the adsorption of PEG can be estimated to be 580/g_{CNC}, i.e. 12 wt %. AFM (Figure 3.C) highlights that after PEG adsorption onto the CNC substrate, the layer appears to be smoother, suggesting that polymer coating onto the CNCs has indeed occurred. By comparison with other studies, when PEG is covalently grafted onto desulfated CNC, (Kloser and Gray 2010) or carboxylated CNC, (Araki *et al.* 2000) the adsorption is significantly higher, approximately 1-1.5 mmol/g_{CNC}.

To summarize, neutral PEG can be physically adsorbed onto CNCs and, due to steric stabilization and non-ionic interactions (hydrogen bonds), the self-assembly of the suspension is retained as previously reported with PEG-grafted CNCs. (Kloser and Gray 2010) Limited interactions were found to originate from the adsorption of anionic PAAS, as expected, and the CNCs maintained their self-assembly properties due to depletion stabilization (i.e. free polymer in the dispersion medium). Next, we will evaluate the influence of these polymers on the final CNC iridescent solid film.

1.3.4 Adsorption phenomena of the water-soluble polymer with CNC

Following the simple evaporation of the CNC suspension, the self-assembly properties are preserved within the solid films, which results in their structural organization as shown in **Fig 3.5**. Similar FE-SEM observations were recently reported by Majoinen *et al.* (2012). At low magnification, FE-SEM analyses (**Fig 3.5.A**) indicate that the layers remain parallel to each other. In contrast, **Fig 3.5.B** gives an interesting indication of the pitch length and the preferential orientation of CNCs (handedness and direction).

The self-assembly of CNCs has also an impact at different scales and not only on the film coloration. For instance, barrier and mechanical properties are different when comparing a structured film to a non-ordered film made from the same CNC suspension. (Bardet *et al.* 2014)

In comparison to a non-ordered film, the mechanical properties for a structural film are low, and generally the iridescent film is very brittle with a high Young's Modulus and a low strain at break.(Bardet *et al.* 2014)

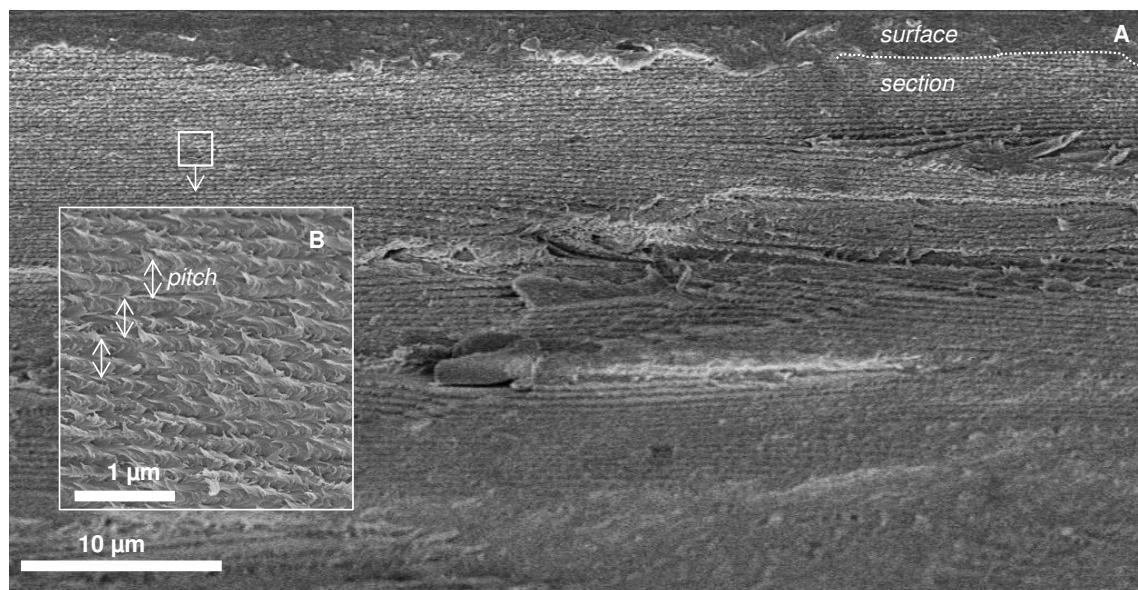


Fig 3.5 - FE-SEM images of a fracture surface across an iridescent CNC film

1.3.5 Tuning of iridescent solid film coloration.

Adjusting the coloration by modifying the chiral-nematic organization and improving the color homogeneity is essential for developing an optical material for anti-counterfeit applications. One effective parameter is the sonication process, which leads to a solid film redshift,(Beck *et al.* 2011) and the addition of monovalent salt (NaCl), which causes a blueshift to the solid film (Dong *et al.* 1996).

However, several limitations exist when monovalent salt is added, namely (i)an irreversible inhibiting effect on self-organization, (ii) tuning coloration with NaCl is limited to a specific range of ionic strengths and (iii) an excess of salt (concentrations greater than 20 mM)(Bardet *et al.* 2014) cause particle agglomeration and suspension gelation. To overcome these issues, neither salt nor cationic polymer was used in this study. Instead the anionic linear polyelectrolyte PAAS with a low molecular weight ($M_w \sim 5000$ g/mol) has been used for tuning coloration.

In contrast to monovalent salt, the high density of negative groups (COO^-) prevents PAAS from adsorbing with the CNC, as confirmed using QCM-D (**Fig 3.3**) and electrokinetic potential analysis (**Table 3.2**).

At the macro-scale, though, the addition of PAAS modifies the rheology and chiral-nematic organization of the CNC suspension, in particular its rheology. **Fig 3.6** presents the

evolution of the suspension viscosity as a function of the PAAS concentration. Upon adding PAAS, the viscosity sharply decreased, reaching a minimum of 4.1 Pa.s at 160 $\mu\text{mol/g}_{\text{CNC}}$ of PAAS. A higher amount of PAAS results in the inhibition of the self-organization of the films, as detected by the disappearance of the fingerprint texture when using higher PAAS concentration than 600 $\mu\text{mol/g}_{\text{CNC}}$.

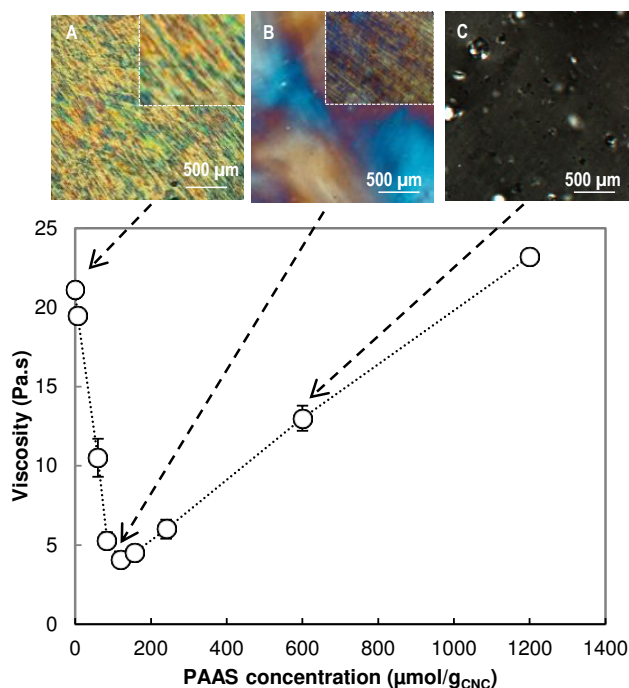


Fig 3.6 - Viscosity of a 5.3 wt % CNC suspension as a function of the PAAS concentration (at 25°C for a shear of 1 Hz), accompanied by fingerprint textures (A, B, and C), as observed using polarized optical microscopy

It has been shown in the previous section there is no adsorption of PAAS with CNC, suggesting depletion stabilization. Even their small size ($R_{\text{gyration}} \approx 3.4 \text{ nm}$), anionic polymer chains will have no tendency to interleave between negatively charged CNCs. PAAS is more likely to move outside crystallites in which electrostatic repulsion will not be predominant. This will lead to a non-homogenous repartition of PAAS within the CNC suspension, leading to a concentration difference around and within crystallites. This concentration difference of PAAS creates an osmotic pressure difference, resulting in a decrease of both chiral nematic pitch and viscosity as illustrated in **Fig 3.7**. Such statement must be assessed by Small angle X-ray diffraction (SAXD) experiments at the nanoscale. (Osorio-Madrado *et al.* 2012)

Another explanation could be the highly hygroscopic behavior of PAAS, which is able to absorb water up to 100 times its initial weight. (Cerolini *et al.* 2009)

Moreover, it has been reported by Zhang *et al.* (2012) that water sorption within CNC iridescent films has caused a redshift. Thus, it can be assumed that the remaining free water molecules may be predominantly absorbed by PAAS, explaining the decrease in pitch in the CNC film.

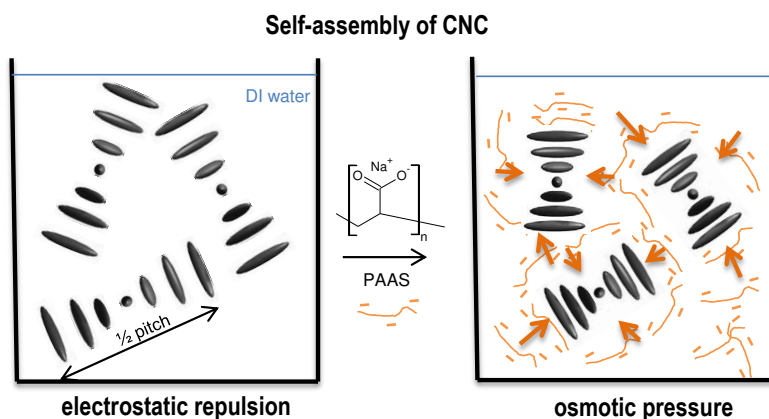


Fig 3.7 - Mechanism that could explain the blueshift occurring upon the addition of PAAS

The analyses were then carried out at solid state by measuring the maximal absorption wavelength (λ_{\max}) and the fingerprint pitch of films, as shown in **Figure 3.7-A**. The addition of PAAS in increasing amounts (ranging from 0 to 160 $\mu\text{mol/g}$) causes a blueshift of solid films without affecting the color intensity as measured by UV-visible absorption measurement at normal incidence. As shown in **Figure 3.7-A**, the neat CNC film absorbs in near-infrared wavelengths with a λ_{\max} at 1006 nm. This results in the absence of coloration in visible wavelengths. In this case, the absence of coloration is explained by the high dispersive energy applied to the CNC suspension (5kJ/g).

A strong sonication treatment is applied to the initial CNC suspension to cover a wide range of coloration with the addition of PAAS. The preservation of the self-assembly at the solid state in neat CNC films is also revealed by the presence of the fingerprint texture observed using polarized optical microscopy (**Figure 3.7-C**). With the addition of an optimal range of PAAS (120-160 $\mu\text{mol/g}$), solid films displayed an intense green coloration (Figure 6-B) with a much narrower absorption peak. Lastly, fingerprint textures are more regular and better pronounced.

To summarize, an anionic linear polymer such as PAAS can be used for tuning the coloration within CNC films. For instance, the addition of approximately 160 $\mu\text{mol/g}_{\text{CNC}}$ of PAAS results in a green coloration ($\lambda_{\max}=600$ nm) and a well-pronounced fingerprint texture.

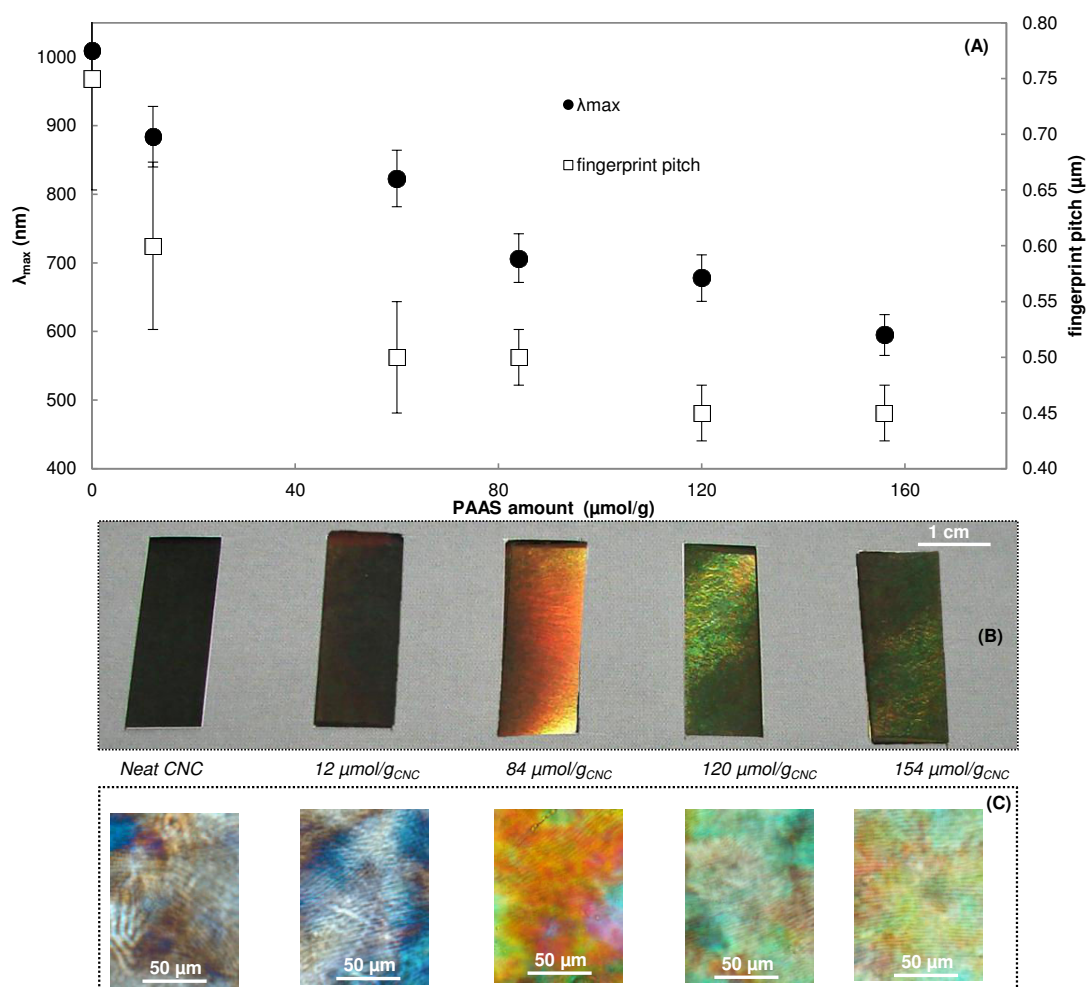


Fig 3.8 - Evolution of the maximum absorption wavelength (λ_{max}) (\square) and average fingerprint pitch (\bullet), as a function of PAAS ratios in 100 g/m^2 CNC films (A). Observation under natural light on a black background of corresponding iridescent CNC films (B), accompanied by the optical microscope image (cross-polarized light) of the film surface (C). Improvement of CNC solid film flexibility using PEG

Even if the coloration of the iridescent CNC film can be finely tuned using PAAS, such films are very brittle, which limits the industrial application of these emerging photonic materials as laminate films or surface coatings. Indeed, as we recently report (Bardet *et al.* 2014) (*Appendix 2-3*), in comparison to a non-ordered film, the mechanical properties for a structural film are low, and generally the iridescent film is very brittle with a high Young's Modulus and a low strain at break. To improve their flexibility and reduce material consumption and cost, PEG was used as a plasticizer of the iridescent solid films. The preservation of their self-organization is expected due to the steric repulsion and non-ionic interaction demonstrated in the previous section. The ratio between PEG and CNC in the prepared films was limited to the equivalent amount previously determined using QCM experiments, $0.6 \text{ mmol/g}_{\text{CNC}}$ (12 wt %).

Table 3.3 - Comparison of optical and mechanical properties of 100 g/m² films produced from the same CNC suspension with increasing amounts of PEG

		Film A (control)	Film B	Film C	Film D
Contexture	PEG to CNC ratio (wt %)	-	2.5	5.0	10.0
	Grammage (g/m ²)	96 (2)	97 (3)	103(3)	98 (5)
	Thickness (μm)	72 (1)	71 (3)	80 (3)	79 (1)
	Density	1.33 (0.06)	1.35 (0.10)	1.28 (0.02)	1.24 (0.08)
Optical	λ _{max} (nm)	595 (13)	585 (25)	615 (5)	623 (25)
	Strain at break (%)	0.70 (0.1)	1.1 (0.3)	1.80% (0.5)	1.70% (0.3)
Mechanical	Force at break (MPa)	35 (7)	30 (3)	29 (7)	19 (9)
	Specific Young Modulus (GPa)	5.8 (1.0)	4.5 (0.3)	2.6 (1.3)	2.4 (1.5)

As presented in **Table 3.3**, the coloration in the CNC films were maintained, resulting in similar iridescent properties to that of the CNC film obtained without plasticizer (Film A). The preservation of iridescent properties was also reported when PVOH was added to CNC.(Beck *et al.* 2013) A moderate redshift was noted, with the coloration (λ_{max}) shifting from 595 nm to 623 nm, upon the addition of 10 wt % PEG. However, this redshift is much less pronounced than that obtained upon the use of glucose as a plasticizer.(Mu and Gray 2014) Two reasons may explain the relatively small effect of PEG on CNC self-assembly into solid films. First, the low molecular weight (200 g/mol, i.e DP≈5) of the polymer favors polymer chain mobility and avoid bridging flocculation. Second, non-ionic interactions with CNC preferentially induce steric stabilization. The mechanical properties decreased with increasing amounts of PEG because of its plasticizing effect. A decrease in the force at break of 45%, a decrease in the Young's Modulus of 55%, and a more than doubling of the strain at break were observed when comparing the reference film (Film A) to a film incorporating 10 wt % PEG (Film D). As a consequence, a flexible and intensely iridescent film is obtained, as presented in **Fig 3.9**.

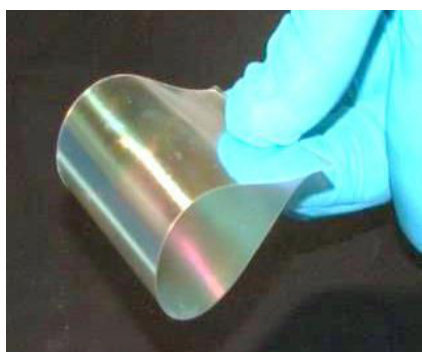


Fig 3.9 - 98 g/m² iridescent CNC film plasticized with 10 wt % PEG (A) and the corresponding film cross-section observed by FE-SEM (B)

When comparing this film with one reinforced with cellulose nanofibers,(Xiong *et al.* 2014) the mechanical properties (Young's modulus, force at break and strain at break) are very similar. However, a moderate iridescence property is observed with the addition of 1 wt % of cellulose nanofibers (CNFs), which allowed preserving the self-assembly of CNC using much less “plasticizer”. Thus, a 10 times lower amount of CNF gave similar results as those reached using PEG.

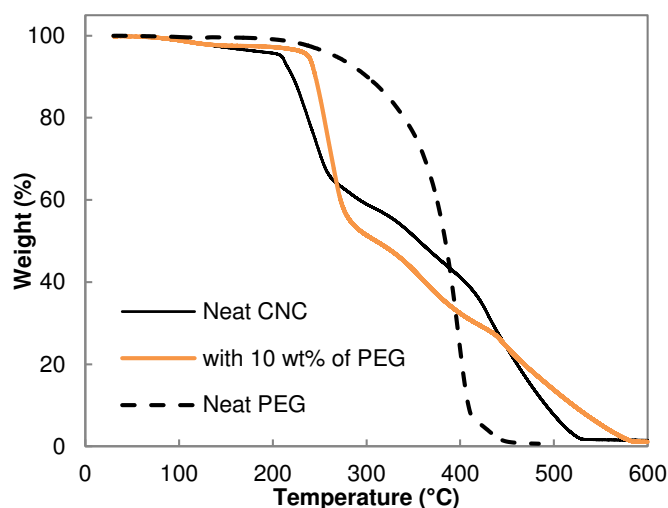


Fig 3.10 - Comparison of TG curves of neat CNC and CNC with 10 wt % of PEG

As revealed with thermal analysis (Figure 7), another benefit of the use of PEG is that it thermally insulates the CNC, increasing its thermal stability. The excellent compatibility between PEG and CNC results in an increase of the onset of thermal temperature degradation by 35°C when comparing neat CNC ($T_{deg}=203^{\circ}\text{C}$) with a film incorporating 10 wt % of PEG ($T_{deg}= 238^{\circ}\text{C}$). Similar results were recently reported for non-iridescent CNC used as reinforcement in extruded composites with higher molecular weight ($M_w=5\times 10^6$ g/mol) PEO (Ben Azouz *et al.* 2011). It is worth noting the advantage of a superior heat resistance in extrusion or lamination treatments. The procedure used in our study is simple to operate, providing a clear advantage in the preparation of CNC-based flexible and strong iridescent films.

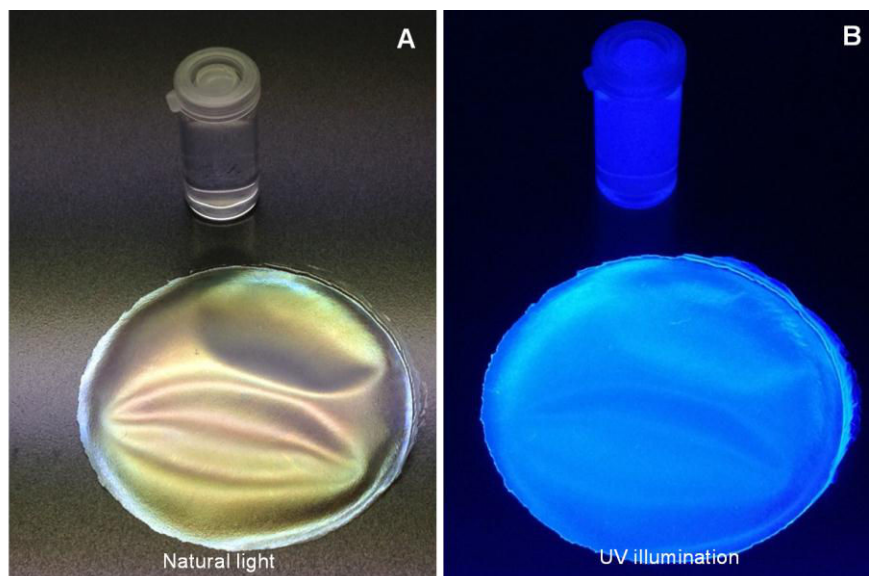
1.4 Conclusion and perspectives

To improve the flexibility and to modulate the coloration of iridescent CNC films, this study investigated the influence of two water-soluble polymers on the self-assembly properties of the suspension of these particles and on the solid film. An anionic polymer, sodium polyacrylate (PAAS), was used to modulate the film coloration and a neutral polymer, polyethylene glycol (PEG), was used to improve the iridescent film flexibility. The average dimensions of CNC used in this study were 5 nm thick by 205 nm long with a surface charge density of 0.56 e/nm². At 5.3 wt %, the CNC suspension is completely anisotropic and a fingerprint texture was observed. The neutral PEG can be physically adsorbed onto CNC and, due to steric stabilization and non-ionic interactions (hydrogen bonds), the self-assembly of the suspended CNC was conserved. Upon the addition of anionic PAAS, limited interactions were observed and the CNCs maintained their self-assembly properties. As a key result, the addition of 10 wt % PEG makes films much more flexible (with double the elongation) while preserving the coloration and increasing the degradation temperature by almost 35°C.

PAAS can be used for tuning the coloration within CNC films. It causes a stronger, narrower coloration in the visible spectrum (higher absorption) with a well-pronounced fingerprint texture. For instance, the addition of approximately 160 μmol/g of PAAS results in an intense green coloration ($\lambda_{\text{max}}=600$ nm). Such results open up the prospect of bio-based materials dedicated to decorative, security and anti-counterfeit flexible films following a biomimetic approach.

2 Self-assembly of cellulose nanocrystals with fluorescent agent in iridescent films

This section is adapted from “Raphael Bardet, Cécile Sillard, Naceur Belgacem, Julien Bras, interactions of the water-soluble polymer with the CNC suspension., Chemistry and Technology (accepted in September 14)”



Abstract

Sulfated cellulose nanocrystals (CNCs) undergo self-organization in concentrated suspensions, leading to formation of an iridescent film under specific drying conditions. In this study, CNCs were combined with the optical brightening agent (OBA), distyrylbiphenyl sulphonate (DSBP), which imparts fluorescence to the iridescent film as an additional property. The influence of DSBP on the CNC suspension is limited, thus the self-organization and the structural coloration (iridescent) of the film obtained by simple evaporation are preserved. The first section of the study outlines the influence of DSPB on the CNC suspension based on various analyses, including zeta potential measurements, dynamic light scattering (DLS), quartz crystal microbalance (QCM), and atomic force microscopy (AFM). From fluorescence spectroscopy, the amount of DSPB labeled onto the CNCs is determined to be $\sim 18 \mu\text{mol/g}$. Solid films based on DSPB-labeled CNC were also produced and characterized via UV spectroscopy. These films appear both colored in natural light due to preservation of the self-assembly of CNC and fluorescent under UV-illumination because of the fluorescent agent.

Keywords: nanocellulose, cellulose nanocrystals, iridescence, fluorescence, film.

2.1 Introduction

The growth of globalized trading and online shopping is accompanied by attendant issues such as counterfeiting of high-value products. According to the Organization for Economic Co-operation and Development (OECD), the value of international trade with counterfeit goods has been estimated at \$500 billion with a growth rate of 1,700% over the past 10 years.(Staake et al. 2009) In parallel, statistics published by the European Commission show that the growth in terms of volume, sophistication, and range of counterfeit goods, as well as the number of affected countries has continued to expand.(Spink et al. 2013) Anti-counterfeiting technology is one method used to protect both companies and customers. In general, anti-counterfeiting technologies should be easily applied but difficult to imitate. Some anti-counterfeiting technologies are low cost and user friendly, while others are highly sophisticated and expensive. Manufacturers have several different technologies to functionalize their products or packaging with anti-counterfeiting features. These include watermarks, specialized printing, the use of holographic labels, and the use of synthetic fibers or additives.(Li 2013)

The use of biomaterials for the design of photonic nanostructures is an emerging perspective in the field of optical encryption technology that was first recognized in 2010. Cellulose nanocrystals (CNCs) are one such biomaterial with the recognized property of self-assembly in a suspension; this leads to formation of an iridescent film under specific drying conditions. Revol, Godbout, and Gray(Revol et al. 1998) presented the pioneering report that the self-organization of oriented CNC may be preserved in a film obtained under free and undisturbed evaporation. As a thumb rule, if the pitch of solid films is approximately the wavelength of visible light, iridescence and colored films are obtained. This is the origin of the structural coloration of films based on CNC, a feature that opened the prospects for new high-value applications of nanocellulose.(Charreau et al. 2013)

In parallel, several studies have investigated the grafting of fluorophore molecules onto CNCs, mainly for sensor or imaging in biomedical applications.(Edwards et al. 2013) This includes aminofluorescein(Abitbol et al. 2013) (DTAF) and fluorescein isothiocyanate (FTIC)(Dong and Roman 2007),(Nielsen et al. 2010) which was fabricated through a three-step reaction.

By exploiting papermaking science, another fluorescent molecule may be labeled onto CNC. Indeed, distyrylbiphenyl sulfonate (DSBP) derivatives are widely used as efficient optical brightening agents (OBAs) to improve the brightness of paper, and these derivatives

exhibit excellent affinity toward cellulose fibers. (Zhang et al. 2009) The combination of a CNC suspension with an OBA agent (Tinopal® HW) has recently been proposed by Zhang and coworkers, (Zhang et al. 2012) who reported a simple and efficient method to manufacture an iridescent film with fluorescent properties.

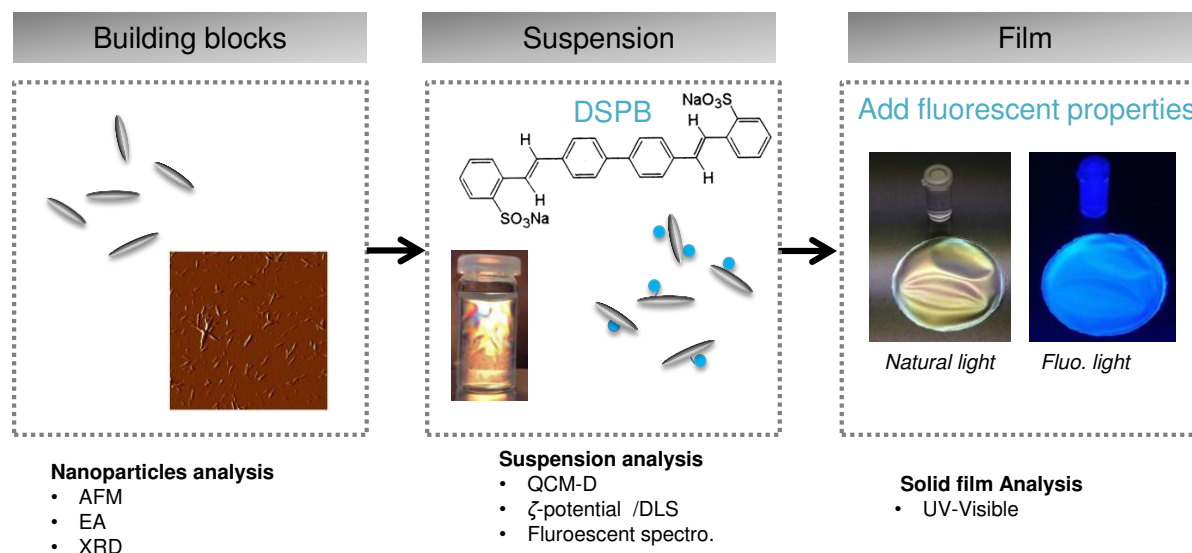


Fig 3.11 – Graphical Abstract

However, they reported a red shift in the emission of the iridescent film with increasing concentration of OBA and no evidence of the labeling with DSPB was reported. Based on these studies, we investigated the functionalization of an iridescent film with another grade of disulfonated DSPB (Tinopal® CBS), as summarized in **Fig 3.11**.

In this study, commercial CNCs produced on the pilot-scale are selected for easier technology transfer. As a preliminary investigation, the labeling of DSPB is investigated based on QCM-D, zeta potential, and AFM analyses. The degree of labeling is also evaluated based on extensive purification of CNC and fluorescence spectroscopy. Furthermore, iridescent and fluorescent films are manufactured and characterized using UV-Visible spectroscopy.

2.2 Experimental section

2.2.1 Materials

The starting material for producing the iridescent solid films is commercial cellulose nanocrystals (CNC), delivered as a dry powder. CNC was purchased from Cellulforce (Allure™, Canada) and isolated from wood pulp by sulfuric acid hydrolysis.

The commercial fluorescent agent (Tinopal® CBS, BASF, Germany) is a 27 wt % solution of 4,4'-distyrylbiphenyl sodium sulphonate salt (DSPB) with a molar weight of 562 g/mol, used as received. Polyethylenimine (PEI) with a molecular weight of 1300 g/mol was purchased from Sigma-Aldrich (USA). Deionized water (5 μS/cm) was used in all experiments.

2.2.2 Methods

Nanoparticle characterization

Individual nanoparticles were imaged using an Atomic Force Microscope (AFM; Nanoscope III®, Veeco, Canada). All samples were pre-diluted to 10⁻⁴ wt % and a 0.2 ml drop of the sample was deposited on freshly cleaved Mica substrates and dried overnight under room conditions. Each sample was characterized with a silicon cantilever (OTESPA®, Bruker, USA) in tapping mode at four different locations and two scanning areas: 3 x 3 μm² and 1 x 1 μm². Topographical as well as phase images were captured, and the resulting images were subjected to 1st-order polynomial flattening to reduce the effects of bowing and tilt. Only the most representative images are presented in this study; however, the morphological dimensions were obtained as an average of at least 50 individual nanoparticles.

The surface charge was determined via conductometric titration. 15 g of the CNC suspension (1 g dried CNC) was stirred with 250 ml of a 0.1 M HCl solution for 10 minutes. The suspension was then extensively dialyzed (Spectra/Por® 4, SpectrumLabs, USA) against a large excess of deionized water over 7 days. Subsequently, the conductivity of the suspension was adjusted to 700 μS/cm by addition of 0.1 M NaCl solution and then titrated with a 10 mM NaOH solution in 0.1 ml increments until all charged groups were neutralized. Each titration was performed in triplicate, and the CNC surface charge was determined as follows:

$$\text{surface charge } (\mu\text{eq/g}) = \frac{C_{\text{NaOH}} \cdot V_{\text{eq}}}{m_{\text{NCC}}} \quad (1)$$

Chemical interactions between CNC and fluorescent agent

The electrophoretic mobility of CNC was measured using a zeta potential analyzer (Zeta2000, Malvern Instruments, USA). CNC suspensions were diluted to around 0.1 wt % in deionized water or in a 100 μM DSBP solution. NaCl solution was added to maintain the conductivity of the suspension ($500 \mu\text{S}\cdot\text{cm}^{-1}$). The electrophoretic mobility (μ_e and zeta potential) reported herein is an average of 10 measurements.

Dynamic light scattering (DLS) was used to measure the size of the nanoparticles (Vasco® I, Corduan Technologies, France). All the samples were previously diluted in DI water to a concentration of 10^{-2} wt %, and the conductivity was adjusted to $500 \mu\text{S}/\text{cm}$ by addition of NaCl solution. The cumulative method was used and two parameters were taken into account, i.e. the hydrodynamic diameter (z^*) and the polydispersity index (*PDI*). For each sample, 10 acquisitions were performed and each measurement was replicated 3 times.

Sorption studies of the water-soluble polymers with the CNC suspension

Adsorption measurements were performed with a Quartz Crystal Microbalance with Dissipation (QCM-D). The instrument (Q-Sense® E1, Biolin Scientific, Sweden) measures the resonance frequency of the oscillation of a quartz crystal based on the fundamental frequency (5 MHz) and selected overtones (15, 25, 35, 45, 55, and 75 MHz). Only the seventh overtone is used in the data evaluation. The adsorbed mass (ng/nm^2) was estimated from the frequency change (Δf) using Sauerbrey's equation. Adsorption curves were acquired using 100 nm gold-coated quartz crystals (QSX301, Biolin Scientific, Sweden). All measurements were performed under constant flow rate ($100 \mu\text{l}/\text{min}$) and temperature (23°C).

Prior to the analyses, the gold surfaces were cleaned by immersion in a "piranha" solution (30% of $\text{H}_2\text{O}_2/\text{NH}_3$, 1:3 by weight) for 20 minutes at 70°C , then rinsed with deionized water and finally subjected to UV/ozone treatment (ProCleaner™, Bioforce, USA) for 20 minutes. Prior to the analysis, a 100 μM cationic polyethylenimine solution (PEI, Sigma Aldrich) was first adsorbed onto the cleaned gold surfaces to facilitate CNC adsorption as well as their irreversible bonding with the crystal sensor. At the beginning of each experiment, deionized water was passed through the chamber until a stable baseline ($\Delta f < 0.05/\text{min}$) was achieved (5–20 minutes).

CNC suspension and DSBP solution preparation

After dilution to 5.0 wt %, the CNC suspension was subjected to dispersion under a force of 1 kJ/g_{CNC} using a 200 W sonication probe (Sonifier® S-250A, Branson, USA) in order to obtain a homogeneous dispersion. A 100 μM solution (500 ml) of DSPB was prepared by diluting the commercial DSPB solution. For spectroscopic analyses, diluted solutions with concentrations ranging from 1 μM to 100 μM were also prepared. All DSBP solutions were mixed in a flask wrapped in aluminum foil to prevent photolysis of OBA.

Fluo-labeled CNC solution and degree of labeling

To achieve a final concentration of 20 μmol/g of DSBP, 0.5 wt % CNC suspension was mixed with a 100 μM DSPB solution and stirred for 20 min at a constant stirring rate. The fluorescent CNC suspension was then purified by prolonged dialysis (Spectra/Por®4, SpectrumLabs, USA) against a large excess of deionized water (in the dark) until the presence of DSBP in the external dialysis reservoir could not be detected (7 days).

The amount of DSBP labeled onto the CNCs was assessed using fluorescence spectroscopy (LS 50B, Perkin-Elmer, USA) at 20°C. The DSBP content of the labeled CNC samples was determined from calibration curves previously established using DSBP standards (0–100 μM range). Fluorescence scans were obtained using the following settings (optimized for a 100 μM DSBP solution): 4 nm slit widths, 350 nm excitation, emission scanned from 360 to 600 nm. Three independent measurements were obtained for each sample.

Solid film formation

Approximately 34 ml of the various 0.5 wt % CNC suspensions (with or without DSPB, before or after dialysis) was casted on a smooth aluminum plate (6 cm diameter) and left to dry for 3 days under room conditions (50% RH, 23°C). For each series, 4 dried free-standing films of 60 g/m² were thus obtained and stored under these conditions until analysis.

Film characterization

The structurally colored films were analyzed using UV-Visible spectroscopy (UV 1800, Shimadzu, Japan). The absorption intensity of the solid film was recorded within the wavelength range of 200 to 1100 nm with a normal incidence. For each sample, three independent measurements and ten scans were recorded and averaged.

2.3 Results and discussion

2.3.1 Nanocellulose characterization and photophysical properties of DSBP

Prior to film formation, the physical and chemical properties of the commercial cellulose nanocrystal (CNC) suspension were determined. As presented in **Fig 3.12-A**, the CNCs had an elongated, rod-like morphology with average dimensions of 8 nm thickness by 174 nm length.

This morphology of the nanoparticles is in accordance with previous studies of CNCs extracted under similar hydrolysis conditions (wood pulp, sulfuric acid). The XRD pattern (not presented) is typical of the crystalline polymorph of neat cellulose I (native cellulose). The major crystalline peak (002) occurs at 22.84° and the associated crystallinity index (CI) is 88%. The surface charge, associated with the content of sulfate ester groups, is about 190 $\mu\text{mol/g}$ (estimated by conductometric titrations).

Based on the surface charge estimation and the geometric dimensions of the CNCs derived from the AFM images, the surface charge density is about 0.38 e/nm^2 . As a comparison, surface charge densities of 0.16 to 0.64 e/nm^2 were reported in self-assembly studies of CNC suspensions. (Dufresne 2012)

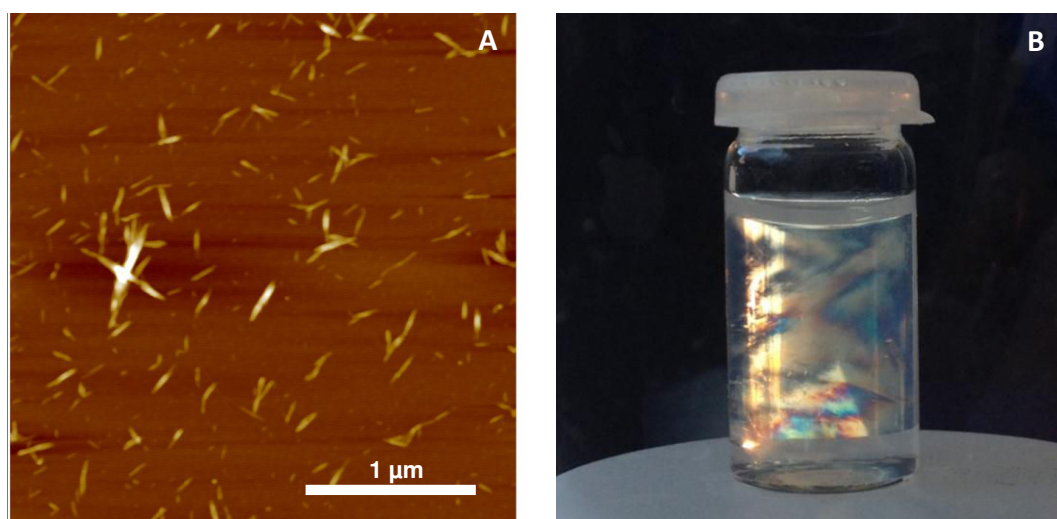


Fig 3.12 - Observation of a 0.5 wt % CNC suspension between cross-polarizers (A) and AFM image showing individualized CNCs (B).

The 0.5 wt % CNC suspension dispersed in water displays intense birefringence patterns (**Fig 3.12-B**). This confirms the absence of agglomeration as well as preservation of the self-assembly properties of CNC in suspension. Thus, it is demonstrated that the CNCs are well isolated from cellulosic fibers; they have a rod-like morphology, and display self-assembly properties in water.

The photo-physical parameters of the distyrylbiphenyl sodium sulphonate (DSBP) salt used as the fluorescent agent were also investigated. **Fig 3.12-A** shows that DSBP adsorbs in the UV spectral range ($\lambda_{\text{abs}} = 351 \text{ nm}$) and emits strong blue fluorescence ($\lambda_{\text{em}} = 425 \text{ nm}$). Such spectral features are in agreement with those reported in other previous studies. (Zhang *et al.* 2012)

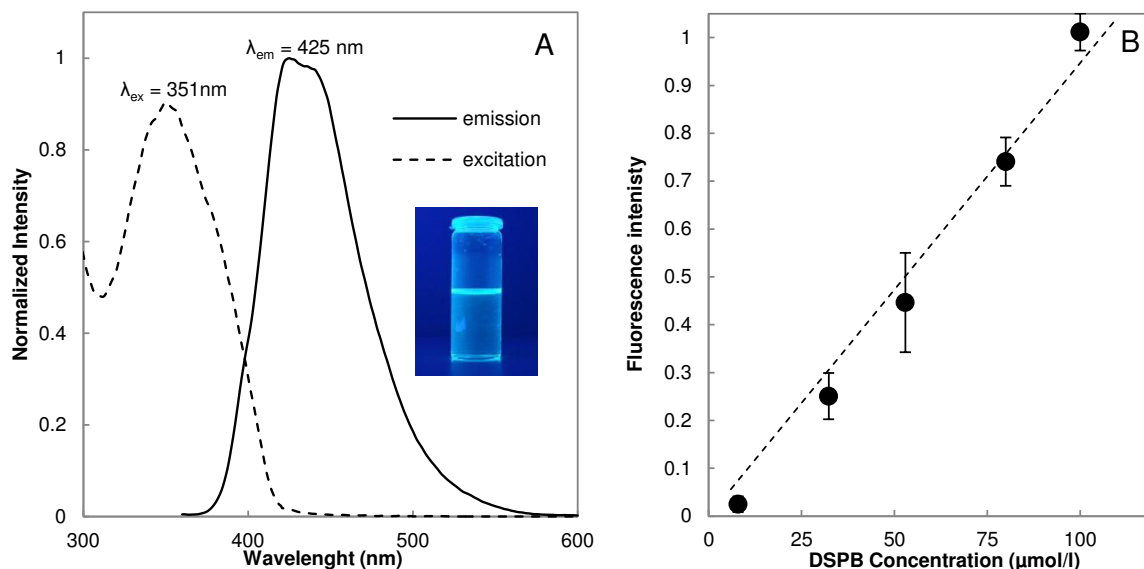


Fig 3.13 – Fluorescence spectra of a 100 μM DSBP solution (A). Calibration curve of DSBP solution from 1 μM to 100 μM using an excitation wavelength of 351 nm (B). Intensities reported in fluorescence spectra and calibration curves were standardized from 100 μM DSBP solutions.

A calibration curve (**Fig 3.13-B**) (normalized fluorescence intensity as a function of the DSBP dosage) was constructed to determine the amount of DSBP labels attached to the CNCs. Good correlation between the fluorescence intensity and DSPB concentration was observed between 0 to 100 μM.

2.3.2 Interactions between CNC particles and DSBP solution

Prior to fabricating the fluorescent and iridescent CNC films, the influence of adding anionic DSBP to the CNC suspension was evaluated. This is a critical point given that the self-organization of CNCs is sensitive to the electrochemical equilibrium. (Araki *et al.* 2000, de Souza Lima and Borsali 2004, Pan *et al.* 2010)

Moreover, the addition of water soluble molecules (monovalent salt, (Revol *et al.* 1998) cationic polymers, (Cheung *et al.* 2013) or surfactants) (Elazzouzi-Hafraoui *et al.* 2009, Kelly *et al.* 2012) can completely modify the CNC self-assembly properties.

The zeta potential is used to quantify the electrostatic repulsive forces and gives an indication of the potential stability of the colloidal system and indirectly of their self-

organization.(Salopek *et al.* 1992) A value lower than ± 15 mV is considered as the onset of particle agglomeration. Values higher than ± 30 mV generally mean that there is sufficient mutual repulsion, which ensures the colloidal stability.(Mirhosseini *et al.* 2008)

Table 3.4 compares the hydrodynamic and electrokinetic parameters of CNC suspended in deionized water with those containing anionic additives. The zeta potential of CNC dispersed in deionized water is highly negative (-45 mV) due to the high surface charge density of the sulfate half-ester groups.(Dong and Gray 1997)

In the presence of anionic DSBP, the mobility remains highly negative and the hydrodynamic diameter is unmodified. Consistent with a previous similar study,(Zhang *et al.* 2012) an increase (-51 mV) of the zeta potential was observed when CNC was suspended in DSBP solution, which can be attributed to absorption of DSBP on the hydroxyl surface groups. The suspension in DSBP solution displays birefringence patterns owing to preservation of the self-organization imparted by the highly negative surface charges of CNC.

In contrast, in the case of dispersion in 100 μ M PEI solution, the flow birefringence disappears and the zeta potential is shifted from -44.5 mV to +15.0 mV. This confirms ionic bonding between the negative sulfated groups of CNC and amino groups of this polymer. This interaction also leads to particle flocculation ($z^* = 856$ nm), as detected via DLS measurement. The dispersion in PEI solution presented above was conducted to evaluate the adsorption phenomena associated with the PEI solutions used for functionalization of the gold-coated mica plate for QCM experiments.

Table 3.4 - Electrokinetic potential, hydrodynamic size, and colloidal behavior of 0.5 wt % CNC suspension dispersed in water and in 100 μ M water-soluble polymer solutions

CNC dispersion (0.5 wt %)	hydrodynamic properties ^a		Electrokinetic potential ^b		Colloidal behavior
	z^* (nm)	PDI	p ζ (mV)	Ue (V)	
Deionized water	105 (5)	0.2	-44.8 (1.2)	-3.5 (0.07)	Birefringent
In DSBP solution (100 μ M)	105 (10)	0.18	-50.8 (0.8)	-3.82 (0.08)	Birefringent
PEI polymer solution (100 μ M)	856 (8)	0.75	15 (1.1)	1.18 (0.09)	no

Measured by DLS^a and Zeta potential^b analyses. Observation between cross-polar after stirring.
Values in brackets indicate the standard deviation.

2.3.3 Adsorption phenomena of DSPB with CNC

Adsorption measurements were performed with a quartz crystal microbalance with dissipation (QCM-D), as shown in **Fig 3.14**.

As a preliminary investigation, the thickness of the adsorbed CNC layer was analyzed to determine if the layer was sufficiently thick to prevent interaction of the positively charged substrate with PEI. Based on the frequency drop ($\Delta f = -62 \pm 2$ Hz) and deduction using Sauerbrey's equation, the average weight of CNC adsorbed on the substrate is 1.1 g/m^2 .

This corresponds to a CNC layer of about 8 nm assuming that the density of the CNC layer is 1.44. Thus, the adsorbed CNC layer is sufficiently thick to prevent artifact absorption with the charged substrate (PEI layer). The amount of adsorbed CNC is similar to that reported (c.a. 10 nm) under equivalent experimental conditions. (Ahola *et al.* 2008)

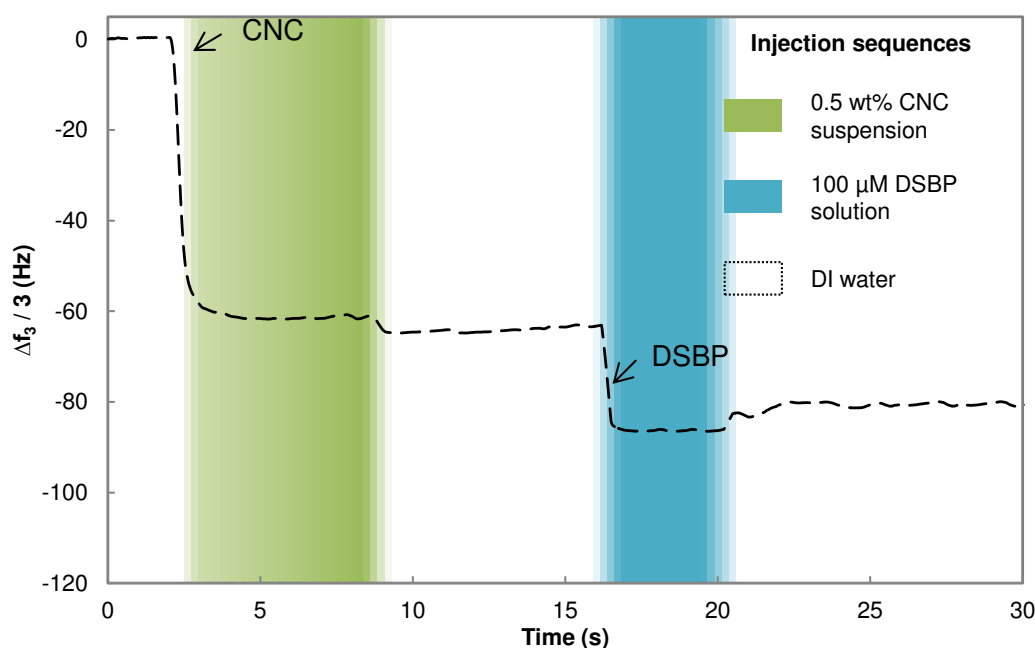


Fig 3.14 – QCM-D study (7th overtone) of CNC and DSPB adsorption on PEI modified gold surface. The 1st injection corresponds to 0.5 wt % CNC suspension (green area) and the 2nd injection is associated with the injection of 100 μM DSPB solution (blue area). Uncolored sections correspond to the rinsing stage with DI water. $\Delta f_3/3$, the frequency drop normalized by the overtone, is a measure of the adsorbed mass including bound water.

AFM analyses were also carried out on the air-dried substrate surface after CNC adsorption and rinsing with DI water (**Fig 3.15-A**). Notably, the adsorbed CNC layer displays good surface coverage with random orientation of the rods. Moreover, the CNC layer formed a three-dimensional network with a large exposed surface area. Instead of uniform adsorption of water-soluble polymers to form a smooth layer, the adsorbed CNC layer formed a non-continuous layer (**Fig 3.15-A**).

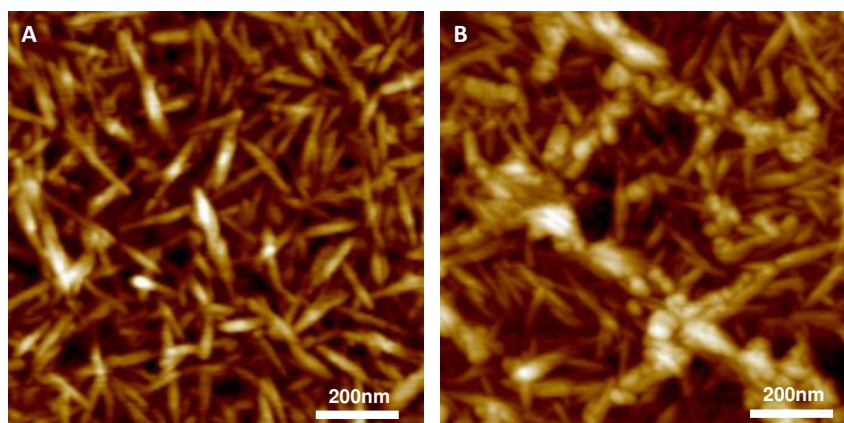


Fig 3.15 – AFM pictures (height sensor) corresponding to air-dried substrate analysis during QCM experiments: after injection of CNC and rinsing (A), after injection of DSPB and rinsing (B).

Consequently, in calculating the mass of DSPB adsorbed on the CNCs, the specific surface topography of the CNC layer must be taken into consideration. (Ahola *et al.* 2008) From a calculation carried out for three $9 \mu\text{m}^2$ scanning areas, the surface formed by the CNC layer is estimated to be $16 \pm 2 \mu\text{m}^2$. This means that, a surface area of 1.8 cm^2 should be considered for 1 cm^2 of the surface sensor. Moreover, based on the heterogeneity of the CNC substrate, the amount of polymer adsorbed should be considered semi-quantitative.

With the addition of DSBP, there is a frequency drop ($\Delta f = -62 \pm 2 \text{ Hz}$) (**Fig 3.14**), suggesting the adsorption of anionic DSBP molecules onto CNC. The nonionic interactions between the additive and the cellulose surface lower the repulsive barrier towards the polyelectrolyte, facilitating adsorption on the CNC surface. Similar to cellulosic fibers, the physical adsorption of DSBP is primarily related to the electrostatic interaction with the surface via the sulfonic groups of DSBP and formation of strong hydrogen bonds. (Iamazaki and Atvars 2007)

Additionally, after injection of DSPB, moderate desorption ($\Delta f \sim +7 \text{ Hz}$) was also observed during rinsing with DI water. Nevertheless, the mass of DSPB adsorbed on CNC remained significant ($\Delta f \sim 21 \text{ Hz}$, i.e. 360 ng/cm^2).

The AFM image (**Fig 3.15-B**) of DSPB adsorbed on CNC suggests that DSPB is not uniformly distributed on the CNC surface. Clustered spherical particles fixed on CNC may undergo agglomeration. Similar aggregation was reported for macroscopic fibers. (Iamazaki *et al.* 2010)

Considering a CNC surface area of about 150 g/m^2 , (Terech *et al.* 1999) and the “real” surface area of the CNC layer, the adsorption of DSPB is estimated to be $53 \pm 11 \mu\text{mol/g}$.

2.3.4 Efficiency of DSPB sorption on CNCs

The affinity of DSPB for the CNCs was evaluated from zeta potential, DLS, and QCM analyses. DSPB could be labeled onto the CNCs at a loading (adsorbed amount) of about $50 \mu\text{mol/g}_{\text{CNC}}$. To confirm the degree of labeling, a 0.5% CNC suspension was mixed with a $100 \mu\text{M}$ DSPB solution (i.e. $50 \mu\text{mol/g}_{\text{CNC}}$).

The CNC and DSPB mixture was sonicated and purified by prolonged dialysis (7 days) to remove the unadsorbed fluorescent agent (**Fig 3.16-B**). Dialysis was discontinued when fluorescence of DSPB could no longer be detected in the contents of the external dialysis reservoir. In parallel, a control solution (without CNC) was also purified (**Fig 3.16-D**). The fluorescence spectra of the dialyzed samples were recorded (**Fig 3.16-C and E**) to determine the degree of labeling using the calibration curve (**Fig 3.13-B**).

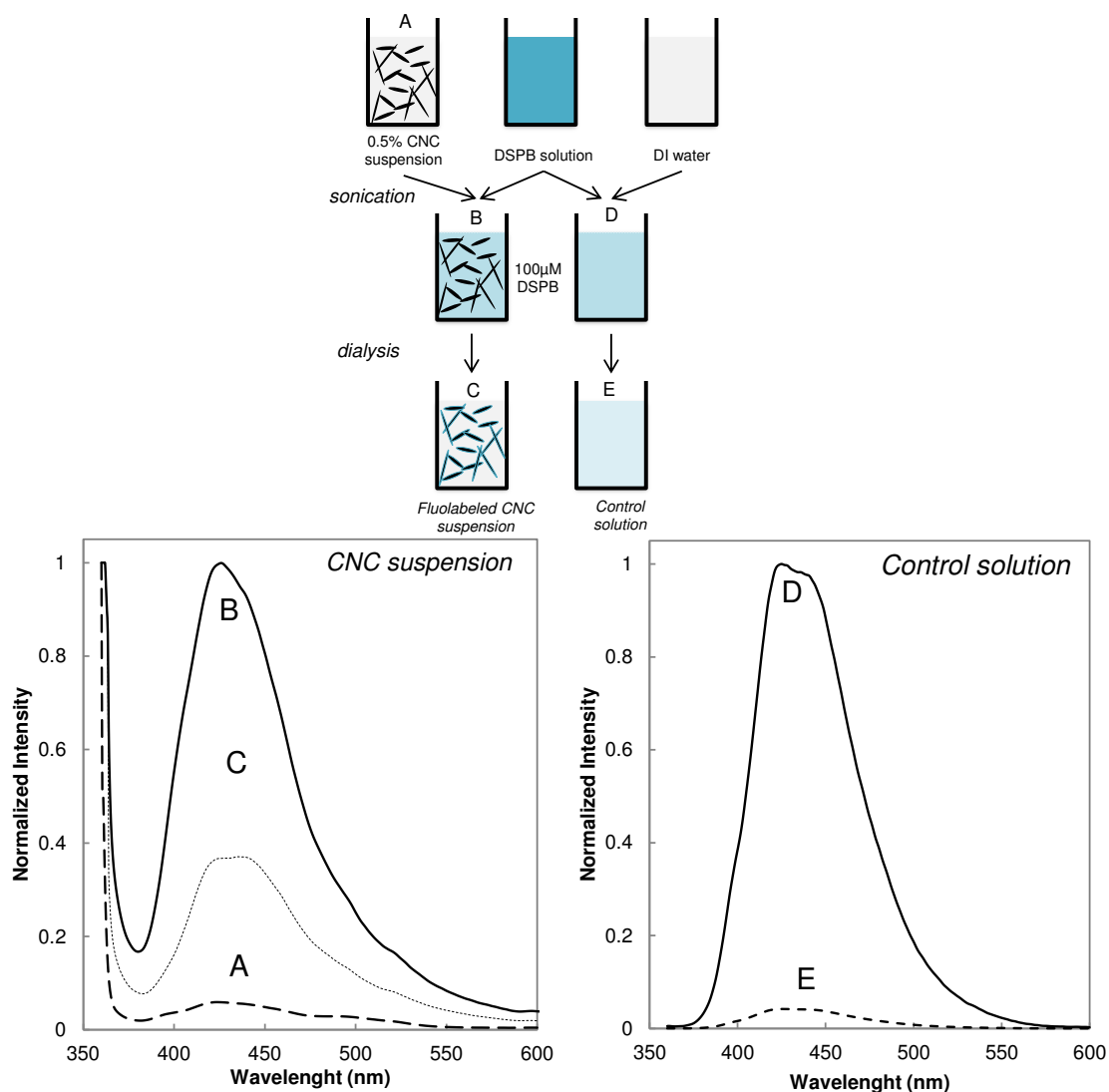


Fig 3.16 – Fluorescence spectra of 0.5 wt % neat CNC suspension (A), with $100 \mu\text{M}$ DSPB solution before (B) and after dialysis (C). Control spectra corresponding to the $100 \mu\text{M}$ DSPB solution before (D) and after dialysis (E). Intensities are standardized with respect to the absorbance of a $100 \mu\text{M}$ DSPB solution. $\lambda_{\text{ex}} = 351 \text{ nm}$.

As expected, the neat CNC suspension was non-fluorescent (**Fig 3.13-A**), whereas CNC suspensions containing DSPB before and after dialysis (**Fig 3.13-B and C**) emitted strong fluorescence ($\lambda_{em} = 425$ nm).

The removal of DSPB molecules from dialyzed CNC was indicated by a decrease in the fluorescence intensity, corresponding to a decrease in the DSPB concentration. From the calibration curve, the amount of DSPB labeled onto CNC is estimated to be 38 ± 3 μM , i.e. 19 $\mu\text{mol/g}_{\text{CNC}}$. For the control solution (100 μM DSPB solution without CNC), the absence of a DSPB absorption peak indicates that almost all of the DSPB in the DI water was removed after purification. It should be noted that the amount of DSPB labeled onto the CNCs reported herein (19 $\mu\text{mol/g}_{\text{CNC}}$) is even lower than the value calculated from QCM (53 $\mu\text{mol/g}_{\text{CNC}}$). This may be due to the assumptions made for the calculation based on QCM experiments, such as the surface area of CNC or the surface topography of the CNC layer. This discrepancy may also be related to the measurement time being too brief during the desorption cycle (only 10 minutes).

As a comparison, a value twenty times lower (1 $\mu\text{mol/g}$) was reported for DSPB adsorbed on cellulosic fibers. (Iamazaki and Atvars 2006) Such a difference may be related to the difference between the surface area of the cellulosic fibers (Scott 1996) and CNCs (Terech *et al.* 1999) of $1-3$ m^2/g and 150 m^2/g , respectively.

Compared with fluorescent molecules grafted onto CNCs, the amount of DSPB is equivalent to fluorescein isothiocyanate (Dong and Roman 2007, Nielsen *et al.* 2010) (FTIC) with values ranging from 3 to 30 $\mu\text{mol/g}$ and several times higher ($5-50$ nmol/g) than that of grafted aminofluorescein (Abitbol *et al.* 2013) (DTAF).

Another point of interest for using DSPB instead of other fluorescent molecules is that the labeling could be carried out without chemical modification and did not require the use of a multistep reaction.

2.3.5 Formation of fluorescent and iridescent film based on CNCs

To prepare 60 g/m² iridescent films with varying amounts of DSBP, the fluolabeled CNC suspension was mixed with neat CNC suspensions. The incorporation of fluorescence properties into the iridescent film may be promising for improving optical encryption of solid films. (Zhang *et al.* 2012)

The ratio of DSPB ranged from 0 μmol/g of DSPB (100% of neat CNC suspension) to 18 μmol/g (100% of fluolabeled CNC suspension).

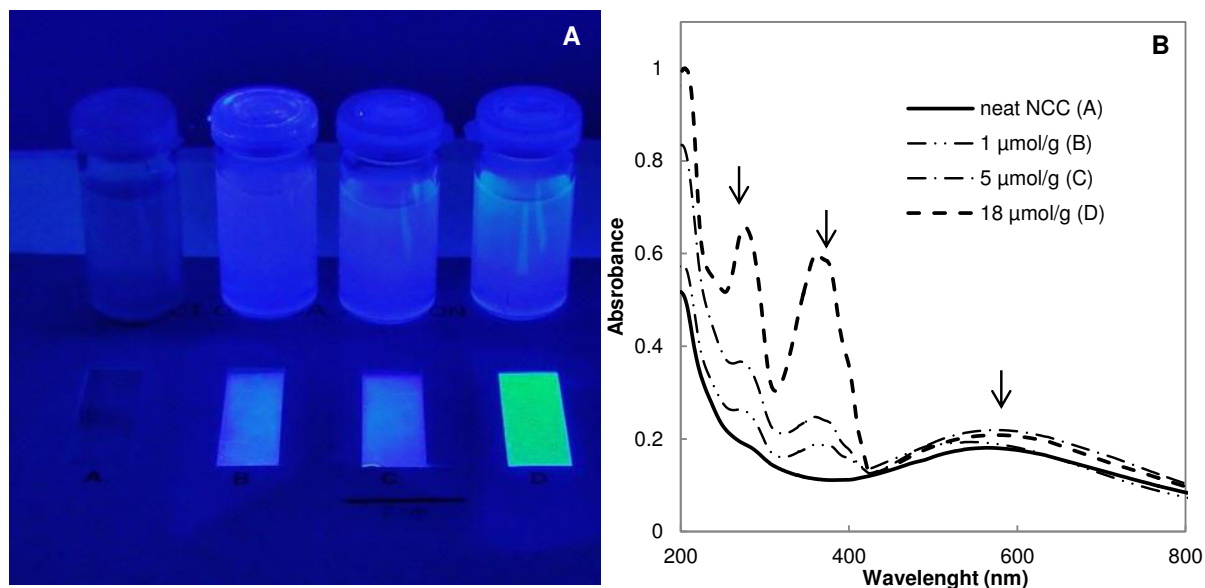


Fig 3.17 – (A) Observation of CNC suspensions and 60 g/m² solid films with increasing amount of DSBP (0 to 11 μmol/g) labeled onto nanoparticles under UV illumination and (B) corresponding UV-visible spectra.

Fig 3.17-A shows moderate fluorescence for the samples containing 1–5 μmol/g of CNC, whereas more intense fluorescence was achieved when more DSBP was used (18 μmol/g). In addition, the coloration under natural light was preserved with a slight red shift from 546 nm to 578 nm of λ_{\max} in the visible spectra.

The absorption peak observed at 367 nm (**Fig 3.17-B**) corresponds to the maximal excitation wavelength of DSBP, the intensity of which increased with the amount of adsorbed DSBP. The prepared films appear colored under natural illumination due to preservation of the self-organized structure of CNC and are fluorescent under UV illumination because of the fluorescent agent.

2.4 Conclusions & perspectives

The adsorption of the anionic fluorescent agent DSPB onto CNCs was confirmed by QCM analyses. Adsorption occurs via electrostatic interaction of the sulfonic groups of DSPB and formation of strong hydrogen bonds with the CNCs. The amount of DSPB adsorbed on the CNCs is about 18 $\mu\text{mol/g}$ based on fluorescence spectroscopy. This limited interaction of DSPB with the CNC suspension preserves the self-assembly of the CNC suspension and the structural coloration (iridescent) of the film obtained by simple evaporation. The combination of CNC with the optical brightening agent, distyrylbiphenyl sulphonate, imparts fluorescence to the iridescent film as an additional property. The prepared films appear colored in natural light because of the preservation of the self-organization of CNC and fluorescent under UV-illumination because of the fluorescent agent.

Concluding remarks

While iridescent films based on CNCs are now commonly widely reported in the literature, the two studies presented here addresses various enhancement in a view of (i) improving the film flexibility,(ii) controlling the coloration, and (iii) incorporating fluorescent properties.

In **Chapter 3.1**, two different water-soluble polymers are used. An anionic polymer, i.e. sodium polyacrylate (PAAS), is used to modulate the film coloration. Moreover, a neutral polymer, i.e. polyethylene glycol (PEG), is used to improve the iridescent film flexibility. As a key result, the addition of 10 wt % of PEG makes films much more flexible (elongation have doubled), the coloration is preserved, and the temperature degradation increased by almost 35°C. The very innovative results is obtained with PAAS, which can be used for tuning the coloration within CNC films. In **Chapter 3.2**, the adsorption of an anionic fluorescent agent DSPB onto CNCs was confirmed. The amount of DSPB adsorbed on the CNCs is about 18 $\mu\text{mol/g}$ based on fluorescence spectroscopy. This limited interaction of DSPB with the CNC suspension allows preserving the self-assembly of the CNC suspension and the structural coloration (iridescent) of the film obtained by simple evaporation. The combination of CNC with the optical brightening agent, i.e (DSBP) distyrylbiphenyl sulphonate, imparts fluorescence to the iridescent film as an additional property. The prepared films appear colored in natural light because of the preservation of the self-organization of CNC and fluorescent under UV-illumination because of the fluorescent agent.

Such results open up the prospect to biobased nanomaterials dedicated to decorative, security and anti-counterfeit flexible films. Even if this is indisputably promising, the uses within specialty papers appear to be limited for several reasons. Indeed, the processing technique for manufacturing iridescent film require several day. In addition, continuous and fast production processes, cannot preserve the structural coloration property. Lastly, CNC as a starting material is not cost-efficient enough to compete with other materials that are already available to display similar iridescent properties, and iridescent films based on CNC are usually very brittle and difficult to process.

In the **Chapter 4.2**, an innovative approach consisting in manufacturing pigments from iridescent CNC films will be presented.

List of Tables

Table 3.1 - Physical and chemical properties of the CNC used in the study	167
Table 3.2 - Electrokinetic potential, hydrodynamic size and colloidal behavior of a 0.5% CNC suspension dispersed in water and 100 μM water-soluble polymer solutions	169
Table 3.3 - Comparison of optical and mechanical properties of 100 g/m^2 films produced from the same CNC suspension with increasing amounts of PEG	177
Table 3.4 - Electrokinetic potential, hydrodynamic size, and colloidal behavior of 0.5 wt % CNC suspension dispersed in water and in 100 μM water-soluble polymer solutions.....	189

List of figures

Fig 3.1 - Viscosity as a function of the CNC concentration (25°C with a shear of 1/s) with the corresponding micrographs between crossed polarizers (A: 2.5 wt % and B: 5.3%)The value of CA^* reported here is in accordance with a more extensive study in which authors reported a value of 6.5 wt % obtained with the study of phase separation of CNC isolated from cotton filter with a surface charge density of 0.35 e/nm^2 .(Ureña-Benavides <i>et al.</i> 2011) 5.3 wt % has been considered as the optimum concentration for casting CNC suspensions to manufacture iridescent solid films considering both the suspension is predominantly anisotropic and not too viscous to obtain a good film by evaporation.....	168
Fig 3.2 - Crossed polarizers observation of 0.5wt % CNC dispersed in water (A) and in 100 μM polymers solutions of PAAS (B), PEG (C), and PEI (D)	169
Fig 3.3 - QCM-D studies (7th overtone) of CNC and polymer (PAAS and PEG) adsorption on a PEI-modified gold surface. The 1st injection corresponds to the 0.5 wt % CNC suspension (green area) whereas the 2nd one injection corresponds to of the 100 μM polymer solutions (orange area). Uncolored sections correspond to the rinsing stage with DI water.	170
Fig 3.4 - AFM pictures (height sensor) corresponding to the air-dried substrate analysis of QCM experiments: after injection of CNC and rinsing (A), after injection of PAAS and rinsing (B), after injection of PEG and rinsing (C).....	171
Fig 3.5 - FE-SEM images of a fracture surface across an iridescent CNC film.....	173
Fig 3.6 - Viscosity of a 5.3 wt % CNC suspension as a function of the PAAS concentration (at 25°C for a shear of 1 Hz), accompanied by fingerprint textures (A,B, and C), as observed using polarized optical microscopy.....	174
Fig 3.7 - Mechanism that could explain the blueshift occurring upon the addition of PAAS	175
Fig 3.7 - Evolution of the maximum absorption wavelength (λ_{max}) (\square) and average fingerprint pitch (\bullet), as a function of PAAS ratios in 100 g/m^2 CNC films (A). Observation under natural light on a black background of corresponding iridescent CNC films (B), accompanied by the optical microscope image (cross-polarized light) of the film surface (C).Improvement of CNC solid film flexibility using PEG	176
Fig 3.9 - 98 g/m^2 iridescent CNC film plasticized with 10 wt % PEG (A) and the corresponding film cross-section observed by FE-SEM (B).....	177
Fig 3.10 - Comparison of TG curves of neat CNC and CNC with 10 wt % of PEG	178
Fig 3.11 – Graphical Abstract.....	183
Fig 3.12 - Observation of a 0.5 wt % CNC suspension between cross-polarizers (A) and AFM image showing individualized CNCs (B).	187

Fig 3.13 – Fluorescence spectra of a 100 μM DSBP solution (A). Calibration curve of DSBP solution from 1 μM to 100 μM using an excitation wavelength of 351 nm (B). Intensities reported in fluorescence spectra and calibration curves were standardized from 100 μM DSBP solutions. 188

Fig 3.14 – QCM-D study (7th overtone) of CNC and DSPB adsorption on PEI modified gold surface. The 1st injection corresponds to 0.5 wt % CNC suspension (green area) and the 2nd injection is associated with the injection of 100 μM DSPB solution (blue area). Uncolored sections correspond to the rinsing stage with DI water. $\Delta f_3/3$, the frequency drop normalized by the overtone, is a measure of the adsorbed mass including bound water. 190

Fig 3.15 – AFM pictures (height sensor) corresponding to air-dried substrate analysis during QCM experiments: after injection of CNC and rinsing (A), after injection of DSPB and rinsing (B). 191

Fig 3.16 – Fluorescence spectra of 0.5 wt % neat CNC suspension (A), with 100 μM DSBP solution before (B) and after dialysis (C). Control spectra corresponding to the 100 μM DSBP solution before (D) and after dialysis (E). Intensities are standardized with respect to the absorbance of a 100 μM DSBP solution. $\lambda_{\text{ex}} = 351$ nm. 192

Fig 3.17 – (A) Observation of CNC suspensions and 60 g/m^2 solid films with increasing amount of DSBP (0 to 11 $\mu\text{mol}/\text{g}$) labeled onto nanoparticles under UV illumination and (B) corresponding UV-visible spectra. . 194

References

1. Abitbol and Cranston, "Chapter 5: Chiral Nematic Self-Assembly of Cellulose Nanocrystals in Suspensions and Solid Films", Handbook of Green Materials (2014).
2. Abitbol, Palermo, *et al.*, "Fluorescent Labeling and Characterization of Cellulose Nanocrystals with Varying Charge Contents", Biomacromolecules 14(9): 3278-3284 (2013).
3. Ahola, Österberg, *et al.*, "Cellulose nanofibrils—adsorption with poly(amideamine) epichlorohydrin studied by QCM-D and application as a paper strength additive", Cellulose 15(2): 303-314 (2008).
4. Ahola, Salmi, *et al.*, "Model Films from Native Cellulose Nanofibrils. Preparation, Swelling, and Surface Interactions", Biomacromolecules 9(4): 1273-1282 (2008).
5. Ahola, Turon, *et al.*, "Enzymatic hydrolysis of native cellulose nanofibrils and other cellulose model films: effect of surface structure", Langmuir 24(20): 11592-11599 (2008).
6. Araki and Kuga, "Effect of Trace Electrolyte on Liquid Crystal Type of Cellulose Microcrystals", Langmuir 17(15): 4493-4496 (2001).
7. Araki, Wada, *et al.*, "Steric Stabilization of a Cellulose Microcrystal Suspension by Poly(ethylene glycol) Grafting", Langmuir 17(1): 21-27 (2000).
8. Araki, Wada, *et al.*, "Birefringent Glassy Phase of a Cellulose Microcrystal Suspension", Langmuir 16(6): 2413-2415 (2000).
9. Bardet, Cancé, *et al.*, "Structural Colored Films Based on Nanocellulose", presented at TAPPI International Conference on Nanotechnology, Vancouver, Canada (2014).
10. Beck, Bouchard, *et al.*, "Controlling the Reflection Wavelength of Iridescent Solid Films of Nanocrystalline Cellulose", Biomacromolecules 12(1): 167-172 (2011).
11. Beck, Bouchard, *et al.*, "Controlled production of patterns in iridescent solid films of cellulose nanocrystals", Cellulose 20(3): 1401-1411 (2013).
12. Beck, Roman, *et al.*, "Effect of Reaction Conditions on the Properties and Behavior of Wood Cellulose Nanocrystal Suspensions", Biomacromolecules 6(2): 1048-1054 (2005).
13. Ben Azouz, Ramires, *et al.*, "Simple Method for the Melt Extrusion of a Cellulose Nanocrystal Reinforced Hydrophobic Polymer", ACS Macro Letters 1(1): 236-240 (2011).
14. Boluk, Zhao, *et al.*, "Dispersions of Nanocrystalline Cellulose in Aqueous Polymer Solutions: Structure Formation of Colloidal Rods", Langmuir 28(14): 6114-6123 (2012).
15. Cerolini, D'orazio, *et al.*, "Moisture buffering capacity of highly absorbing materials", Energy and Buildings 41(2): 164-168 (2009).
16. Charreau, L Foresti, *et al.*, "Nanocellulose patents trends: A comprehensive review on patents on cellulose nanocrystals, microfibrillated and bacterial cellulose", Recent patents on nanotechnology 7(1): 56-80 (2013).
17. Cheung, Giese, *et al.*, "Iridescent Chiral Nematic Cellulose Nanocrystal/Polymer Composites Assembled in Organic Solvents", ACS Macro Letters 2(11): 1016-1020 (2013).
18. De Souza Lima and Borsali, "Rodlike Cellulose Microcrystals: Structure, Properties, and Applications", Macromolecular Rapid Communications 25(7): 771-787 (2004).

19. Dong and Gray, "Effect of Counterions on Ordered Phase Formation in Suspensions of Charged Rodlike Cellulose Crystallites", Langmuir 13(8): 2404-2409 (1997).
20. Dong, Kimura, *et al.*, "Effects of Ionic Strength on the Isotropic–Chiral Nematic Phase Transition of Suspensions of Cellulose Crystallites", Langmuir 12(8): 2076-2082 (1996).
21. Dong, Revol, *et al.*, "Effect of microcrystallite preparation conditions on the formation of colloid crystals of cellulose", Cellulose 5(1): 19-32 (1998).
22. Dong and Roman, "Fluorescently Labeled Cellulose Nanocrystals for Bioimaging Applications", Journal of the American Chemical Society 129(45): 13810-13811 (2007).
23. Dorris and Gray, "Gelation of cellulose nanocrystal suspensions in glycerol", Cellulose 19(3): 687-694 (2012).
24. Dufresne, "Nanocellulose, From Nature to High Performance Tailored Materials", edited by De Gruyter (2012).
25. Edwards, Prevost, *et al.*, "Nanocellulose-based biosensors: design, preparation, and activity of peptide-linked cotton cellulose nanocrystals having fluorimetric and colorimetric elastase detection sensitivity", Engineering 5: 20 (2013).
26. Elazzouzi-Hafraoui, Putaux, *et al.*, "Self-assembling and Chiral Nematic Properties of Organophilic Cellulose Nanocrystals", The Journal of Physical Chemistry B 113(32): 11069-11075 (2009).
27. Hu, Cranston, *et al.*, "Tuning Cellulose Nanocrystal Gelation with Polysaccharides and Surfactants", Langmuir 30(10): 2684-2692 (2014).
28. Hu, Cranston, *et al.*, "Tuning Cellulose Nanocrystal Gelation with Polysaccharides and Surfactants", Langmuir (2014).
29. Iamazaki and Atvars, "Role of Surfactants in the Sorption of the Whitening Agent Tinopal CBS onto Viscose Fibers: A Fluorescence Spectroscopy Study", Langmuir 22(24): 9866-9873 (2006).
30. Iamazaki and Atvars, "Sorption of a Fluorescent Whitening Agent (Tinopal CBS) onto Modified Cellulose Fibers in the Presence of Surfactants and Salt", Langmuir 23(26): 12886-12892 (2007).
31. Iamazaki, Pereira-Da-Silva, *et al.*, "A morphological view of the sodium 4,4'-distyrylbiphenyl sulfonate fluorescent brightness distribution on regenerated cellulose fibers", Journal of Applied Polymer Science 118(4): 2321-2327 (2010).
32. Kelly, Shopsowitz, *et al.*, "Chiral Nematic Stained Glass: Controlling the Optical Properties of Nanocrystalline Cellulose-Templated Materials", Langmuir 28(50): 17256-17262 (2012).
33. Kelly, Yu, *et al.*, "Large, Crack-Free Freestanding Films with Chiral Nematic Structures", Advanced Optical Materials 1(4): 295-299 (2013).
34. Kinoshita, Yoshioka, *et al.*, "Physics of structural colors", Reports on Progress in Physics 71(7): 076401 (2008).
35. Kloser and Gray, "Surface Grafting of Cellulose Nanocrystals with Poly(ethylene oxide) in Aqueous Media", Langmuir 26(16): 13450-13456 (2010).
36. Li, "Technology designed to combat fakes in the global supply chain", Business Horizons 56(2): 167-177 (2013).
37. Majoinen, Kontturi, *et al.*, "SEM imaging of chiral nematic films cast from cellulose nanocrystal suspensions", Cellulose 19(5): 1599-1605 (2012).

-
38. Mirhosseini, Tan, *et al.*, "Effect of Arabic gum, xanthan gum and orange oil contents on ζ -potential, conductivity, stability, size index and pH of orange beverage emulsion", Colloids and Surfaces A: Physicochemical and Engineering Aspects 315(1–3): 47-56 (2008).
 39. Moon, Martini, *et al.*, "Cellulose nanomaterials review: structure, properties and nanocomposites", Chemical Society Reviews 40(7): 3941-3994 (2011).
 40. Mu and Gray, "Formation of Chiral Nematic Films from Cellulose Nanocrystal Suspensions Is a Two-Stage Process", Langmuir 30(31): 9256-9260 (2014).
 41. Nielsen, Eyley, *et al.*, "Dual fluorescent labelling of cellulose nanocrystals for pH sensing", Chem. Commun. 46: 8929-8931 (2010).
 42. Pan, Hamad, *et al.*, "Parameters Affecting the Chiral Nematic Phase of Nanocrystalline Cellulose Films", Macromolecules 43(8): 3851-3858 (2010).
 43. Parker and Townley, "Biomimetics of photonic nanostructures", Nat Nano 2(6): 347-353 (2007).
 44. Revol, Godbout, *et al.*, "Solid self-assembled films of cellulose with chiral nematic order and optically variable properties", Journal of Pulp and Paper Science 24(5): 146-149 (1998).
 45. Revol, J.-F., *et al.*, "Solid self-assembled films of cellulose with chiral nematic order and optically variable properties", Tappi Journal 24(5) (1998).
 46. Salopek, Krasić, *et al.*, "Measurement and application of zeta-potential", edited by Rudarsko-geološko-naftni fakultet (1992).
 47. Scott, "Principles of wet end chemistry", edited by Tappi Press Atlanta, Georgia (1996).
 48. Shafiei-Sabet, Hamad, *et al.*, "Rheology of Nanocrystalline Cellulose Aqueous Suspensions", Langmuir 28(49): 17124-17133 (2012).
 49. Spink, Moyer, *et al.*, "Defining the types of counterfeiters, counterfeiting, and offender organizations", Crime Science 2(1): 1-10 (2013).
 50. Staake, Thiesse, *et al.*, "The emergence of counterfeit trade: a literature review", European Journal of Marketing 43(3/4): 320-349 (2009).
 51. Terech, Chazeau, *et al.*, "A Small-Angle Scattering Study of Cellulose Whiskers in Aqueous Suspensions", Macromolecules 32(6): 1872-1875 (1999).
 52. Xiong, Han, *et al.*, "Flexible, highly transparent and iridescent all-cellulose hybrid nanopaper with enhanced mechanical strength and writable surface", Carbohydrate Polymers 113(0): 264-271 (2014).
 53. Zhang, Chodavarapu, *et al.*, "Nanocrystalline cellulose for covert optical encryption", Organic Photonic Materials and Devices Xiv 8258, edited by (2012).
 54. Zhang, Chodavarapu, *et al.*, "Structured color humidity indicator from reversible pitch tuning in self-assembled nanocrystalline cellulose films", Sensors and Actuators B: Chemical(0) (2012).
 55. Zhang, He, *et al.*, "Using optical brightening agents (OBA) for improving the optical properties of HYP-containing paper sheets", Pulp and paper Canada 110(8): 20 (2009).
- Zou, Tan, *et al.*, "Flexible, iridescent nanocrystalline cellulose film, and method for preparation", Fpinnovations, Can. . WO2010124378A1 (2010).

Chapter4

**Nanocelluloses as
potential material for
specialty papers**

Table of contents

Introduction	209
1 Cost-effective approach for limiting TiO₂ in paper formulation with surface coating based on CNF	211
1.1 Introduction	211
1.2 Experimental section	213
1.2.1 Materials	213
1.2.2 Methods.....	213
1.3 Results and discussions	217
1.3.1 Comparison between CNF-TiO ₂ in bulk addition or as surface coating ..	217
1.3.2 Comparison between conventional coating and CNF based-coating.....	218
1.3.3 Experimental validation of CNF-TiO ₂	220
1.3.4 Cost efficiency study.....	222
1.3.5 Upscaling CNF-TiO ₂ based coating for lightweight paper.....	223
1.4 Conclusions & Perspectives	228
2 Engineered pigments based on iridescent cellulose nanocrystal films	229
Abstract	229
2.1 Introduction	230
2.2 Experimental	231
2.2.1.1 Materials	231
2.2.2 Methods.....	231
2.3 Results and Discussion.....	234
2.3.1 Cellulose nanocrystals characterization	234
2.3.2 Formation of the nanostructured iridescent film.....	235
2.3.3 Dry fine grinding.....	236
2.3.4 Compatibilization techniques o for film manufacturing.....	239
2.3.5 Improving the thermal resistance of the CNC-based pigment.....	240
2.3.6 Improving the water resistance of the CNC-based pigment	242
2.3.7 Upscaling the manufacturing of iridescent pigments.....	244
2.3.8 Addition of iridescent pigments in paper at industrial scale.....	245
2.4 Conclusion and perspectives	250
Concluding remarks.....	251
List of Tables.....	253
List of figures	253
References	255

Introduction

To conclude, this chapter concerns the implementation at an industrial scale within the papermaking process of the results obtained for nanocellulose films to be considered as model surface layer for paper. It aims to assess the potential use of nanocellulose in specialty papers based on two concrete applications: the use of CNF based material as a coating or iridescent pigment.

From the results obtained in *Chapter 2*, a cost-effective solution for saving opacifying pigment is presented. The approach is to determine to estimate an acceptable CNF cost for further industrial uses in order to be cost-effective. Upscaling lab experiments to a pilot trial are described. Finally, the results of the trials have been positive because the coating material of CNF-TiO₂ is promising in regards to the process runnability and end-use properties.

Based on the finding of *Chapter 3*, *Chapter 4.2* describes how to engineer iridescent pigments from films based on cellulose nanocrystal (CNC). An efficient method is also proposed using fine grinding and various post-treatments depending on the end-use application. Such pigments can be used for a number of applications, such as food, pharmaceutical, and cosmetic packaging, in which anti-counterfeiting functions could be targeted. In the last section of *Chapter 4.2*, a description of the manufacturing and use of iridescent pigment during the papermaking process is also provided.

These approaches have been validated at lab scale, but also which is unusual, on a pilot scale. They are mainly inspired from different patent applications, industrial trial reports, and one scientific paper.

.

1 Cost-effective approach for limiting TiO₂ in paper formulation with surface coating based on CNF

This section is inspired from “Julien Bras, Naceur Belgacem, Raphael Bardet, Philippe Agut, Jocelyne Dumas, Opacifying layer for a paper medium, Grenoble INP ; Papeteries du Leman, WO 2014033409 A1 (2014)”.

1.1 Introduction

Context. As mentioned in **Chapter 1**, Titanium Dioxide (TiO₂) is one of the most efficient mineral pigment regarding its opacifying and covering effects.(Nelson et al. 2008) This is related to its high refractive index (2.55-2.75), high reflectance in the visible region of light, as well as the optimal particle size of these opacifying particles, which makes them the most effective white opacifying pigments. (Laufmann et al. 2006) For all these reasons, TiO₂ is preferentially used when high level of covering and brightness of thin materials are a key issue: paints (50%), plastics (30%) and papers (5%).(Braun 1997)

However, because of its scarcity and extraction cost, TiO₂ is the most expensive pigment in the paper industry, it costs 10 times more than bleached pulp and 20 times more than Calcium carbonate. Since the year 2008, there has been a sharp increase of TiO₂ price (from 2,000€/t to 3,200€/t) because of a rise demand from non-paper industries, and increasing consumption from emerging markets like China. It is therefore estimated that the price of titanium oxide could break the 3,500 €/ton barrier in the near future. In paper industry, TiO₂ is mainly used within specialty papers often for low basis weights with particularly high demand in opacity and sheet brightness. TiO₂ is used in Bible, label paper and decor paper. The level of TiO₂ is adjusted depending on the final optical and cost goals.

Generally, magazine and light business paper contains 0-5% of TiO₂, up to 10% for bible and offset paper and up to 30% in the laminate papers (Braun et al. 1992). During the papermaking process, TiO₂ can be introduced in two ways: during the wet-end preparation (bulk) or as a surface treatment (paper coating). In the wet-end addition, pigment dispersion is added directly to the pulp suspension. However, the addition of TiO₂ presents many challenges. It leads to an increase of the chemicals due to their high specific area (10m²/g) and their interaction with the cationic wet-end additives. Furthermore, without appropriate retention agents, the retention of TiO₂ (during first pass) is only 50–60%.(Jaycock et al. 1976)

At an industrial level, TiO₂ pigments are difficult to retain in the paper web because of their fine dimension (average particle size 0.2–0.25 μm), and their high density (3.8-4.2

g/cm³). In surface coating, 5-10 wt % of TiO₂ is generally combined with Calcium Carbonate or Kaolin Clay and 10 wt % of binder. (Barke et al. 1984) The use of TiO₂ in surface coating is also challenging for specialty papers. Indeed, such particles are very abrasive which reduced the lifetime of metering and coating elements. This can be overcome by using a mixture of hydrous silica and alumina. (Hirani et al. 2006) Lastly, at high amount of TiO₂, particles are not well dispersed and tend to agglomerate, which induces the overlapping of their light scattering zones, thus reducing their opacifying effect.

Purpose of the study. Different cost-effective approaches for optimizing paper formulations are outlined in the literature. They generally consists of using TiO₂ extender as spacing particle to optimize hiding efficiency of TiO₂ and avoid crowding, (Adkins 1992) or to use specific polyelectrolyte as retention aids during paper formation (Gesenhues 2011). More recently, the use of TiO₂ nano-powders as special paper coating pigments has also been proposed. (El-Sherbiny et al. 2014). As previously described in **Chapter 2.1**, high opacity film can also be obtained using TiO₂ particles dispersed in CNF network. (Bardet et al. 2013) Based on the gel-like properties of CNF suspensions and the ability of CNF to form a well-entangled nanofibers network, spherical shape particles could be entrapped and physically dispersed within the thickness of the CNF films. Meanwhile, several studies have proposed to use CNF in paper coating for barrier or printing applications as reported in **Chapter 1.2**, (Bardet et al. 2014) and in a recent review (Fredrik Wernersson Brodin et al. 2014).

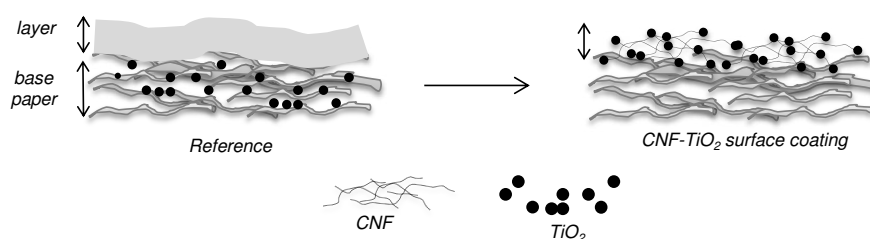


Fig 4.1 - Cost-effective approach for limiting TiO₂ in paper formulation

Based on these statements, the present work investigates the possibility of surface treatment of CNF and TiO₂ onto thin papers as summarized in **Fig 4.1**. It aims to propose a sustainable and cost-effective approach for limiting petro-based latex and saving TiO₂ in specialty paper like opaque lightweight papers. It includes lab scale experiments, a brief economic analysis, and it ends by pilot scale trials. Based on such promising results a patent has been submitted in 2012 and accepted in 2014. This patent is available in **Appendix 1.1** and the reader is invited to consult it for more detailed description of the approach envisaged. (Bras et al. 2014)

1.2 Experimental section

1.2.1 Materials

Cellulose nanofiber (CNF) suspension was produced at pilot scale (CTP, France). According to protocol developed during SUNPAP project, CNF was isolated from sulphite softwood-dissolving pulp (Cellulose Plus®, Domsjö, Sweden) using refining and enzymatic pretreatments and a then homogenized (Ariete NS3075, GEA Niro Soavi, Italy). Five passes (one at 1000 bar and four at 1450 bar) were successively performed into the homogenizer to produce a homogenous and gel-like CNF suspension at 2 wt % consistency.

Pigments used in the study are a 71 wt % slurry of Titanium Dioxide (TiO₂) (Tiona®, Millennium Chemicals, England) and a slurry of precipitated Calcium Carbonate (PCC) (Precarb 120, Scaeffler Kalk, Germany). Their average diameter D₅₀ measured by laser granulometry (1190 Particle Size Analyzer®, Cilas, France) are 0.40±0.07 μm and 1.04±0.05 μm and, for TiO₂ and PCC, respectively.

1.2.2 Methods

Manufacturing of base papers

Two different 30 g/m² base papers were used: one at lab-scale and the other from industrial production. Labsheets were prepared according to *ISO:5269-1* for adjusting the TiO₂ amount (0 to 9 wt %) within the base paper. The suspension is a mixture of softwood (70 wt %) and hardwood (30 wt %). The degree of refining of suspensions (measured according to *ISO:5267*) is 72°SR. Fibers average length is 0.68±0.01 mm and their width is 22±5 μm. The suspension morphology was measured using MorFi fiber analyzer following procedure describes by Lehto (2004). Secondly, an industrial base paper (MSP34WUS, Papeteries du Léman, France) was collected before the surface coating and soft-calendaring sections. This is a 30g/m² lightweight-coated paper dedicated to the offset lithography printing. This paper is **composed** with 81 wt % of refined pulp and filled with 19 wt % of kaolin clay.

Coating Preparation

Three different types of coating formulations were tested: a conventional coating formulation used for lithography offset paper, a CNF-TiO₂ formulation, and a control formulation. The conventional coating (first one) consisted in a suspension of Kaolin Clay

with SBR latex and starch binders. This coating color was taken during the paper production and used “as it is”. The CNF-TiO₂ coating consists of a mixture of Cellulose nanofibers and a TiO₂. Three amounts of TiO₂ were tested: 20, 50, and 70 wt %. These formulations were prepared as claim by Bras et al. (2012). For the control coating, a 1:1 mixture of SB latex and starch replaced the entire amount of CNF with same amounts of TiO₂.

Surface coating systems

Two different coating systems were used. For lab scale experiments, “Labor Size Press SP” (Mathis AG, Switzerland) was used. Handsheets were pressed between the two rolls at 2 bars at a speed of 20 m/min. Papers were then coated onto both sides and dried with a contact drying system under tension at 105°C for 3 min. These steps were repeated two times to reach a coating deposition of about 4 g/m². For pilot scale trials, an industrial flexographic press (Onyx 108GL, UTECO, Germany) is used. This industrial coating machine is based in Italy and has been specially adapted for the project in order to simulate surface coating of a paper machine (e.g. speed of 100m/min). A technical comparison between the both surface coating systems is provided in **Table 4.1**.

Table 4.1 - Technical comparison between the two surface coating systems

	Lab scale	Pilotscale	Challenge for upscaling	Recommendations
Base paper	30g/m ² handsheets	30 g/m ² industrial base paper		
Coating preparation	500ml batches Mixing with homogenizer	40l batches Mechanical stirring	Ensure a good dispersion with an industrial stirring	Continuous and high mechanical stirring
Pumping and feeding	-	Peristaltic pump Recirculation	avoid clogging in pipes	Adapt viscosity to pumping and feeding equipment Decrease dry matter (if requires) Maintain a high shear rate throughout the coating process
Coating deposition	Blade coating Several passes possible Pressure	Film-press Anilox volume (10-30cm ³)	Reach the targeted coating weigh (>2g/m ²).	Adjust by using different anilox parameter and machine speed.
Drying	Air drying system Long drying time available	Industrial online infrared system	Evaporation of additional water contains in the low consistency coating	Increase drying temperature
Speed	20 m/min	100m/min	Paper runnability	<i>Adjust machine parameters</i>

Optical and physical properties

Before characterization, all the samples were conditioned at room temperature and at 23°C with 50% of relative humidity, for at least 48 h. They were characterized in term of optical, mechanical, and printing properties by using standards as summarized below (**Table 4.2**) :

Table 4.2 - Recap of the ISO standards used to characterized the properties of paper samples

	Properties	Units	Standards
General	Grammage	g/m ²	ISO 535:1991
	Coat weight	g/m ²	
	Thickness	μm	ISO 534:2005
	Density	g/cm ³	
	Filler content residue on ignition at 525 °C	%	ISO 1762:2001
	TiO ₂ content spectrophotometric procedure	%	ISO 2144:1997
Optical	ISO Opacity		ISO 2471:2008
	ISO Brightness		ISO 2470-2:2008
Mechanical	Bending stiffness		ISO 2493-2:2011

Printing properties

For simulating offset lithography and to predict the print-through, papers were printed with a printability tester (IGT C1 Printability tester, IGT, Netherland). This method consists of applying a homogenous layer of standardized black ink onto the paper strip under dynamic, controlled and reproducible conditions. Then, the dry weight of printed ink, the printing density, and the reflectance are measured. For each sample series, two paper strips of 45x280mm were printed (75.3 cm² per strip) with ink weight ranging from 0.5 to 2 g/m² of standardized black ink. Printing conditions are described in **Table 4.3**.

Table 4.3 - Printing parameters of the offset lithography test

Parameters	Values
Atmospheric conditions during printing	23 °C, 50 %RH
Standardized black ink	Sunlit Exact PSO Process Black, SunChemical®, UK
Speed	1m /s
Force	500 N
Drying time	12 hours, room temperature

For calculation of the black print density, a reflection densimeter (R410e, Techkon®, Germany) has been used. For each printed paper strips, 4 measures have been made on the front of the printed strip. The print-through is expressed by the following formula:

$$Print\ through = -\ln\left(\frac{R_{printed}}{R_{\infty}}\right)$$

The print-through has been evaluated using a spectrophotometer (Elrepho2000, Datacolor, Switzerland). Ten layers of (non-printed) papers were superimposed in order to obtain a pad thick enough to be opaque. Afterward, two measures are taken: the luminance factor (R_{∞}) of the unprinted pad and the luminance factor ($R_{printed}$) of the pad with the printed sample on the inside to the pad.

Surface topography of the coated papers

E-SEM (Environmental Scanning Electron Microscope) in backscattered electron mode (BSE) was used to evaluate the thickness of uncoated and coated samples (Quanta 200©, FEI, Japan). Then, the fillers repartition of the samples cross-section were obtained by EDS (quantitative x-ray mapping) of C,O, Ca,, Si, Mg and Ti elements. Samples were previously conditioned and coated with carbon and observed using an applied tension of 15 kV.

FE-SEM (*Field-Emission Scanning Electron Microscope*) was used to observe the nanostructure of the surface of samples (Ultra 55 ©, Zeiss, Germany). Samples were covered with carbon tape and coated with a 2nm layer of gold/palladium to ensure the conductivity of all samples. The accelerating voltage (EHT) was 3 kV for a working distance of 6.4 mm.

1.3 Results and discussions

1.3.1 Comparison between CNF-TiO₂ in bulk addition or as surface coating

As explained in the introduction, there are two different ways to introduce TiO₂ pigments, i.e. directly in the base paper or as a layer (surface coating). To confirm the approach of using CNF-TiO₂ coating is cost-effective and to justify further industrial trials, the following section is focused on the comparison of these two approaches.

Fig 4.2 shows the two different approaches. The different grey-levels observed in the BSE-images can be used as an efficient tool to evaluate the repartition of TiO₂ within the cellulosic materials including CNFs and fibers. **Fig 4.2-A**, the repartition of TiO₂ particles are distributed outside fiber walls. A higher concentration is found in the fibers entanglement area. This contrasts with **Fig 4.2-B** in which TiO₂ pigments are only located at the coated surface (upper side). **Fig 4.2-B** also confirms TiO₂ particles are well retained in the CNF layer. However, Because of low coating weight (<3 g/m²), it is difficult to estimate the surface layer thickness.

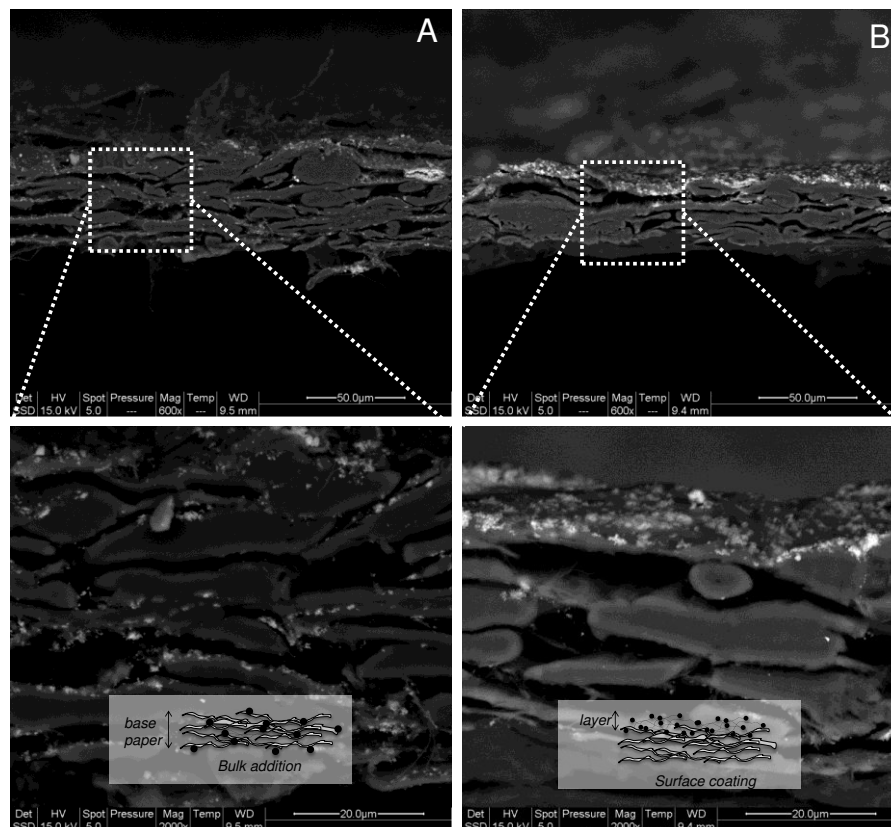


Fig 4.2 - SEM images (in BSE mode) of 30 g/m² paper cross-sections which consists of fibers (94%), CNFs (3%) and TiO₂ (3%). Addition of CNFs and TiO₂ during the labsheet formation (A) or as surface treatment (B).

The key result is obtained when comparing the opacity of the two papers. With the same amount of TiO₂ (3 wt %) in handsheets, the opacity is about 10 percent higher for TiO₂ introduced as a surface layer than in the base paper (70.3±0.9 instead of 63.8±1.4 %). This difference in opacity is huge. The low filler retention of TiO₂ during handsheets formation mainly explains the lower opacity reported for sample in which TiO₂ is incorporated during handsheets manufacturing. In case of TiO₂ incorporate in the base paper, about 45 % are retained. (Gesenhues 2011) Here the retention of TiO₂ is almost total in case of when TiO₂ is coated and about 50 wt % when added in the bulk. However, it is worth noting that the two paper compared have similar final TiO₂ quantity. In addition, several studies report that the retention of CNF themselves is low and especially for lightweight papers.(Hamann 2011).

In addition, there are several drawbacks of using CNF as bulk additives can be addressed as mentioned in the **Chapter 1.3**:

- The cost is relatively high in comparison with other retention aids commonly used in the wet-end process.
- In addition, a negative impact on the drainage properties that directly affect the papermaking process, and more precisely, the drying and pressing sections is often reported.

It is also necessary to point out that the retention TiO₂ (as well as CNF) is almost total with the surface treatment and the impact on papermaking is limited to the coating section. In addition, TiO₂ particles are well retained in the CNF layer. With the same amount of TiO₂, the opacity is about 11 % higher for TiO₂ introduced as a surface layer than in the base paper.

1.3.2 Comparison between conventional coating and CNF based-coating

As discussed in the previous section, the cost-effective approach for a lightweight paper (30 g/m²) is to introduce a mixture of CNF and TiO₂ as a coating layer. The selection of CNF as binder can be questioned because other effective binder can be used such as CMC, PVA, latex or starch.

However, in our previous study, it has been reported that CNFs promote the dispersion of TiO₂ particle because of the formation of entangled networks of nanofibers.(Bardet et al. 2013) Thus, thin films based on CNF are systematically more opaque than the other ones. As a finding, for producing opaque films with the same optical properties, about 60 wt % of TiO₂ can be saved in comparison with standard binder. Indeed, several differences exist between the opaque film obtained by casting method and the surface layer coated in a base paper. It

includes a lower thickness (few μm instead $30\ \mu\text{m}$), interaction with the paper surface, a layer formation under high shear stress and a fast drying (instead of a simple evaporation).

To validate the results collected with the “model film” to the “paper coating”, similar coating formulations were coated on a $30\ \text{g/m}^2$ paper. Coating formulations are based on varying amount of TiO_2 (0 to 6 wt % as final ratio in the coated paper) and conventional binders (SB latex and starch) are compared with CNF.

Fig 4.3 presents the evolution of opacity ISO as a function of the total amount of TiO_2 and compares conventional binders (starch and latex) with CNF.

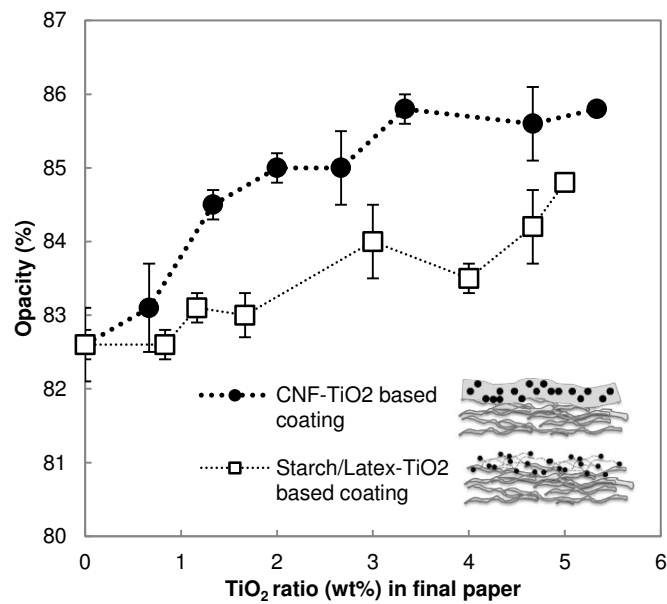


Fig 4.3 - Opacity as a function of TiO_2 ratio in a paper. Comparison between CNF (●) and Starch/SB latex (□) based coating formulations.

Not surprisingly, the opacity increases with the amount of TiO_2 in the paper. At very low amount of TiO_2 ($< 1\ \text{wt}\%$), there is no significant difference between the two formulations. However, for ratio higher than $1\ \text{wt}\%$, the opacifying effect is much better for CNF based coating. Such difference of opacity at this high level of opacity is very significant. These results confirm the very positive effect of CNF for dispersing TiO_2 . Therefore, when high opacity of the coating layer is targeted, CNFs is worthwhile to substitute conventional binder in printing coating.

As shown in **Fig 4.4**, the difference between the entangled networks of nanofibers (A) and the continuous matrix (B) may explain the difference of opacity. This is due to a better dispersion of solids particles (i.e. TiO_2) within the NFC network as already reported (Bardet et al. 2013).

In addition, it can be also related to the higher porosity within CNF-TiO₂ layer. Indeed the presence of small air voids may promote light scattering (Nelson et al. 2008). It explains because “air” has a lower refractive index (1.0) compared with starch, latex (1.5) or cellulose (1.53). So the light scattering is enhanced because of additional refraction upon incorporation of nanoporosity (air voids).

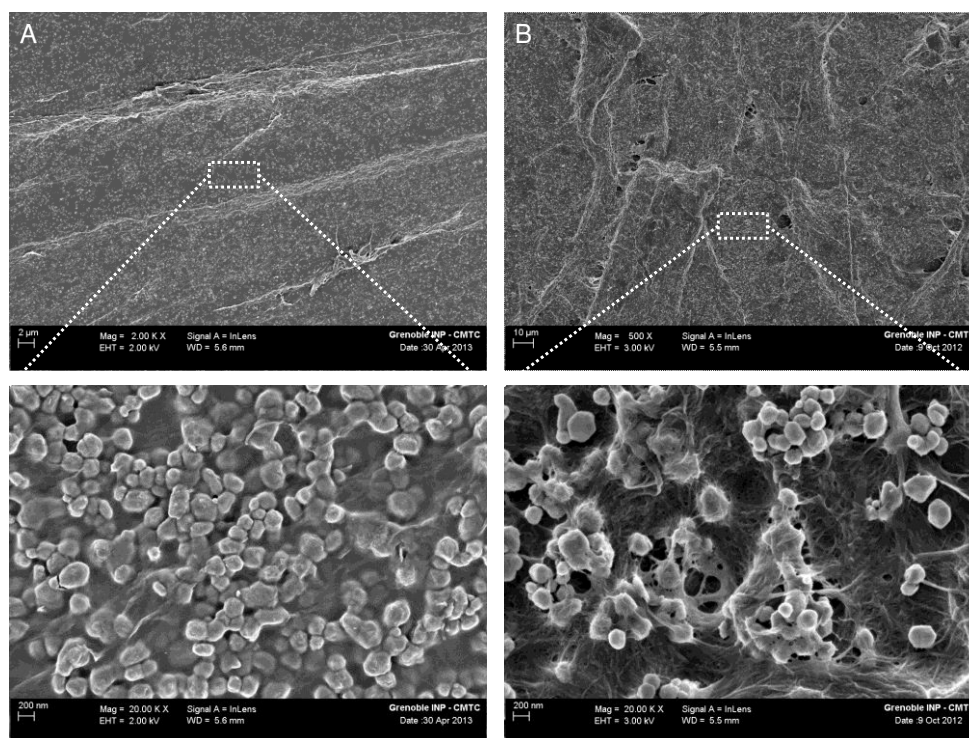


Fig 4.4 - FE-SEM pictures of paper surface coated with Starch-Latex TiO₂

This section demonstrates that CNF can replace with success conventional binders such as latex and starch in surface coating formulations. So, a second source of saving TiO₂ is identified after the possibility of coating instead of bulk addition. Moreover, it is worth to highlight that CNFs used as a binder in paper have the advantage of being more environmentally friendly in comparison to petrol-based SB latex or even starch extracted from food resources.

1.3.3 Experimental validation of CNF-TiO₂ surface coating for lightweight paper

First results are promising because for the same amount of TiO₂, it demonstrates that the paper opacity is higher with a CNF-TiO₂ than for TiO₂ introduced in the base paper or coated with common binder. With an industrial perspective, it sounds more interesting to estimate the potential save of TiO₂ for the same opacity. Thus, two additional series of handsheets were prepared with TiO₂ varying from 0% to 9% as summarized in **Fig 4.5**. The ratio corresponds to the final ratio of TiO₂ measured in the coated paper.

To do so, TiO_2 is introduced either in the base paper (reference) or in the surface layer (CNF- TiO_2 coating). The final filler ratio is adjusted to 25 wt % with PCC fillers. The weight of the base paper (i.e. handsheet) is 30 g/m² and the average coating weight is about 4 g/m². “Reference” samples correspond to the current approach used for manufacturing opaque lightweight papers. In this case, TiO_2 is introduced in the base paper and then coated with Kaolin, SB latex/Starch formulation. Series called “CNF- TiO_2 coating” corresponds to a mixture of CNF and a TiO_2 . prepared as claims by Bras et al. (2012).

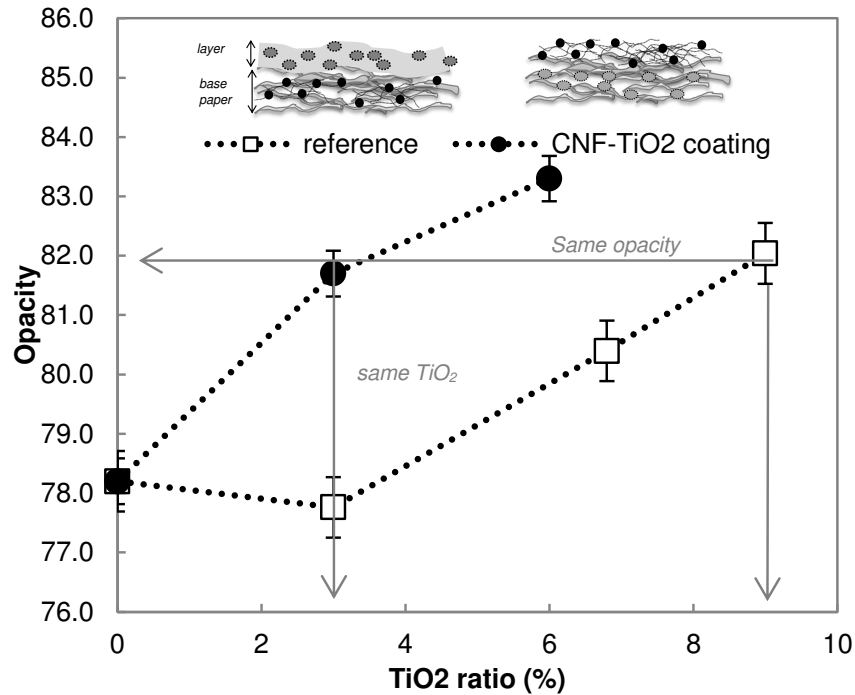


Fig 4.5 - Comparison of the opacity between CNF- TiO_2 coated paper (●) and reference coated paper (□) for different TiO_2 ratio

The results presented in **Fig 4.5** are promising and confirm the interest of using CNF- TiO_2 mixture as a coating formulation for opaque lightweight paper. Indeed, for exactly the same TiO_2 ratio (measured in the paper), there is about three opacity points of difference between the “reference” sample and “CNF- TiO_2 coating” sample.

For instance, with 9 wt % of TiO_2 (contains in the base paper), the paper opacity is 82 ± 0.8 %, however the same opacity can be obtained with only 3% of TiO_2 with a CNF- TiO_2 surface coating. Dividing by 3 the quantity of TiO_2 represents an important saving of TiO_2 ¹.

¹ At beginning of the PhD thesis, the TiO_2 consumption for the industrial partnership is about 1 250 tons of TiO_2 per year (i.e. 4 900 K€ per year)

1.3.4 Cost efficiency study

Based on these experimental results, the cost-efficiency of CNF-based coating can be evaluated. Because CNFs are not yet commercially available, the economic gain is difficult to assess. However, based on the potential save of TiO_2 ; the “acceptable” CNF price can be estimated. This price is determined in order to reach the same material cost for a 34 g/m^2 coated paper. To do so, the following assumptions were taken as summarized in **Table 4.4**

Table 4.4 - Hypothesis undertaken for the technico-economic

		Current solution	CNF-Based coating		
Overview	base paper		30 g/m ²		
	coating		4 g/m ²		
	filler ratio		25%		
Paper formulation	Base paper (as wt %)	fiber	79	75	
		PCC	18 to 10	22	
		TiO_2	0 to 8	-	
	Composition	Additives		3%	
		Surface coating (as wt %)	Binder	78	50
			Pigment	20	50
			Additives	2	-
	raw materials cost (€ / kg)	Fiber		0.54	
		PCC		0.3	
		TiO_2		2 or 3	
Binder			0.8		
additives			1		

Main assumptions: TiO_2 save for CNF- TiO_2 coated is estimated by assuming a linear interpolation of the curve presented in Fig 4.5. The over drying cost due the low consistency of CNF- TiO_2 coating is not considered. End-use properties (printing and mechanical) remains equivalent

Fig 4.6 presents the cost of acceptance of CNF for two different prices of TiO_2 and different ratio additions. The CNF cost is ranging from 0.70€/kg to 2.5€/kg depending on the TiO_2 ratio (or the targeted opacity).

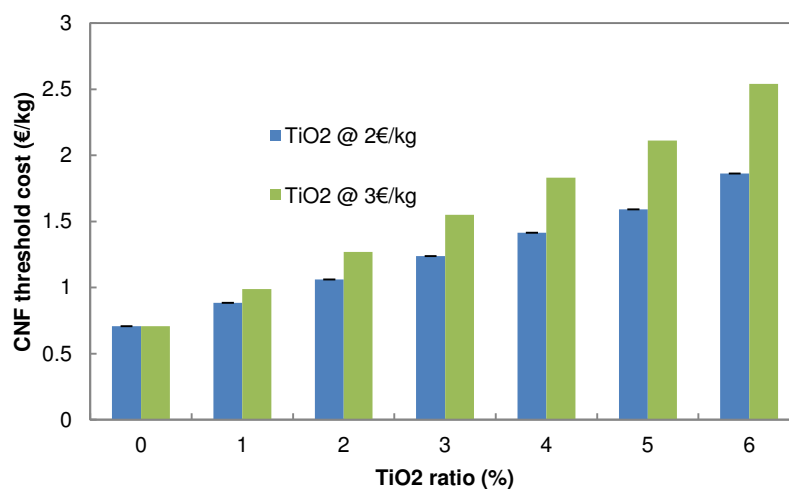


Fig 4.6 - Threshold price for CNF giving the equivalent costs for 34 g/m^2 lightweight paper

The range of CNF price reported here is in the same order than the one reported in a study Torvinen et al. (2011) in which CNF was used to increase the filler content in soft-calendared paper. In this study, they estimates that CNF price should be below 2 €/kg to be cost-efficient. Even if such calculated price reported here is much lower than announced commercial price for CNF (3-10€/kg), it remains in the range to the estimated manufacturing cost of CNF.(Miller 2014)

This result confirms that an *in-situ* production of CNF with TiO₂ (as a satellite within the mill) is the most appropriate strategy. This why up-scaling has been considered for this use of nanocellulose in specialty paper.

1.3.5 Upscaling CNF-TiO₂ based coating for lightweight paper

This last section is dedicated to evaluate whether or not CNF based coating is promising regarding the potential save of TiO₂. Indeed, in spite of very promising lab-scale results, still some questions are pending: influence of speed (shear rate) during coating, possibility of pumping the gel-like structure, drying possibility for this low solid-content coating suspensions, etc...

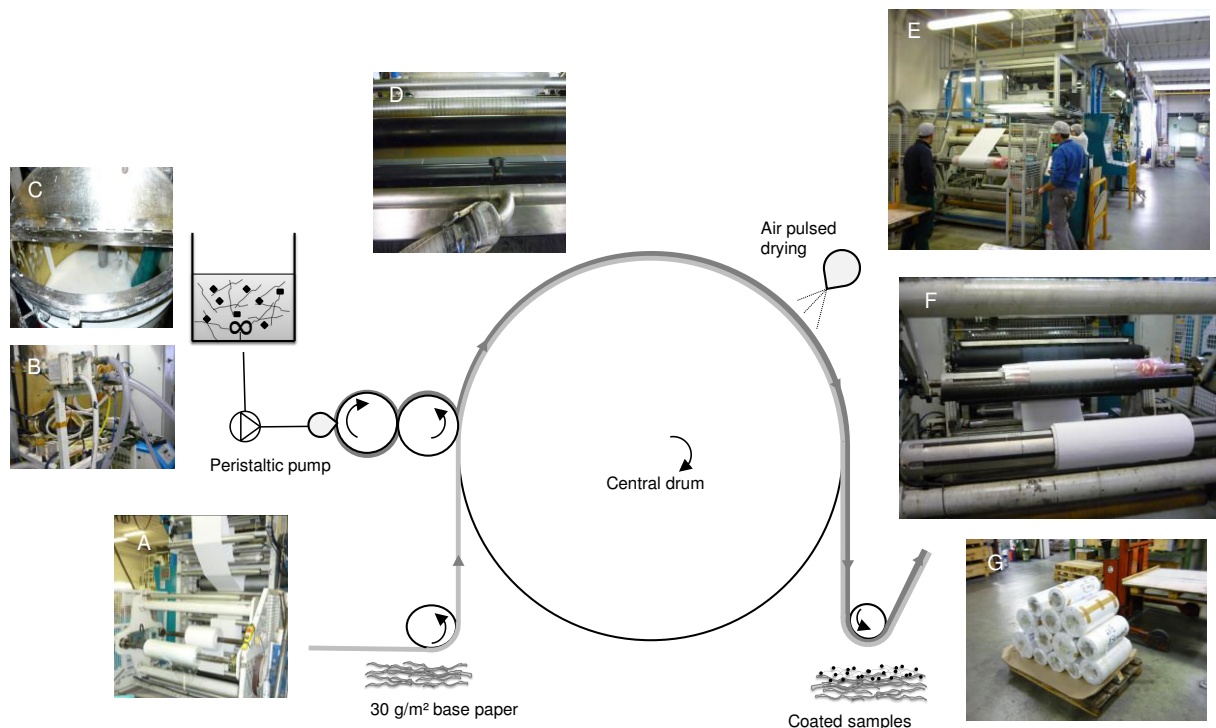


Fig 4.7 - Overview of the pilot coating machine

For upscaling the study, coating trials (one week campaign) has been implemented on industrial flexographic press (Onyx 108GL, UTECO, Germany). This industrial coating machine has been specially adapted for the project in order to simulate the surface coating of

a paper machine² (see experimental section). A scheme of the pilot coating is presented in **Fig 4.7**. The base paper (reel of 60 cm width) is conveyed to a central drum (A). The surface treatment is carried out on one side of the base paper thanks to two-transfer rolls (anilox) (D). The coating formulation is mixed with a mechanical stirring (C) and pumped with a peristaltic pump from the reservoir tank (B) to the anilox (D). The excess of coating is recirculated to the initial tank. The drying is ensured with an air pulsed system at the end of drum. Finally the coated paper is reeled.

Coating preparation and pumping

The rheological behavior of a CNF-TiO₂ coating is critical in both handling operations (pumping, feeding and storage) and during the coating application onto the base paper (**Fig 4.8**). Indeed viscosities of such coating vary widely with the shear rate and so throughout the coating process. This is because most of paper coatings as well as CNF suspensions have a non-Newtonian behavior.

As highlighted in **Fig 4.8**, at low shear rate (corresponding to pumping or mixing operations), the viscosity is very high for both formulations (i.e. about 10⁵ the viscosity of water at 23°C).

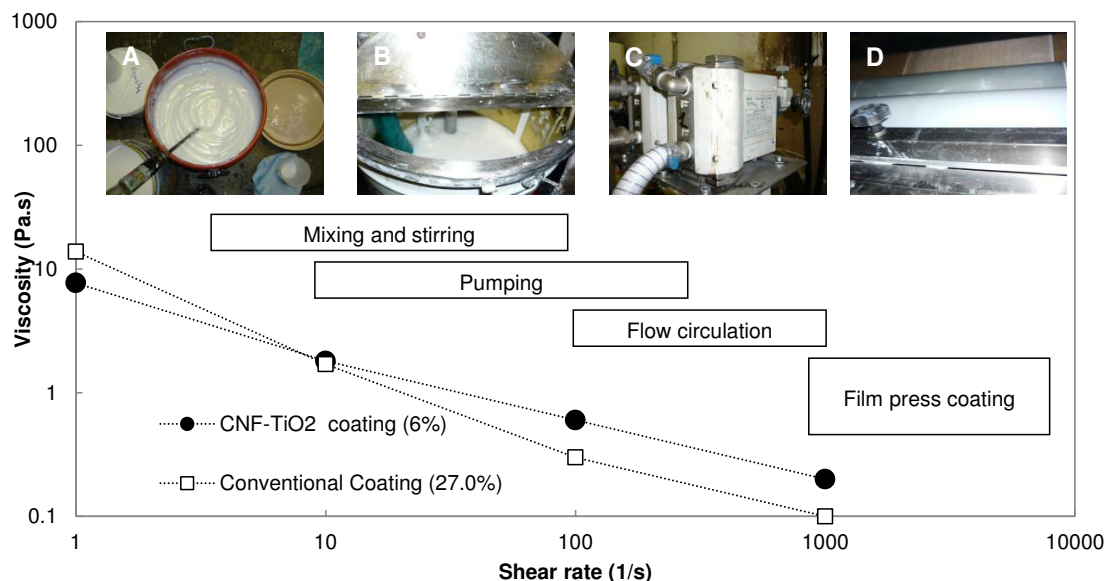


Fig 4.8 - Viscosity as a function of the shear rate for a 27 wt % conventional coating and a 6 wt % CNF-TiO₂ coating. Pictures of the coating process: coating preparation(A), pumping system(B), flow circulation(C), and surface coating(D). Boxes correspond to the characteristic shear-rate ranges occurring during the paper coating.

² Trial had not been implemented directly on paper machine because the coating preparation on requires a significant volume of coating (4000-6000 l per coating preparation). At the time of the trial such quantity of CNF was not available. This is why it has been chosen to firstly implement on such coating machine

However, the rheological behavior is equivalent in the range of shear rate from 0.1 to 10 s⁻¹. Beyond 10 s⁻¹, the CNF-TiO₂ based coating is slightly more viscous than a conventional coating. In comparison to a neat CNF suspension (not presented), CNF-TiO₂ suspension presented several advantages because the introduction of mineral pigment such as TiO₂ increases from 2.0 % to 6.0 % the dry matter of a CNF-based coating but also decreases the viscosity of the ensued suspension.

This rheological investigation tends to confirm the CNF-TiO₂ coating formulation is suitable for pilot scale and probably for industrial production. It is important to notice that results presented here only provide a general trend about the feasibility of coating CNF-TiO₂ throughout the coating process. Indeed to be relevant a more complete study should include investigation at higher shear rate (i.e. from 10⁵ to 10⁶) with a capillarity rheometer.

Key findings

The results of the pilot-scale trials have been very positive. Indeed the CNF-TiO₂ coating scale-up is possible and efficient as summarized in **Table 4.4**

Table 4.4 - Trial overview

	Parameters	results
Coating machine	Average coating weight	3 coating weight 0.6-3.0 g/m ²
	Coating formulation	3 formulation -CNF-TiO ₂ -Starch-Latex TiO ₂ -Conventional coating
	Speed	80-100 m/min
	Drying temperature	100-120 °C
Sample production overview	Duration of mill trials	29 hours
	Trial production	13 reels of 1000m in length

During the trials (about 30 hours), 3 coating formulations were tested as well as different coating weight from 0.6 to 2.8 g/m². Thus, 13 reels of about 1000 m long were coated and then characterized. The runnability of paper and the surface treatment-using pilot coating machine are successful for CNF-TiO₂ coating (as well for conventional coating).

The following section focuses on the evaluation of the end-use properties of paper coated with the pilot coating machine.

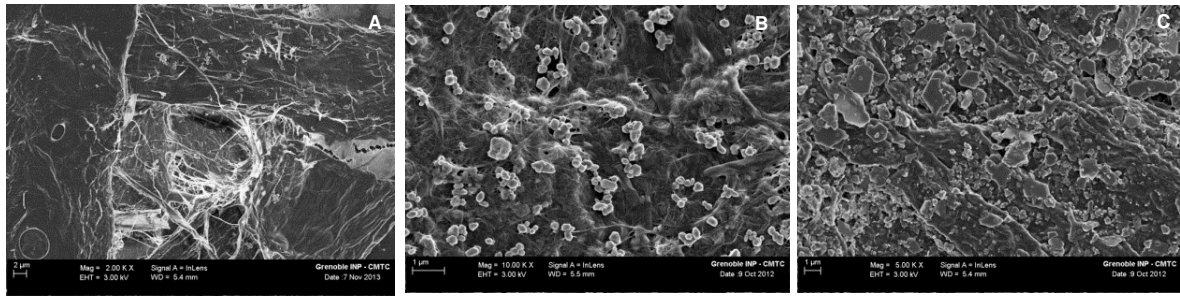


Fig 4.9 - FE-SEM pictures of the 30 g/m² uncoated base paper (A), coated with 1.4 g/m² of CNF-TiO₂ (B), and 2.5 g/m² of conventional formulation (C)

As presented in **Fig 4.9**, the microstructure of a base paper differs between the base paper (sample A) and coated samples (sample B and C). As for lab experiment (**Fig 4.4-B**), this highlights the good coverage of the coating in spite of a low coating weight deposition during the pilot-scale trials (1.5 g/m²).

However, there is a difference regarding their surface. This was expected because kaolin clay (platelet-like particles) are substituted by TiO₂ particles whereas CNF is used a binder instead of SB latex and starch. Lastly, the good dispersion of TiO₂ particles is also confirmed. As expected, the increase of opacity is a function of the coating weight (**Fig 4.10**).

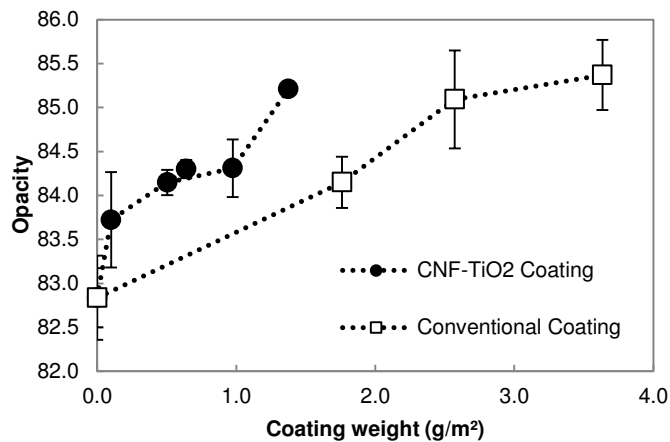


Fig 4.10 - Opacity as a function of coating weight for a 30 g/m² industrial base paper coated with a CNF-TiO₂ (●) or conventional (□) formulations

Similar to the lab experiment, there is also a gap between the two formulations regarding the evolution the opacity. Thus, an equivalent opacity (i.e. 85%) is reached with 1.5 g/m² of coating formulation whereas about 3.0 g/m² of conventional coating are necessary. This very positive.

Even if results are promising, paper analyses should not be restricted to opacity because such lightweight papers dedicated to offset lithography require also a high bending stiffness, surface strength as well as low print-through.

For this purpose, mechanical and printing properties were also investigated (but not presented). In comparison to a conventional coating, no significant difference was revealed when measuring brightness, bending stiffness or dusting propensity.

Concerning the print-through properties, a difference appears. Print-through is an often-encountered issue in lightweight papers mainly caused by ink penetration and insufficient opacity of the paper. (Pianta 1998)

As described in the experimental section, the print-through is measured as the print density of the reverse side of the printed-paper, which is printed at a standard print density. In other words, the lower the print-through, the better the paper is.

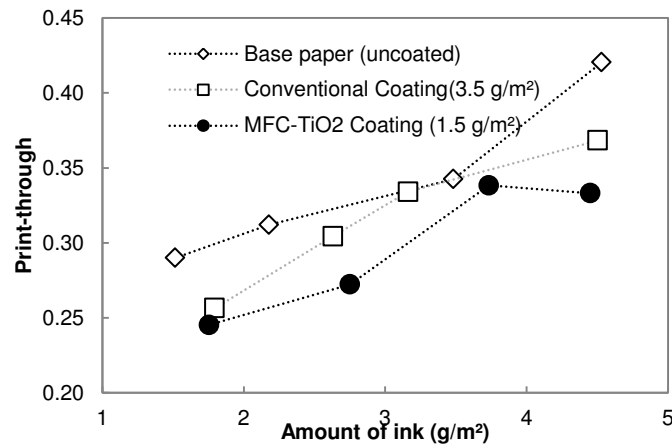


Fig 4.11 - Print-through as a function of amount of black ink printed on the industrial base paper (◇), coated with 3.5 g/m² of conventional formulation (□) and 1.5 g/m² of CNF-TiO₂ (●)

As described in **Fig 4.11**, the print-through increases with the amount of ink whatever the sample. The uncoated base paper shows higher print-through whereas coated papers are systematically better. As their surface is more open, the ink tends to penetrate more.

For CNF coated paper, ink remains on the paper surface in spite of nanoporosity. In addition, a reduction of the print-through was found for CNF-TiO₂ paper, even though the surface layer is lower (1.5 instead of 3.5 g/m²). This positive results may be the results of the formation of dense network of CNF as already reported by Song et al. (2010).

Therefore, the pilot-scale study proves the feasibility of our strategy patented, confirms the positive impact of coating CNF-TiO₂ system regarding opacity but also indicates other advantages like print-through properties or sustainability. Based on that such positive results, Papeteries du Lemans has decided in February 2014 to launch a trial (and then a production) in their paper machine. Unfortunately, since that time, it has not been possible to order large amount of CNF at “acceptable” price in spite of contacts with several suppliers. These discussions and trials should carry on in the coming months.

1.4 Conclusions & Perspectives

The goal of this chapter was to present an overview of how CNF-TiO₂ coating may be cost-effective for saving TiO₂ in lightweight coated papers. This study started from lab experiments and was completed by pilot scale trials.

First, the addition of CNF-TiO₂ suspension was demonstrated to be more effective as a surface coating than in addition to the bulk paper. This is due to the low retention of CNF and TiO₂ in thin base paper because of their small sizes. Then, CNF used as binder in paper coating was compared to conventional binder (latex and starch) currently used in industrial papermaking. It has been shown that for the same TiO₂ ratio, CNF gives a better much opacity than a conventional binders (starch, and SB latex).

To confirm CNF surface coating is cost-effective, two different series of paper were then prepared : one that contains CNF-TiO₂ in the base paper and coated with a conventional coating, and the other one that is coated with CNF-TiO₂. To ensure the comparison, paper samples were formulated at the same filler ratio, coating and final weight. The same opacity was measured for a reference paper containing 9 wt % of TiO₂ while only 2.8 wt % of TiO₂ was required when TiO₂ was coated with CNF. This solution is then very promising as no retention issues occurred and 3 times less TiO₂ is necessary. This key result was one of several considerations that justified the patent application and the pilot scale trials.

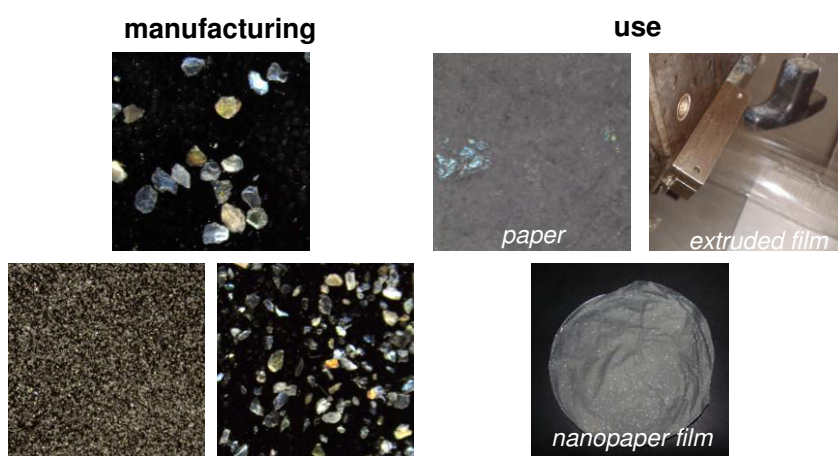
Based on such lab results, the cost-efficiency was investigated to determine an acceptable CNF cost for further industrial uses. It gives an average value between 0.70 €/kg to 2.5 €/kg depending of the TiO₂ ratio in the paper. Such preliminary results emphasize that the solution proposed here is only cost-efficient in the case of an in-situ production of CNF.

The last section was dedicated to the upscaling of lab experiments. A 30 g/m² lightweight paper dedicated to the offset lithography printing was used as base paper. The surface coating was carried out at pilot-scale on an industrial flexographic press adapted to simulate the on-line surface coating of a paper machine. Several process parameters were checked and adapted such as the coating preparation, pumping and drying. Finally, the results of the trials are positive because the coating of a CNF-TiO₂ coating was adapted regarding both the process runnability and end-use properties. During the trial, three coating formulations were tested and different coating weights were deposited. Thus thirteen reels of about 1000g long were produced and then analyzed. As a conclusion, the feasibility and efficiency of CNF-TiO₂ coating was demonstrated.

2 Engineered pigments based on iridescent cellulose nanocrystal films

This section is adapted from “Raphael Bardet, Francine Roussel, Stéphane Coindeau Naceur Belgacem, Julien Bras, Engineered pigments based on iridescent cellulose nanocrystal films, Carbohydrate Polymers (accepted in September 2014)”.

And inspired from “Raphael Bardet, Julien Bras, Naceur Belgacem, Philippe Agut, Jocelyne Dumas, Method for marking paper, Grenoble INP ; Papeteries du Lemans, WO 2014118466 A1 (2014)”



Abstract

A simple method to produce biobased iridescent pigments from cellulose nanocrystal (CNC) films is reported. The process consists of forming nanostructured films from a CNC liquid-crystalline suspension and an appropriate dry grinding. The features of the iridescent pigments are described; they have a flake-like morphology with a thickness of 25 μm . However, because of the presence of sulfate groups, thermal degradation and high redispersion in water occur, which affect the iridescent property of these biobased pigments. To overcome such limitations, two post-treatments are proposed. The sulfate ester groups are removed from the iridescent pigments with vacuum overdrying. The mass loss of iridescent pigment in water is reduced with an increase of the ionic strength in the aqueous medium by NaCl addition. These post-treatments have proven to be efficient and engineered pigments based on CNC films can be used to add anticounterfeiting features to packaging manufactured by classical paper techniques or extrusion

Keywords: nanocellulose, cellulose nanocrystals, iridescence, pigment grinding

2.1 Introduction

Derived from the well-known property of CNCs to display liquid-crystalline behavior in water (Gray 1994) and non-aqueous suspensions (Heux et al. 2000), one outstanding application is the manufacturing of iridescent materials as patented in 1995 (Revol et al. 1995). Revol et al. (1998) were the first to report that the self-organization can be preserved by simple evaporation.

Even if this nanostructured material is indisputably promising as reported in *Chapter 3*, end applications appear to be limited to the lab scale because a processing technique that can be completed within one day is required for manufacturing iridescent films.

Continuous and fast production processes, such as surface treatment, extrusion, lamination, or paper-like techniques, cannot preserve the structural coloration property. In addition, CNC as a starting material is not cost-efficient enough to compete with other materials that are able to display similar photonic properties, and iridescent films based on CNC are usually very brittle and difficult to process.

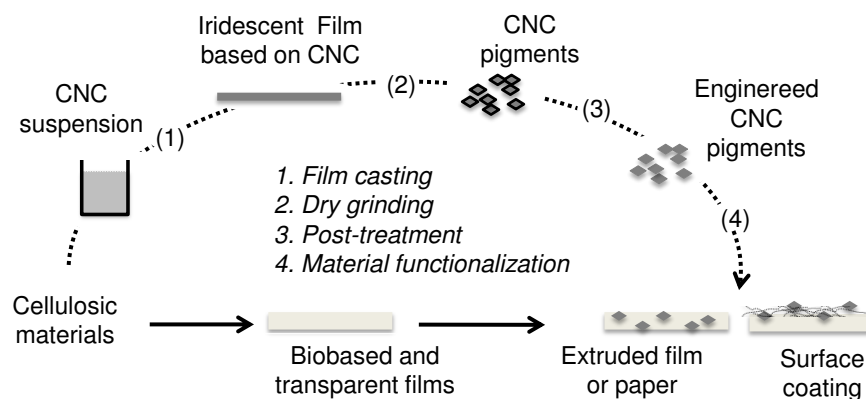


Fig 4.12 - The proposed approach for engineering pigments from iridescent films based on CNCs

In this context, this study proposes to overcome these limitations by manufacturing pigments from iridescent CNC films and then incorporating them within flexible and transparent films, as described in **Fig 4.11**.

In the first part, the CNCs and the iridescent film were characterized. Then, the optimized procedure for manufacturing the pigment with dry grinding is described. The chemical and morphological features of the pigments are also summarized.

In addition to the elaboration and characterization of the ground pigment, two main drawbacks that limit the industrial application of such pigments are addressed, i.e., the low thermal stability due to surface sulfate groups and the water sensitivity. For this, various treatments are also investigated, i.e., obtaining engineered iridescent pigment based on CNCs.

2.2 Experimental

2.2.1 Materials

The starting material for producing iridescent solid films is commercial cellulose nanocrystals (CNCs) delivered as a dry powder. It was purchased from Cellulforce (Canada) and isolated from wood pulp by sulfuric acid hydrolysis. CAB (CAB-381-20, Eastman Chemical Company™, USA) is a thermoplastic polymer based on cellulose. The butyryl, acetyl and hydroxyl contents are 37.0, 13.5 and 1.8 wt %, respectively, with a molecular weight of 70,000 g/mol. The CAB used has a glass transition temperature of 141 °C and a melting point ranging from 195 to 205 °C, as reported by the supplier. NaCl solutions were prepared by dissolving salt purchased from Sigma-Aldrich (France) in deionized water.

2.3 Methods

Manufacturing of the iridescent solid film

After being diluted to 5.0 wt %, the CNC suspension was submitted to a dispersion energy of 1 kJ/g using a 200-Watt sonication probe (Sonifier® S-250A, Branson, USA), to obtain a homogeneous dispersion. Films were obtained by simple evaporation of the suspension. Approximately 200 ml of the suspension was gently poured into a rectangular glass container (40x30 cm²) and evaporated at room conditions (23°C, 50% RH) over 24 h. An iridescent film based only on CNCs with an average thickness of approximately 75 µm (basis weight of approximately 100 g/m²) was obtained.

Iridescent-pigment preparation

Approximately 10 g of the iridescent film was previously cut into small pieces (0.5*0.5 cm²) with a knife mill (GM300, Retsch, Germany) and then dry-crushed using an ultracentrifugal mill (ZM 200, Retsch, Germany). To separate the finest and coarsest elements, the ground materials were successively screened between two sieves of 60 and 270 mesh.

Nanoparticle characterization

Individual nanoparticles were imaged using atomic force microscopy, AFM, (Nanoscope III®, Veeco, Canada). All samples were previously diluted at 10⁻⁴ wt %, and a drop of 0.2 ml was deposited onto freshly cleaved mica substrates and dried overnight under room conditions. Each sample was characterized in tapping mode with a silicon cantilever

(OTESPA®, Bruker, USA) at four different locations with a scanning area of 3x3 μm². Both topographical and phase images were captured, and the AFM images were subjected to first-order polynomial flattening to reduce the effects of bowing and tilt. Only the most representative images were presented in this study; however, the morphological dimensions were calculated as an average of at least 50 individual nanoparticles.

Dynamic light scattering (DLS) was used to measure the size of the nanoparticles (Vasco® I, Corduan Technologies, France). All of the samples were previously diluted in DI water at 10⁻² wt %. A cumulative method was used, and two parameters were taken into account: the hydrodynamic diameter (*z**) and the polydispersity index (PDI). For each sample, ten acquisitions were performed, and each measurement was replicated three times.

The X-ray diffraction (XRD) patterns were obtained with an X-ray diffractometer (PANalytical®, X'Pert PRO MPD). The operating conditions for the refractometer were Cu Kα radiation (1.54 Å), a 2θ Bragg angle range between 5 and 60°, a step size of 0.067° and a counting time of 90 s. The cellulose crystallinity index (CI) was evaluated using an empirical method developed by Segal et al. (1959). For each XRD pattern, the experiments were duplicated and then averaged.

The electrophoretic mobility of the CNCs was measured using a zeta potential analyzer (Zeta 2000, Malvern, UK). The CNC suspensions were diluted to approximately 0.05 wt % in deionized water in the presence of a NaCl solution to maintain a constant ionic strength (500 μS/cm). The reported zeta potential corresponded to the average value of ten measurements

The sulfur (%S) content was determined by inductively coupled plasma atomic emission spectroscopy (iCAP 6300 ICP Spectrometer, Thermo Scientific, USA). The analysis was performed at the “Institut des Sciences Analytiques” (CNRS, France). Each elemental analysis (EA) was duplicated and averaged. The surface-charge density was estimated from the sulfur content and assuming the geometrical dimensions obtained from AFM:

$$\sigma(e/nm^2) = \frac{M_{SO_3} * \%S * Na}{S_{A:V}/d_{cell}}$$

where M_{SO_3} corresponds to half of the sulfate ester molecular weight, %S is the sulfur content, Na is Avogadro's constant, $S_{A:V}$ refers to the surface-to-volume ratio and d_{cell} corresponds to the density of the cellulose crystals.

Iridescent film and pigment characterization

Field-emission scanning electron microscopy was used to observe the film nanostructure (cross section and surface) of the iridescent films and pigments (Ultra 55©, Zeiss, Germany).

The samples were glued onto a specialized holder and coated with a 2-nm layer of gold/palladium to ensure the conductivity of all samples. The accelerating voltage (EHT) was 3 kV for a working distance of 6.4 mm.

The thermal degradation of the investigated samples was monitored by thermogravimetric analysis (TGA, using the thermogravimetric analyzer STA 6000®, Perkin Elmer Instruments, England). The weight-loss and heat-flow curves were recorded for a 30 mg subsample at a heating rate of 10°C/min in the temperature range of 30-950°C under oxidizing atmosphere (air). The analyses were duplicate and averaged.

The thicknesses were determined from the FE-SEM micrographs of the film cross-sections. For each film, six measurements were performed at four different locations, and the basis weight was evaluated using the ISO-536:1995 standard. The film density was estimated by dividing the basis weight by the film thickness.

The structurally colored films were analyzed using UV-Visible spectroscopy (UV 1800, Shimadzu, Japan). The absorption intensity of the solid film was recorded in the wavelength range from 200 to 1100 nm with normal incidence. For each sample, three different measurements and ten scans were recorded and averaged.

Pictures of the iridescent pigment in the powder state or incorporated into transparent films were taken with an optical stereo microscope (Stereo Discovery V20, Zeiss, Germany) equipped with a digital camera (AxioCamICc5, Zeiss, Germany)

Functionalization of extruded films with iridescent pigments based on CNCs

For the extruded films, iridescent pigments were mixed with 15 g of CAB in a pigment-to-CAB ratio of 10 mg/g. The films were extruded using a lab extruder (HAAKE™ MiniLab II Micro Compounder, Thermo Fisher Scientific, USA) during 15 min at 100 rpm, and the extrusion temperature was set to 185°C. Extruded films, based on CAB and the iridescent pigments, with an average thickness of approximately 70 µm and a width of 5 cm were obtained.

2.4 Results and Discussion

2.4.1 Cellulose nanocrystals characterization

The physical and chemical properties of cellulose nanocrystal (CNC) suspension are summarized in **Table 4.4**.

Table 4.4 - Physical and chemical properties of CNCs used in the study.

	Properties	Value
Morphology	Length ^a (nm)	174 (83)
	Thickness ^a (nm)	8 (3)
	Aspect ratio	22 (13)
	Crystallinity Index ^b (%)	88 (2)
Chemical	Sulfur content ^c ($\mu\text{mol/g}$ CNC)	244 (16)
	Zeta potential ^d (mV)	- 41 (2.5)
Physicochemical	Surface charge density ^e (e/nm^2)	0.36 (0.02)

Values measured from AFM^a, XRD^b, EA^c, conductivity adjusted to 500 $\mu\text{S}/\text{cm}$ by the addition of NaCl solution^d, and calculation based on both AFM and EA^e. Value in brackets refers to the standard deviation.

The observation between cross polarizers of the prepared CNC suspension (**Fig 4.13-A**) shows a well-pronounced optical fingerprint texture that is considered to be one of the properties of a lyotropic liquid crystal (Gray 1994).

As shown by AFM analysis (**Fig 4.13-B**), the rod-like CNCs are elongated with average dimensions of 8 nm thick by 174 nm long. The zeta potential can be used as a measure of the electrostatic repulsive forces, which can provide an indication of the potential stability of the suspension and, indirectly, its self-organization capacity.

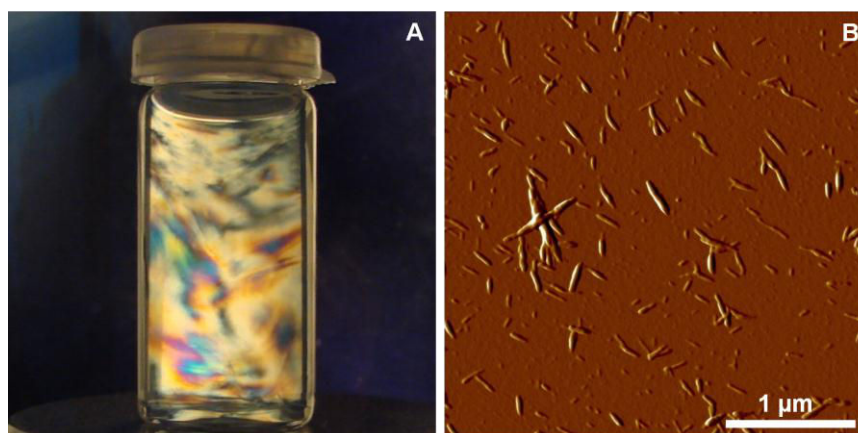


Fig 4.13 - Observation of a 5 wt % CNC suspension between cross-polarizers (A) and AFM image showing individualized CNC nanoparticles (B)

The zeta potential of CNCs dispersed in deionized water is highly negative (-41 mV) due to the high surface-charge density of the sulfate half-ester groups.

The estimated negative surface-charge density (0.36 e/nm^2) is in accordance with previously reported values for nanoparticles extracted under similar hydrolysis conditions (wood pulp, sulfuric acid). (Beck et al. 2013)

2.4.2 Formation of the nanostructured iridescent film

As explained in the introduction, our approach is to engineer iridescent pigments from a nanostructured films based on CNCs. The next section addresses film manufacturing by the simple evaporation of a CNC suspension previously diluted at 5.0% and submitted to a dispersion-sonication treatment, as described in the experimental section.

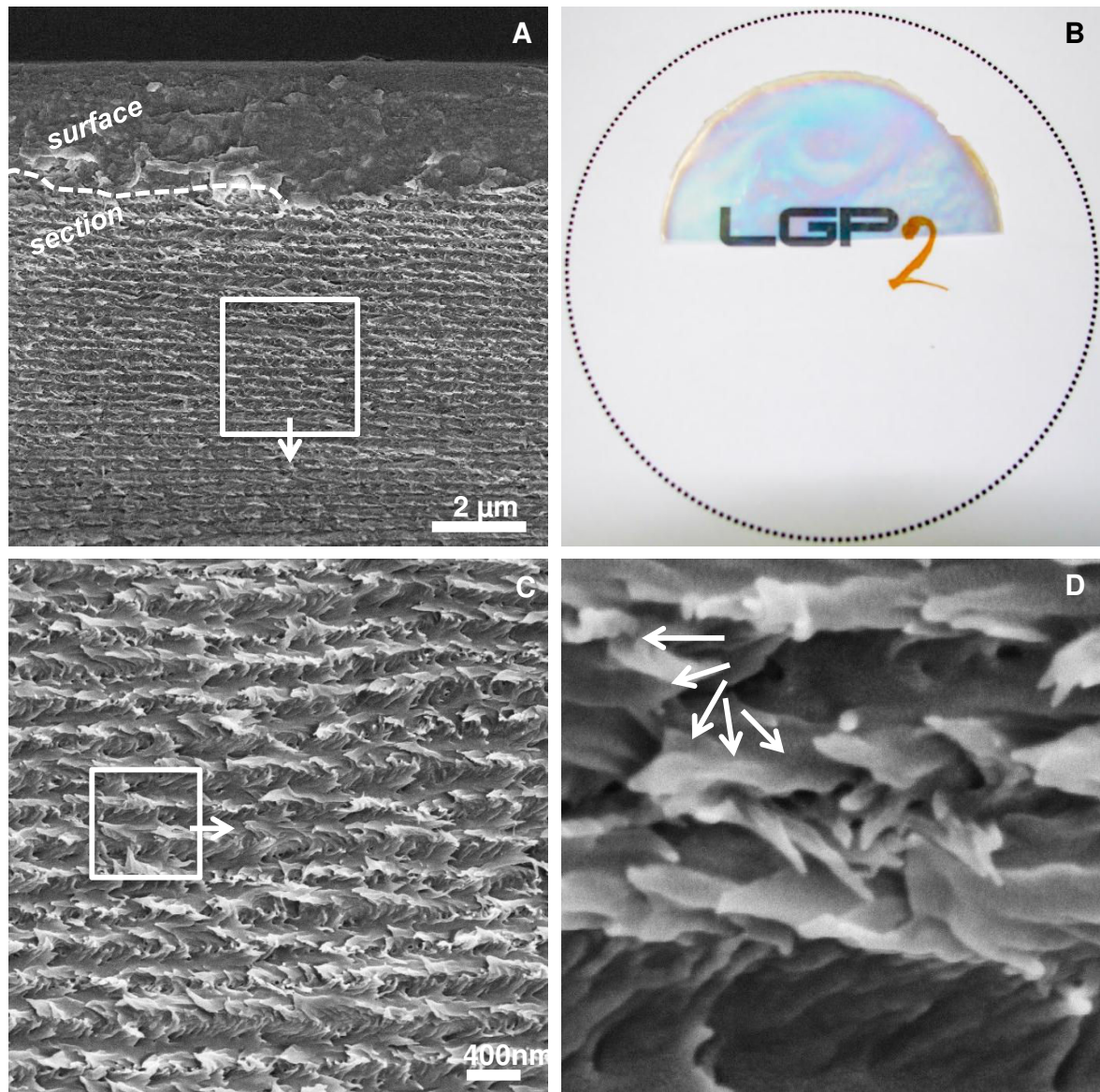


Fig 4.14 - Iridescent film (B) and the corresponding film cross-sections observed by FE-SEM at various magnifications (A, C, and D)

The CNC film exhibits an intense blue coloration (**Fig 4.14-B**) with a maximal absorption λ_{\max} at 540 nm (Table 2). When modifying the illumination angle (or observation), the surface coloration changes, which characterizes an iridescent surface (Doucet et al. 2009). The formation of a multilayer, self-organized film is shown in **Fig 4.14-A, C, and D**. This highlights that the film is composed of several layers of stacked and oriented CNCs. Horizontal alignment and lateral orientation of the nanoparticles can be observed, as shown by the orientations of the white arrows (**Fig 4.14-D**).

The FE-SEM observations of the cross-section of the film are consistent with the results of recent studies (Majoinen et al. 2012) (Dumanli et al. 2014). It is noteworthy that the colored aspect is caused by the nanostructure. Structural coloration is distinct from coloration generated by a solid pigment, such as chromophore molecules (dyes) and/or a metal surface that generally absorbs or emits light in the visible region.

2.4.3 Dry fine grinding of the CNC films: selection of the grinding technology

As reported in **Table 4.5** iridescent films are highly brittle. This is because of the high intrinsic stiffness of the CNCs (Xiong et al. 2014).

Table 4.5 - Optical and mechanical properties of an iridescent film based on CNCs.

	Properties	Value
Contexture	Thickness (μm)	72 (1)
	Grammage (g/m^2)	96 (3)
	Density	1.33 (0.04)
Optical	Visual aspect	Iridescent with blue coloration
	λ_{\max}^a (nm)	570 (13)
Mechanical	Strain at break (%)	0.7 (0.1)
	Stress at break (MPa)	35 (7)
	Specific Young's modulus (GPa)	5.8 (1)

^aMaximal absorption wavelength at normal incidence. Value in brackets refers to the standard deviation.

Therefore, the processing from film to pigment is easily achieved using fine grinding equipment (see the experimental section). The grinding technology is chosen, and parameters are optimized with two main objectives. First, the coloration caused by the nanostructured organization within the powdered film should be preserved. Second, a pigment with an average thickness of 20-50 μm should be engineered because this average dimension is suitable for the targeted end-use applications (extruded film or nanopaper)

Granulometry analysis (not presented) highlights that the pigments have a heterogeneous size distribution varying from approximately ten to several hundred micrometers.

Consequently, the pigments were screened using a vibrating sifting system specially designed with two sieves of 50 and 250 μm . Thus, three-particle size fractions are obtained, namely, residues (A), iridescent pigment (B) and coarse pigment (C), as presented in **Fig 4.15**.

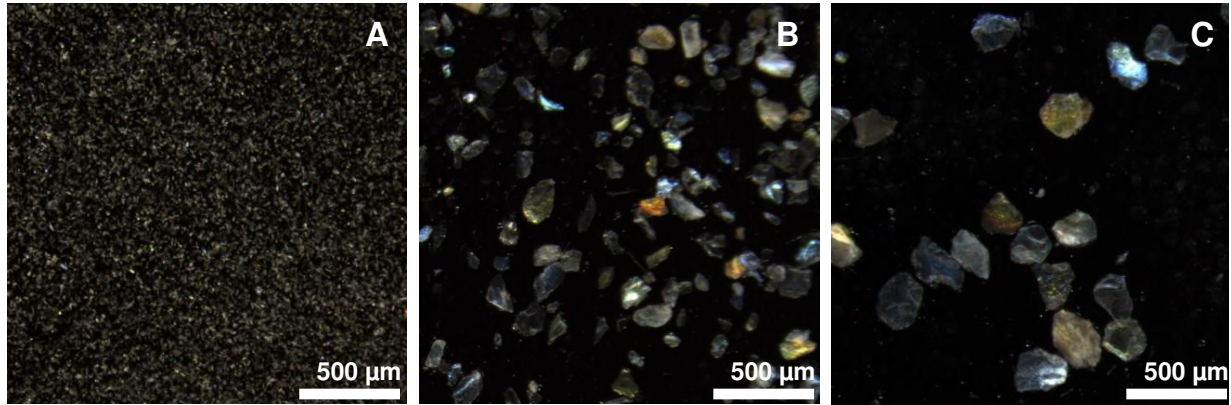


Fig 4.15 - Optical analysis of the powdered film divided into three classes: residues (A), iridescent pigment (B), and coarse pigment (C)

It was observed that approximately 90% (by weight) of the ground pigment had the desired size and a flake-like morphology that is suitable for end-use applications (**Table 4.6**).

Table 4.6 - Main features of a pigment based on a CNC iridescent film

Properties		Value		
Types of pigments		Residue (A)	Iridescent pigment (B)	Coarse pigment (C)
Screening parameters	Sieves	<50 μm	50<...<250	>250 μm
	Fraction ratio (wt %)	6 (3)	89 (5)	4 (3)
Morphology ^a	Shape	Needle	Fine flake	Coarse flake
	Surface (mm^2)	0.002 (10^{-4})	0.20 (0.07)	0.5 (0.2)
	Circularity	0.4 (0.2)	0.8 (0.1)	0.8 (0.1)
	Thickness	43 (20)	25 (5)	7 (5)
Iridescence and Coloration detection ^b		No	Ok	Ok

Parameters determined from FE-SEM micrographs^a and evaluated from optical stereomicroscope images^b. Value in brackets refers to the standard deviation.

The remaining 10% of pigments (including residues or coarse pigment) can be reused for various purposes.

When residues are suspended in water, submitted to strong dispersion energy, and filtered through Whatman® paper, an iridescent film based on the CNC suspension is obtained again.

The coarse pigment can be submitted to a secondary grinding to obtain the required particle sizes. A negligible matter loss occurs after recycling the residues and regrinding the coarse pigment.

It has been reported that mechanical treatment by fine grinding of clay minerals can produce important changes in powdered materials. This phenomenon occurs during a prolonged grinding time because of the high thermomechanical exposure.(Hrachová et al. 2007).

FE-SEM analysis was performed to confirm that the nanostructure is retained during pigment comminution (**Fig 4.16**). A similar organization within the iridescent pigment is observed (**Fig 4.16-C**) as that in the iridescent films (**Fig 4.14-C**).

This appears to confirm that the nanostructure is preserved during the grinding process and explains the coloration of the pigment.

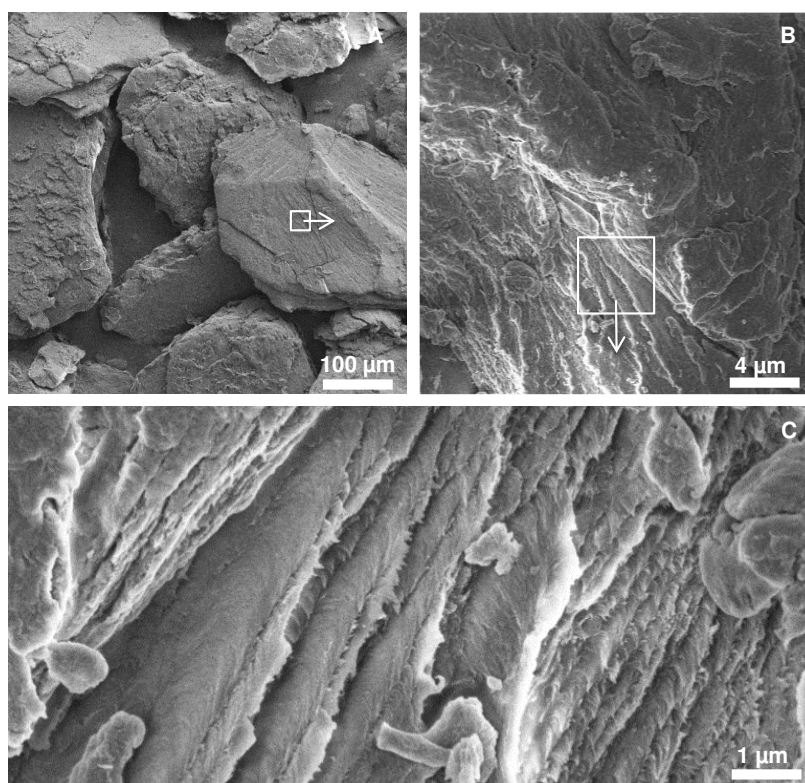


Fig 4.16 - FE-SEM pictures of the iridescent pigments from their bulk morphology within their nanostructure

To check these results in further detail, the crystallinity of the CNC-based materials at various physical states was investigated by XRD analysis, as presented in **Fig 4.17**.

All of the XRD patterns of the samples are characteristic of native cellulose (semicrystalline cellulose I β). The major crystalline peak (002) occurs at 22.8°, and the associated crystallinity index (CI) is approximately 88% for all of the analyzed samples.

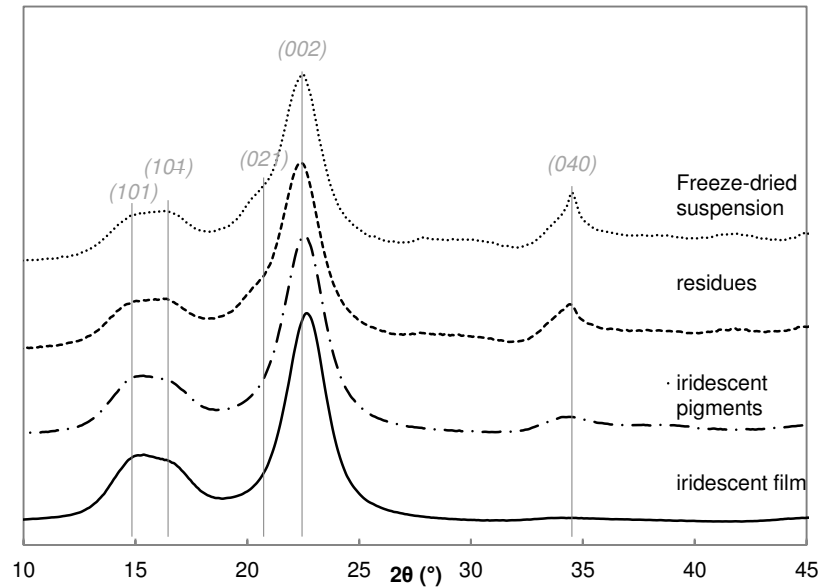


Fig 4.17 - XRD patterns of the various CNC forms. Comparison between a solid film, coarse pigment, residues, and freeze-dried suspension.

However, when comparing a film and pigments with a freeze-dried suspension and residues, several differences exist. More intense peaks are identified at 20.5° and 33.3° for the freeze-dried sample and residues.

The appearance of this characteristic (021) and (040) lattice peak clearly indicates a difference between the stacked CNCs and the more randomly oriented nanoparticles in the residues and freeze-dried sample. This cannot be related to the differences within the nanocrystals, but it can only be caused by the self-organization of nanoparticles during free evaporation of the CNC suspension.

As a key result, the iridescent pigments based on CNC films obtained by centrifugal milling have a platelet shape and an average thickness of $25\ \mu\text{m}$. In addition, they exhibit a strong iridescence because the structural coloration is preserved in the film powdering during dry fine grinding.

2.4.4 Compatibilization techniques of iridescent pigments with existing processes for film manufacturing

Even if iridescent pigments have a platelet shape, an average thickness of $25\ \mu\text{m}$ and strong iridescence, they cannot be used “as is” in extrusion or water processes. Without any modification of the pigment, they completely blacken when heated over 185°C (**Fig 4.18-A**) or are redispersed in aqueous medium (**Fig 4.18-B**).

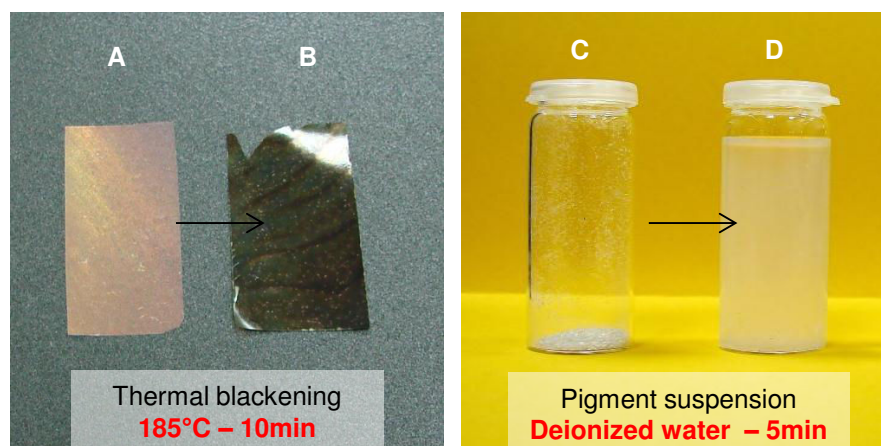


Fig 4.18 - Two limitations of end-use applications of neat iridescent pigments: thermal degradation (A), and water redispersion (B)

It is assumed that, to limit their thermal degradation, iridescent materials should be sulfur-free. It is also assumed that, to prevent the redispersion of pigments in water, CNCs should remain agglomerated for a prolonged time. However, no chemical modification can be achieved before the film formation because the structural coloration of this material is based on the self-organization of the CNCs.(Dong et al. 1998)

Our approach is therefore to modify the material after the film formation and fine grinding.

2.4.5 Improving the thermal resistance of the CNC-based pigment

During the extrusion of common thermoplastic biobased polymers such as polylactic acid (PLA) or cellulose acetate butyrate (CAB), the melting temperature is approximately 170-200°C over 5-20 min.(Oksman et al. 2006, Dufresne 2008)

Even if iridescent pigments have high-temperature degradation (255°C), pigment blackening occurs after extrusion with CAB (see experimental section), which leads to a loss of iridescent coloration (**Fig 4.21-A**). This happens before the onset of thermal degradation of CNC is reached (**Fig 4.21-C**). It is well known that the presence of sulfate groups degrades the thermal stability of CNC.(Wang et al. 2007)

To remove sulfate ester groups, four methods are proposed in the literature, including mild acid hydrolysis,(Pomin et al. 2005) alkaline treatment,(Wang et al. 2007) solvolysis (Jiang et al. 2010), and glycerolysis (Dorris et al. 2012).

In this work, these techniques present several limitations because desulfation reactions occur in aqueous or organic media and use additional chemicals. Therefore, the CNC self-organization in the suspension and the film iridescence are no longer guaranteed.

Recently, Beck and Bouchard have proposed auto-catalyzed acidic desulfation in the dry state of CNC films (Beck et al. 2014). They have succeeded in removing two-thirds of the sulfur content in only 5 min by heating at 105°C in an oven.

Based on this study, the sulfate ester groups were removed from the iridescent pigments with vacuum overdrying (Fig 4.21). In the study, this treatment was performed over 1 h, under a more moderate heating temperature (75°C) and vacuum (40 mBar).

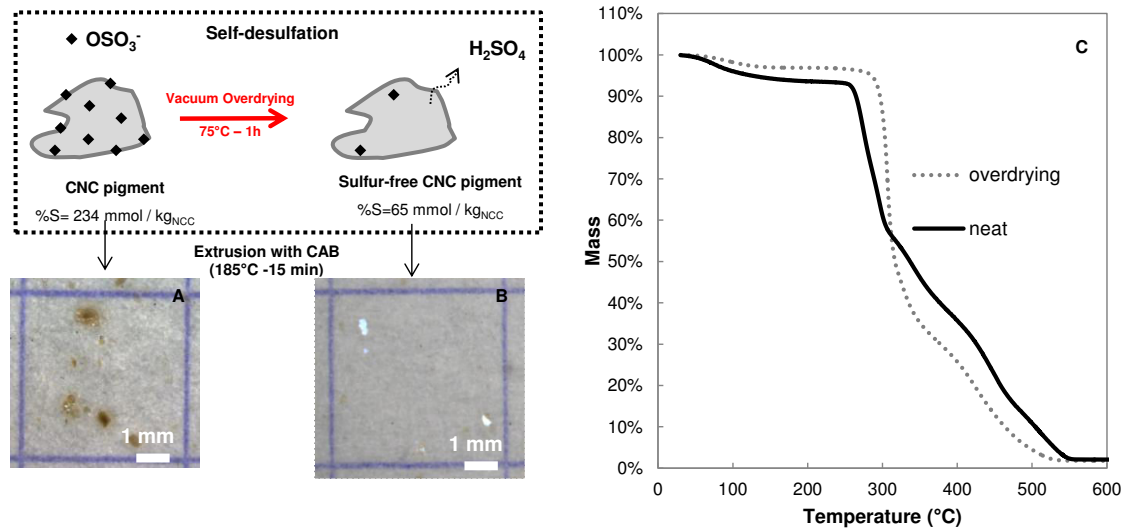


Fig 4.19 - Pictures corresponding to the iridescent pigments incorporated into CAB-extruded films and observed by optical microscopy. Comparison between the neat CNC pigment (A) and a sulfur-free CNC pigment (B). TG curves (C) for the neat CNC pigment (continuous line) and sulfur-free CNC pigment (dotted line) at a heating rate of 10°C/min in oxidizing atmosphere in the temperature range of 30-600°C.

The desulfation reaction was confirmed by EA with approximately 75% of the sulfur groups removed in only 1 h under vacuum overdrying (75°C). It was also supported by the onset of the degradation temperature measured by the TGA shifting from 255° to 280°, which appears to indicate a low sulfur content (Fig 4.21-C).

After resuspension (mechanical shearing and sonication) of over-dried pigments in water, the zeta potential of the desulfated CNCs decreases to -25 mV, whereas a value of -41 mV was measured for the neat CNC suspension. All of these analyses tend to confirm desulfation of the iridescent pigment. The continuous vacuum may also lead to the partial dehydration of free water molecules.

The mechanism of self-desulfation observed here tends to contradict the statement made by Dong et al. (1997), in which, for CNC dried in a vacuum oven at 35°C for 24 h, they observed negligible desulfation. The analyses presented here confirm that self-desulfation can occur in the dry state. The main difference from the result of the previous study is the

presence of a continuous vacuum and a higher heating temperature that appear to improve the desulfation reaction because of the removal of gaseous H_2SO_4 . After melting and processing with CAB, the coloration of the iridescence is preserved in the extruded, flexible film (**Fig 4.21-B**) with the vacuum-overdrying treatment.

2.4.6 Improving the water resistance of the CNC-based pigment

Instead of using pigments in extrusion, a papermaking technique, i.e., a water based-process, can be used. However, the introduction of pigments into water remains challenging. When they are introduced into deionized water, they quickly redisperse and form a cloudy colloidal suspension. This results in the nearly complete destruction of the visible iridescent particles after less than 1 h (**Fig 4.20-D**).

In an aqueous medium, negatively charged CNCs are thermodynamically favorable, which results in a stable colloidal suspension. Thus, the instability of iridescent pigments (considered to be aggregated CNCs) causing their resuspension can be explained because the repulsive forces induced by negatively charged groups are higher than the attractive interactions caused by hydrogen bonds. (Verwey 1947)

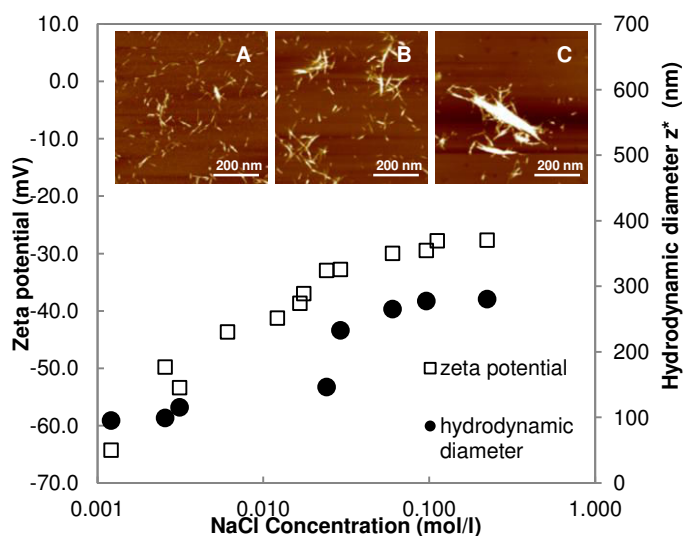


Fig 4.20 - Zeta potential (\square) and average hydrodynamic diameter of CNC (\bullet), as a function of the NaCl concentration. AFM pictures correspond to CNCs in deionized water (A), in a 25 mM NaCl solution (B), and in a 250 mM solution (C).

In the recent literature, the high dispersivity of nanoparticles is generally targeted, as it is expected for providing dried nanocellulose at the industrial scale (Beck et al. 2012) (Missoum et al. 2012). Protonation of the sulfate ester groups of CNCs (strong acidic groups) can be achieved by decreasing the pH of the suspension under strongly acidic conditions (pH=1). This approach (protonation) has not been tested because it may degrade the pigment, and a

strong acidic condition is not compatible with the papermaking process. In contrast, few studies have tried to limit this redispersion. A reduction in the surface charge can be achieved by protonating or reducing the surface charge of the nanoparticles.

Starting with the approach that the agglomeration phenomena in a suspension of charged nanoparticles are related to the pH, ionic strength or electrolyte ion valence, a monovalent salt was added to “screen” the charged groups of the CNCs. An increase in the NaCl concentration (i.e., the ionic strength) results in an increase in the hydrodynamic dynamic diameter (z^*) and a decrease in the zeta potential (**Fig 4.21**). This indicates that agglomeration occurs between individual nanoparticles (also confirmed by AFM images), which confirms the screening of negative charges in the presence of NaCl.

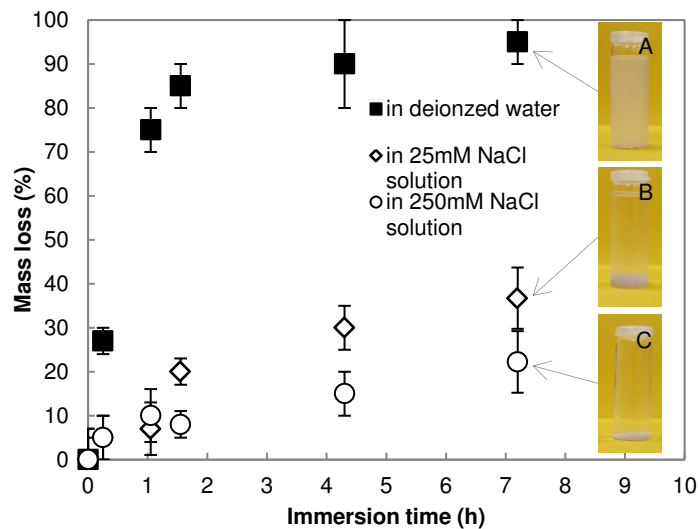


Fig 4.21 - Evolution of the mass loss of the iridescent pigment with immersion time in deionized water (■), a 25 mM NaCl solution (◊) and a 250 mM NaCl solution (○). The iridescent pigment concentration for the three suspensions is 25 g/l, and the mass losses were estimated from the dried mass of the iridescent pigments collected after a screening on a 270-mesh sieve. Images A, B and C correspond to 1 g of iridescent pigment after 7h in suspension, in deionized water (A), in a 25 mM NaCl solution (B), and in a 250 mM NaCl solution (C).

Based on these findings, the evolution of the mass loss of the iridescent pigment with immersion time was estimated in deionized water, a 25 mM NaCl solution, and a 250 mM solution, as presented in **Fig 4.21**. The presence of NaCl (25 or 250 mM) in the suspension results in a low matter loss of the iridescent pigment. This can be explained because the CNC remains agglomerated within the iridescent pigment because of the screening of the negative charges. The mass loss is low, even after a very long immersion time. Thus, after 7 h in suspension, more than $63\pm 7\%$ and $78\pm 10\%$ of the iridescent pigment remains for the 25 mM (**Fig 4.21-B**) and 250 mM NaCl (**Fig 4.21-C**) solutions, respectively. For the same immersion

time in deionized water (**Fig 4.21-A**), only 5 wt % of iridescent pigment remains. For an immersion time of 1 h, the mass loss of iridescent pigment in a saline solution can be considered negligible (between 7 to 10 wt %). This corresponds to the conditions generally required for the preparation of a water-based surface coating or for the papermaking process.

The increase in the ionic strength in the aqueous medium by NaCl addition is particularly successful. This leads to a slight matter loss while preserving the optical properties of the iridescent pigment.

2.4.7 Upscaling the manufacturing of iridescent pigments³

The simple and innovative approach for manufacturing iridescent pigments has been detailed in last sections. However, at lab scale, the amount of iridescent pigment produced is only about 10 g maximum. Such quantity cannot be suitable for performing an industrial trial. That is why several technical investigations were carried out for up-scaling iridescent pigment production. The main unit operations as well as the equipment used are detailed in **Table 4.7**. The recap presented here (**Table 4.7**) describes only the most efficient technique based on multiple previous attempts (not presented here).

Considering the formation of iridescent films, the main challenges was to :

- redisperse air-dried CNC in suspension without agglomerate
- determine the best CNC concentration, the volume of suspension to evaporate
- find the appropriate substrate (Teflon®, glass, aluminum)
- determine the correct specific energy to apply for dispersing CNC in water suspension
- adjust the concentration of NaCl solution
- find the good temperature and drying parameters during the water evaporation

For instance, using Teflon large plates or a drying over 70°C disturb the self-assembly of CNC and form a transparent film. In addition, the key steps for producing a large amount of pigments remain the grinding and the screening of pigments. Several grinder manufacturers have been contacted and in collaboration with Retsch has allowed producing pigment powder.

Considering the grinding of pigments, the main challenges was to :

- determine the optimum granulometry of iridescent pigment to be used within papers
- find a grinding technology suitable for this material (machine configuration)
- preserve the film microstructure during grinding (time, grinding power)

³ The next sections have been added from the initial scientific paper. It provides more detail about : the process for producing iridescent pigments at pilot-scale for paper machine trials. The approaches being considered to add iridescent pigment within specialty papers production with a paper machine from Papeteries du Léman

Actually, more than 1 kg of iridescent pigments have been successfully produced for the purpose of industrial trials. Based on these results, it assumed a pigment production could be easily done in less than 1 week.

Table 4.7 - Recap of the different unit operations for the production of 1kg of iridescent pigment

	Goal	Unit operations	Equipment	Parameters
Suspension 	To suspend air-dried NCC in deionized water and limit presence of agglomerate	High mechanical shearing homogenization	Ultra-turrax® T25 <i>IKA, France</i>	10 min 12,500 rpm
	To disperse NCC suspension at a specific dispersive energy	Sonication dispersion	Sonifier® 250, <i>Emerson, USA</i>	3 cycles 10minutes under continuous stirring 1.3kJ/g
Film formation 	To form iridescent film by free evaporation	Casting	Aluminum pan, <i>Fischer Scientific, UK</i>	23°C – 50%HR, 24 h- 48 h
Dry grinding 	To obtain iridescent pigment with a precise size and shape	Precutting - Knife milling	GM 300®, <i>Retsch, Germany</i>	10s, 2 000 rpm
		Fine grinding – Centrifugal milling	ZM 200®, <i>Retsch, Germany</i>	18000 rpm, One pass
Screening 	To fractionate and separate coarse particles, iridescent pigments and fines residues	Screening – sieve shaking	AS 200®, <i>Retsch, Germany</i>	10min – 50 Hz Sieves : -35 mesh (500µm) -60 mesh (250µm) -270 mesh (50µm)

2.4.8 Addition of iridescent pigments in paper at industrial scale

Detection of iridescent pigment in lab sheet paper

Afterwards, iridescent pigment can incorporated either in the base of paper or in the paper coating (using carbohydrate coating). Such mentioned approaches were done first with a 30g/m² lab sheet paper by using starch coating color. Because of the relative fine dimension of iridescent pigment, their detection without microscopy tool is not so evident. With the use of POM, the presence of iridescent pigments can be easily confirmed as presented in **Fig 4.22**.

Thus, intense colored pigments are detected both in the base paper (A) and in the surface layer (B).

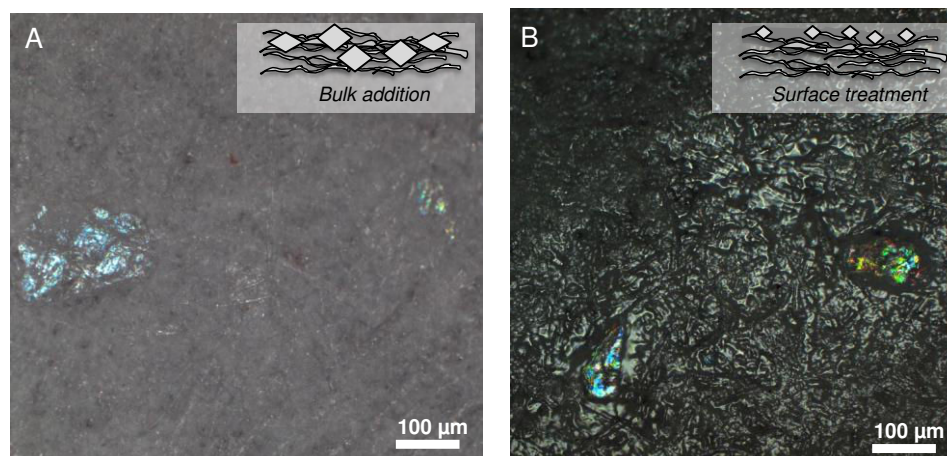


Fig 4.22 - Optical Microscopy micrographs of the surface of a 30g/m² lab hand sheets in which iridescent pigment are introduced in the base paper (A) or coated (B)

Additional analysis can be carried out in order to analyze the chemical composition of the iridescent pigment, which will be used as a security features.

To do so, the grey level contrast in SEM micrographs (in BSE mode) can be used because heavy elements (high atomic number) more strongly scatter electron than light elements (low atomic number). **Fig 4.23** highlights the different grey level between the surface of an uncoated base paper (A) and after coating with a mixture of starch and iridescent pigments (B and C).

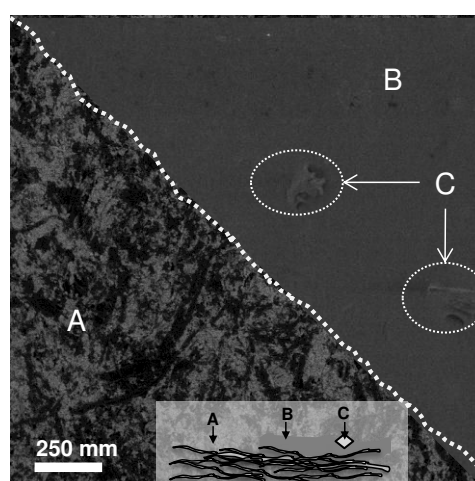


Fig 4.23 - E-SEM images in BSE mode corresponding to an uncoated base paper (A) and a 5g/m² coated paper with a mixture of (B) starch and iridescent pigments (C)

In **Fig 4.23-B and C** corresponding to the coated surface, no mineral filler can be identified anymore, however two particles (iridescent pigments) are observed. The grey level seems to confirm the chemical compositions of iridescent particles close to the starch polymer

coating. However, such SEM analysis gives no more indication on the precise chemical composition of the iridescent pigments. That is why EDS analyses were carried out on the base paper (a), on the starch-coated surface (b) and on one iridescent particle (C) as presented in Fig 4.24.

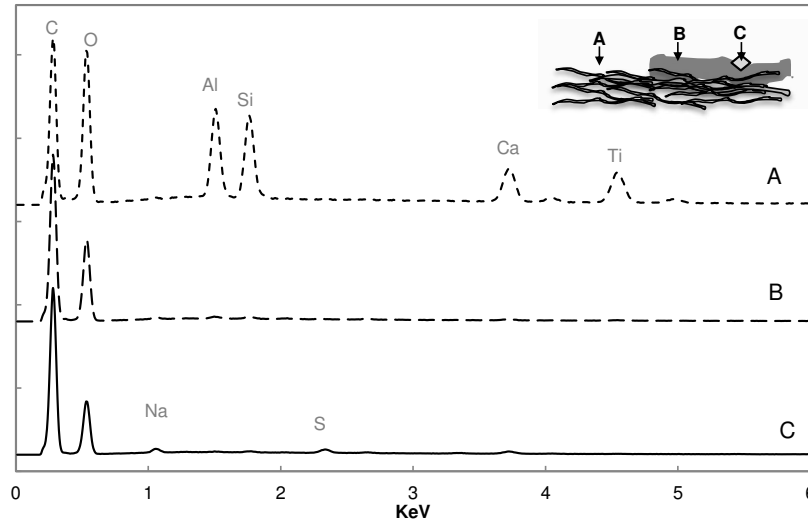


Fig 4.24 - EDS spectra corresponding to (A) uncoated base paper (B) starch coated surface and iridescent pigment (C)

Regarding the base paper, Carbon and Oxygen elements are detected which is assigned to Cellulosic fibers. In addition, four mineral elements are detected: Aluminum, Silica, Calcium, and Titanium. These peaks are assigned to the mineral elements used as white fillers in the base paper that are Kaolin Clay ($\text{Al}_2\text{Si}_2\text{O}_5(\text{OH})_4$), Calcium Carbonate (CaCO_3), and Titanium Dioxide (TiO_2).

This contrasts with the surface coated layer (Fig 4.24-B) in which only organic component appears. EDS spectrum carried out on one iridescent pigment (**Fig 4.24-C**) indicates its chemical composition is mainly organic with some traces amount of sodium and sulfur. The presence of sulfur is expected because of the presence of sulfate ester groups. Sodium may originate from NaCl which is used in the drying process of nanocellulose to make NCC non redispersible. (Beck et al. 2012) For iridescent pigments, a sulfur content of 0.82 wt % and a sodium content 0.60 wt were measured by Elemental analysis

To conclude, the detection of iridescent particles can be easily operated by POM analysis for iridescent particles incorporated in the base paper as well as for surface coating. SEM in BSE mode and EDS analyses highlight the chemical nature of iridescent pigment based on CNC is almost the same than carbohydrates (starch or cellulose). Therefore, this proves that CNC iridescent pigments are difficult to counterfeit because of their complex manufacturing as well as their unusual chemical composition as a security feature.

Iridescent pigments in paper: ratio optimizing

In first trial, the pigment were roughly added in the paper and so not cost-effective. Initially, the pigment-to-paper ratio was fixed to 10 milligram of iridescent pigments per gram of paper (for a 30 g/m² paper). In such a way, the number of iridescent pigments was too high for a discrete paper marking. In addition, the overcost (due to the incorporation of iridescent pigments) multiplied by six the cost of the base paper.

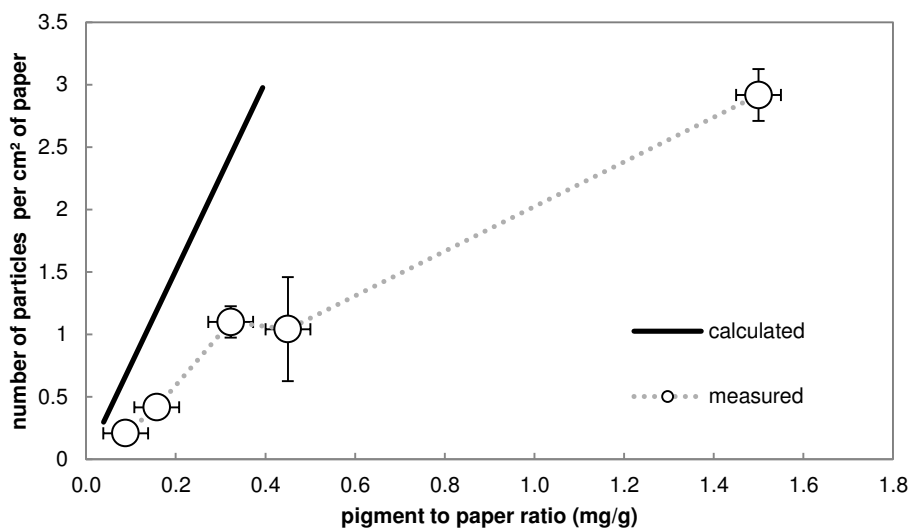


Fig 4.25 - Number of iridescent pigment per square centimeter of paper as a function of iridescent pigment to paper ratio Comparison between calibration curve estimated from calculation based on their average dimension (bold line) and counted pigments with POM in a 30 g/m² handsheets made with increasing amount of iridescent particles (dotted line)

In order to ascertain the number of iridescent pigment per the surface of paper as a function of pigment to paper ratio, calibration curve was done, as presented in **Fig 4.25**. This graph gives the number of particles per square centimeter as a function of the amount of iridescent pigment. A slight difference can be found between calculated calibration curves from average dimension of iridescent particles and experimental curves estimated from particles counting using POM. Lastly, for a discrete marking of a 30 g/m² paper with iridescent pigment, i.e. one pigment per square centimeter, the optimum ratio is ranging between 0.32 to 0.42 mg of iridescent per gram of paper. The optimization of the amount of iridescent pigment has reduced the overcost of using iridescent pigments within specialty papers to less than 10 % the initial cost. This is a key result that proves the economic feasibility of such anti-counterfeiting strategies.

Industrial trials

It became possible to use iridescent pigments within the papermaking conditions. Indeed the main challenges for using iridescent are now overcome:

- the technique for limiting the re-suspension of iridescent pigments in water processes which consists of dispersing iridescent pigments in saline solution (0.250 mM)
- the capacity to produce enough quantity of iridescent pigment (1 kg)
- the determination of the amount of iridescent pigment to add in paper (0.5 mg/g)

The next section briefly described how to do it at the industrial level.

As proposed, addition of iridescent particles could be done either in bulk paper formation or in a surface treatment. Trials were performed on a specialty paper machine from Papeteries du Lemans during the production of a 30 g/m² paper, at a speed of 550 m/min. Up to now, two industrial trials (about 30 minutes per trials in June 2014 and July 2014) have been performed following two different strategies and at different place at the machine as shown in figure below (Fig 4.26).

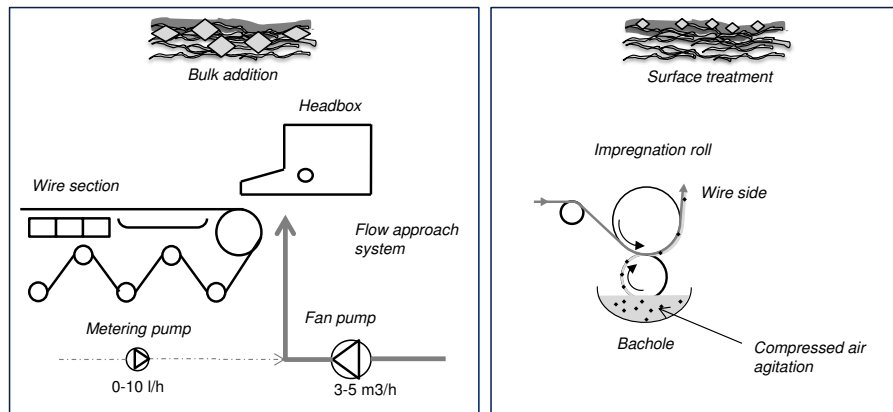


Fig 4.26 - General scheme of the configuration of the paper machine during industrial trials

During trials, no problem regarding the paper manufacturing was revealed and no paper break was noted. This is key point because it means that the introduction following these approaches does not affect the papermaking process. To avoid pigments sedimentation, a compressed air agitation has been specially installed during the second trials.

For the coating strategy, pigment non redispersion has been checked. The main challenges for these two trials are the pigment presence onto final materials, which is too low to be visible.

Other trials should be performed by changing some parameter to limit the degradation of pigments.

2.5 Conclusion and perspectives

The main goal of this study was to engineer iridescent pigments from films based on cellulose nanocrystal (CNC). An efficient method is proposed using fine grinding and various post-treatments depending on the end-use applications. The CNC-based pigments thus obtained have a platelet shape and an average thickness of 25 μm . They exhibit strong iridescence because the structural coloration is preserved during the film powdering. However, because of the presence of sulfate groups, thermal degradation and high redispersion in water occur, which irreversibly affect the unique optical properties of these biobased pigments. This represents the major issue for using these pigments in extrusion or in water-based processes (papermaking or surface coating). To overcome such limitations, two different post-treatments were proposed to remove sulfur or to screen negative charges with NaCl addition. These easy and simple post-treatments have proven to be efficient because sulfur-free pigments (75% of the sulfur groups are removed) can be obtained and the redispersion in water is strongly reduced even after a very long immersion time (15 days). These results are promising because they open up the prospect of new functional materials using these engineered CNC pigments within industrial processes. Such pigments can be used for a number of applications, such as food, pharmaceutical and cosmetic packaging in which anti-counterfeiting functions could be targeted. Afterwards, the engineered iridescent pigments are manufactured at pilot scale in order to supply enough quantity for the.

In the last section of the *Chapter 4.2*, a description of the manufacturing and use of iridescent pigment during the papermaking process is also provided. Consequently, such pigments appear to be easily applied but difficult to imitate.

Their main advantages can be highlighted:

- relatively low-cost
- biobased, biocompatible
- difficult to duplicate
- easily identifiable visually without the need of special equipment
- hard to re-label or reuse
- easily noticeable when tampered with

Therefore, it can be considered that iridescent pigments based on CNCs can be a sustainable and cost-efficient alternative to security features commonly used in specialty paper.

Concluding remarks

The results obtained from a model surface layer based on nanocellulose (*Chapter 2 and Chapter 3*) have been implemented at the industrial scale within the papermaking process.

From the results obtained in *Chapter 2*, a cost-effective solution for saving opacifying pigment is presented in *Chapter 4.1*. The CNF based coating appears to be a sustainable and cost-effective approach for limiting TiO₂ in opaque lightweight-coated paper.

This study started from a lab experiment and was completed by pilot scale trials. The same opacity was measured from a reference paper containing 9 wt % of TiO₂ while only 3 wt % of TiO₂ was required when TiO₂ was coated with CNF. This key result was one of several considerations that justified a patent application and the pilot scale trials.

Based on such lab results, the cost-efficiency of the approach was determined to estimate an acceptable CNF cost for further industrial uses. It gives an average value between 0.70 €/kg to 2.5 €/kg depending of the TiO₂ ratio in the paper. Such preliminary results emphasize that the solution proposed is only cost-efficient in the case of an in-situ production of CNF.

The last section was dedicated to upscaling lab experiments into pilot trial. Several process parameters were checked and optimized such as the coating preparation, pumping, and drying.

Finally, the results of the trials are extremely positive because the CNF-TiO₂ coating had favorable process runnability and end-use properties. As a conclusion, the feasibility and efficiency of CNF-TiO₂ coating was clearly demonstrated and further industrial trials are expected.

Chapter 4.2 describes how to engineer iridescent pigments from films based on cellulose nanocrystal (CNC). An efficient method is proposed using fine grinding and various post-treatments depending on the end-use applications. The CNC-based pigments thus obtained have a platelet shape and an average thickness of 25 μm. They exhibit strong iridescence because the structural coloration is preserved during the film powdering.

However, because of the presence of sulfate groups, thermal degradation and high re-dispersion in water occurs, which irreversibly affect the unique optical properties of these biobased pigments. This represents the major issue for using these pigments in extrusion or in water-based processes (papermaking or surface coating).

To overcome such limitations, two different post-treatments were proposed, with success, to remove sulfur or to screen negative charges with NaCl addition.

Such promising pigments have been patented can be used for a number of applications, such as food, pharmaceutical and cosmetic packaging in which anti-counterfeiting functions could be targeted. Industrial trials are in progress at the end of the PhD for specialty papers.

Chapter 4, which is the applied part of this industrial PhD, can be considered as being very successful. Promising approaches have been proposed and patented, some challenges have been overcome, and pilot-scale or even industrial trials have been performed. So, depending on availability of nanocellulose, industrial application of nanocellulose within specialty papers can be envisaged thanks to this PhD project, which is one of the first “stones of the wall” in this field.

List of Tables

Table 4.1 - Technical comparison between the two surface coating systems	214
Table 4.2 - Recap of the ISO standards used to characterized the properties of paper samples	215
Table 4.3 - Printing parameters of the offset lithography test	215
Table 4.4 - Physical and chemical properties of CNCs used in the study.	234
Table 4.5 - Optical and mechanical properties of an iridescent film based on CNCs.	236
Table 4.6 - Main features of a pigment based on a CNC iridescent film	237
Table 4.7 - Recap of the different unit operations for the production of 1kg of iridescent pigment	245

List of figures

Fig 4.1 - Cost-effective approach for limiting TiO ₂ in paper formulation	212
Fig 4.2 - SEM images (in BSE mode) of 30 g/m ² paper cross-sections which consists of fibers (94%), CNFs (3%) and TiO ₂ (3%). Addition of CNFs and TiO ₂ during the labsheet formation (A) or as surface treatment (B).	217
Fig 4.3 - Opacity as a function of TiO ₂ ratio in a paper. Comparison between CNF (●) and Starch/SB latex (□) based coating formulations.	219
Fig 4.4 - FE-SEM pictures of paper surface coated with Starch-Latex TiO ₂	220
Fig 4.5 - Comparison of the opacity between CNF-TiO ₂ coated paper (●) and reference coated paper(□) for different TiO ₂ ratio	221
Fig 4.6 - Threshold price for CNF giving the equivalent costs for 34g/m ² lightweight paper	222
Fig 4.7 - Overview of the pilot coating machine	223
Fig 4.8 - Viscosity as a function of the shear rate for a 27 wt % conventional coating and a 6 wt % CNF-TiO ₂ coating. Pictures of the coating process: coating preparation(A), pumping system(B), flow circulation(C), and surface coating(D). Boxes correspond to the characteristic shear-rate ranges occurring during the paper coating.....	224
Fig 4.9 - FE-SEM pictures of the 30 g/m ² uncoated base paper (A), coated with 1.4 g/m ² of CNF-TiO ₂ (B), and 2.5 g/m ² of conventional formulation(C).....	226
Fig 4.10 - Opacity as a function of coating weight for a 30 g/m ² industrial base paper coated with a CNF-TiO ₂ (●) or conventional (□) formulations.....	226
Fig 4.11 - Print-through as a function of amount of black ink printed on the industrial base paper (◇), coated with 3.5 g/m ² of conventional formulation (□) and 1.5 g/m ² of CNF-TiO ₂ (●)	227
Fig 4.12 - The proposed approach for engineering pigments from iridescent films based on CNCs	230
Fig 4.13 - Observation of a 5 wt % CNC suspension between cross-polarizers (A) and AFM image showing individualize CNC nanoparticles (B)	234

- Fig 4.14** - Iridescent film (B) and the corresponding film cross-sections observed by FE-SEM at various magnifications (A, C, and D) 235
- Fig 4.15** - Optical analysis of the powdered film divided into three classes: residues (A), iridescent pigment (B), and coarse pigment(C) 237
- Fig 4.16** - FE-SEM pictures of the iridescent pigments from their bulk morphology within their nanostructure 238
- Fig 4.17** - XRD patterns of the various CNC forms. Comparison between a solid film, coarse pigment, residues, and freeze-dried suspension. 239
- Fig 4.18** - Two limitations of end-use applications of neat iridescent pigments: thermal degradation (A), and water redispersion (B) 240
- Fig 4.19** - Pictures corresponding to the iridescent pigments incorporated into CAB-extruded films and observed by optical microscopy. Comparison between the neat CNC pigment (A) and a sulfur-free CNC pigment (B). TG curves (C) for the neat CNC pigment (continuous line) and sulfur-free CNC pigment (dotted line) at a heating rate of 10°C/min in oxidizing atmosphere in the temperature range of 30-600°C. 241
- Fig 4.20** - Zeta potential (\square) and average hydrodynamic diameter of CNC (\bullet), as a function of the NaCl concentration. AFM pictures correspond to CNCs in deionized water (A), in a 25 mM NaCl solution (B), and in a 250 mM solution (C). 242
- Fig 4.21** - Evolution of the mass loss of the iridescent pigment with immersion time in deionized water (\square), a 25 mM NaCl solution (\blacklozenge) and a 250 mM NaCl solution (\bullet). The iridescent pigment concentration for the three suspensions is 25 g/l, and the mass losses were estimated from the dried mass of the iridescent pigments collected after a screening on a 270-mesh sieve. Images A, B and C correspond to 1 g of iridescent pigment after 7h in suspension, in deionized water (A), in a 25 mM NaCl solution (B), and in a 250 mM NaCl solution (C). 243
- Fig 4.22** - Optical Microscopy micrographs of the surface of a 30g/m² lab hand sheets in which iridescent pigment are introduced in the base paper (A) or coated (B) 246
- Fig 4.23** - E-SEM images in BSE mode corresponding to an uncoated base paper (A) and a 5g/m² coated paper with a mixture of (B) starch and iridescent pigments (C) 246
- Fig 4.24** - EDS spectra corresponding to (A) uncoated base paper (B) starch coated surface and iridescent pigment (C) 247
- Fig 4.25** - Number of iridescent pigment per square centimeter of paper as a function of iridescent pigment to paper ratio Comparison between calibration curve estimated from calculation based on their average dimension (bold line) and counted pigments with POM in a 30 g/m² handsheets made with increasing amount of iridescent particles (dotted line) 248
- Fig 4.26** - General scheme of the configuration of the paper machine during industrial trials 249

References

1. Adkins, "Spacer/extender for titanium dioxide in pigment systems for coatings", Aluminum Company Of America, CA2083397A1 (1992).
2. Bardet, Belgacem, *et al.*, "Different strategies for obtaining high opacity films of MFC with TiO₂ pigments", Cellulose: 1-13 (2013).
3. Bardet and Bras, "Cellulose Nanofibers and Their Use in Paper Industry", Handbook of Green Materials: 207-232, edited by World Scientific (2014).
4. Barke and Luebke, "Seed having high opacity coatings", Cargill, CA1159667A1 (1984).
5. Beck and Bouchard, "Auto-catalyzed acidic desulfation of cellulose nanocrystals", Nordic Pulp and Paper Research Journal 29(01): 006-014 (2014).
6. Beck, Bouchard, *et al.*, "Dispersibility in Water of Dried Nanocrystalline Cellulose", Biomacromolecules 13(5): 1486-1494 (2012).
7. Beck, Bouchard, *et al.*, "Controlled production of patterns in iridescent solid films of cellulose nanocrystals", Cellulose 20(3): 1401-1411 (2013).
8. Bras, Belgacem, *et al.*, "Opacifying layer for a paper medium", Institut Polytechnique de Grenoble, Fr.; Papeteries du Leman . WO2014033409A1 (2014).
9. Bras, Belgacem, *et al.*, "Couche d'opacification d'un support papier", INSTITUT POLYTECHNIQUE DE GRENOBLE, WO201258093 (2012).
10. Braun, "Titanium dioxide: A review", JCT, Journal of coatings technology 69(868): 59-72 (1997).
11. Braun, Baidins, *et al.*, "TiO₂ pigment technology: a review", Progress in Organic Coatings 20(2): 105-138 (1992).
12. Dong and Gray, "Effect of Counterions on Ordered Phase Formation in Suspensions of Charged Rodlike Cellulose Crystallites", Langmuir 13(8): 2404-2409 (1997).
13. Dong, Revol, *et al.*, "Effect of microcrystallite preparation conditions on the formation of colloid crystals of cellulose", Cellulose 5(1): 19-32 (1998).
14. Dorris and Gray, "Gelation of cellulose nanocrystal suspensions in glycerol", Cellulose 19(3): 687-694 (2012).
15. Doucet and Meadows, "Iridescence: a functional perspective", Journal of The Royal Society Interface 6(Suppl 2): S115-S132 (2009).
16. Dufresne, "Polysaccharide nano crystal reinforced nanocomposites", Canadian Journal of Chemistry- Revue Canadienne De Chimie 86(6): 484-494 (2008).
17. Dumanli, Van Der Kooij, *et al.*, "Digital color in cellulose nanocrystal films", ACS Applied Materials & Interfaces (2014).
18. El-Sherbiny, Morsy, *et al.*, "Synthesis, characterization and application of TiO₂ nanopowders as special paper coating pigment", Applied Nanoscience 4(3): 305-313 (2014).
19. Fredrik Wernersson Brodin, Gregersen, *et al.*, "Cellulose nanofibrils: Challenges and possibilities as a paper additive or coating material – A review", Nordic Pulp and Paper Research Journal 29(01): 156-166 (2014).

20. Gesenhues, "The mechanism of polyelectrolyte-assisted retention of TiO₂ filler particles during paper formation", Advances in Colloid and Interface Science 162(1–2): 1-21 (2011).
21. Gray, "Chiral nematic ordering of polysaccharides", Carbohydrate Polymers 25(4): 277-284 (1994).
22. Hamann, "Wet-End Applications of NFC", presented at SUNPAP Workshop, Espoo, Finland (2011).
23. Heux, Chauve, *et al.*, "Nonflocculating and chiral-nematic self-ordering of cellulose microcrystals suspensions in nonpolar solvents", Langmuir 16(21): 8210-8212 (2000).
24. Hirani, Dighe, *et al.*, "Effective cost saving in high Performance coating by replacing titanium dioxide with calcium aluminum silicate & magnesium aluminum silicate", Paintindia 56(10): 75-90 (2006).
25. Hrachová, Komadel, *et al.*, "The effect of mechanical treatment on the structure of montmorillonite", Materials Letters 61(16): 3361-3365 (2007).
26. Jaycock and Pearson, "A study of the retention of pigment during paper formation", Journal of Colloid and Interface Science 55(1): 181-190 (1976).
27. Jiang, Esker, *et al.*, "Acid-catalyzed and solvolytic desulfation of H₂SO₄-hydrolyzed cellulose nanocrystals", Langmuir 26(23): 17919-17925 (2010).
28. Laufmann and Hubschmid, "Mineral Fillers in Papermaking", Handbook of Paper and Board: Volume 1&2: 109-143 (2006).
29. Lehto, "Characterization of mechanical and chemical pulp fibers", Appita Annu. Conf. Exhib. 58th: 349-356 (2004).
30. Majoinen, Kontturi, *et al.*, "SEM imaging of chiral nematic films cast from cellulose nanocrystal suspensions", Cellulose 19(5): 1599-1605 (2012).
31. Miller, "Nanocellulose: Technology Applications, and Markets", presented at TAPPI International Conference on Nanotechnology, Vancouver, Canada (2014).
32. Missoum, Bras, *et al.*, "Water Redispersible Dried Nanofibrillated Cellulose by Adding Sodium Chloride", Biomacromolecules 13(12): 4118-4125 (2012).
33. Nelson and Deng, "Enhanced light scattering from hollow polycrystalline TiO₂ particles in a cellulose matrix", Langmuir 24(3): 975-982 (2008).
34. Oksman, Mathew, *et al.*, "Manufacturing process of cellulose whiskers/polylactic acid nanocomposites", Composites Science and Technology 66(15): 2776-2784 (2006).
35. Pianta, "Contribution à l'amélioration de l'opacité et de la transvision des papiers minces destinés à l'impression écrite", PhD Thesis, Institut National Polytechnique de Grenoble (1998).
36. Pomin, Valente, *et al.*, "Mild acid hydrolysis of sulfated fucans: a selective 2-desulfation reaction and an alternative approach for preparing tailored sulfated oligosaccharides", Glycobiology 15(12): 1376-1385 (2005).
37. Revol, Godbout, *et al.*, "Solidified liquid crystals of cellulose with optically variable properties", Pulp and Paper Research Institute of Canada, WO9521901A1 (1995).
38. Revol, Godbout, *et al.*, "Solid self-assembled films of cellulose with chiral nematic order and optically variable properties", Journal of Pulp and Paper Science 24(5): 146-149 (1998).
39. Segal, Creely, *et al.*, "An empirical method for estimating the degree of crystallinity of native cellulose using the x-ray diffractometer", Text. Res. J. 29: 786-794 (1959).

40. Song, Ankerfors, *et al.*, "*Reduction of the linting and dusting propensity of newspaper using starch and microfibrillated cellulose*", Nord. Pulp Pap. Res. J. 25: 495-504 (2010).
41. Torvinen, Helin, *et al.*, "*Nano fibrillated cellulose as a strength additive in filler-rich SC paper*", presented at 2011 TAPPI International Conference on Nanotechnology for Renewable Materials, Arlington, USA (2011).
42. Verwey, "*Theory of the Stability of Lyophobic Colloids*", The Journal of Physical and Colloid Chemistry 51(3): 631-636 (1947).
43. Wang, Ding, *et al.*, "*Thermal degradation behaviors of spherical cellulose nanocrystals with sulfate groups*", Polymer 48(12): 3486-3493 (2007).
44. Xiong, Han, *et al.*, "*Flexible, highly transparent and iridescent all-cellulose hybrid nanopaper with enhanced mechanical strength and writable surface*", Carbohydrate Polymers 113(0): 264-271 (2014).

General Conclusion

The main objective of this work was dedicated to the contribution of nanocellulose for improving or modifying the properties of specialty papers as shown in **Figure 1**.

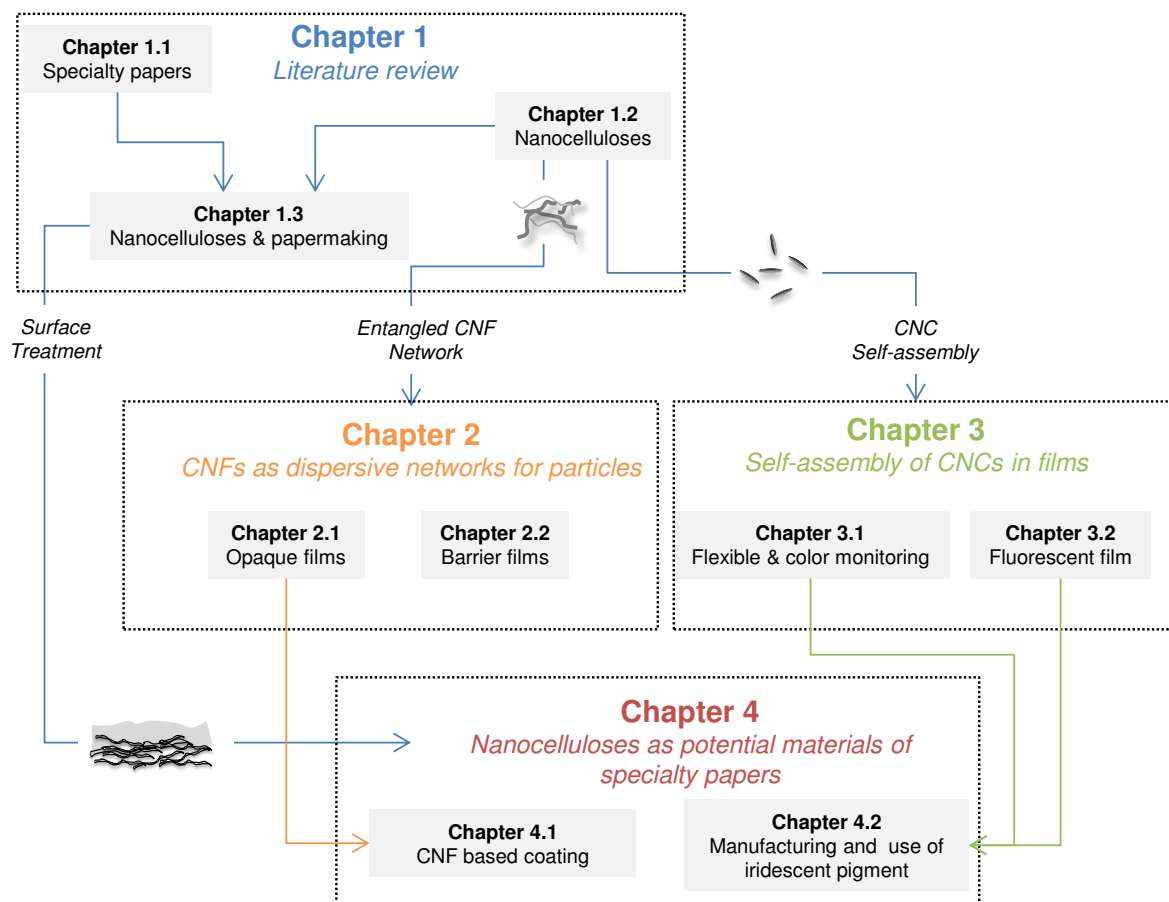


Figure 1- Schematic view of the manuscript organization

The different chapters highlight that nanocellulose is a sustainable and cost-effective alternative. In particular, nanocellulose can be used for improving end-use properties, i.e. printability and opacity, and for imparting functional properties, i.e. anticounterfeiting.

Nanocellulose from 2011 to 2014. **Table 1** summarizes the main evolution in the field of nanocellulose during this PhD project. Over the last three years, the number of publications has tripled and the number of patents has multiplied by a factor of ten. Substantial progress has been made in the field of the standardization and characterization, as well as in the evaluation of the nanotoxicology and risk assessments.

Before this project, nanocomposites and films were predominately explored; research and innovation are now more focused on smart and biomedical applications.

During the last two years, nanocellulose has been marketed. Therefore, during this PhD, we had the opportunity to work with different commercial nanocellulose, thereby facilitating the implementation at industrial scale.

Table 1- Main evolutions in the general field of nanocellulose and important developments in the scientific themes over the three years of the PhD project

Themes	Before the project (October 2011)	End of the project (October 2011)
Nanocellulose overview	<ul style="list-style-type: none"> nanoparticles characterization production optimization main applications in nanocomposites <p>1315 articles 239 patents</p>	<ul style="list-style-type: none"> chemical modification main application in smart and biomedical materials <p>3201 articles 436 patents</p>
Industrialization	<ul style="list-style-type: none"> only at lab scale /few in situ pilot plant no commercialization 	<ul style="list-style-type: none"> 4 joint ventures/ 5 start-ups commercialization almost available
Toxicology	<ul style="list-style-type: none"> limited data available <p>3 papers</p>	<ul style="list-style-type: none"> currently under investigation in principle non-toxic <p>31 papers</p>
Standardization	<ul style="list-style-type: none"> no standardization, no characterization many different terms used 	<ul style="list-style-type: none"> recommendations from TAPPI about nomenclature and appropriate techniques and methodologies
Chapter 2 CNFs as dispersive network	<p><i>Opaque films</i></p> <ul style="list-style-type: none"> 3 patents for manufacturing hybrid CNF suspension <p><i>Barrier films</i></p> <ul style="list-style-type: none"> transparency of CNF film is targeted good barrier properties of CNF films (air, grease, oxygen) <p>41 papers 13 patents</p>	<p><i>Opaque films</i></p> <ul style="list-style-type: none"> several patents dedicated to the manufacturing of hybrid CNF suspension <p><i>Barrier films</i></p> <ul style="list-style-type: none"> incorporation of Nanoclay and use of hydrophilic CNF investigation of barrier properties at high moisture content development of conductive film <p>142 papers 20 patents</p>
Chapter 3 Self-assembly of CNCs in films	<ul style="list-style-type: none"> self-assembly of CNCs in water and organic solvent method for manufacturing iridescent films use of NaCl for tuning coloration <p>5 papers 3 patents</p>	<ul style="list-style-type: none"> several parameters for tuning coloration mesoporous organosilica films detailed SEM/AFM imaging of iridescent film <p>25 papers 4 patents</p>
Chapter 4 Nanocelluloses as potential material of specialty papers	<p><i>CNF based coating</i></p> <ul style="list-style-type: none"> only at lab scale CNF as surface coating for improving barrier, printing and mechanical properties <p>24 articles 10 patents</p> <p>Iridescent pigments</p> <ul style="list-style-type: none"> only vaguely mentioned as perspectives in some patents or conference. 	<p><i>CNF based coating</i></p> <ul style="list-style-type: none"> several pilot trials reported multiple coating techniques/multilayer in a mixture with polymer or as a coating additives <p>73 articles 28 patents</p> <p><i>Iridescent pigments</i></p> <ul style="list-style-type: none"> no significant progress

Considering the ever-increasing number of communications in the field of nanocellulose, the contribution of this PhD remains modest. However, regarding the different scientific themes address in the framework of the PhD, i.e. CNF as dispersive network (**Chapter 2**), the self-assembly of CNC in films (**Chapter 3**), and lastly the use of nanocellulose within the papermaking process (**Chapter 4**), even if several new contributions are also proposed, none of them have similar key results.

Key results and main contributions. As summarized in **Table 2**, this PhD project paved the way for the use of nanocellulose in specialty papers. Several inputs were proposed both regarding the scientific understanding and for the applied research.

Table 2- The key endpoints of the PhD project

Scientific themes	Key results
Chapter 2 CNFs as dispersive network	<p><i>Opaque films</i></p> <ul style="list-style-type: none"> • use of CNF as dispersive network • 3 processes for manufacturing hybrid CNF-TiO₂ suspension <ul style="list-style-type: none"> -blend -during CNF fibrillation -by sol-gel process <p>➤ High opacity from 5 wt% TiO₂</p>
	<p><i>Barrier films</i></p> <ul style="list-style-type: none"> • substitution of nanoclay with CNCs • positive impact of thermal treatment on barrier properties at high moisture content <p>➤ all-nanocellulose films with high barrier properties at high moisture content</p> <p style="text-align: right;">2 scientific papers</p>
Chapter 3 Self-assembly of CNCs in films	<p><i>Iridescent films</i></p> <ul style="list-style-type: none"> • sorption of molecule and water soluble polymers onto CNCs <ul style="list-style-type: none"> - High absorption for PEG (0.6 mmol /g_{CNC}) - moderate for I'OBA (18 μmol /g_{NCC}) - none for PAAS • PEG (10 wt%) used plasticizer improve <ul style="list-style-type: none"> -flexibility (x2) -thermal stability (+35 °C) • PAAS used for the coloration monitoring (0-160 μmol/g_{NCC}) • use of OBA imparts fluorescent property under UV-illumination <p>➤ 3 levels of optical encryption (iridescent, polarized and fluorescent)</p> <p style="text-align: right;">2 scientific papers</p>
	<p><i>CNF based coating</i></p> <ul style="list-style-type: none"> • CNF-TiO₂ coating provide a 2.5x reduction of the amount of TiO₂ for the same paper opacity • successfully carried out at pilot scale • average acceptable CNF costs : 0.7-2.5 €/kg <p>➤ sustainable and cost-effective approach for limiting TiO₂</p>
Chapter 4 Nanocelluloses as potential material of specialty papers	<p><i>Manufacturing and use of iridescent pigments</i></p> <ul style="list-style-type: none"> • Innovative method for manufacturing 1 kg of iridescent pigment • Two simple post-treatments to overcome technical limitations <ul style="list-style-type: none"> -Use of NaCl solution (>25 mM) in water-based processes -Self-desulfation of pigment (vacuum overdrying, 60 °C, 2 hours) <p>➤ Two tested possibilities for incorporating iridescent pigment in papermaking process</p> <p style="text-align: right;">2 patents -2 pilots trials -1 scientific paper</p>

In **Chapter 2**, CNFs were used with success as dispersive network for particles to (i) replace existing polymer in thin opaque films or (ii) as a substitute for mineral nanoparticles in barrier materials. One target of **Chapter 2.1** was to obtain an opaque solid film using TiO₂ particles dispersed in a CNF network. This study proposes different solutions for obtaining

highly opaque hybrid CNF films and opens up prospects for a new generation of opaque films for light barrier packaging or printed electronics. The aim of **Chapter 2.2** was to design a transparent and barrier film only based on nanocellulose with the same properties as films reinforced with nanoclay (i.e sodium Montmorillonite, MMT). A key result was the oxygen permeability is about the same to CNF reinforced with MMT. This work paves the way for future studies or applications of all-cellulose barrier films or surface coatings. Results obtained for the CNF model films demonstrate the potential of CNF for coating applications.

The self-assembly properties of CNCs to display iridescent films in a dry state were investigated in **Chapter 3**. While iridescent films based on CNCs are widely reported in the literature, it addresses various enhancements in (i) improving the film flexibility,(ii) controlling the coloration, and (iii) incorporating fluorescent properties. The main inputs of the **Chapter 3.1** were the addition of 10 wt % PEG makes films much more flexible, and the addition of PAAS can be used for tuning the coloration within CNC films. In **Chapter 3.2**, the combination of CNCs with the optical brightening agent, distyrylbiphenyl sulphonate, imparts fluorescence to the iridescent film as an additional property. The prepared films appear colored in natural light because of the preservation of the self-organization of CNCs and fluorescent under UV-illumination. Such results create possibilities for the design of bio-based materials dedicated to decorative, security, and anti-counterfeit flexible films.

In **Chapter 4**, the results obtained for model surface layer based on nanocellulose (**Chapter 2** and **Chapter 3**) were carried out at the industrial scale within the papermaking process. From the results obtained in **Chapter 2**, a cost-effective solution for saving opacifying pigment was presented in **Chapter 4.1**. The cost-efficiency of the approach was determined to estimate an acceptable CNF cost for further industrial uses. Such preliminary results emphasize that the solution proposed here is cost-efficient in the case of an in-situ production of CNF. Upscaling lab experiments to a pilot trial is however proposed. Finally, the results of the trials are positive because the coating of CNF-TiO₂ is a promising material in regards to the process runnability and end-use properties. In conclusion, the feasibility and efficiency of CNF-TiO₂ coating was demonstrated. **Chapter 4.2** describes how to engineer iridescent pigments from films based on cellulose nanocrystal (CNC). An efficient method was proposed using fine grinding and various post-treatments depending on the end-use applications. Two different post-treatments were proposed to remove sulfur, or to screen negative charges with NaCl addition. Such pigments can be used for a number of applications,

such as food, pharmaceutical, and cosmetic packaging, in which anti-counterfeiting functions could be targeted. In the last section of the **Chapter 4.2**, a description of the manufacturing and use of iridescent pigment during the papermaking process is also provided.

Open questions and perspectives. Through these findings, several perspectives can be developed as described in **Table 3**.

Table 3- Ideas and propositions as further work and perspectives

Scientific themes	Further work and perspectives
Chapter 2 CNFs as dispersive network	<i>Opaque films</i> <ul style="list-style-type: none"> Investigate other mineral fillers for manufacturing hybrid CNF suspensions Use of TiO₂ nanoparticles for their photocatalytic and anti-microbial properties Confirm the impact of abrasive particles during the CNF isolation (energy consumption)
	<i>Barrier films</i> <ul style="list-style-type: none"> Identify the main difference between a model film and surface coating (interaction with substrate) Implement CNF film manufacturing on papermaking process Replace neat CNF by acetylated or carboxymethylated CNF
Chapter 3 Self-assembly of CNCs in films	<ul style="list-style-type: none"> Substitute plasticizer with another matrix polymer matrix (PLA, CAB,) Investigate mechanical and barrier properties of self-assembly CNC film vs non-organized CNC film Development of an advanced characterization tool for evaluating iridescent properties
Chapter 4 Nanocellulose as potential material of specialty papers	<i>CNF based coating</i> <ul style="list-style-type: none"> Confirm pilot scale results during industrial papermaking and printing Surface coating with modified CNF or with chemical additives (AKD, PAE) in a view of imparting paper hydrophobicity and wet resistance Test another surface treatment techniques such as spray coating or curtain coating Rheological studies on CNF suspension (neat or hybrid) throughout the coating preparation
	<i>Manufacturing and use of iridescent pigment</i> <ul style="list-style-type: none"> Additional industrial papermaking trials Combine iridescent pigments with CNF based coating Investigate alternative use of iridescent pigments

In conclusion, this PhD project provides interesting results regarding the use of nanocellulose in specialty papers. Two main sustainable approaches were proposed such as CNF based coating or iridescent pigment. These approaches have been validated at lab scale but also which is unusual, at pilot scale. Five scientific papers and two patent applications were achieved proving the quality of results and envisaged approaches at the starting of the project. It is hoped that this will provide a sustainable and profitable growth for the industrial partnership.

**Extended abstract in
French**

Sommaire

1	Positionnement du projet.....	271
2	Organisation du projet.....	276
3	Principaux résultats	278
3.1	Les MFCs comme réseaux d'enchevêtrement.....	278
3.1.1	Films opaques	278
3.1.2	Films barrières	281
3.1.3	Conclusions et perspectives	283
3.2	L'auto-assemblage des NCCs	284
3.2.1	Influence des polymères solubles sur l'auto-assemblage des NCCs	287
3.2.1	Influence d'un agent fluorescent sur l'auto-assemblage des NCCs.....	287
3.2.2	Conclusions et perspectives.....	288
3.3	Contribution des nanocelluloses pour l'amélioration et la fonctionnalisation des papiers spéciaux	289
3.3.1	Réduction de la consommation de TiO ₂ dans la formulation des papiers minces avec un traitement de surface à base MFC	289
3.3.2	Production, caractérisation et utilisation de pigments iridescents	293
4	Conclusions et perspectives.	297
	Listes des tableaux.....	299
	Listes des figures.....	299
	Références	301

Extended abstract in French

1 Positionnement du projet

L'industrie papetière en Europe. Aujourd'hui, le papier est omniprésent dans la vie de tous les jours. Le papier contribue au développement de l'industrie, à la dissémination des connaissances ou à la distribution des biens manufacturiers. Il est par exemple utilisé dans les livres, les emballages, les papiers peints, les billets de banques. Les différents types de papiers sont généralement regroupés en quatre catégories : les papiers d'impression-écriture, les emballages, les papiers hygiéniques et les papiers spéciaux. Les deux premiers groupes représentent près de 80% pour une production totale de plus de 420 million de tonnes par an.

Avec un accroissement mondial de 2 % / an, la consommation de papier est fortement liée au niveau de vie des pays. Ainsi en France, la consommation annuelle par habitant est de 150 kg alors qu'elle est supérieure à 230 kg aux Etats-Unis contre moins de 10 kg en Inde.

Celle-ci stagne ou décroît pour les pays développés (Europe de l'Ouest, pays scandinaves, Amérique du nord et Japon) et s'accroît fortement pour les pays émergents et les BRICS (Brésil, Russie, Inde, Chine, Afrique du Sud). Bien que la production européenne de papier ait augmenté de près de 40 % lors de ces vingt dernières années, près de 900 machines à papier et 228 000 emplois directs ont été détruits. Au niveau de la France, la consommation des papiers a chuté de 1,3% entre 2000 et 2010. La croissance de la production papetière en Europe est essentiellement portée par le secteur de l'emballage et celui des papiers spéciaux.

Cette croissance dans ces secteurs permet de maintenir et de poursuivre le développement de l'industrie papetière européenne. Il permet notamment de faire face au déclin des papiers à usage graphiques ou pour les journaux qui ont vu leur demande fortement impactée avec l'émergence dans les années 2000 de l'Internet et de la dématérialisation. (Ahmadi Achachlouei 2013)

Les papiers spéciaux. Ils englobent une large diversité de produits et de domaines d'applications : les papiers thermiques, les papiers fins pour cigarette, les filtres, le fiduciaire, les emballages spéciaux et les papiers peints. Même si les papiers spéciaux ne représentent que 6 % de la production totale, ils sont un des principaux relais de croissance pour les papetiers européens. La demande globale de papiers spéciaux est estimée à 24.4 millions de

tonnes en 2013 et devrait atteindre près de 26 millions de tonnes en 2014. D'autre part la forte demande de la part des marchés émergents, la faible offre, et la complexité de leur procédé de fabrication permettent à ces papiers d'être vendus à des prix largement supérieurs aux papiers de commodités. Ils permettent aux papetiers de diversifier leurs gammes de produits, d'améliorer leurs performances financières avec des prix de vente élevés et relativement stables au cours du temps.

Les papiers spéciaux sont caractérisés par des propriétés additionnelles ou fonctionnelles qui les distinguent des autres segments. Parmi ces propriétés spécifiques, il peut être mentionné l'hydrophobicité, (Samain et al. 2013) la conduction électrique, (Hu et al. 2009) l'antimicrobien, (Rodriguez et al. 2007) la résistance aux graisses, (Vaswani et al. 2005) ou l'anti-contrefaçon (van Renesse 1997). Pour obtenir ces propriétés, des procédés et des matériaux spécifiques sont mis en œuvre. Le support ou la couche externe sont ainsi chimiquement ou physiquement modifiés en utilisant des procédés et des matériaux appropriés.

Les nanomatériaux et nanocelluloses. Parmi les solutions envisageables, les nanomatériaux¹ sont une importante voie de recherches et sont aujourd'hui largement utilisés dans l'industrie papetière. (Scott 1996) L'introduction de nanoparticules intervient à la fois dans l'amélioration du procédé de fabrication et l'amélioration des propriétés finales.

Par exemple, des nanoparticules de silices colloïdales ou de bentonites sont utilisés en partie humide pour améliorer la rétention des éléments fins, l'égouttage et la formation de feuille. (Scott 1996) D'autres nanoparticules, principalement d'origine minérale sont utilisées dans la composition des couches des papiers spéciaux :

- pour l'amélioration de l'imprimabilité (nano charges) (Juuti et al. 2009)
- l'élaboration de couches barrières (nano argiles), (Sun et al. 2007)
- le développement de propriétés antimicrobiennes (nanoparticules d'oxydes métalliques) (Liu et al. 2009).

Alors que la plupart des nanomatériaux sont issus de ressources minérales ou dérivés de la pétrochimie, les nanomatériaux extraits de la biomasse représentent une solution alternative pertinente. (Buzea et al. 2007)

¹ D'après la norme ISO/TC 229, le terme «nanomatériau» désigne une particule possédant au moins une dimension inférieure à 100 nm.

Parmi ces nanomatériaux biosourcés, le développement des nanocelluloses connaît un accroissement accéléré comme en témoigne l'augmentation exponentielle du nombre de publications ou de brevets depuis 2007 (**Figure 1**).

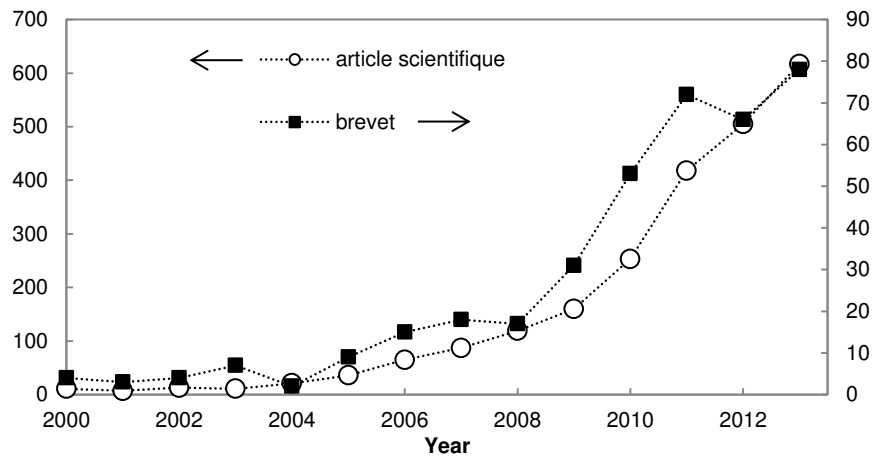


Figure 1 – Evolution du nombre annuel de brevets et d'articles scientifiques dédiés aux nanocelluloses (données extraites de Scifinder, Septembre 2014)

Le terme nanocellulose désigne les nanoparticules extraites de fibres végétales cellulosiques. Les nanocelluloses peuvent être extraites à partir de différents constituants issus de la biomasse végétale : de pâte à papier provenant de résineux ou de feuillus, de plantes annuelles, de résidus de l'agriculture voire même de certaines algues.

En comparaison avec la plupart des nanomatériaux, les nanocelluloses présentent de nombreux d'avantages :

- une surface spécifique (>100 m²/g) et un facteur de forme très élevé (>20)
- une densité équivalente à celle de la plupart des polymères organiques (1.5 g/cm³)
- une chimie de surface réactive une bonne biocompatibilité et une faible toxicité
- des propriétés spécifiques à l'état de suspension et à l'état sec.

De plus, il a été montré que les nanocelluloses pouvaient apporter un effet de renfort à de nombreux matériaux (papier, gel, et composites) et permettre l'élaboration de nouveaux matériaux (aérogel, film flexible, biomatériau).(Dufresne 2012)

Ainsi, les principaux domaines d'applications brevetées des nanocelluloses couvrent le domaine des films, des nanocomposites, de la filtration, des encres, des peintures, du biomédical et de l'industrie papetière.(Charreau et al. 2013)

Selon une récente estimation, la demande annuelle pourrait atteindre 1 à 3 millions de tonnes dans les cinq prochaines années (2015-2020).(Cowie et al. 2014)

Les nanocelluloses sont divisées en deux familles, les microfibrilles de cellulose (MFCs) et les nanocristaux de celluloses (NCCs). L'extraction de ces nanoparticules est basée sur une déstructuration à l'échelle nanométrique de fibres de cellulose. Deux principales voies permettent d'effectuer cette déstructuration à l'échelle nanométrique :

- une voie chimique (hydrolyse acide) pour les NCCs
- une voie mécanique pour les MFCs

Les MFCs sont obtenues principalement par un intense traitement mécanique.(Turbak et al. 1983) Ce traitement mécanique peut-être réalisé en utilisant différentes techniques comme l'homogénéisation à haute pression, l'ultra-raffinage ou la micro-fluidisation.(Siró et al. 2010) Pour faciliter l'isolation des MFCs, les fibres de celluloses sont généralement soumises à un prétraitement chimique (Saito et al. 2006), mécanique ou enzymatique (Henriksson et al. 2007). L'objectif du prétraitement est multiple et permet notamment de faciliter l'extraction des nanocelluloses en purifiant et homogénéisant la suspension, tout en réduisant significativement la demande énergétique requise pour isoler les nanocelluloses.

Les NCCs sont obtenus après une forte hydrolyse acide ou une réaction d'oxydation. La réaction chimique entraîne une dissolution préférentielle des zones amorphes des fibres de cellulose et libère les zones cristallines (cristallites).(Ranby 1949).

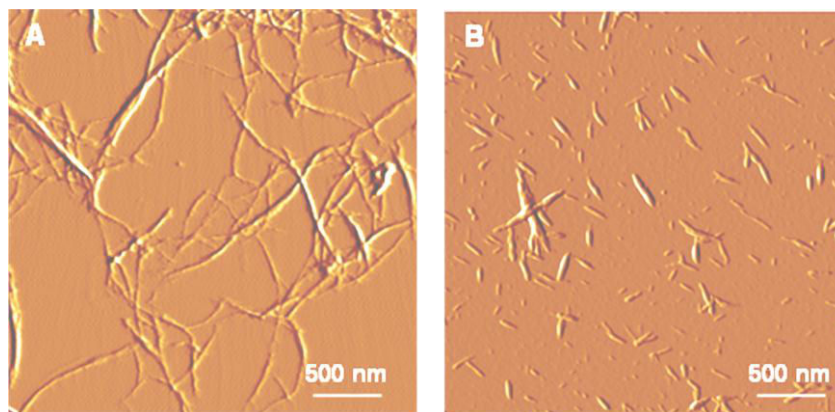


Figure 2 – Observation par microscopie à force atomique de particules individualisées de nanocellulose : MFC(A) et NCC(B)

La morphologie et les propriétés physico-chimiques des MFCs sont fortement dépendantes du traitement mécanique et des prétraitements subis par les fibres. Comme l'illustre la **Figure 2-A**, les MFCs de la se présentent sous la forme de faisceaux de fibrilles agrégées ayant une longueur moyenne de l'ordre du micromètre et un diamètre compris entre 20 et 60 nm. Les NCCs correspondent, au contraire, aux plus petites particules pouvant être extraites à partir de fibres de cellulose. Ces NCCs peuvent être considérés comme des cristaux rigides modèles dont les dimensions varient en fonction du matériau cellulosique de départ.

Ainsi des NCCs extraits de sources marines sont généralement plus longs (500-1500 nm) que ceux isolés à partir de coton ou de bois (100-300 nm) (**Figure 2-B**), leurs dimensions latérales varient entre 5 et 10 nm. Contrairement aux MFCs dont la chimie de surface reste très proche de celles des fibres cellululosiques, les NCCs présentent une charge de surface négative portée par les esters de sulfate ($-\text{SO}^3^-$) résultant de la réaction de l'acide sulfurique avec les groupements hydroxyles ($-\text{OH}$).

Principales propriétés des nanocelluloses. Les différences morphologiques et chimiques entre les MFCs et les NCCs, leur confèrent des propriétés et des applications très différentes. Ainsi à l'état de suspension, les MFCs ont un aspect de gels (**Figure 3-A**) ayant un comportement de fluide à seuil rhéofluodifiant. (Iotti et al. 2011) Ce comportement rhéologique peut être attribué à la capacité des MFCs à former un réseau d'enchevêtrement maintenu entre autre par des liaisons de types *Van der Waals*.

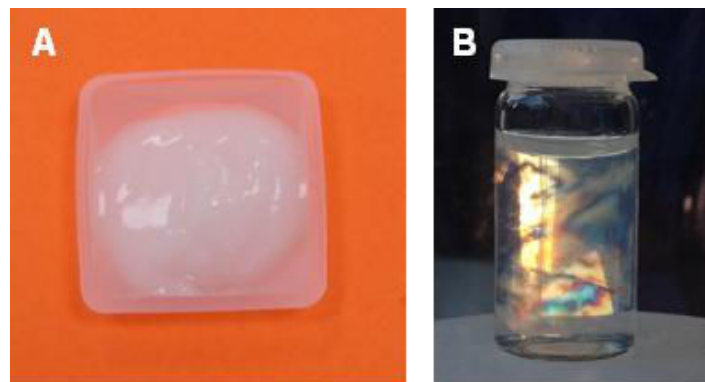


Figure 3 – Observation de suspensions à 2 % de MFC (A) et NCC (B).

Au contraire, les NCCs préparés par hydrolyse à l'acide sulfurique se présentent sous forme de bâtonnets rigides stabilisés par la présence de charges électrostatiques répulsives qui leurs confèrent des propriétés d'auto-assemblage. Ainsi, lorsqu'une suspension de NCCs est éclairée entre deux polariseurs croisés, (**Figure 3-B**) une biréfringence caractéristique similaire à celle observée pour les cristaux liquides cholestériques peut être observée.

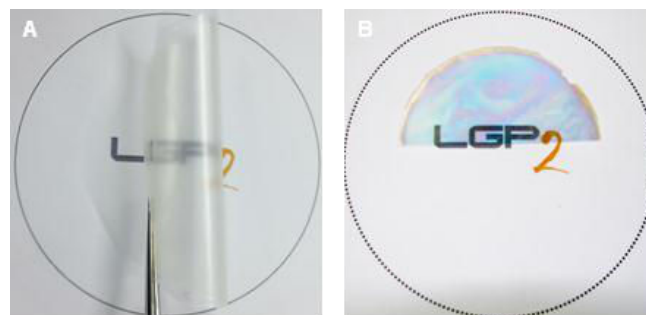


Figure 4 – Observation des films de 60 g/m² de MFC (A) et NCC (B) obtenus par simple coulée et évaporation.

Lors de l'évaporation, l'enchevêtrement des MFCs est préservé grâce à la formation de nombreuses liaisons hydrogènes. Le matériau ainsi obtenu s'apparente à un film dense transparent possédant d'excellentes propriétés barrières et mécaniques (**Figure 4-A**).

Au contraire, lors de l'évaporation d'une suspension de NCCs, la propriété d'auto-assemblage peut être préservée permettant l'obtention d'un film coloré ayant des propriétés d'iridescence (**Figure 4-B**).

L'utilisation des nanocelluloses dans l'industrie papetière. En comparaison du nombre total de publications (3201) et de brevets (436), on compte moins d'une centaine de publications concernant l'utilisation de nanocelluloses pour l'industrie papetière et une tendance bien plus importante au regard du nombre de brevets puisque un tiers de brevets couvrant le domaine papetier. Les différentes approches reportées dans la littérature peuvent être divisées en deux approches :

- le traitement de surface
- l'introduction en partie humide dans le support de base

L'utilisation des nanocelluloses permet une amélioration du procédé de fabrication (partie humide de couchage) ainsi qu'une amélioration significative des propriétés finales du papier. Il ressort de l'analyse de l'état de l'art que l'approche la plus prometteuse consiste à introduire les nanocelluloses en surface des papiers. C'est donc celle-ci qui a été envisagée au cours de ce projet.

2 Organisation du projet

L'originalité de ce projet est de s'appuyer sur les deux types de nanocelluloses (les MFCs et les NCCs) pour à la fois améliorer et fonctionnaliser les papiers spéciaux comme le décrit la **Figure 5**. Il s'inscrit dans le cadre d'une thèse industrielle (CIFRE N° 325/2011) avec les Papeteries du Léman (France).

Dans un premier temps, des films modèles de nanocelluloses ont été étudiés (**Chapitre 2 et 3**) puis des stratégies d'applications aux papiers spéciaux ont été proposées de l'échelle pilote à industrielle.

Les contributions des MFCs sont regroupées dans le **Chapitre 2** et se focalisent sur la dispersion de particules dans un réseau d'enchevêtrement. Le but était (i) d'étudier la dispersion de particules minérales pour élaborer des films minces présentant une excellente

opacité et (ii) d'élaborer un film à base de nanocelluloses qui soit à la fois flexible, transparent et ayant d'excellentes propriétés barrières à forte humidité relative.

Le **Chapitre 3** qui étudie l'auto-assemblage des NCCs pour élaborer des films iridescents, décrit les interactions des NCCs avec :

- deux polymères solubles (neutre ou anionique) pour améliorer la flexibilité et d'ajuster la coloration du film de NCCs
- une molécule photochimique (azurant optique) pour élaborer un film à base de NCCs qui soit iridescent lorsqu'il est observé sous éclairage naturel et fluorescent quand il est observé avec un éclairage ultraviolet.

Enfin, le **Chapitre 4** concerne l'implémentation dans le procédé industriel papetier des précédents chapitres dédiés à l'élaboration de films opaques ou barrières à base de MFCs (**Chapitre 2**) et à l'élaboration de films iridescents (**Chapitre 3**) à base de NCCs. Le principal objectif de ce dernier chapitre est de confirmer le potentiel des nanocelluloses pour améliorer et fonctionnaliser les papiers spéciaux. Ce chapitre synthétise les campagnes d'essais industriels et présente les principales raisons à l'origine du dépôt des deux brevets au cours du projet.

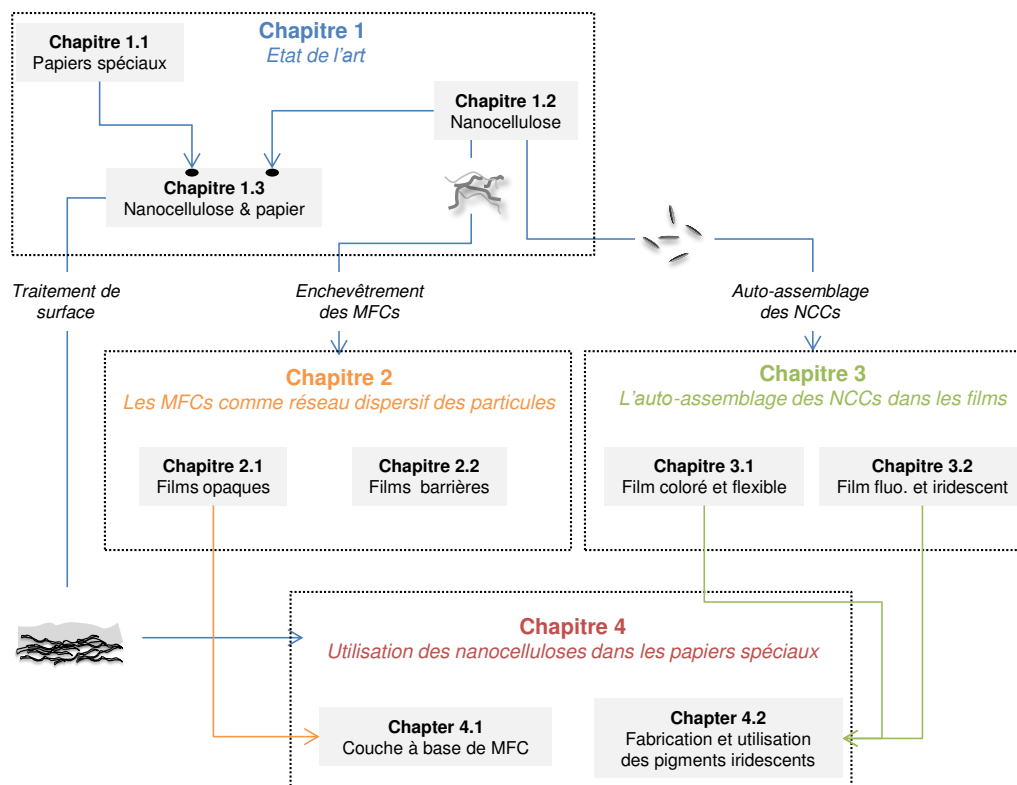


Figure 5 – Schéma de thèse

3 Principaux résultats

Les trois chapitres de résultats ont permis de confirmer que les nanocelluloses sont bien une alternative prometteuse pour

- améliorer les propriétés finales des papiers spéciaux telles que l'opacité et l'imprimabilité
- conférer des propriétés fonctionnelles comme l'anti contrefaçon

Les apports de ce travail permettent d'améliorer la compréhension scientifique des mécanismes mis en jeu et de favoriser le passage de la recherche aux applications. Les résultats ont été publiés (3 publications acceptées, deux en cours de soumission) ou brevetés (deux brevets publiés). Le contexte des différentes études et les principaux résultats sont détaillés ci-dessous.

3.1 Les MFCs comme réseaux d'enchevêtrement

Dans le but d'étudier la dispersion de particules dans un réseau de MFC enchevêtrées, le *Chapitre 2* est divisé en deux études distinctes :

- L'étude de la dispersion de particules minérales pour élaborer des films minces présentant une excellente opacité.
- L'élaboration d'un film à base de nanocelluloses qui soit à la fois flexible, transparent et présentant d'excellentes propriétés barrières à forte humidité relative

3.1.1 Films opaques

Contexte. Cette étude décrit différentes méthodes de production de films opaques à partir de particules de TiO_2 dispersées dans une suspension de MFCs. L'objectif de cette étude est de répondre à une demande du partenaire industriel pour réduire sa consommation de TiO_2 dans les papiers minces opaques. Cette étude a servi de base préliminaire pour la rédaction du brevet 1 et a été publiée dans le journal *Cellulose*.

Principaux résultats. Il a été démontré que l'excellente dispersion de particules de TiO_2 (sans l'aide d'aucun dispersant chimique) provient uniquement de l'aspect gel de la suspension de MFCs et de leurs enchevêtrements pour former un réseau dense de fibrilles. Ainsi des analyses en microscopie électronique à balayage (MEB) montrent que les particules sphériques de TiO_2 sont réparties de manière homogène dans l'épaisseur du film (**Figure 6**).

La dispersion de particules minérales est optimale avec ce réseau de MFCs car une très faible quantité de TiO_2 (dès 5 wt %) est suffisante pour obtenir un film opaque. Il a été estimé que le ratio optimum de TiO_2 se situe à 20% wt.

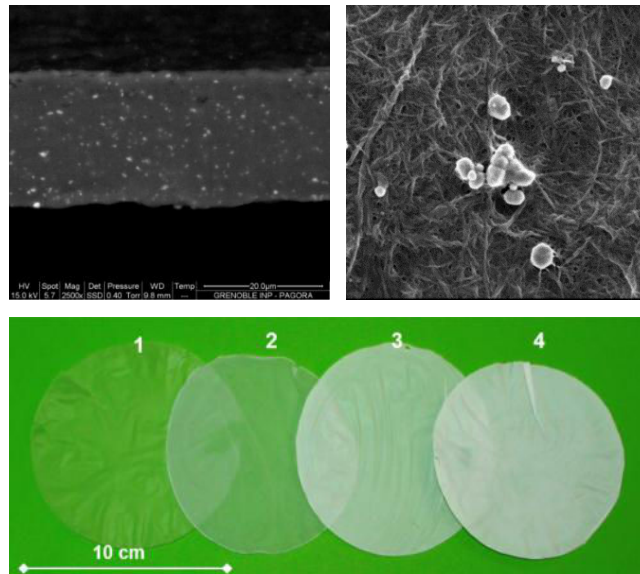


Figure 6 – Observation d'un film de 30 g/m² de MFCs contenant 10 wt% de TiO_2 . (A) correspondent à la coupe observée par E-SEM (BSE mode) et (B) à la surface du film. Les photos 1 à 4 correspondent à des films de MFCs obtenus avec un taux croissant de TiO_2 (0, 2, 7 et 20 wt%).

Puis, trois différentes approches (**Figure 7**) pour la fabrication de suspensions hybrides MFC- TiO_2 sont proposées :

- La première consiste à simplement mélanger la suspension de MFC avec le TiO_2 .
- Dans la deuxième approche, la charge minérale est introduite avant l'étape de fibrillation.
- Enfin dans la dernière approche, les particules de TiO_2 sont générées « in-situ » par une réaction sol-gel.

Les différents paramètres pour les deux dernières approches (« premix » et « sol- gel ») ont été optimisés.

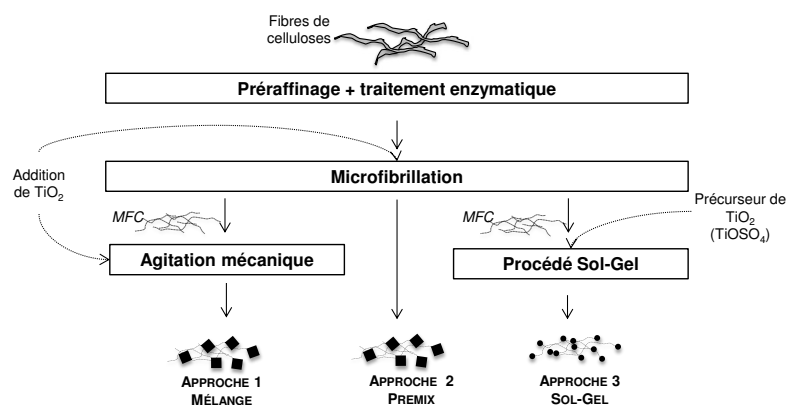


Figure 7 - Schéma des trois procédés de production de suspension hybrides de MFC/ TiO_2

Il a été constaté que par rapport à un film de MFCs seul, les propriétés mécaniques des films hybrides de MFCs contenant du TiO_2 sont réduites. Cette dégradation des propriétés mécaniques est attribuée à la création de points faibles dans le réseau d'enchevêtrements des MFCs.

Ainsi le module d'élasticité spécifique décroît de 12.3 GPa à 5.2 GPa pour un film contenant 20 wt% de TiO_2 . Ensuite, les propriétés des films de MFC ont été comparées à trois matrices polymères : l'amidon, la carboxyméthylcellulose (CMC), et l'alcool polyvinylique (PVOH). Ces polymères ont été sélectionnés car ils sont utilisés comme liant dans la formulation de sauce de couchage de certains papiers spéciaux.

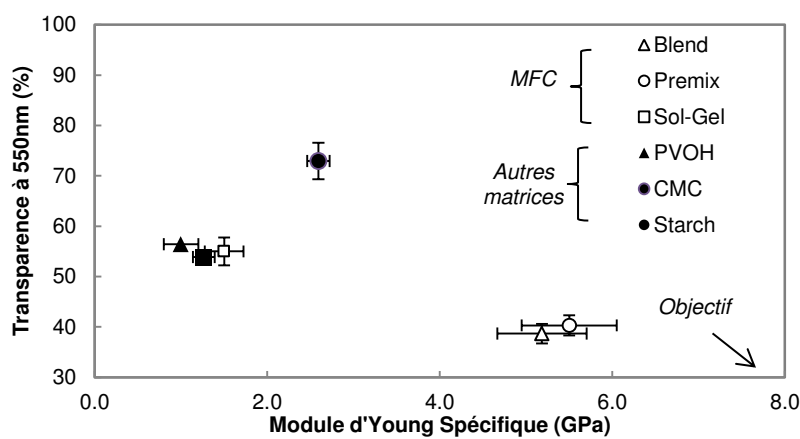


Figure 8 – Module d'Young spécifique et transparence d'un film de 30 g/m^2 contenant 20 wt% de TiO_2 : comparaison entre les trois approches d'obtention de suspension hybride ainsi qu'avec trois autres matrices polymères

Comme le montre la **Figure 8**, pour une quantité identique de TiO_2 (20 wt %), les propriétés mécaniques et surtout l'opacité des films à base de MFCs sont systématiquement meilleures que celles obtenues avec les autres matrices polymères. Dans le cas des films de MFCs, les particules de TiO_2 sont dispersées dans le réseau d'enchevêtrement tandis que les matrices polymères (amidon, CMC et PVOH) forment un film continu plus fragile.

Conclusion. Le principal intérêt de cette étude est de démontrer que pour un même niveau de TiO_2 , l'opacité est systématiquement plus élevée pour un film de MFCs. Ainsi, à niveau d'opacité équivalente, une réduction de la quantité de TiO_2 (ou une diminution de l'épaisseur) peut être envisagée. Dans l'objectif de l'élaboration des films minces, cette étude confirme la dispersion de particules minérales dans une suspension de MFCs, sans additif chimique (dispersant) et en utilisant une simple homogénéisation mécanique

3.1.2 Films barrières

Contexte. Contrairement à l'étude précédente qui consiste à étudier la dispersion de particules minérales pour améliorer l'opacité des films de MFCs, cette étude propose de substituer les nanoargiles par des NCCs modifiées pour élaborer un film 100% nanocellulose présentant de très bonnes propriétés barrières à haute humidité relative (>70% HR). Cette étude préliminaire a été menée pour étudier la possibilité de développer une couche barrière pour les papiers spéciaux sans utiliser de nanoparticules minérales. L'approche envisagée est schématisée dans la **Figure 9**.

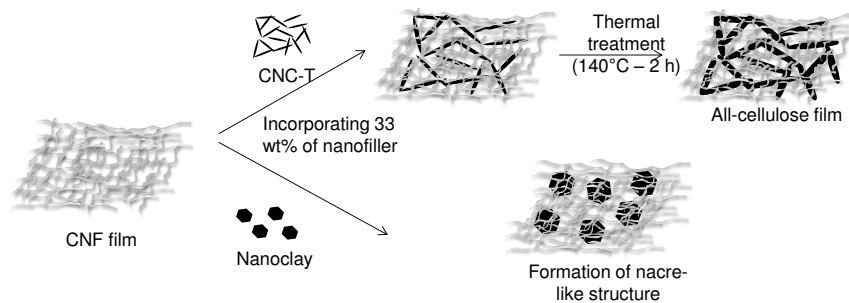


Figure 9 – Approche envisagée pour améliorer les propriétés barrières d'un film de MFCs.

Principaux résultats. Les propriétés optiques, barrières et mécaniques d'un film de MFCs (40 g/m²) ont été caractérisées. Celui-ci possède de bonnes propriétés mécaniques avec un module d'Young à 7.5 GPa et une résistance à la rupture de près de 100 MPa. Il possède aussi d'excellentes propriétés barrières (à la graisse et à l'oxygène) à faible humidité relative. Cependant, comme le montre la **Figure 10**, la perméabilité à l'oxygène augmente significativement à partir de 70% d'humidité relative. Ainsi, la perméabilité à l'oxygène du film de MFCs passe de 1 à plus de 13 cm³.μm/m².dkPa pour une humidité relative de 20% à 90%,

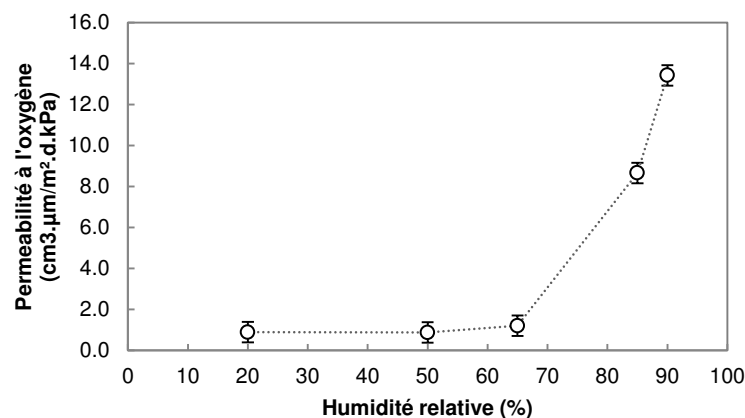


Figure 10 – Evolution de la perméabilité à l'oxygène en fonction de l'humidité relative pour un film de MFC

Il a été ainsi proposé de réduire cette sensibilité à la vapeur d'eau en incorporant deux types de nanocharges : une dispersion minérale de nanoclay (MMT) ou une dispersion de NCC comme décrit dans la **Figure 9**.

Dans cette étude, le film MFC/MMT a été considéré comme la référence à atteindre en termes de propriétés barrières à forte humidité relative. En effet, il a été largement démontré dans la littérature que l'incorporation de MMT dans un film de MFCs améliorerait significativement les propriétés barrières. (Wu et al. 2012)

Les conclusions tirées de précédentes études sur cette thématique ont permis de sélectionner le type de nanocharges minérales le plus adapté (nanoargiles de type Montmorillonite) et aussi de fixer la proportion optimale de nanocharge à ajouter aux MFCs (32.5 wt %). (Sehaqui et al. 2010, Liu et al. 2012) Ensuite, pour favoriser les interactions entre les nanocelluloses, les NCCs ont été oxydées par une réaction TEMPO selon celui décrit par les travaux de Saito et al. (2007).

L'incorporation de 32.5 % de NCC-T dans un film de MFCs a un effet très positif :

- la perméabilité à l'oxygène (90% HR) est réduite de moitié
- la perméabilité à la vapeur d'eau (à 50% HR) est également diminuée de plus de 70%
- il a été aussi montré que cela avait des conséquences notables sur le module d'élasticité (+34%) ainsi que sur la transparence du film (+8%)

Cependant cette amélioration des propriétés barrières à haute humidité est inattendue car lors de l'oxydation des NCCs, les groupements hydroxyles (-OH) sont substitués par des groupements carboxyles (-COOH) de nature plus hydrophile. Cette amélioration est expliquée uniquement par une modification de la structure du film. Il en résulte une légère augmentation de l'indice de cristallinité (+4%), une augmentation significative de la densité (+28%), et une diminution importante de la porosité (+57%) du film. Par ailleurs, cette amélioration n'a pas été constatée pour des NCCs natifs.

Le résultat clé de cette étude est que l'incorporation de NCC-T permet d'obtenir un film plus cohésif et cristallin ce qui semble principalement expliquer l'amélioration des propriétés barrières pour de forte humidité sans pourtant rendre le matériau hydrophobe.

La dernière partie de l'étude est consacrée à l'étude de l'influence du séchage. Les films obtenus par une simple évaporation de la suspension ont été séchés à 140°C pendant 2 heures. L'approche envisagée ici était de favoriser le mécanisme d'hornification ainsi que la réticulation par une réaction d'estérification des groupements carboxyles de surface des NCC-T avec les groupements hydroxyles de la cellulose. La spectroscopie RMN du ¹³C a mis en évidence qu'aucune nouvelle liaison covalente n'est formée au niveau de la cellulose. Il

semblerait donc que le mécanisme prédominant soit uniquement l'augmentation du nombre de liaisons hydrogènes (irréversibles) qui assurent une forte cohésion au film même en présence d'une teneur en eau importante.

Comme il est montré dans la **Figure 11**, le traitement thermique permet d'améliorer les perméabilités à l'oxygène et à la vapeur d'eau.

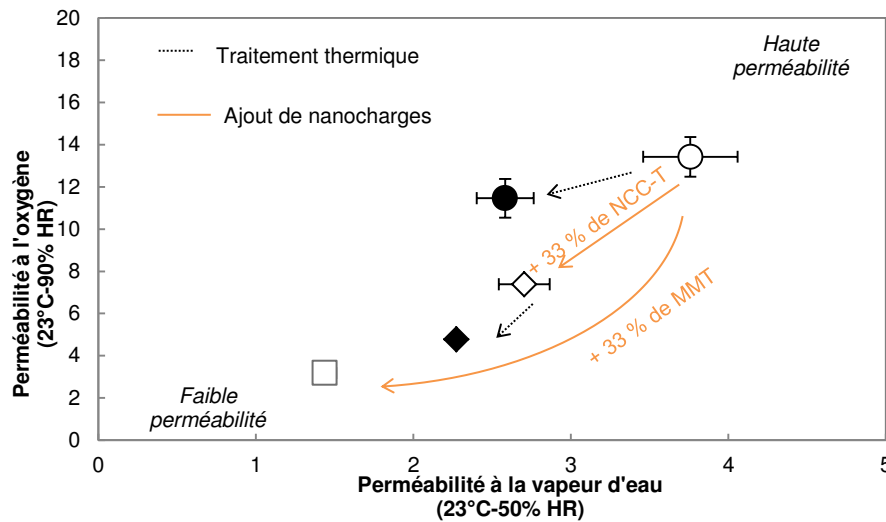


Figure 11 – Perméabilité à l'oxygène et à la vapeur d'eau pour différents films de nanocellulose de 40 g/m² : MFC seule, renforcé avec des nanocharges, et avec ou sans traitement thermique

En conclusion, il a été montré pour la première fois qu'une substitution des nanoargiles par des nanoparticules isolées de fibres de celluloses (NCC-T) est envisageable. Les propriétés barrières obtenues après un traitement thermique du film (2 heures à 140°C) sont proches de celles du film renforcé avec la MMT. De plus, le film composé uniquement de nanocelluloses présente de nombreux avantages car outre l'aspect 100% cellulose, celui-ci possède de meilleures propriétés mécaniques et une transparence plus importante.

3.1.3 Conclusions et perspectives

Le **Chapitre 2** est principalement axé sur l'étude de la dispersion de particules dans un réseau d'enchevêtrements de MFCs.

Dans le **Chapitre 2.1**, la dispersion de particules de TiO₂ a été étudiée de manière à élaborer des films minces présentant une excellente opacité. Le principal intérêt de cette étude est de montrer que pour un même niveau de TiO₂, l'opacité est systématiquement meilleure pour un film de MFCs que pour une autre matrice polymère. Cette étude confirme aussi qu'il est possible de disperser des particules minérales dans une suspension de MFCs, sans additif chimique (dispersant), en utilisant une simple homogénéisation mécanique.

Dans le **Chapitre 2.2**, il a été montré qu'il était possible d'obtenir des films composés uniquement de nanocelluloses qui soit à la fois flexible, transparent et ayant d'excellentes propriétés barrières à forte humidité relative. Ainsi, une substitution des nanoargiles par des nanoparticules isolées de fibres de celluloses (NCC-T) est envisageable.

3.2 L'auto-assemblage des NCCs

Contexte. Contrairement aux MFCs qui forment un réseau d'enchevêtrements lors du séchage et conduisent à la formation d'un film flexible et transparent, les NCCs se caractérisent par des propriétés d'auto-organisation en suspension aqueuse ou dans certains solvants. Il en résulte une propriété optique spécifique lors du séchage du film appelée « iridescence ». L'iridescence est la propriété d'une surface à changer de couleur avec l'angle d'éclairage ou d'observation (Revol et al. 1998). Comme décrit dans la **Figure 12**, dans un matériau iridescent, la coloration est uniquement due à la microstructure et à l'auto-assemblage spécifique des nanoparticules

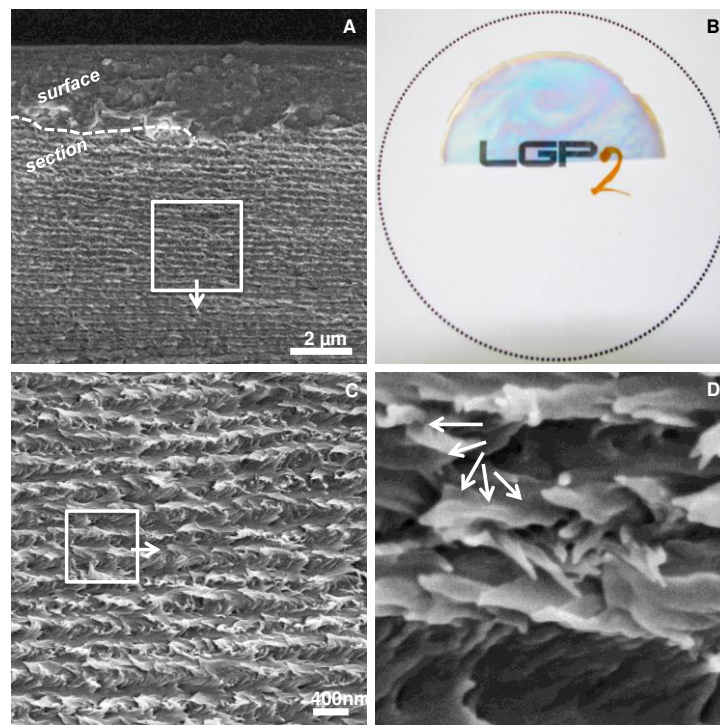


Figure 12 – Photographie d'un film de NCC iridescent sous illumination et incidence normale (B) et observation en microscopie électronique à balayage de section d'un film à différents grossissements (A, C, et D)

Dans ce projet, l'idée finale sera d'utiliser des films iridescents à base de NCC dans l'élaboration de papiers anti-contrefaçon. Le **Chapitre 3** est consacré dans un premier temps à la fabrication de films modèles et plus particulièrement à l'étude des interactions des NCCs avec différents additifs.

Ainsi deux polymères solubles ont été utilisés (neutre ou anionique) pour améliorer la flexibilité et ajuster la coloration du film de NCC (*Chapitre 3.1*).

Ensuite, une molécule photochimique (azurant optique) a permis d'élaborer un film qui soit iridescent sous éclairage naturel et fluorescent sou un éclairage ultraviolet (*Chapitre 3.2*)

Comme le décrit la **Figure 13**, les deux sous-chapitres sont structurés selon le même plan :

- une première partie a été consacrée à la caractérisation des NCCs et à leur propriété d'auto-assemblage en suspension
- une deuxième partie est consacrée à l'étude des interactions physico-chimiques avec les différents additifs
- la dernière partie se consacre aux propriétés (thermomécaniques et optiques) des films.

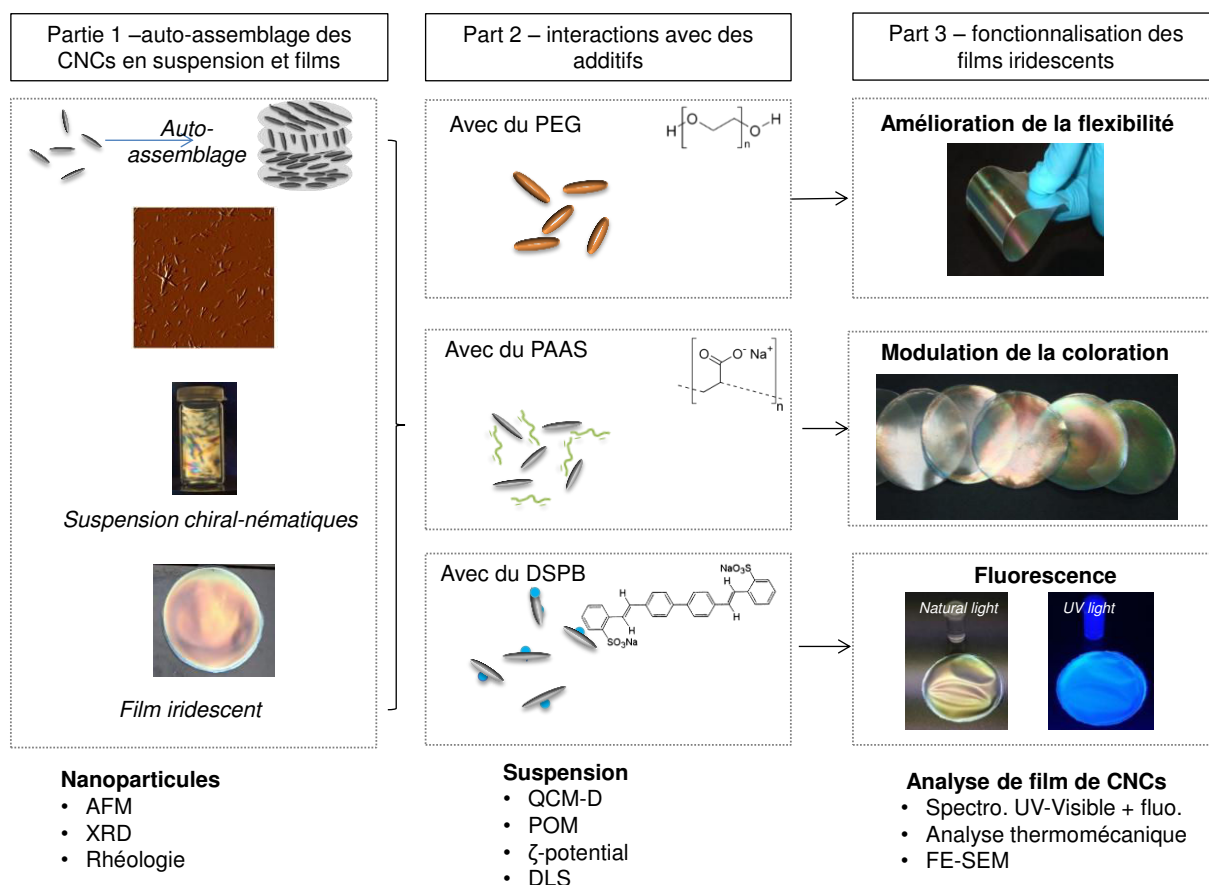


Figure 13 – Schéma récapitulatif du *Chapitre 3* dédié à l'étude de l'auto-organisation des nanocristaux de cellulose pour la formation de film iridescent

Comme mentionné précédemment, la modulation de la couleur des films iridescents est recherchée pour élaborer un matériau permettant l'authentification ou l'anti-contrefaçon. Plusieurs paramètres peuvent être utilisés comme l'ajout de sel monovalent permettant un décalage de la coloration dans le bleu (blueshift) ou comme le traitement par ultrason permettant un décalage dans le rouge (redshift). (Beck et al. 2010)

Les principaux inconvénients d'un film iridescent de NCCs sont entre autres sa fragilité et son manque de flexibilité. Il est ainsi très difficile de le manipuler et de l'utiliser. Il existe très peu de travaux qui ont proposé de limiter cet inconvénient. Par exemple, il a été proposé d'utiliser l'alcool polyvinylique ou un latex de type styrène-butadiène pour améliorer la flexibilité des films (Zou et al. 2010).

Principaux résultats. Pour faciliter l'application industrielle des résultats obtenus dans ce chapitre, deux types de NCCs disponibles commercialement ont été utilisés au cours des études suivantes. Les NCCs ont été fournies par :

- l'usine pilote de l'Université du Maine (Forest Product Lab., USA) pour le **Chapitre 3.1**
- la première usine semi-industrielle de fabrication de NCCs (Celluforce, Canada) pour le **Chapitre 3.2**

Durant ce projet, il a donc été possible de se rapprocher, par des accords de confidentialité, de deux fournisseurs pouvant délivrer une qualité de NCCs suffisante dans la perspective de la fabrication de films iridescents au niveau industrielle. Leurs principales caractéristiques sont reprises dans le **Tableau 1**.

Tableau 1– Récapitulatif des propriétés morphologiques et chimiques des deux t

		Source 1	Source 2
Caractéristiques			
Fournisseur		FPL, USA	Celluforce, Canada
Source		Pâte kraft de résineux blanchie	
Procédé de fabrication		Hydrolyse acide	
Etat		Suspension 6.5%	à Sec
Prix d'achat (en kg/sec)		310 €/kg	90 €/kg
Propriétés			
Morphologies	Longueur (nm)	205 (83)	174 (53)
	Epaisseur (nm)	5 (3)	8 (2)
	Facteur de forme	41 (30)	22 (9)
	Indice de cristallinité (%)	88 (2)	88 (3)
Chemical	Taux de sulfate ($\mu\text{mol/g}_{\text{NCC}}$)	370 (16)	244 (16)
	Potentiel zêta (mV)	-45 (1.2)	-41 (2.5)
Physico-chimique	densité de charge (e/nm^2)	0.56 (0.02)	0.36 0.02

3.2.1 Influence des polymères solubles sur l'auto-assemblage des NCCs

Premièrement, un polymère anionique, le *Polyacrylate de Sodium* (PAAS), a été utilisé pour modifier la coloration des films. Secondement, un polymère neutre, le *polyéthylène glycol* (PEG), a été utilisé pour améliorer la flexibilité du film. Plusieurs raisons ont justifié ce choix de polymères :

- Leur nature chimique (non cationique) et leur masse molaire (faible) ne risquent pas d'entraîner une floculation avec les NCCs
- Leur rôle de plastifiant ou dispersant a déjà été avéré.
- Ces deux produits commerciaux sont utilisés par le partenaire industriel.

Il est montré que l'auto-assemblage des NCCs dans une solution de PEG est conservé par stabilisation stérique et par l'absence de liaisons ioniques. Par ailleurs, le PEG est physiquement adsorbé (liaisons hydrogènes) à la surface des NCCs. Ainsi l'addition de 10 wt % de PEG a permis de doubler la flexibilité du film iridescent avec un impact négligeable sur l'iridescence du film obtenu. Il a été aussi démontré que le PEG permettait d'augmenter la température de dégradation d'environ 35 °C.

A l'opposé, l'importante anionicité (due aux groupements carboxyliques) du PAAS empêche son adsorption à la surface des NCCs eux aussi fortement anioniques. Cependant, une modification de l'auto-organisation des NCCs est constatée. Ainsi, le PAAS a pu être utilisé pour moduler la coloration (blueshift) d'un film iridescent sur une large gamme du spectre visible (**Figure 13**). De plus, il permet d'obtenir une coloration plus homogène et intense. Cette modulation sera très utile pour l'application anti-contrefaçon. Ainsi, le contrefacteur aura des difficultés à contrefaire la couleur choisie par l'industriel et fabriquée sur site.

3.2.1 Influence d'un agent fluorescent sur l'auto-assemblage des NCCs

Dans un second temps (**Chapitre 3.2**), il est proposé d'ajouter une troisième signature optique en incorporant un agent fluorescent. Il a été envisagé d'utiliser une autre famille de composés fluorescents à base de stilbène.

Le *Distyrylbiphenyl Disulfonate* (DSBP) est un azurant optique (OBA) dont l'utilisation est généralisée dans la papeterie ou le textile pour obtenir des matériaux à haute blancheur. L'adsorption du DSPB sur les NCCs a été observée par analyse QCM et mesurée à 18 $\mu\text{mol/g}_{\text{NCC}}$ par une analyse en spectroscopie de fluorescence après une longue purification (dialyse). L'impact du DSPB est limité, il n'affecte pas l'auto-assemblage des NCCs à l'état de film : aucune modification de la coloration n'a été constatée.

Une utilisation des NCCs comme marqueur fluorescent peut ainsi être envisagée. La sélection d'un agent photochimique déjà utilisé dans l'industrie papetière permet de proposer une méthode simple et robuste pour adsorber un agent fluorescent sans affecter leur propriété d'auto-assemblage.

3.2.2 Conclusions et perspectives.

La propriété d'auto-assemblage des NCCs a été utilisée dans le *Chapitre 3* pour obtenir des films iridescents dont la principale application sera le développement de matériaux anti-contrefaçon.

L'amélioration des propriétés optiques et physiques du film a été proposée en utilisant un plastifiant pour améliorer sa flexibilité et un polymère anionique pour moduler sa coloration. Le résultat clé de ce chapitre est qu'il est donc possible d'obtenir un matériau flexible avec trois niveaux de signature optique :

- D'une part la « couleur » du film peut être analysée par spectroscopie d'absorption dans l'UV-visible.
- D'autre part, la texturation en « fingerprint » due à l'organisation chiral-nématique propre à chaque film de NCCs peut être analysée par Microscopie Optique à Lumière Polarisée.
- Enfin un agent fluorescent a été utilisé pour élaborer un matériau présentant une troisième signature optique lorsqu'il est illuminé sous UV.

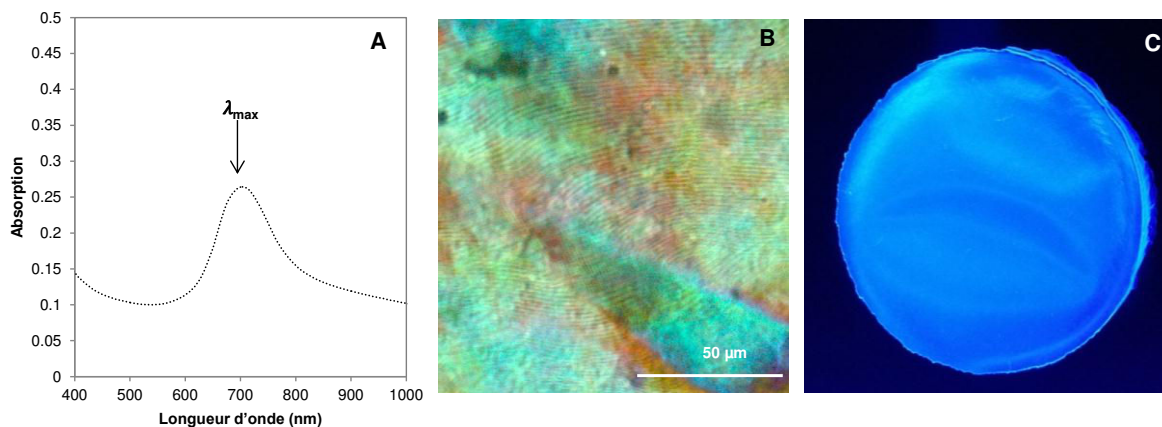


Figure 14 – Observation des trois signatures optiques d'un film iridescent à base de NCC par analyses spectroscopie UV-visible (a), Microscopie Optique à Lumière Polarisée (b) et une observation sous éclairage UV.

Ces trois niveaux permettront de limiter fortement toute contrefaçon. De plus, le produit obtenu (film de NCCs iridescent) répond aux attentes de la législation propre à la fabrication de cigarette et permet ainsi d'envisager de nouvelles opportunités dans ce domaine.

3.3 Contribution des nanocelluloses pour l'amélioration et la fonctionnalisation des papiers spéciaux

Le *Chapitre 4* concerne l'implémentation dans le procédé industriel papetier des résultats des précédents chapitres qui ont été dédiés : à l'élaboration de films opaques (ou barrières) à base de MFCs (*Chapitre 2*) et de films iridescents à base de NCCs (*Chapitre 3*).

Le principal objectif de ce chapitre est de confirmer le potentiel des nanocelluloses pour améliorer et fonctionnaliser les papiers spéciaux. Ce chapitre est organisé de manière à synthétiser à la fois les campagnes d'essais laboratoires, pilotes et industriels mais aussi pour présenter les principales raisons qui ont justifiées le dépôt des deux brevets.

3.3.1 Réduction de la consommation de TiO₂ dans la formulation des papiers minces avec un traitement de surface à base MFC

Contexte. Le TiO₂ est le pigment le plus cher utilisé dans l'industrie papetière. Son coût représente près de 10 fois celui de la pâte à papier et près de 20 fois celui du Carbonate de Calcium broyé (GCC) ou précipité (PCC). Ce coût fluctue aussi énormément et parfois très rapidement : il a en effet augmenté de près de 50 % au cours de l'année 2011. Tout ceci est dû à sa faible abondance, sa provenance géographique, le coût des procédés d'extraction et de purification et la demande croissante de la part des marchés émergents (Nelson et al. 2008). Ainsi les différentes projections estiment que son prix devrait dépasser les 3500 € par tonne dans les prochaines années contre 2500 aujourd'hui. Il existe des solutions techniques pour limiter son utilisation :

- la mise en œuvre de pigments de substitution (Carbonate de Calcium précipité, Kaolin Calciné, pigments plastiques) (Johnson et al. 1997)
- l'utilisation d'additifs chimiques permettant de favoriser sa dispersion et sa rétention (Adkins 1992)

Il reste indispensable dans la plupart des papiers à faible grammage dont l'opacité est une spécification requise. Généralement, les papiers pour les catalogues industriels ou magazines contiennent jusqu'à 5 % de TiO₂, plus de 10 % pour les papiers destinés à la littérature religieuse, et jusqu'à 30 % pour les papiers laminés. (Braun et al. 1992)

L'introduction de TiO₂ dans le papier peut se faire soit par en partie humide (dans la masse du support) ou lors du traitement du surface (dans la couche). L'introduction en partie humide présente des inconvénients car elle entraîne une surconsommation de produits chimiques à cause de leur surface spécifique élevée (10 m²/g). La faible granulométrie (0.2

μm à $0.5 \mu\text{m}$) et la densité élevée du TiO_2 entraîne aussi une très faible rétention du TiO_2 (50 – 60%).

Lorsque le TiO_2 est employé dans une sauce de couchage pigmentaire pour limiter son agglomération, il est généralement combiné avec d'autres charges minérales (GCC ou PCC). Cependant, la forte abrasivité de pigment cause souvent une usure prématurée des équipements d'enduction. Les principaux résultats expérimentaux du **Chapitre 2** ont permis d'élaborer un film opaque à partir d'une suspension hybride de MFCs contenant une quantité optimisée de TiO_2 .

D'autre part, la revue bibliographique a montré qu'une suspension de MFCs pouvait être utilisée dans la formulation de couchage pour des applications dans l'impression ou le packaging. Le **Chapitre 3.1** inclut donc une partie expérimentale à l'échelle du laboratoire, une analyse économique permettant d'estimer un prix seuil des MFCs. Il s'achève par une présentation des résultats obtenus lors d'une campagne d'essais pilotes.

Principaux résultats. Cette étude s'est focalisée sur le traitement de surface à partir d'un mélange hybride de MFCs et de TiO_2 dans le but de limiter la quantité de TiO_2 dans les papiers spéciaux. Une partie des résultats présentés ici a servi de base pour l'élaboration d'un brevet (accepté en 2014). La préparation de suspension hybride a été réalisée selon les principales revendications décrites dans le **Brevet 1**. Il est consultable en annexe 1.

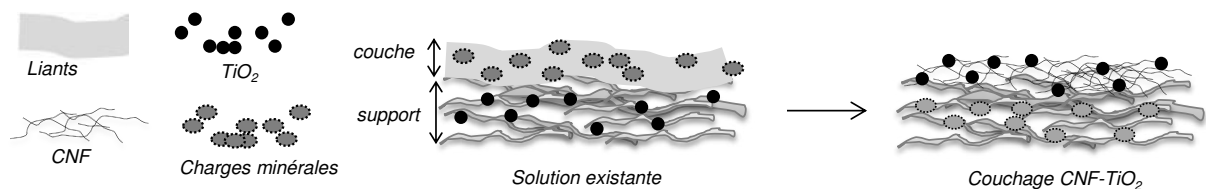


Figure 15 – Approche envisagée pour optimiser la quantité de TiO_2 dans la formulation des papiers minces

Comme indiqué sur la figure ci-dessus, la suspension hybride a été enduite sur un support papier ($30\text{g}/\text{m}^2$) et comparée à un mélange de liants contenant le même taux de TiO_2 . Par rapport à une couche composée de liants conventionnels (Latex SB et amidon), la suspension hybride permet d'obtenir une meilleure opacité quelle que soit la quantité de TiO_2 . Cela peut être attribué à la fois à une meilleure dispersion du TiO_2 à travers le réseau d'enchevêtrements des MFCs qui crée une microporosité dans la couche pouvant favoriser la diffusion de la lumière.

Ensuite, deux compositions de papier ont été comparées (**Figure 16**). Dans un cas, la suspension hybride MFC-TiO₂ a été introduite dans le support de base qui est ensuite enduit avec une couche standard (référence). Dans l'autre cas, la suspension hybride a été couchée sur le support. Par ailleurs, les deux séries de papiers ont été obtenus à taux de charge (25%), poids de couche (4 g/m²) et grammage constant (30 g/m²). Ainsi, pour atteindre le même niveau d'opacité pour un papier contenant 9 % de TiO₂ (introduit en masse), seulement 3 % de TiO₂ sont nécessaires lorsqu'il est couché avec une suspension de MFCs ()

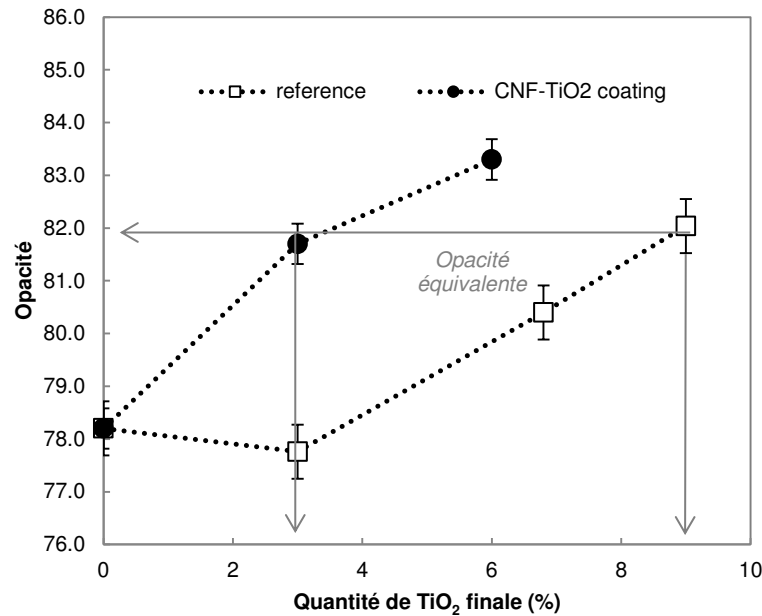


Figure 16 – Comparaison entre l'opacité d'un papier couché avec la suspension hybride MFC/TiO₂ et un papier couché de référence en fonction de la quantité de TiO₂

Ce résultat est extrêmement positif. Il prouve à l'échelle laboratoire qu'il est possible de diminuer fortement le TiO₂ consommé dans ces papiers spéciaux en divisant le tonnage par 3. A partir de ces résultats, il a été possible de déterminer le prix seuil des MFCs. En fonction de la quantité de TiO₂ dans le papier et de sa rétention, ce prix varie de 0.7 € à plus de 2.5 € par kg de MFCs. Il est donc démontré que le couchage d'une suspension hybride MFC-TiO₂ n'est viable industriellement que lors d'une production de MFCs in-situ moins onéreuse.

Les résultats obtenus au laboratoire ont ensuite été validés à l'échelle pilote. Pour ce faire, une machine dédiée à l'impression flexographique a été spécialement adaptée dans le but de simuler un couchage industriel (**Figure 17**).

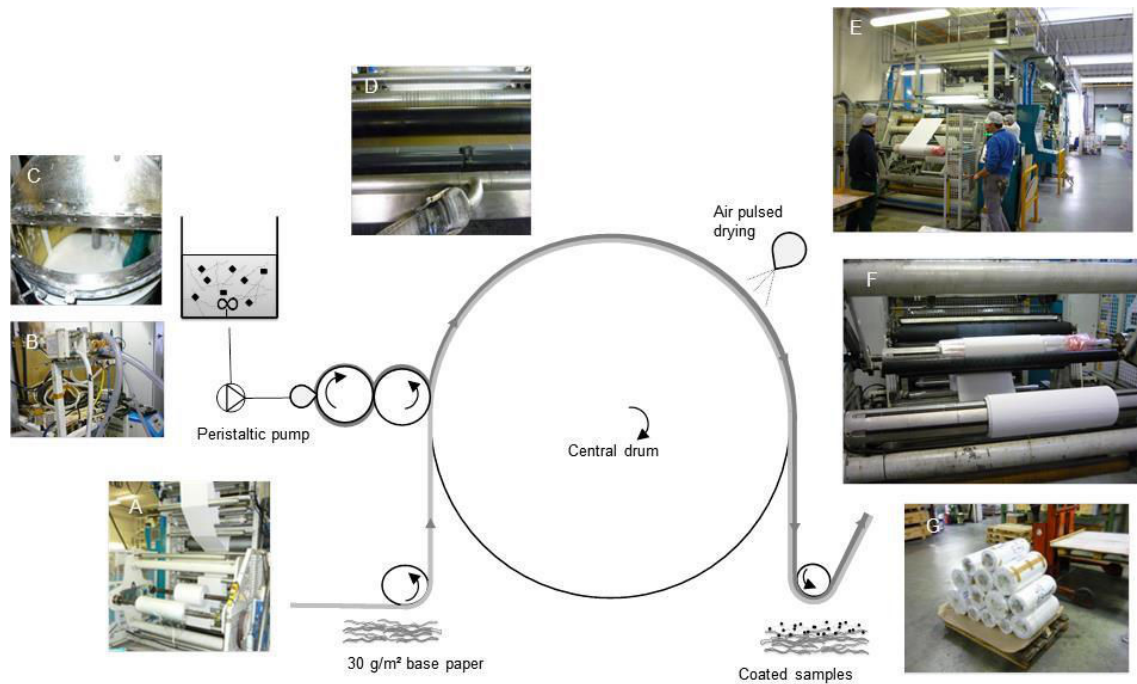


Figure 17 – Schéma du dispositif pilote utilisée pour les essais d'enduction

Durant ces essais avec un partenaire Italien (30 heures), trois différentes formulations de couches ont été testées ainsi que différents poids de couches allant de 0.6 à 2.8 g/m². Au final, treize bobines de 1000 m de long ont été couchées et ensuite caractérisées. L'évaluation des propriétés optiques et d'imprimabilité des papiers met en évidence une plus forte opacité ainsi que de meilleures propriétés d'imprimabilité pour une couche de 1.5 g/m² de MFC-TiO₂ en comparaison avec un couche classique de 3.5 g/m² utilisée lors de la fabrication de papier mince opaque. Les essais pilotes ont donc confirmé tout l'intérêt de cette stratégie et des essais industriels ont été envisagés et actés.

Malheureusement, il n'a pas été possible, pour l'instant, de directement coucher une suspension hybride de MFC-TiO₂ lors d'une fabrication industrielle de papier. En effet, aucun fournisseur de nanocelluloses n'était en mesure de fournir la quantité nécessaire de nanocelluloses pour faire cet essai industriel (entre 4000 à 5000 l). Ceci devrait être le cas dans les années à venir, en attendant des préconisations ont été proposées.

3.3.2 Production, caractérisation et utilisation de pigments iridescents

Contexte. L'élaboration d'un dispositif anti-contrefaçon à partir de NCCs est la principale application des films iridescents ciblée dans ce projet. En effet, avoir des papiers cigarette difficiles à contrefaire est un des objectifs fort de l'industriel finançant cette thèse. Pour des raisons évidentes de sécurité et santé, la liste des produits utilisables dans ces papiers est très limitée, mais bien évidemment la cellulose (et donc les nanocristaux de cellulose) en fait partie. Il a été montré dans le **Chapitre 3** qu'il était possible de fabriquer un film à partir de NCCs disponibles commercialement.

Néanmoins l'utilisation de films iridescents présente de nombreux inconvénients qui limitent son application industrielle. Bien qu'il soit probable que le coût des NCCs puisse être encore largement réduit avec l'émergence de nouveaux sites de production, son coût reste aujourd'hui très élevé (90 € à 370 € /kg). Pour obtenir une surface iridescente, il a été démontré que l'épaisseur optimum était d'environ 60 μm et que même en améliorant la flexibilité du film, il restait très fragile et difficile à manipuler. D'autre part, pour ne pas perturber l'auto-assemblage des NCCs, un film iridescent ne peut être obtenu qu'à partir d'une évaporation sans contrainte (1 à 2 jours). Pour ces raisons, il est impossible d'obtenir un film iridescent par des procédés industriels en continu comme le couchage ou l'extrusion.

Enfin d'un point de vue technico économique, un film iridescent à base NCCs n'est pas compétitif avec les autres matériaux utilisés actuellement. Pour résoudre ces différentes contraintes, une nouvelle approche a été proposée (**Figure 18**). Celle-ci consiste à fabriquer des pigments à partir du film iridescent de NCCs et ensuite de les incorporer dans un matériau flexible (film ou papier).

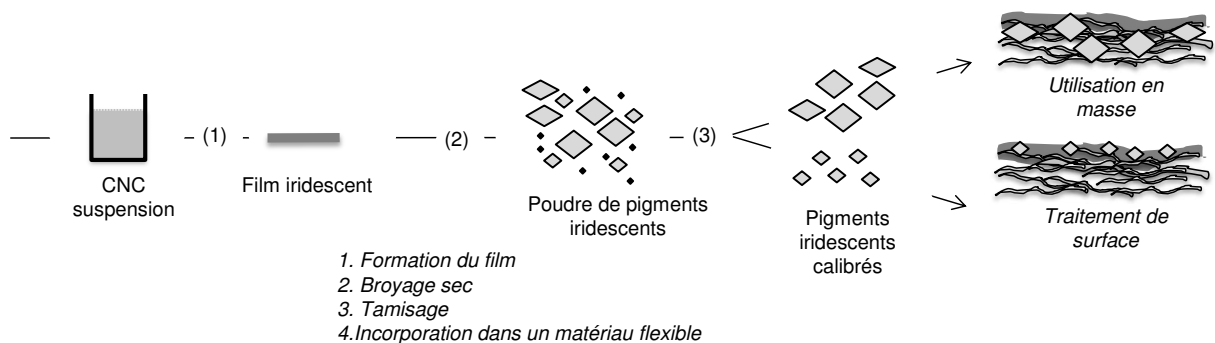


Figure 18 – Schéma du procédé de fabrication de pigments iridescents à partir d'une suspension de NCC

Principaux résultats. Dans la première partie de l'étude, la procédure pour fabriquer des pigments iridescents par broyage à l'état sec est décrite. Les pigments obtenus sont iridescents et ont une épaisseur de l'ordre de 25µm. Ils sont caractérisés par une intense coloration car l'auto-organisation des NCCs dans le film est conservé au cours du broyage (**Figure 19**).

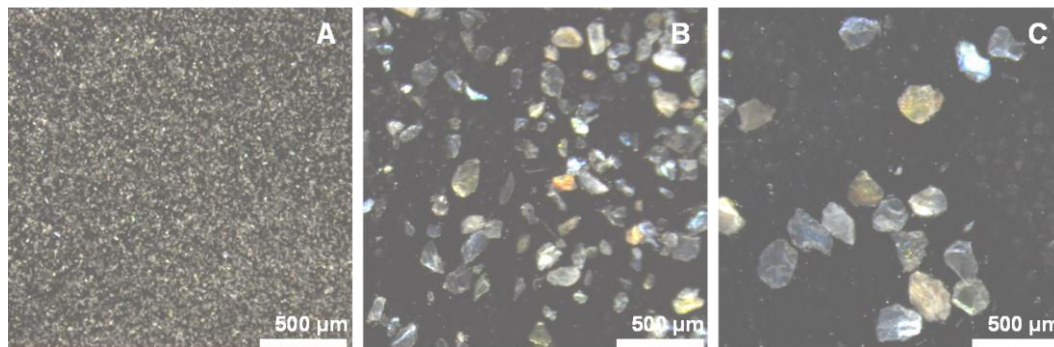


Figure 19 – Observation en microscopie optique des trois différentes granulométries de pigments obtenues au cours du broyage des pigments

A cause de la présence de groupement sulfate, les pigments iridescents ne peuvent pas être incorporés car ils noircissent en présence de chaleur (à partir de 180°C) et ils se redispersent rapidement au contact de l'eau. Pour cela, deux post-traitements ont été proposés (**Figure 20**).

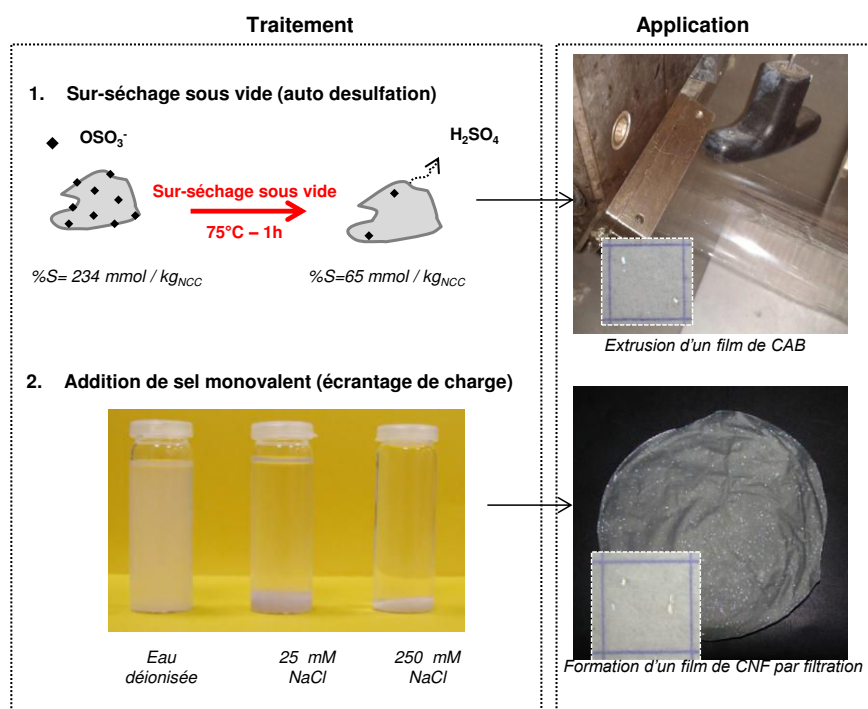


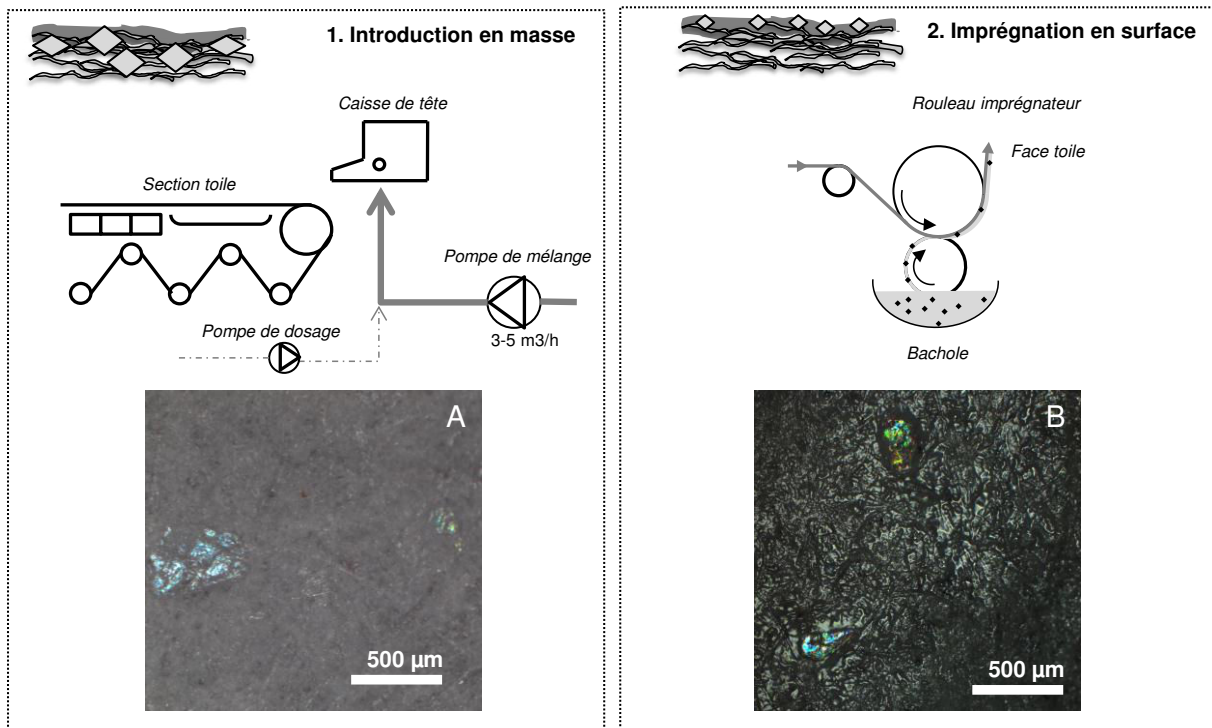
Figure 20 – Récapitulatif des deux post traitements des pigments iridescents et deux exemples d'application permettant l'incorporation des pigments iridescents dans un matériau transparent et flexible

Le premier post-traitement consiste à sur-sécher sous vide (1 heure à 75°C) les pigments iridescents pour retirer les groupements sulfate. Cette technique est efficace car environ 75%

des groupements sulfates sont retirés par un mécanisme d'« auto-desulfation ». Les pigments peuvent être ainsi extrudés jusqu'à une température d'environ 190°C. Par exemple, l'extrusion des pigments iridescents avec l'Acétate-Butyrate de cellulose (CAB) a permis d'obtenir un film transparent incorporant des pigments iridescents.

Pour limiter la désagglomération de pigments iridescents dans l'eau, l'approche proposée a été d'utiliser une solution de NaCl concentré (>25 mM) pour écranter les charges négatives des NCCs après formation des films et broyage des films. Cette approche simple a permis ainsi d'augmenter significativement la stabilité des pigments iridescents durant un temps prolongé d'immersion. Ainsi pour le même temps d'immersion (1 heure), la perte de pigment est inférieure à 10 % dans une solution de NaCl alors que près de la totalité des pigments se dispersent dans l'eau déionisée. Ce résultat est déterminant car il est maintenant possible d'utiliser les pigments iridescents dans la plupart des procédés en milieu aqueux ou d'extrusion.

L'incorporation de pigments iridescents a ensuite été proposée dans un support papier à l'échelle industrielle soit (i) par une introduction dans la masse du papier (en partie humide), soit (ii) soit par un traitement de surface (par imprégnation) comme le décrit la **Figure 21**.



Une partie importante de la préparation des essais a consisté à produire une quantité suffisante de pigments iridescents (environ 1 kg). Ensuite, deux campagnes d'essai ont été

réalisées sur une machine à papier (550 m/min) lors de la production d'un papier de 30 g/m². Ces essais ont permis de lever les principaux verrous techniques liés à l'introduction de pigments iridescents dans le procédé papetier. Le bilan des essais est encourageant et a démontré sa faisabilité industrielle. Plusieurs points positifs ont été relevés lors des essais, car l'introduction de pigments iridescents n'a pas d'impact sur le procédé de fabrication du papier et n'altèrent pas les propriétés du papier. Par ailleurs, il a été estimé que moins de 500 g de pigments iridescents par tonne de papier était nécessaire pour avoir environ un pigment iridescent par cm² de papier. Le surcoût lié à l'introduction de pigments iridescents incluant le coût d'achat des NCCs et le coût de fabrication des pigments est inférieure à 5% celui du coût de fabrication d'un papier de spécialités.

Conclusion et perspectives. En se basant sur les principaux résultats du **Chapitre 3**, une solution innovante est proposée pour élaborer un support flexible (papier, film,...) incorporant des pigments iridescents. Ces pigments sont obtenus à partir du broyage à l'état sec d'un film de NCCs iridescents. Deux solutions simples sont proposées pour améliorer l'utilisation des pigments iridescents dans un procédé industriel en milieu aqueux ou d'extrusion. L'incorporation de pigments iridescents a ensuite été proposée dans un support papier et réalisée sur une machine à papier. Il a pu être réalisé soit par une introduction dans la masse du papier (en partie humide) soit par un traitement de surface (par imprégnation. Bien que les pigments iridescents composés de nanocellulose présentent plusieurs avantages, ils sont toutefois difficiles :

- à caractériser et à détecter car ils ne présentent aucune similitude avec les autres solutions existantes et sont très proches chimiquement de n'importe quels hydrates de carbone (ex cellulose, amidon)
- à reproduire car le procédé de fabrication est complexe et unique.

Ainsi cette approche permet de conférer aux papiers spéciaux une propriété d'anti-contrefaçon pour un coût relativement limité du fait de la faible quantité des pigments iridescents requise sans pour autant altérer l'aspect générale du papier. Enfin, parce que ces pigments iridescents sont élaborés à partir de nanocelluloses extraites de fibres de cellulose, ils permettent de répondre à une législation plus restrictive, leur utilisation peut être envisagée dans l'élaboration d'emballage ou de notice destinées à l'alimentaire, le cosmétique et le médical.

4 Conclusions et perspectives.

L'originalité de ce travail est d'étudier la contribution des nanocelluloses pour la fonctionnalisation des papiers spéciaux. Les principaux résultats sont résumés dans **Tableau 2**.

Tableau 2 - Résultats clés du projet de thèse

Thématiques scientifiques	Résultats clés
<p>Chapitre 2 Les MFCs comme réseau dispersif des particules</p>	<p>Films opaques</p> <ul style="list-style-type: none"> • utilisation des MFCs comme un réseau dispersif • trois procédés pour obtenir des suspensions hybrides MFC-TiO₂ <p>-par mélange -pendant la fibrillation des MFCs -par procédé sol-gel</p> <p>➤ film de MFCs opaque avec 5 wt% de TiO₂</p> <p>Films barrières</p> <ul style="list-style-type: none"> • substitution des nano argiles par des NCCs modifiés • mise en évidence de l'impact positif du traitement thermique <p>➤ film uniquement 100% nanocellulose avec de très bonnes propriétés barrières à haute humidité</p>
	2 papiers
<p>Chapitre 3 L'auto-assemblage des NCCs dans les films</p>	<p>Films iridescents</p> <ul style="list-style-type: none"> • absorption des additifs (molécules et polymère) sur les NCCs <p>- forte absorption du PEG (0.6 mmol /g_{NCC}) - modérée de l'OBA (18 µmol /g_{NCC}) - nulle pour le PAAS</p> <ul style="list-style-type: none"> • le PEG (10 wt%) améliore <p>-la flexibilité (x2) -la stabilité thermique (+35°C) †</p> <ul style="list-style-type: none"> • le PAAS permet l'ajustement de la coloration (0-160 µmol/g_{NCC}) • l'OBA permet d'obtenir des films fluorescents sous éclairage UV <p>➤ trois niveaux de signature optique (iridescent, polarisé et fluorescent)</p>
	2 papiers
<p>Chapitre 4 Utilisation des nanocelluloses dans les papiers spéciaux</p>	<p>Traitement de surface à base de MFC</p> <ul style="list-style-type: none"> • couchage MFC-TiO₂ permet de réduire de 2.5x la quantité de TiO₂ à opacité constante • valider à l'échelle pilote • détermination du prix seuil des MFCs : 0.7-2.5 €/kg <p>➤ solution vertueuse et économique pour limiter la quantité de TiO₂</p> <p>Fabrication et utilisation des pigments iridescents</p> <ul style="list-style-type: none"> • méthode simple permettant la fabrication de 1 kg pigments iridescents • traitements permettant de limiter la resuspension et le noircissement des pigments <p>-utilisation de NaCl (>25 mM) dans les procédés aqueux -auto desulfation des pigments (séchage sous vide, 60 °C, 2 heures)</p> <p>➤ deux stratégies d'introduction (en masse et en couche) dans le procédé papetier</p>
	2 brevets -2 essais pilote ou industriel -1 papier

Il y a des différences entre les deux types de nanocellulose, *i.e.*, les nanocristaux de cellulose (NCCs) et les microfibrilles de cellulose (MFCs), au niveau de leur morphologie et leur chimie de surface. Il en résulte des propriétés différentes à l'état de suspension et à l'état sec. La propriété remarquable des MFCs à former un réseau d'enchevêtrement est utilisée pour la dispersion des particules. L'auto-assemblage des NCCs a permis d'élaborer des films iridescents. Ces films ont été considérés comme couches modèles et mis en œuvre dans le procédé de fabrication des papiers. Il a été vérifié que :

- L'utilisation des MFCs dans le couchage permettait de réduire fortement la quantité de pigments opacifiants pour les papiers minces,
- Des pigments iridescents pouvaient être utilisés pour obtenir des propriétés d'anti-contrefaçon.

Ces approches innovantes ont été étudiées à l'échelle laboratoire, brevetées et validées à l'échelle pilote ou industrielle.

Listes des tableaux

Tableau 1 – Récapitulatif des propriétés morphologiques et chimiques des deux t.....	286
Tableau 2 - Résultats clés du projet de thèse	297

Listes des figures

Figure 1 – Evolution du nombre annuel de brevets et d’articles scientifiques dédiés aux nanocelluloses (données extraites de Scifinder, Septembre 2014)	273
Figure 2 – Observation par microscopie à force atomique de particules individualisées de nanocellulose : MFC(A) et NCC(B)	274
Figure 3 – Observation de suspensions à 2 % de MFC (A) et NCC (B).	275
Figure 4 – Observation des films de 60 g/m ² de MFC (A) et NCC (B) obtenus par simple coulée et évaporation.....	275
Figure 5 – Schéma de thèse.....	277
Figure 6 – Observation d’un film de 30 g/m ² de MFCs contenant 10 wt% de TiO ₂ . (A) correspondent à la coupe observée par E-SEM (BSE mode) et (B) à la surface du film. Les photos 1 à 4 correspondent à des films de MFCs obtenus avec un taux croissant de TiO ₂ (0, 2, 7 et 20 wt%).	279
Figure 7 - Schéma des trois procédés de production de suspension hybrides de MFC/TiO ₂	279
Figure 8 – Module d’Young spécifique et transparence d’un film de 30 g/m ² contenant 20 wt% de TiO ₂ : comparaison entre les trois approches d’obtention de suspension hybride ainsi qu’avec trois autres matrices polymères.....	280
Figure 9 – Approche envisagée pour améliorer les propriétés barrières d’un film de MFCs.....	281
Figure 10 – Evolution de la perméabilité à l’oxygène en fonction de l’humidité relative pour un film de MFC	281
Figure 11 – Perméabilité à l’oxygène et à la vapeur d’eau pour différents films de nanocellulose de 40 g/m ² : MFC seule, renforcé avec des nanocharges, et avec ou sans traitement thermique.....	283
Figure 12 – Photographie d’un film de NCC iridescent sous illumination et incidence normale (B) et observation en microscopie électronique à balayage de section d’un film à différents grossissement (A, C, et D)	284
Figure 13 – Schéma récapitulatif du Chapitre 3 dédié à l’étude de l’auto-organisation des nanocristaux de cellulose pour la formation de film iridescent.....	285
Figure 14 – Observation des trois signatures optiques d’un film iridescent à base de NCC par analyses spectroscopie UV-visible (a), Microscopie Optique à Lumière Polarisée (b) et une observation sous éclairage UV.....	288
Figure 15 – Approche envisagée pour optimiser la quantité de TiO ₂ dans la formulation des papiers minces	290

Figure 16 – Comparaison entre l'opacité d'un papier couché avec la suspension hybride MFC/TiO ₂ et un papier couché de référence en fonction de la quantité de TiO ₂	291
Figure 17 – Schéma du dispositif pilote utilisée pour les essais d'enduction	292
Figure 18 – Schéma du procédé de fabrication de pigments iridescents à partir d'une suspension de NCC	293
Figure 19 – Observation en microscopie optique des trois différentes granulométries de pigments obtenues au cours du broyage des pigments.....	294
Figure 20 – Récapitulatif des deux post traitements des pigments iridescents et deux exemples d'application permettant l'incorporation des pigments iridescents dans un matériau transparent et flexible	294
Figure 21 – Schéma des deux procédés d'incorporation des pigments iridescents dans un papier de spécialité accompagnée de leur observation au microscope optique : en masse (a) et en couche (b)	295

Références

1. Adkins, "Spacer/extender for titanium dioxide in pigment systems for coatings", Aluminum Company Of America, CA2083397A1 (1992).
2. Ahmadi Achachlouei, "Environmental Impacts of Electronic Media: A Comparison of a Magazine's Tablet and Print Editions", PhD Thesis, KTH Royal Institute of Technology, Sweden (2013).
3. Beck, Bouchard, *et al.*, "Iridescent solid nanocrystalline cellulose films incorporating patterns and their production", Fpinnovations, Can. . WO2010066029A1 (2010).
4. Braun, Baidins, *et al.*, "TiO₂ pigment technology: a review", Progress in Organic Coatings 20(2): 105-138 (1992).
5. Buzea, Pacheco, *et al.*, "Nanomaterials and nanoparticles: sources and toxicity", Biointerphases 2(4): MR17-MR71 (2007).
6. Charreau, L Foresti, *et al.*, "Nanocellulose patents trends: A comprehensive review on patents on cellulose nanocrystals, microfibrillated and bacterial cellulose", Recent patents on nanotechnology 7(1): 56-80 (2013).
7. Cowie, Bilek, *et al.*, "Market projections of cellulose nanomaterial-enabled products—Part 2: Volume estimates", Tappi Journal 13(6) (2014).
8. Dufresne, "Nanocellulose, From Nature to High Performance Tailored Materials", edited by De Gruyter (2012).
9. Henriksson, Henriksson, *et al.*, "An environmentally friendly method for enzyme-assisted preparation of microfibrillated cellulose (MFC) nanofibers", European Polymer Journal 43(8): 3434-3441 (2007).
10. Hu, Choi, *et al.*, "Highly conductive paper for energy-storage devices", Proceedings of the National Academy of Sciences 106(51): 21490-21494 (2009).
11. Iotti, Gregersen, *et al.*, "Rheological Studies of Microfibrillar Cellulose Water Dispersions", Journal of Polymers and the Environment 19(1): 137-145 (2011).
12. Johnson, Thiele, *et al.*, "Lightscattering efficiency white pigments: an analysis of model core-shell pigments vs. optimized rutile TiO₂", Tappi Journal 80(11): 233-239 (1997).
13. Juuti, Koivunen, *et al.*, "Light scattering study from nanoparticle-coated pigments of paper", Colloids and Surfaces A: Physicochemical and Engineering Aspects 352(1-3): 94-98 (2009).
14. Liu and Berglund, "Clay nanopaper composites of nacre-like structure based on montmorillonite and cellulose nanofibers—Improvements due to chitosan addition", Carbohydrate Polymers 87(1): 53-60 (2012).
15. Liu, He, *et al.*, "Antibacterial activities of zinc oxide nanoparticles against *Escherichia coli* O157:H7", Journal of Applied Microbiology 107(4): 1193-1201 (2009).
16. Nelson and Deng, "Enhanced light scattering from hollow polycrystalline TiO₂ particles in a cellulose matrix", Langmuir 24(3): 975-982 (2008).
17. Ranby, "Aqueous colloidal solutions of cellulose micelles", Acta Chem. Scand. (1947-1973) 3: 649-650 (1949).
18. Revol, J.-F., *et al.*, "Solid self-assembled films of cellulose with chiral nematic order and optically variable properties", Tappi Journal 24(5) (1998).

19. Rodriguez, Batlle, *et al.*, "The use of natural essential oils as antimicrobial solutions in paper packaging. Part II", Progress in Organic Coatings 60(1): 33-38 (2007).
20. Saito, Kimura, *et al.*, "Cellulose Nanofibers Prepared by TEMPO-Mediated Oxidation of Native Cellulose", Biomacromolecules 8(8): 2485-2491 (2007).
21. Saito, Nishiyama, *et al.*, "Homogeneous Suspensions of Individualized Microfibrils from TEMPO-Catalyzed Oxidation of Native Cellulose", Biomacromolecules 7(6): 1687-1691 (2006).
22. Samain and Stinga, "Procédé et dispositif de traitement par greffage chromatogénique d'un substrat hydroxyle", WO2013093113A3 (2013).
23. Scott, "Principles of wet end chemistry", edited by Tappi Press Atlanta, Georgia (1996).
24. Sehaqui, Liu, *et al.*, "Fast preparation procedure for large, flat cellulose and cellulose/inorganic nanopaper structures", Biomacromolecules 11(9): 2195-2198 (2010).
25. Siró and Plackett, "Microfibrillated cellulose and new nanocomposite materials: a review", Cellulose 17(3): 459-494 (2010).
26. Sun, Schork, *et al.*, "Water-based polymer/clay nanocomposite suspension for improving water and moisture barrier in coating", Composites Science and Technology 67(9): 1823-1829 (2007).
27. Turbak, Snyder, *et al.*, "Microfibrillated cellulose, a new cellulose product: properties, uses, and commercial potential", Journal of applied polymer science 37: 815-827 (1983).
28. Van Renesse (1997), "Paper based document security-a review". European Conference on Security and Detection. London, England.
29. Vaswani, Koskinen, *et al.*, "Surface modification of paper and cellulose by plasma-assisted deposition of fluorocarbon films", Surface and Coatings Technology 195(2): 121-129 (2005).
30. Wu, Saito, *et al.*, "Ultrastrong and High Gas-Barrier Nanocellulose/Clay-Layered Composites", Biomacromolecules 13(6): 1927-1932 (2012).
31. Zou, Tan, *et al.*, "Flexible, iridescent nanocrystalline cellulose film, and method for preparation", Fpinnovations, Can. . WO2010124378A1 (2010).

Appendix 1

Patents

(19) Organisation Mondiale de la Propriété Intellectuelle
Bureau international



(10) Numéro de publication internationale
WO 2014/033409 A1

1

(43) Date de la publication internationale
6 mars 2014 (06.03.2014)

WIPO | PCT

(51) Classification internationale des brevets :
D21H 17/25 (2006.01) D21H 21/28 (2006.01)
D21H 17/67 (2006.01) D21H 21/52 (2006.01)
D21H 17/00 (2006.01) C09D 101/02 (2006.01)
D21H 19/38 (2006.01) C09D 7/12 (2006.01)

(74) Mandataire : CABINET BEAUMONT; 1, Rue Champollion, F-38000 Grenoble (FR).

(81) États désignés (sauf indication contraire, pour tout titre de protection nationale disponible) : AE, AG, AL, AM, AO, AT, AU, AZ, BA, BB, BG, BH, BR, BW, BY, BZ, CA, CH, CL, CN, CO, CR, CU, CZ, DE, DK, DM, DO, DZ, EC, EE, EG, ES, FI, GB, GD, GE, GH, GM, GT, HN, HR, HU, ID, IL, IN, IS, JP, KE, KG, KN, KP, KR, KZ, LA, LC, LK, LR, LS, LT, LU, LY, MA, MD, ME, MG, MK, MN, MW, MX, MY, MZ, NA, NG, NI, NO, NZ, OM, PA, PE, PG, PH, PL, PT, QA, RO, RS, RU, RW, SA, SC, SD, SE, SG, SK, SL, SM, ST, SV, SY, TH, TJ, TM, TN, TR, TT, TZ, UA, UG, US, UZ, VC, VN, ZA, ZM, ZW.

(84) États désignés (sauf indication contraire, pour tout titre de protection régionale disponible) : ARPO (BW, GH, GM, KE, LR, LS, MW, MZ, NA, RW, SD, SL, SZ, TZ, UG, ZM, ZW), eurasset (AM, AZ, BY, KG, KZ, RU, TJ, TM), europasn (AL, AT, BE, BG, CH, CY, CZ, DE, DK, EE, ES, FI, FR, GB, GR, HR, HU, IE, IS, IT, LT, LU, LV, MC, MK, MT, NL, NO, PL, PT, RO, RS, SE, SI, SK, SM, TR), OAPI (BF, BJ, CF, CG, CI, CM, GA, GN, GQ, GW, KM, ML, MR, NE, SN, TD, TG).

(21) Numéro de la demande internationale : PCT/FR2013/051997

(22) Date de dépôt international : 29 août 2013 (29.08.2013)

(25) Langue de dépôt : français

(26) Langue de publication : français

(30) Données relatives à la priorité : 1258093 30 août 2012 (30.08.2012) FR

(71) Déposants : INSTITUT POLYTECHNIQUE DE GRENOBLE [FR/FR]; 46, Avenue Félix Viallet, F-38000 Grenoble (FR). PAPETERIES DU LEMAN [FR/FR]; 1080, Rue des Vignes Rouges, F-74500 Amphion Les Bains (FR).

(72) Inventeurs : BRAS, Julien; 15, Rue Jean Prévost, F-38000 Grenoble (FR). BELGACEM, Naceur; 53, Chemin des Rivollets, F-38320 Brié Et Angonnes (FR). BARDET, Raphaël; c/o Papeteries Du Lemans, 1080, Rue des Vignes Rouges, F-74500 Amphion-les-Bains (FR). AGUT, Philippe; c/o Papeteries Du Lemans, 1080, Rue des Vignes Rouges, F-74500 Amphion-les-Bains (FR). DUMAS, Jocelyne; c/o Papeteries du Léman, 1080 rue des Vignes Rouges, F-74500 Amphion les Bains (FR).

Publiée : avec rapport de recherche internationale (Art. 21(3))

COUCHE D'OPACIFICATION D'UN SUPPORT PAPIER

Domaine de l'invention

L'invention concerne une composition pigmentaire à base de microfibrilles de cellulose (MicroFibrillated Cellulose, ou MFC) et un procédé d'enduction de cette composition pigmentaire.

Dans de nombreux domaines, on cherche à déposer sur un support une couche d'un matériau conférant à ce support des caractéristiques particulières (aspect, imprimabilité, résistance...). Par souci de simplicité, les exemples donnés ci-après le seront essentiellement dans le domaine de la papeterie et dans le cas où on cherche à conférer à un papier un aspect opaque, notamment dans le cas où celui-ci doit être imprimé. Toutefois, il faut souligner, comme on le verra ci-après que l'invention n'est pas limitée à ce domaine et à cette application particulière.

Exposé de l'art antérieur

Une première solution pour opacifier un papier consiste à introduire pendant la fabrication de ce papier des charges et des pigments dans le matelas fibreux constituant le papier. Ces éléments, se présentant sous forme sèche ou de poudres pré-dispersées en milieu aqueux, peuvent être ajoutés en amont ou en aval de la formation du matelas fibreux. Parmi les

WO 2014/033409 A1

(54) Title : OPACIFYING LAYER FOR A PAPER MEDIUM

(54) Titre : COUCHE D'OPACIFICATION D'UN SUPPORT PAPIER

(57) Abstract : The invention relates to a layer for coating a medium, comprising a mixture of cellulose nanofibres and grains of a filler or pigment, in which the cellulose nanofibres have a diameter of less than 50 nm and a shape factor greater than 30, and at least 50% of the grains have a size smaller than 500 nm.

(57) Abstré : L'invention concerne une couche de revêtement d'un support comprenant un mélange de nanofibres de cellulose et de grains d'une charge ou d'un pigment, dans laquelle : les nanofibres de cellulose ont un diamètre inférieur à 50 nm et un facteur de forme supérieur à 30, et au moins 50 % des grains ont une dimension inférieure à 500 nm.

2

3

différentes charges et pigments utilisés, on peut mentionner des carbonates de calcium broyés ou précipités, du kaolin natif ou calciné, du talc, du dioxyde de titane (TiO₂).

Pour opacifier un support mince, le TiO₂ est le pigment le plus efficace parmi les pigments utilisés car il possède d'excellentes propriétés de diffusion de la lumière. En effet il possède un indice de réfraction élevé (2,55 à 2,70) par rapport aux autres charges.

Néanmoins, l'introduction de charges ou de pigments opacifiants dans une pâte à papier présente de nombreux inconvénients parmi lesquels on peut mentionner les suivants :

- détérioration des caractéristiques mécaniques (longueur de rupture, éclatement, déchirure et rigidité),
- mauvaise rétention des pigments par le matelas fibreux du papier, d'où il résulte un entraînement dans les eaux blanches c'est-à-dire les eaux d'égouttage recyclées,
- augmentation de la masse volumique,
- augmentation de la quantité d'additifs chimiques nécessaire pour le procédé de fabrication (agent de floculation, de rétention...) ou pour les propriétés finales du papier (collage, résistance à l'état sec ou humide...).

Pour les supports les plus légers (25-35 g/m²), la quantité nécessaire de dioxyde de titane (TiO₂) requise pour atteindre une opacité acceptable peut représenter jusqu'à 10 % (massique). Cependant, du fait de leur faible dimension et de leur densité élevée (3,9 à 4,2), les pigments de TiO₂ ont une très faible rétention pouvant atteindre moins de 50 % même en utilisant un système optimisé de récupération des eaux résiduaires.

De plus, le TiO₂ est un pigment très cher, les sources d'approvisionnement en titane sont limitées géographiquement, et les procédés d'extraction et de purification du titane sont polluants. La réduction de la consommation de TiO₂ présente un double intérêt, à la fois économique et environnemental.

Une deuxième solution pour réaliser une opacification consiste à déposer une couche supplémentaire sur au moins une face du papier. La couche supplémentaire est déposée à partir de saucées de couchage (un mélange en suspension aqueuse). Les saucées de couchage couramment utilisées sont des mélanges de liants tels que des latex (acrylique ou styrène-butadiène) ou des polymères hydrosolubles (amidon, CMC, PVA, caséine) et de charges pigmentaires minérales (carbonate de calcium broyé ou précipité, kaolin, talc, TiO₂) ou organiques. Certains adjuvants comme des dispersants, des azurants optiques, des antimousses, des insolubilisants, des lubrifiants, etc. peuvent être aussi ajoutés. Cela permet entre autres d'améliorer l'état de surface du papier, son opacité, son imprimabilité ou de lui conférer des propriétés additionnelles (barrière aux graisses, à l'eau...).

Dans le cas où on recherche une opacification et où la saucée de couchage contient du TiO₂, la quantité nécessaire de TiO₂ requise pour atteindre une opacité acceptable peut, ici encore, représenter jusqu'à 10 % (massique). Même alors, l'utilisation de charges opacifiantes telles que le TiO₂ dans les saucées de couchage traditionnelles n'est cependant pas adaptée aux procédés d'enduction traditionnels car les pigments ont tendance à s'agglomérer, ce qui génère des hétérogénéités dans le traitement de surface et entraîne des variations locales d'opacité. De plus, et du fait de sa forte abrasivité le TiO₂ entraîne une usure prématurée des dispositifs d'enduction.

Il est également connu, pour protéger, étanchéifier, colorer des supports papier, de les revêtir d'un tapis de microfibrilles de cellulose, MFC, ou cellulose microfibrillée (en anglais MicroFibrillated Cellulose) additionnées notamment d'un pigment. Un tel procédé est décrit dans la demande de brevet WO2011/14877. Néanmoins cette demande de brevet ne propose pas l'utilisation de ce procédé pour l'opacification d'un support papier et notamment d'un support papier fin et ne précise aucune caractéristique dimensionnelle ni pour les MFC ni pour les pigments.

Il existe donc un besoin d'une structure de couche d'opacification d'un support papier fin qui assure une opacification satisfaisante et n'entraîne pas une augmentation significative de l'épaisseur et du poids par unité de surface du papier.

Résumé

Pour satisfaire à ce besoin et à d'autres, on propose ici d'utiliser des microfibrilles de cellulose (MFC) de dimensions submicrométriques qui seront appelées nanofibrilles de cellulose ou NFC (NanoFibrillated Cellulose). Ces nanofibrilles de cellulose ont un diamètre inférieur à 50 nm avec un facteur de forme supérieur à 30 (par exemple une longueur de l'ordre de 1 µm). Une dispersion de NFC se présente sous la forme d'un gel transparent ou semi transparent à une concentration comprise entre 2 et 4 %. Au-delà, cette dispersion aura tendance à s'agglomérer et à ne plus être homogène.

Un mode de réalisation de la présente invention prévoit une couche de revêtement d'un support comprenant un mélange de nanofibres de cellulose et de grains d'une charge ou d'un pigment, dans laquelle les nanofibres de cellulose ont un diamètre inférieur à 50 nm et un facteur de forme supérieur à 30, et au moins 50 % des grains ont une dimension inférieure à 500 nm.

Un mode de réalisation de la présente invention prévoit une couche d'opacification d'un support papier comprenant un mélange de nanofibres de cellulose et de grains de TiO₂, dans laquelle les nanofibres de cellulose ont un diamètre inférieur à 30 nm, et au moins 50 % des grains de TiO₂ ont une dimension inférieure à 500 nm.

Selon un mode de réalisation de la présente invention, les grains de TiO₂ sont de structure rutile.

Selon un mode de réalisation de la présente invention, les nanofibres de cellulose ont une longueur supérieure à 1 µm.

Selon un mode de réalisation de la présente invention, le support papier a un grammage de 10 à 40 g/m² et la couche a un grammage à l'état anhydre de 0,5 à 3 g/m² par face enduite.

Selon un mode de réalisation de la présente invention, la proportion massique entre les grains de TiO₂ et les nanofibres de cellulose est située dans une plage de 10 à 50 %.

Selon un mode de réalisation de la présente invention, l'épaisseur de la couche d'opacification a au minimum 3 fois le diamètre moyen des pigments opacifiants et au maximum 10 % de l'épaisseur du support à opacifier.

Un mode de réalisation de la présente invention prévoit une feuille de papier d'un grammage de 10 à 40 g/m² revêtue sur au moins une face d'une couche d'opacification telle que ci-dessus.

Un mode de réalisation de la présente invention prévoit une suspension aqueuse destinée à la formation d'une couche homogène sur un support telle que ci-dessus, dans laquelle la viscosité de la suspension est comprise dans une plage de 1000 à 2000 mPa.s.

Selon un mode de réalisation de la présente invention, le pigment est composé de particules minérales ou organiques choisies parmi les carbonates de calcium broyés ou précipités (calcite ou aragonite) et les dioxydes de titane (rutile ou anatase) ainsi que tout mélange des deux groupes.

Selon un mode de réalisation de la présente invention, le pigment est dans une proportion de 10 à 50 % en poids par rapport aux nanofibres de cellulose.

Un mode de réalisation de la présente invention prévoit un procédé de préparation d'une suspension aqueuse telle que ci-dessus, comprenant les étapes successives consistant à introduire sous forte agitation mécanique et à température ambiante des nanofibres de cellulose, et à introduire sous forte agitation mécanique et à température ambiante des pigments, la quantité d'eau étant ajustée pour que la suspension pigmentaire ait une viscosité comprise entre 1000 et 2000 mPa.s.

Brève description des dessins

Ces objets, caractéristiques et avantages, ainsi que d'autres seront exposés en détail dans la description suivante de modes de réalisation particuliers faite à titre non limitatif en relation avec les figures jointes parmi lesquelles :

la figure 1 représente une cuve d'agitation contenant une suspension de NFC et de TiO₂ ; et

la figure 2 représente un support papier revêtu d'une couche d'opacification.

Description détaillée

Les inventeurs ont cherché à obtenir une couche d'opacification sur un support papier en partant des enseignements de la demande de brevet WO 2011/14877 et ont constaté que les résultats obtenus n'étaient généralement pas satisfaisants. Les essais réalisés par les inventeurs ont montré qu'il n'était possible d'obtenir une couche d'opacification satisfaisante que si certaines conditions particulières étaient satisfaites en ce qui concerne au moins certaines des caractéristiques suivantes :

- la viscosité de la suspension de MFC pigmentaire à partir de laquelle est formée l'enduction de la couche recherchée,
- le ratio pigment/MFC dans la suspension,
- la dimension et la nature chimique des pigments,
- les propriétés morphologiques (diamètre et facteur de forme) des MFC, et/ou
- l'épaisseur du film déposé.

Ces conditions particulières vont être exposées ci-après.

La figure 1 représente une cuve 1 contenant une suspension pigmentaire 2 comprenant un mélange de MFC 4 et de pigments 6 obtenu à partir d'un dispositif d'agitation mécanique non représenté.

La figure 2 illustre un support fibreux 10, par exemple du papier, revêtu d'une couche 12 obtenue par enduction et séchage à partir de la suspension 2.

On notera que, en figures 1 et 2, les MFC 4 et les pigments 6 sont illustrés uniquement de façon à faire comprendre la présente description mais ne sont pas représentés à l'échelle, ni en ce qui concerne leurs dimensions ni en ce qui concerne leurs proportions.

On constate, comme l'illustre très schématiquement la figure 2, que l'on obtient une dispersion très régulière des pigments fins repartis de manière homogène dans le réseau nanofibreux de MFC si certaines conditions particulières sont respectées.

En particulier, il convient que la suspension pigmentaire présente les caractéristiques suivantes :

- le diamètre des MFC est inférieur à 50 nm (ce sont des NFC) et leur facteur de forme est supérieur à 30,
- les particules de pigments fins ont au moins 50 % de leurs diamètres inférieurs à 500 nm ($d_{50} < 500$ nm), et
- la viscosité de la suspension pigmentaire se situe entre 1000 et 2000 mPa.s.

L'ordre d'introduction des deux composés joue un rôle important dans la qualité de la dispersion pigmentaire. Il est préférable d'introduire en premier lieu les NFC tout en procédant à une agitation mécanique pour fluidifier et homogénéiser la suspension aqueuse. Ensuite il convient d'introduire progressivement les pigments fins tout en maintenant l'agitation pendant au moins 5 minutes.

Le choix d'une plage de viscosité située entre 1000 et 2000 mPa.s (viscosité Brookfield mesurée à 23°C) pour la suspension pigmentaire est réalisé pour limiter la sédimentation et l'agglomération des pigments fins et permettre son pompage vers un dispositif d'enduction.

La suspension pigmentaire peut-être déposée par différentes méthodes d'enduction en milieux aqueux comme par exemple par couchage par transfert de film, couchage à lame, couchage rideau...

Bien que l'on ait décrit précédemment une couche d'opacification déposée sur une seule face du matériau, il peut être envisagé de déposer cette couche simultanément sur les deux faces.

L'utilisation d'une couche d'opacification d'un support papier telle que décrite ici présente par rapport aux procédés connus d'opacification par introduction de pigments fins comme le TiO₂ dans la masse du papier les avantages suivants :

- diminution de la quantité de TiO₂ utilisé,
- diminution de la quantité d'additifs chimiques requis dans le support de base (dispersant, agent de rétention,...),
- facilitation du traitement des eaux de recirculation (circuit primaire et secondaire) et réduction de l'impact final du TiO₂ sur le recyclage des boues et effluents.

De plus, la composition de couche proposée ici présente des avantages par rapport à une formulation de couche traditionnelle :

- agents de couchage d'origine biologique et biodégradables,
- aucun liant n'est nécessaire, les NFC permettant de remplacer le liant (amidon et latex) grâce à la création d'un réseau de nanofibrilles dans lequel est dispersé le pigment fin opacifiant,
- l'agent épaississant (dérivé issu de la pétrochimie) n'est plus nécessaire compte tenu d'un comportement rhéologique de la suspension de NFC.

Par rapport aux saucées de couchage traditionnelles, les saucées composées de NFC et de pigments dans les conditions décrites ici ont une meilleure stabilité dans le temps (pas de rétrogradation ou prise en masse de la saucée de couchage) et sont capables de supporter de larges variations de températures sans aucune altération. De plus, le stockage à froid de la saucée de couchage est possible et ce pendant une longue période et sans agitation.

Cellulose (NanoCristaux de Cellulose). MCC provient des termes anglo-saxons (MicroCristaux de Cellulose).

2. Suspension pigmentaire

Les suspensions de nanocelluloses (NFC, MFC, NCC, MCC) ont été préalablement homogénéisées pendant 2 minutes à 6500 tr/min. Leur concentration initiale est située entre 2,5 et 3 %.

Des pigments ont été ajoutés pour réaliser des suspensions pigmentaires. Dans le cas où les pigments sont de la poudre de TiO₂ rutile (Ti-pure RPS Vantage®, DuPont®) ou anatase (TionaAT-1®, Millenium Chemicals®), on a essayé :

- des pigments "fins" c'est-à-dire des pigments dont au moins 50% ont une dimension inférieure à 500 nm, et
- des pigments "gros" obtenus par filtration de la suspension de pigments fins (toile filtrante) permettant d'éliminer les pigments les plus fins de dimension inférieure à 500 nm pour obtenir des pigments dont au moins 50% ont une dimension comprise entre 500 nm et 1 µm.

3. Réalisation de films

A partir des suspensions pigmentaires, on a réalisé des films d'une épaisseur correspondant à une masse surfacique (grammage) de l'ordre de 30 g/m² avec une proportion de 90% (massique) de nanocellulose et 10% (massique) de pigments, par évaporation dans une étuve (50°C) pendant 4 à 5 heures. Ensuite, ces films ont été séchés à l'air libre dans une salle conditionnée (23°C, 50% HR) pendant 12 heures.

L'homogénéité de la dispersion a été évaluée en utilisant des images réalisées par microscopie électronique à balayage (SEM, de l'anglais Scanning Electron Microscopy) en électrons secondaires de manière à obtenir une image avec un bon contraste entre la cellulose et les pigments minéraux. Les zones "claires" correspondent aux zones contenant des éléments minéraux (TiO₂) et les zones "sombres" correspondent à des zones contenant des éléments organiques (cellulose).

De préférence, la proportion massique entre les pigments fins utilisés et les microfibrilles de cellulose est située dans une plage de 10 à 90 %, et c'est ce qui donne les résultats en termes d'opacification indiqués ici. De plus, les grains de TiO₂ sont de préférence de structure rutile plutôt qu'anatase pour améliorer le pouvoir opacifiant.

La couche d'opacification décrite ci-dessus peut être soumise à des traitements supplémentaires pendant le procédé de fabrication du papier ou hors ligne comme :

- un couchage additionnel,
- un traitement thermomécanique dit calandrage pour améliorer l'état de surface du papier,
- une imprégnation d'une résine (organosilane) pour obtenir ainsi un matériau laminé opaque.

15 ESSAIS COMPARATIFS

1. Divers types de MFC

Diverses suspensions de cellulose micro- ou nano-fibrillée, appelées ici NFC, MFC, NCC et MCC, ont été essayées pour mettre en évidence l'importance de la morphologie et de la taille des nanocelluloses. Leurs caractéristiques sont données par le tableau 1 ci-dessous.

Tableau 1

	NFC	MFC	NCC	MCC
morphologie	fibrille	fibrille	cristaux	granulaire
longueur	≈0,2-3µm	≈50µm	100-200nm	
diamètre	10nm<.<50nm	1µm<.<300µm	5-20nm	9µm
facteur de forme	>30	5-10		
taux de cristallinité		71%	80%	75%
concentration massique (%)	2,7%	3,0%	2,5%	9,8%

NFC provient des termes anglo-saxons NanoFibrillated Cellulose (NanoCellulose Fibrillée). MFC provient des termes anglo-saxons MicroFibrillated Cellulose (Cellulose Micro-Fibrillée). NCC provient des termes anglo-saxons NanoCrystalline

La qualité de la dispersion dans le film a été obtenue en réalisant un traitement d'image des coupes des films avec le logiciel ImageJ®. Ce logiciel a été utilisé pour évaluer l'aire et le diamètre moyen des particules et/ou agglomérats de TiO₂. A partir des images acquises, on a obtenu que, pour une poudre pigmentaire identique et une même proportion massique dans le film, plus le diamètre moyen sera proche de celui mesuré par granulométrie, plus la dispersion (à l'état sec) sera bonne et donc plus l'opacité sera homogène et élevée.

Le tableau 2 indique l'opacité du film obtenu et la qualité de la dispersion de pigments dans le film pour un mélange contenant 10% de TiO₂ et 90% de MFC pour divers types de MFC et divers types de pigments, la viscosité de la suspension de départ étant de 1500 mPa.s.

Tableau 2

Essai	COMPOSITION PIGMENTAIRE DU FILM		Paramètres des nanocelluloses			Opacité	QUALITE DE LA DISPERSION	PRESENCE DE FIBRES MACROSCOPQUES A LA SURFACE DU FILM
	NANOCCELLULOSE (90%)	PIGMENT FIN (10%)	LONGUEUR MOYENNE	forme	FACTEUR DE FORME			
1	NFC	TiO ₂ rutile (d50=0,5)	0,2-3µm	nanofibrille	>30	81,0±0,5	++	non
2	NCC	TiO ₂ rutile (d50=0,5)	150-250 nm	nanocristal	5-10	74,0±0,5	-	non
3	50% NFC - 50% MFC	TiO ₂ rutile (d50=0,5)	0,2-300 µm	nanofibrille	5-30	80,5±0,3	+	non
4	MFC	TiO ₂ rutile (d50=0,5)	1-300µm	microfibrille	10-40	78,5±0,3	-	oui
5	MCC	TiO ₂ rutile (d50=0,5)	1-300µm	granulaire	3-4	-	-	non-formation du film impossible

On constate que le meilleur résultat en termes d'homogénéité est obtenu dans le cas de l'essai 1 : NFC de facteur de forme supérieur à 30 et pigments fins. Ce résultat s'accompagne des meilleures performances en matière d'opacité du film.

12

On a également testé l'impact de la viscosité des suspensions pigmentaires sur la qualité du film. Les résultats en sont donnés dans le tableau 3.

Tableau 3

Essai	Viscosité mPa.s	Qualité de la dispersion dans le film	Opacité	Observations
1-0	2650+/-350	++	81.5±0.5	Présence de bulles d'air
1-1	1950+/-200	++	81.0±0.2	OK
1-2	1400+/-150	++	51.5±0.3	OK
1-3	450+/-50	-	80.2±0.7	OK
1-4	280+/-100	-	79.9±0.5	OK

Ainsi, en faisant varier la viscosité de la suspension pigmentaire et pour un même ratio de NFC/TiO₂ et une masse surfacique des films identique (30 g/m²), il a été constaté expérimentalement que :

- au-delà de 2000 mPa.s, la suspension pigmentaire se présente sous la forme d'une pâte. Il a été constaté expérimentalement que l'agitation mécanique introduit des bulles d'air qui se retrouvent alors piégées dans le film et nuisent à une utilisation ultérieure du film,

- pour une faible valeur de viscosité (< 500 mPa.s), la suspension pigmentaire est très fluide, mais des images acquises au microscopique électronique ont montré qu'une partie du TiO₂ avait tendance à sédimenter, se traduisant par une plus faible opacité.

On a également testé l'impact de la nature et du polymorphisme des particules de TiO₂. Les résultats en sont donnés dans le tableau 4.

Tableau 4

Essai	Composition pigmentaire du film				Opacité	Qualité de la dispersion
	NFC	TiO ₂ rutile d ₅₀ ±0.50 µm	TiO ₂ rutile d ₅₀ ±0.97 µm	TiO ₂ anatase d ₅₀ ±0.50 µm		
1	90	10			81.5±0.5	++
2	90	5	5		80.8±0.1	++
3	90		10		80.9±0.2	-
4	90			10	80.2±0.5	++

13

Pour un même ratio de NFC/TiO₂, une viscosité ajustée à 1500 mPa.s, une masse surfacique identique (30 g/m²), il a été constaté expérimentalement que :

- l'opacité la plus élevée du film est atteinte avec un mélange de TiO₂ rutile ayant un d₅₀≈ 0.50µm,
- pour une dimension de particule équivalente, le TiO₂ rutile confère une meilleure opacité par rapport à l'autre forme polymorphique du TiO₂, l'anatase.

4. Réalisation de couches minces sur papier

Pour la suite des exemples, les grammages des couches (g/m²) correspondent à la masse de couche anhydre par unité de surface.

Des sauces de couchage ont été préparées de la même manière en respectant les ordres d'introduction suivants : pigments (i), liants (ii), et additifs (iii), sauf dans le cas des sauces contenant une proportion de NFC. Dans ce cas, les NFC ont été introduites en premier.

Les sauces de couchage ont été enduites sur du papier avec un appareil d'enduction à lame de laboratoire en faisant varier les paramètres de pression et d'épaisseur de lame qui permettent d'obtenir un poids de couche situé entre 1,5 et 2,0 g/m²/face tout en obtenant un état de surface optimal.

Les papiers enduits ont ensuite été séchés pendant trois minutes à 110°C (sècheur de laboratoire, Techpap®). Ce dispositif de séchage permet de sécher les échantillons par conduction thermique et permet d'obtenir un séchage de l'échantillon sans retrait. Après séchage, les échantillons sont immédiatement conditionnés pendant 24 heures à 23°C et 50 % d'humidité relative.

Le support de base utilisé ici est un papier issu d'une production industrielle, il n'est ni couché ni calandré et présente les caractéristiques indiquées dans le tableau 5.

14

Tableau 5

PROPRIETES	Propriétés		Unité	Valeur
CONTEXTURE	Épaisseur		µm	30±2
	Volume massique		cm ³ /g	1,10±0
	Grammage		g/m ²	27,5±0,2
COMPOSITION	Ratio fibres longues/fibres courtes		%	75-25
	Taux de charges		%	20±4
	Opacité		%	82,5±0,1
PROPRIETES OPTIQUES	Blancheur		%	79,3±0,3

Des essais ont été effectués pour des sauces ayant les formulations F1 à F7 indiquées dans le tableau 6.

Tableau 6

Formulation	FORMULATION DE LA SAUCE PIGMENTAIRE								COMPORTEMENT RHEOLOGIQUE DES SAUCES			
	Pigments				Liants				Additifs	Matière sèche	pH	Viscosité
	GCC	Kaolin	TiO ₂	PCC	Latex	Amidon	NFC	Agent épaississant				
F1	40	60			7	15		0,15	25,2%	9,5	1250	
F2			100		7	15		0,30	25,0%	9,5	1150	
F3				100	7	15		0,30	25,0%	9,5	1250	
F4			82				18		13,1%	7	>2000	
F5			50				50		5,2%	7	>2000	
F6			10				90		2,9%	7	>2000	
F7				82			18		8,4%	7	>2000	

Des essais plus détaillés ont été faits pour des suspensions de NFC et de TiO₂ et des suspensions de mélange de liants et d'additif et de TiO₂, en faisant varier les pourcentages de TiO₂. Les résultats en sont donnés dans les tableaux 7 et 8.

15

Tableau 7

Essai	Composition		Opacité
	NFC	TiO ₂	
1	90	10	83.1±0.5
2	80	20	84.5±0.5
3	70	30	85.0±0.5
4	60	40	85.0±0.2
5	50	50	85.8±0.9
6	30	70	85.6±0.2
7	20	80	85.8±0.1

Tableau 8

Essai	Composition		Opacité
	Liant & additifs	TiO ₂	
C1	90	10	82.2±0.8
C2	80	20	83.1±0.1
C3	70	30	83.0±0.6
C4	60	40	83.5±0.4
C5	50	50	83.5±0.1
C6	30	70	83.2±0.0
C7	20	80	83.4±0.3

Le tableau 7 montre qu'avec une suspension de NFC et de TiO₂ dont la proportion de TiO₂ est supérieure à 50 %, on obtient une opacité sensiblement constante, supérieure à 85,5 %, valeur qui ne peut pas être obtenue avec des mélanges classiques de dispersants et de liants.

Le tableau 9 présente les résultats (blancheur et opacité tels que définies par la norme ISO) obtenus sur une feuille de papier telle que définie au tableau 5 avec les différentes sauces d'enduction F1 à F7 définies au tableau 6, pour un grammage déposé compris entre 1,5 et 2,0 g/m² :

Tableau 9

Formulation	GRAMMAGE DEPOSE (g/m ²)	OPACITE	BLANCHEUR
F1	2,0±0,1	82,6±0,3	77,3
F2	1,7±0,4	83,4±1,2	78,2
F3	1,8±0,4	82,8±0,5	77,9
F4	2,1±0,4	85,8±0,5	80,5
F5	1,5±0,4	84,5±0,5	78,2
F6	1,7±0,4	83,1±0,5	77,2
F7	1,6±0,4	82,2±0,5	77,6

Pour une couche de formulation F1 classiquement utilisée pour l'impression offset des papiers minces, le niveau d'opacité est de 82,6 pour une blancheur de 77,3 pour 2,0 g/m².

En remplaçant, le couple pigmentaire Kaolin-GCC par le TiO₂ (formulation F2), le gain est de 1 % et 1,2 % pour l'opacité et la blancheur, respectivement. Cependant la sauce de couchage n'est pas adaptée à un couchage classique. En effet, un phénomène d'agglomération du TiO₂ a été constaté. L'agglomération du TiO₂ se traduit par un état de surface hétérogène et d'importantes variations d'opacité (cf. écart-type).

En remplaçant, le couple pigmentaire Kaolin-GCC par le PCC (formulation F3) le gain d'opacité est de 0,2% et 0,8% pour l'opacité et la blancheur respectivement.

Les couches de formulation F4, F5, F6 sont les formulations pigmentaires comprenant un mélange de NFC et de TiO₂ avec différents ratios de TiO₂ et NFC. Le gain d'opacité par rapport à une formulation contenant le même pourcentage de TiO₂ (voir formulations F4 et F2) est de 3,0 % pour l'opacité et la blancheur.

Pour un pourcentage de TiO₂ (formulation F5) 33 % plus faible par rapport à la formulation F2, une augmentation de l'opacité de près de 1 % a été constatée.

Pour un pourcentage de TiO₂ de près de 83 % plus faible par rapport à la formulation F2, un niveau équivalent d'opacité a été constaté.

Un niveau équivalent d'opacité a été constaté pour une couche NFC-PCC (formulation F7) par rapport à une couche classique contenant la même proportion de TiO₂.

Des tests complémentaires de rigidité à la flexion et d'imprimabilité ont montré qu'il n'y avait aucun impact (amélioration/dégradation) sur ces deux propriétés essentielles pour les papiers minces destinés à être imprimés en offset.

Bien que les exemples donnés ci-dessus l'aient été essentiellement dans le domaine de la papeterie dans le cas où on cherche à conférer à un papier un aspect opaque et dans le cas où le pigment est du TiO₂, l'homme de l'art notera que l'invention s'applique de façon générale au cas où l'on souhaite déposer sur un support une couche comprenant une répartition homogène de pigments ou autre charge. Il faut alors utiliser les relations dimensionnelles indiquées ici, tant pour les MFC (NFC) que pour les charges.

REVENDICATIONS

1. Couche d'opacification d'un support papier comprenant un mélange de nanofibres de cellulose et de grains d'un pigment composé de particules minérales ou organiques choisies parmi les carbonates de calcium broyés ou précipités, calcite ou aragonite, et les dioxydes de titane, rutilite ou anatase, ainsi que tout mélange des deux groupes, dans laquelle :

les nanofibres de cellulose ont un diamètre inférieur à 30 nm et un facteur de forme supérieur à 30, et

au moins 50 % des grains ont une dimension inférieure à 500 nm,

la proportion massique entre les grains et les nanofibres de cellulose est située dans une plage de 10 à 50 %, et

l'épaisseur de la couche d'opacification a au minimum 3 fois le diamètre moyen des pigments opacifiants.

2. Couche d'opacification selon la revendication 1, dans laquelle les grains de pigment sont des grains de TiO₂ de structure rutilite.

3. Couche d'opacification selon la revendication 1 ou 2, dans laquelle le support papier a un grammage de 10 à 40 g/m² et la couche a un grammage à l'état anhydre de 0,5 à 3 g/m² par face enduite.

4. Couche d'opacification selon l'une quelconque des revendications 1 à 3, dans laquelle l'épaisseur de la couche d'opacification est au maximum égale à 10 % de l'épaisseur du support à opacifier.

5. Feuille de papier d'un grammage de 10 à 40 g/m² revêtue sur au moins une face d'une couche d'opacification selon l'une quelconque des revendications 1 à 4.

6. Suspension aqueuse destinée à la formation d'une couche homogène sur un support selon l'une quelconque des revendications 1 à 5, dans laquelle la viscosité de la suspension est comprise dans une plage de 1000 à 2000 mPa.s.

7. Suspension selon la revendication 6, dans laquelle le pigment est dans une proportion de 10 à 50 % en poids par rapport aux nanofibres de cellulose.

8. Procédé de préparation d'une suspension aqueuse selon la revendication 6 ou 7, comprenant les étapes successives suivantes :

introduire sous forte agitation mécanique et à température ambiante des nanofibres de cellulose, et

introduire sous forte agitation mécanique et à température ambiante des pigments,

la quantité d'eau étant ajustée pour que la suspension pigmentaire ait une viscosité comprise entre 1000 et 2000 mPa.s.

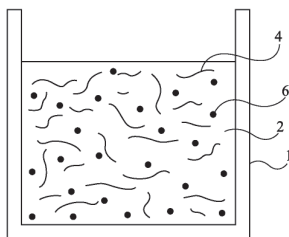


Fig 1

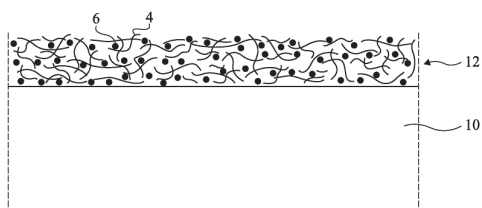


Fig 2

INTERNATIONAL SEARCH REPORT

International application No
PCT/FR2013/051997

A. CLASSIFICATION OF SUBJECT MATTER Inv. D21H17/25 D21H17/67 D21H17/00 D21H19/38 D21H21/28 D21H21/52 C09D101/02 C09D7/12		
B. FIELDS SEARCHED Minimum documentation searched (classification system followed by classification symbols) D21H C09D Documentation searched other than minimum documentation to the extent that such documents are included in the fields searched Electronic data base consulted during the international search (name of data base and, where practicable, search terms used) EPO-Internal, WPI Data		
C. DOCUMENTS CONSIDERED TO BE RELEVANT		
Category*	Citation of document, with indication, where appropriate, of the relevant passages	Relevant to claim No.
A	EP 1 323 674 A1 (NITTETSU MINING CO LTD [JP]) 2 July 2003 (2003-07-02) claims 1-12 paragraphs [0090], [0091]	1-8
A	WO 2010/142846 A1 (UPM KYMMENE CORP [FI]; STORA ENSO OYJ [FI]; HENTZE HANS-PETER [FI]; S1) 16 December 2010 (2010-12-16) claims 1-21	1-8
A	WO 2010/112519 A1 (OMYA DEVELOPMENT AG [CH]; GANE PATRICK A C [CH]; SCHOELKOPF JOACHIM [C]) 7 October 2010 (2010-10-07) claims 1-24 page 20, line 16 - line 17 page 5, line 9 - line 10	1-8
<input checked="" type="checkbox"/> Further documents are listed in the continuation of Box C. <input checked="" type="checkbox"/> See patent family annex.		
* Special categories of cited documents : "A" document defining the general state of the art which is not considered to be of particular relevance "E" earlier application or patent but published on or after the international filing date "L" document which may throw doubts on priority claim(s) or which is cited to establish the publication date of another citation or other special reason (as specified) "O" document referring to an oral disclosure, use, exhibition or other means "P" document published prior to the international filing date but later than the priority date claimed		"T" later document published after the international filing date or priority date and not in conflict with the application but cited to understand the principle or theory underlying the invention "X" document of particular relevance; the claimed invention cannot be considered novel or cannot be considered to involve an inventive step when the document is taken alone "Y" document of particular relevance; the claimed invention cannot be considered to involve an inventive step when the document is combined with one or more other such documents, such combination being obvious to a person skilled in the art "Z" document member of the same patent family
Date of the actual completion of the international search		Date of mailing of the international search report
28 October 2013		08/11/2013
Name and mailing address of the ISA/ European Patent Office, P.B. 5818 Patentaan 2 NL - 2280 HV Rijswijk Tel. (+31-70) 340-2040, Fax: (+31-70) 340-3016		Authorized officer Ponsaud, Philippe

INTERNATIONAL SEARCH REPORT

International application No
PCT/FR2013/051997

C(Continuation). DOCUMENTS CONSIDERED TO BE RELEVANT		
Category*	Citation of document, with indication, where appropriate, of the relevant passages	Relevant to claim No.
A	WO 2010/125247 A2 (UPM KYMMENE CORP; LAINE JÄNNE [FI]; OESTERBERG MONIKA [FI]; DELPHINE M) 4 November 2010 (2010-11-04) page 5, line 25 - line 29	1-8
A	WO 2010/142845 A1 (UPM KYMMENE CORP [FI]; STORA ENSO OYJ [FI]; HENTZE HANS-PETER [FI]; S1) 16 December 2010 (2010-12-16) claims 1-25	1-8

INTERNATIONAL SEARCH REPORT

Information on patent family members

International application No
PCT/FR2013/051997

Patent document cited in search report	Publication date	Patent family member(s)	Publication date
EP 1323674 A1	02-07-2003	AU 6943001 A	14-01-2002
		CN 1444543 A	24-09-2003
		EP 1323674 A1	02-07-2003
		JP 3392109 B2	31-03-2003
		JP 2002029739 A	29-01-2002
		US 2003121451 A1	03-07-2003
		WO 0202462 A1	10-01-2002
		WO 2010142846 A1	16-12-2010
		CA 2764223 A1	16-12-2010
		EP 2440705 A1	18-04-2012
FI 20095634 A	09-12-2010		
JP 2012529572 A	22-11-2012		
US 2012132380 A1	31-05-2012		
WO 2010142846 A1	16-12-2010		
WO 2010112519 A1	07-10-2010	AR 075960 A1	11-05-2011
		CA 2755493 A1	07-10-2010
		CN 102378839 A	14-03-2012
		CO 6450680 A2	31-05-2012
		EP 2236664 A1	06-10-2010
		EP 2414584 A1	08-02-2012
		JP 2012522145 A	20-09-2012
		KR 20120004478 A	12-01-2012
		RU 2011143811 A	10-05-2013
		TW 201038788 A	01-11-2010
		US 2012094953 A1	19-04-2012
		UY 32533 A	29-10-2010
		WO 2010112519 A1	07-10-2010
		WO 2010125247 A2	04-11-2010
CN 102439226 A	02-05-2012		
EP 2425057 A2	07-03-2012		
EP 2615207 A1	17-07-2013		
EP 2615208 A1	17-07-2013		
FI 20095480 A	30-10-2010		
JP 2012525509 A	22-10-2012		
KR 20120014573 A	17-02-2012		
RU 2011148392 A	10-06-2013		
US 2012132383 A1	31-05-2012		
WO 2010125247 A2	04-11-2010		
WO 2010142845 A1	16-12-2010	CA 2764221 A1	16-12-2010
		EP 2440704 A1	18-04-2012
		FI 20095635 A	09-12-2010
		JP 2012529571 A	22-11-2012
		US 2012132381 A1	31-05-2012
		WO 2010142845 A1	16-12-2010

RAPPORT DE RECHERCHE INTERNATIONALE

Demande internationale n°
PCT/FR2013/051997

A. CLASSEMENT DE L'OBJET DE LA DEMANDE INV. D21H17/25 D21H17/67 D21H17/00 D21H19/38 D21H21/28 D21H21/52 C09D101/02 C09D7/12			
Selon la classification internationale des brevets (CIB) ou à la fois selon la classification nationale et la CIB			
B. DOMAINES SUR LESQUELS LA RECHERCHE A PORTE Documentation minimale consultée (système de classification suivi des symboles de classement) D21H C09D			
Documentation consultée autre que la documentation minimale dans la mesure où ces documents relèvent des domaines sur lesquels a porté la recherche			
Base de données électronique consultée au cours de la recherche internationale (nom de la base de données, et si celle-ci est réalisable, termes de recherche utilisés) EPO-Internal, WPI Data			
C. DOCUMENTS CONSIDERES COMME PERTINENTS			
Catégorie	Identification des documents cités, avec, le cas échéant, l'indication des passages pertinents	no. des revendications visées	
A	EP 1 323 674 A1 (NITTETSU MINING CO LTD [JP]) 2 juillet 2003 (2003-07-02) revendications 1-12 alinéas [0090], [0091]	1-8	
A	WO 2010/142846 A1 (UPM KYMMENE CORP [FI]; STORA ENSO OYJ [FI]; HENTZE HANS-PETER [FI]; SI) 16 décembre 2010 (2010-12-16) revendications 1-21	1-8	
A	WO 2010/112519 A1 (OMYA DEVELOPMENT AG [CH]; GANE PATRICK A C [CH]; SCHOELKOPF JOACHIM [C]) 7 octobre 2010 (2010-10-07) revendications 1-24 page 20, ligne 16 - ligne 17 page 5, ligne 9 - ligne 10	1-8	
-/-			
<input checked="" type="checkbox"/> Voir la suite du cadre C pour la fin de la liste des documents		<input checked="" type="checkbox"/> Les documents de familles de brevets sont indiqués en annexe	
* Catégories spéciales de documents cités:			
"A" document définissant l'état général de la technique, non considéré comme particulièrement pertinent		"T" document ultérieur publié après la date de dépôt international ou la date de priorité et n'appartenant pas à l'état de la technique pertinent, mais cité pour comprendre le principe ou la théorie constituant la base de l'invention	
"E" document antérieur, mais publié à la date de dépôt international ou après cette date		"X" document particulièrement pertinent; l'invention revendiquée ne peut être considérée comme nouvelle ou comme impliquant une activité inventive par rapport au document considéré isolément	
"L" document pouvant jeter un doute sur une revendication de priorité ou cité pour déterminer la date de publication d'une autre citation ou pour une raison spéciale (elle qu'indiquée)		"Y" document particulièrement pertinent; l'invention revendiquée ne peut être considérée comme impliquant une activité inventive lorsque le document est associé à un ou plusieurs autres documents de même nature, cette combinaison étant évidente pour une personne du métier	
"O" document se référant à une divulgation orale, à un usage, à une exposition ou tous autres moyens		"S" document qui fait partie de la même famille de brevets	
"P" document publié avant la date de dépôt international, mais postérieurement à la date de priorité revendiquée			
Date à laquelle la recherche internationale a été effectivement achevée 28 octobre 2013		Date d'expédition du présent rapport de recherche internationale 08/11/2013	
Nom et adresse postale de l'administration chargée de la recherche internationale Office Européen des Brevets, P.B. 5818 Patentaan 2 NL - 2280 HV Rijswijk Tel. (+31-70) 340-2040, Fax. (+31-70) 340-2016		Fonctionnaire autorisé Ponsaud, Philippe	

RAPPORT DE RECHERCHE INTERNATIONALE

Demande internationale n°
PCT/FR2013/051997

C(suite). DOCUMENTS CONSIDERES COMME PERTINENTS		
Catégorie	Identification des documents cités, avec, le cas échéant, l'indication des passages pertinents	no. des revendications visées
A	WO 2010/125247 A2 (UPM KYMMENE CORP; LAINE JANNE [FI]; OESTERBERG MONIKA [FI]; DELPHINE M) 4 novembre 2010 (2010-11-04) page 5, ligne 25 - ligne 29	1-8
A	WO 2010/142845 A1 (UPM KYMMENE CORP [FI]; STORA ENSO OYJ [FI]; HENTZE HANS-PETER [FI]; SI) 16 décembre 2010 (2010-12-16) revendications 1-25	1-8

RAPPORT DE RECHERCHE INTERNATIONALE

Renseignements relatifs aux membres de familles de brevets

Demande internationale n°
PCT/FR2013/051997

Document brevet cité au rapport de recherche	Date de publication	Membre(s) de la famille de brevet(s)	Date de publication		
EP 1323674 A1	02-07-2003	AU 6943001 A	14-01-2002		
		CN 1444543 A	24-09-2003		
		EP 1323674 A1	02-07-2003		
		JP 3392109 B2	31-03-2003		
		JP 2002029739 A	29-01-2002		
		US 2003121451 A1	03-07-2003		
		WO 0202462 A1	10-01-2002		

		WO 2010142846 A1	16-12-2010	CA 2764223 A1	16-12-2010
				EP 2440705 A1	18-04-2012
FI 20095634 A	09-12-2010				
JP 2012529572 A	22-11-2012				
US 2012132380 A1	31-05-2012				
WO 2010142846 A1	16-12-2010				

WO 2010112519 A1	07-10-2010	AR 075960 A1	11-05-2011		
		CA 2755493 A1	07-10-2010		
		CN 102378339 A	14-03-2012		
		CO 6450680 A2	31-05-2012		
		EP 2236664 A1	06-10-2010		
		EP 2414584 A1	08-02-2012		
		JP 2012522145 A	20-09-2012		
		KR 20120004478 A	12-01-2012		
		RU 2011143811 A	10-05-2013		
		TW 201038788 A	01-11-2010		
		US 2012094953 A1	19-04-2012		
		UY 32533 A	29-10-2010		
		WO 2010112519 A1	07-10-2010		

		WO 2010125247 A2	04-11-2010	CA 2757576 A1	04-11-2010
CN 102439226 A	02-05-2012				
EP 2425057 A2	07-03-2012				
EP 2615207 A1	17-07-2013				
EP 2615208 A1	17-07-2013				
FI 20095480 A	30-10-2010				
JP 2012525509 A	22-10-2012				
KR 20120014573 A	17-02-2012				
RU 2011148392 A	10-06-2013				
US 2012132383 A1	31-05-2012				
WO 2010125247 A2	04-11-2010				

WO 2010142845 A1	16-12-2010	CA 2764221 A1	16-12-2010		
		EP 2440704 A1	18-04-2012		
		FI 20095635 A	09-12-2010		
		JP 2012529571 A	22-11-2012		
		US 2012132381 A1	31-05-2012		
		WO 2010142845 A1	16-12-2010		

(19) Organisation Mondiale de la Propriété Intellectuelle
Bureau international



(10) Numéro de publication internationale
WO 2014/118466 A1

(43) Date de la publication internationale
7 août 2014 (07.08.2014)

(51) Classification internationale des brevets :
D21H 19/42 (2006.01) D21H 21/52 (2006.01)
A24D 1/02 (2006.01) D21H 27/00 (2006.01)
D21H 19/52 (2006.01) C09D 101/02 (2006.01)
D21H 19/54 (2006.01) C08L 101/02 (2006.01)
D21H 19/66 (2006.01) C08B 1/02 (2006.01)
D21H 21/40 (2006.01)

Rue des Vignes Rouges, F-74500 Amphion Les Bains (FR).

(72) Inventeurs : BARDET, Raphael; c/o Papeteries du Leman, 1080, Rue des Vignes Rouges, F-74500 Amphion Les Bains (FR). BRAS, Julien; 15, Rue Jean Prévost, F-38000 Grenoble (FR). BELGACEM, Naceur; 53, Chemin des Rivollets, F-38320 Brie Et Angonnes (FR). AGUT, Philippe; c/o Papeteries du Leman, 1080, Rue des Vignes Rouges, F-74500 Amphion Les Bains (FR). DUMAS, Jocelyne; 354, Rue de la Combaz, F-73460 Saint Vital (FR).

(21) Numéro de la demande internationale : PCT/FR2014/050159

(22) Date de dépôt international : 29 janvier 2014 (29.01.2014)

(74) Mandataire : THIBON, Laurent; Cabinet Beaumont, 1, Rue Champollion, F-38000 Grenoble (FR).

(25) Langue de dépôt : français

(26) Langue de publication : français

(30) Données relatives à la priorité : 1350795 30 janvier 2013 (30.01.2013) FR

(81) États désignés (sauf indication contraire, pour tout titre de protection nationale disponible) : AE, AG, AL, AM, AO, AT, AU, AZ, BA, BB, BG, BH, BN, BR, BW, BY, BZ, CA, CH, CL, CN, CO, CR, CU, CZ, DE, DK, DM, DO, DZ, EC, EE, EG, ES, FI, GB, GD, GE, GH, GM, GT, HN, HR, HU, ID, IL, IN, IR, IS, JP, KE, KG, KN, KP, KR, KZ, LA, LC, LK, LR, LS, LT, LU, LY, MA, MD, ME, MG, MK, MN, MW, MX, MY, MZ, NA, NG, NI, NO, NZ,

(71) Déposants : INSTITUT POLYTECHNIQUE DE GRENOBLE [FR/FR]; 46, Avenue Félix Viallet, F-38000 Grenoble (FR). PAPERIES DU LEMAN [FR/FR]; 1080,

[Suite sur la page suivante]

(54) Titre : METHOD FOR MARKING PAPER

(54) Titre : PROCÉDÉ DE MARQUAGE D'UN PAPIER

(57) Abstract : The invention relates to a method for marking paper including the following steps: forming an iridescent cellulose nanocrystal film from cellulose nanoparticles, dry-grinding the film into grains, incorporating the grains to serve as pigments in an aqueous mixture containing a binder, coating the paper with the aqueous mixture, and drying; wherein the step of forming the film includes three main sub-steps: manufacturing cellulose nanocrystals (CNC), placing same in suspension and forming a film; and wherein, during the sub-step of manufacturing cellulose nanocrystals (CNC), cellulose nanoparticles, having an elongate rod-like morphology, a form factor of 20 to 70, preferably 40 to 60, and a polydispersity index (PDI) of less than 0.1 are used as a starting material.

(57) Abrégé : L'invention concerne un procédé de marquage d'un papier comprenant les étapes suivantes; former un film iridescent de nanocristaux de cellulose à partir de nanoparticules de cellulose, broyer par voie sèche le film en grains, incorporer les grains en tant que pigments dans un mélange aqueux contenant un liant, revêtir le papier du mélange aqueux, et sécher, dans lequel, l'étape de formation comprend trois sous-étapes principales; fabrication de nanocristaux de cellulose (NCC), mise en suspension, formation d'un film, et dans lequel, pendant la sous-étape de fabrication de nanocristaux de cellulose (NCC), on part de nanoparticules de cellulose ayant une morphologie allongée, en bâtonnets, avec un facteur de forme compris entre 20 et 70, de préférence entre 40 et 60, et un indice de polydispersité, PDI, inférieur à 0,1.

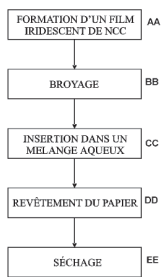


Fig 1

AA Formation of an iridescent CNC film
BB Grinding
CC Insertion in an aqueous mixture
DD Coating the paper
EE Drying

WO 2014/118466 A1

WO 2014/118466

PCT/FR2014/050159

1

PROCÉDE DE MARQUAGE D'UN PAPIER

Domaine

La présente invention vise un procédé de marquage d'un papier par un matériau iridescent et plus particulièrement un marquage dans un but d'authentification.

Devant l'afflux des contrefaçons, on cherche à marquer des papiers de manière à pouvoir vérifier qu'il s'agit de papiers commercialisés par un fabricant donné. Ceci s'applique notamment au marquage de papier à cigarette, la contrefaçon de cigarettes prenant actuellement des proportions importantes. Plus généralement, on cherche à marquer des papiers fins (d'un grammage inférieur à 60 g/m²) tels que des notices pharmaceutiques ou des papiers d'emballage alimentaire par des produits non toxiques.

Exposé de l'art antérieur

On rappelle tout d'abord que l'iridescence est la propriété optique de certains matériaux polycristallins de présenter une réflexion et une absorption différentes selon la longueur d'onde et selon l'incidence d'observation. Ainsi, un film iridescent éclairé en lumière blanche apparaîtra coloré en réflexion, la couleur observée variant selon l'incidence d'observation.

WO 2014/118466

PCT/FR2014/050159

2

Divers documents, par exemple les demandes de brevet PCT WO 2010/066029 et WO 95/21901 décrivent la fabrication et l'utilisation de films iridescents de nanocristaux de cellulose (NCC).

Les films décrits dans les deux demandes de brevet susmentionnées n'ont pas de caractéristiques optiques homogènes sur toute leur étendue, et sont peu adaptés au marquage de matériaux souples tels que des feuilles de papier fin.

La demande de brevet PCT WO 95/21901 mentionne une utilisation de particules issues d'un film de nanocristaux pour un vernis, une peinture ou une encre, ces particules étant dispersées dans un liquide non aqueux.

Résumé

Les demandeurs ont tenté de reproduire le procédé de fabrication de films iridescents de nanocristaux de cellulose décrits dans les demandes de brevet PCT WO 2010/066029 et WO 95/21901 susmentionnées, mais ne sont arrivés à réaliser les résultats annoncés dans ces documents qu'après plusieurs années de recherche et de nombreux essais, les enseignements de ces documents étant insuffisants pour atteindre les résultats annoncés. Notamment, l'utilisation directe des enseignements de ces documents conduit à des films de nanocristaux de cellulose transparents mais non iridescents.

On cherche ici à prévoir un procédé de marquage d'un papier, et plus particulièrement d'un papier à cigarette, par des matériaux iridescents à base de nanocristaux de cellulose.

On cherche à prévoir un tel procédé mettant en oeuvre des matériaux non toxiques issus de ressources renouvelables.

On cherche à prévoir un tel procédé de marquage dans lequel le marquage soit détectable en lumière naturelle, non polarisée.

On cherche à prévoir un tel procédé de marquage adaptable au marquage de papiers fins.

On cherche à prévoir un procédé de fabrication de films de nanocristaux de cellulose conduisant de façon certaine à l'obtention de films iridescents.

On cherche à prévoir un tel procédé de fabrication dans lequel le film iridescent ait une signature optique (homogénéité et reproductibilité des couleurs) précise.

Ainsi, un mode de réalisation prévoit un procédé de marquage d'un papier comprenant les étapes suivantes :

former un film iridescent de nanocristaux de cellulose à partir de nanoparticules de cellulose, broyer par voie sèche le film en grains, incorporer les grains en tant que pigments dans un mélange aqueux contenant un liant, revêtir le papier du mélange aqueux, et sécher, dans lequel, l'étape de formation comprend trois sous-étapes principales :

- fabrication de nanocristaux de cellulose (NCC),
- mise en suspension,
- formation d'un film, et

dans lequel, pendant la sous-étape de fabrication de nanocristaux de cellulose (NCC), on part de nanoparticules de cellulose ayant une morphologie allongée, en bâtonnets, avec un facteur de forme compris entre 20 et 70, de préférence entre 40 et 60, et un indice de polydispersité, PDI, inférieur à 0,1.

Selon un mode de réalisation, les nanoparticules de cellulose sont formées par une forte hydrolyse par de l'acide sulfurique.

Selon un mode de réalisation, les nanoparticules de cellulose ont un indice de cristallinité, Xc, supérieur à 80 % et de préférence supérieur à 85 %.

Selon un mode de réalisation, pendant l'étape de formation d'un film, les conditions d'évaporation sont choisies pour que la vitesse d'évaporation soit comprise entre 0,1 mm et 25 mm d'eau évaporée par heure de séchage.

Selon un mode de réalisation, pendant l'étape de formation d'un film, la température de séchage est inférieure à 100°C et de préférence inférieure à 80°C.

Selon un mode de réalisation, à l'issue de l'étape de formation d'un film, la teneur finale en eau du film sec est inférieure à 10 %.

Selon un mode de réalisation, à l'issue de l'étape de formation d'un film, le film a une épaisseur comprise entre 20 et 50 µm.

Selon un mode de réalisation, après l'étape de broyage, les grains sont tels que leur plus grande dimension est inférieure à 30 µm.

Selon un mode de réalisation, les nanocristaux de cellulose sont mis dans une solution aqueuse avec une concentration massique comprise entre 10 et 40 grammes par litre.

Selon un mode de réalisation, l'organisation de nanocristaux en suspension aqueuse est modifiée par ajout d'un composé chimique choisi dans le groupe comprenant un sel mono ou divalent, et un poly-électrolyte anionique de faible poids moléculaire.

Selon un mode de réalisation, le polyélectrolyte anionique de faible poids moléculaire est un agent choisi parmi la famille comprenant les composés suivants : benzoxazolines, biphenyl-stilbènes, coumarins, diazoles, imidazolines, triazoles, triazine-stilbènes.

Selon un mode de réalisation, le liant du mélange aqueux est une suspension de microfibrilles de cellulose.

Selon un mode de réalisation, la proportion de grains iridescents dans le mélange aqueux est comprise entre 0,01 et 10 % et de préférence entre 0,1 et 10 % en poids sec.

Selon un mode de réalisation, on choisit de façon précise les paramètres suivants :

- le facteur de forme de la nanocellulose,

-la charge de surface de la nanocellulose, comprise entre 100 et 500 micromoles par gramme avec un taux de sulfate compris entre 0,5 et 1,0 % en poids sec, et de préférence entre 0,6 et 0,8 %,

-l'énergie dispersive appliquée à la suspension de nanocristaux, dans une plage de 1 à 50 kJ/g,

-la vitesse et la température de séchage du film comprise entre 0,1 et 25 mm d'eau évaporée par heure de séchage, et

-l'épaisseur du film comprise entre 20 et 300 µm et de préférence inférieure à 150 µm.

Un mode de réalisation prévoit un papier à cigarette marqué par des grains de nanocristaux de cellulose obtenus par le procédé ci-dessus.

Brève description des dessins

Ces caractéristiques et avantages, ainsi que d'autres, seront exposés en détail dans la description suivante de modes de réalisation particuliers faite à titre non limitatif en relation avec la figure 1 ci-jointe qui illustre les principales étapes d'un procédé selon l'invention.

Description détaillée

Comme on l'a indiqué précédemment, divers procédés ont été décrits dans l'art antérieur pour obtenir des films iridescents à partir de nanocristaux de cellulose (NCC).

Pour le marquage d'un matériau souple tel qu'une feuille de papier, on propose ici de procéder successivement aux étapes suivantes :

- formation d'un film iridescent de NCC,
- broyage,
- insertion dans un mélange aqueux contenant un liant,
- revêtement du papier, et
- séchage.

Dans le cas où le produit à marquer est une feuille de papier à cigarette, on notera qu'actuellement, les cigarettes sont souvent munies de zones annulaires successives comportant

un revêtement formé par exemple à partir d'une solution d'amidon qui sert d'élément d'extinction quand le consommateur arrête de tirer sur sa cigarette. Ce revêtement, dit LIP (Low ignition propensity), est tel que l'incandescence du tabac n'est plus suffisante pour que la cigarette se consume toute seule jusqu'au bout lorsque la cigarette est posée sur un substrat conformément aux tests ASTM E2187-04 et ISO12863, comme cela est décrit dans la demande de brevet WO 2011/144701. Dans le cadre de cette application particulière, on utilisera ici un mélange aqueux

constitué d'une suspension aqueuse de polysaccharides (amidon, carboxy-méthyl-cellulose...) ou de nanofibres de cellulose à laquelle auront été ajoutés à titre de pigments des grains obtenus à partir de films iridescents de nanocristaux de cellulose. On notera que la nature chimique des nanocristaux de cellulose est très proche de celle des polysaccharides ou des nanofibres de cellulose et que cela n'altère en rien les propriétés gustatives et toxicologiques de la cigarette.

On va maintenant détailler les diverses étapes d'un mode de réalisation d'un procédé de marquage, notamment dans le cas où on cherche à obtenir des grains de cristaux iridescents ayant des signatures spécifiques très difficiles à reproduire.

1. FORMATION D'UN FILM DE NANOCRISTAUX DE CELLULOSE.

Cette formation comprend trois sous-étapes principales décrites en particulier dans les documents susmentionnés :

- fabrication de nanocristaux de cellulose (NCC),
- mise en suspension,
- formation d'un film.

1.1 Fabrication de nanocristaux de cellulose

Les inventeurs ont montré que pour que le film iridescent que l'on cherche à obtenir ait des caractéristiques optiques homogènes, déterminées et reproductibles, il convenait que, pendant l'étape de fabrication de nanocristaux de cellulose à partir de nanoparticules de cellulose, au moins certaines des conditions indiquées aux points (1) à (7) ci-après soient respectées.

(1) Les nanoparticules de cellulose sont formées principalement par hydrolyse par de l'acide sulfurique.

(2) Ces nanoparticules ont une morphologie allongée, dite en bâtonnets ou en aiguilles.

5 (3) Ces nanoparticules ont un facteur de forme compris entre 20 et 70, de préférence entre 40 et 60.

(4) L'indice de polydispersité, PDI, doit être inférieur à 0,20 pour obtenir un film iridescent et inférieur à 0,1 pour obtenir un film iridescent de caractéristiques optiques homogènes.

10 (5) L'indice de cristallinité, X_c , est supérieur à 80 % et de préférence supérieur à 85 %.

(6) Une modification des propriétés de greffage en surface des groupements ester de sulfate est effectuée par un procédé chimique qui consiste à modifier le pH de la suspension par ajout de quelques millimoles d'un acide fort ou d'une base forte dans la solution.

(7) La charge de surface est comprise entre 100 et 500 micromoles par gramme avec un taux de sulfate compris entre 0,5 et 1,0 % en poids sec.

1.2 Mise en suspension

25 Les inventeurs ont montré que, pour que le film iridescent que l'on cherche à obtenir ait des caractéristiques homogènes, déterminées et reproductibles, il convenait que, pendant l'étape de mise en suspension, au moins certaines des conditions indiquées aux points (8) à (10) ci-après soient respectées.

(8) La concentration massique des nanocristaux de cellulose est comprise entre 1 et 70 grammes par litre, de préférence entre 10 et 40 grammes par litre.

(9) Une modification de l'organisation de nanocristaux en suspension aqueuse est réalisée par un ajout en faible quantité d'un composé chimique comme par exemple un sel mono ou divalent, un poly-électrolyte de faible poids moléculaire ou un plastifiant.

(10) Une modification de l'organisation des nanocristaux en suspension aqueuse est obtenue en appliquant à la suspension de nanocristaux une énergie dispersive spécifique comprise entre 1 et 50 kJ par gramme de nanocristaux sec par un traitement aux ultrasons, micro-ondes ou infrarouges ou une homogénéisation mécanique.

1.3 Formation d'un film

10 Les inventeurs ont montré que, pour que le film iridescent que l'on cherche à obtenir ait des caractéristiques homogènes, déterminées et reproductibles, il convenait que, pendant cette étape de formation d'un film, au moins certaines des conditions indiquées aux points (11) à (15) ci-après soient respectées.

(11) La suspension obtenue est déversée sur un support plan, horizontal, et un film homogène d'épaisseur régulière est obtenu par séchage sans agitation de la suspension aqueuse préservant l'organisation stratifiée des nanocristaux selon un plan normal à la surface du film.

(12) Les conditions d'évaporation sont choisies pour que la vitesse d'évaporation soit comprise entre 0,1 et 25 mm d'eau évaporée par heure de séchage.

(13) La température de séchage est de préférence inférieure à 100°C et encore de préférence inférieure à 80°C. Le séchage est réalisé en minimisant le flux d'air chaud et il doit être homogène sur toute la surface du film.

(14) La teneur finale en eau du film sec est inférieure à 10 % et de préférence inférieure à 5 %.

(15) On choisit de préférence de former un film d'une épaisseur comprise entre 10 et 100 µm, de préférence entre 20 et 30 µm.

2. BROYAGE.

30 Le film de NCC iridescent sous lumière naturelle ainsi obtenu est ensuite broyé pour obtenir des grains dont la plus grande dimension est inférieure à 30 µm, pour au moins 50 %

d'entre eux. Ce broyage est réalisé par voie sèche en utilisant par exemple un broyage à disque, à billes ou à jet d'air.

3. MELANGE AQUEUX

5 Les grains ainsi obtenus sont incorporés dans un mélange aqueux contenant un liant (ou sauce d'enduction). Cette sauce comprend par exemple une suspension aqueuse de polysaccharides (amidon, carboxy-méthyl-cellulose...) ou de nanofibres de cellulose. On pourra choisir une formulation dans laquelle les grains iridescents sont dans une proportion de 0,1 à 50 %, de préférence entre 1 et 10 %, en poids à sec par rapport à la matrice organique.

10 On pourra choisir d'insérer dans le mélange aqueux contenant un liant un ou plusieurs types de grains obtenus à partir de films différents.

15 La sauce d'enduction est homogénéisée par agitation mécanique douce ne limitant pas la redispersion de nanocristaux contenus dans un grain iridescent.

20 On a constaté que, contrairement à un préjugé, les grains de nanocristaux de cellulose obtenus par broyage du film ne se délitent pas et ne perdent pas leurs caractéristiques, et notamment pas leurs caractéristiques d'iridescence, même après une durée d'immersion des grains de plus de 2 heures dans un mélange aqueux contenant un liant.

4. REVÊTEMENT DU PAPIER

25 Le papier est revêtu à partir du mélange aqueux contenant les grains de nanocristaux de cellulose en utilisant l'une des techniques de couchage courantes comme le couchage à barre, à rideau, à lame ou à pulvérisation. Le revêtement peut-être réalisé en utilisant des techniques d'impression comme la flexographie.

5. SÉCHAGE

30 Le séchage est effectué de façon que le poids sec de couche soit compris entre 1 et 40 g/m², de préférence entre 2 et 10 g/m². Ainsi, l'épaisseur moyenne de couche déposée sur le support fin est comprise entre 2 et 10 µm.

OBSERVATIONS

5 Une fois tout le processus effectué, la présence des nanocristaux de cellulose sur le papier, par exemple du papier à cigarette n'est pas facilement détectable à l'oeil nu. Toutefois, les nanocristaux sont facilement détectables avec un microscope optique classique ayant par exemple un grossissement de 5 à 40. On pourra en outre par une technique d'analyse chimique comme la méthode SEM-EDX (Scanning Electron Microscopy - Energy Dispersive X-ray Analyser) ou la spectrométrie FT-IR constater qu'il n'y a aucune différence de composition chimique entre les pigments de NCC et la sauce sèche, étant donné que le procédé de marquage n'implique que des polysaccharides.

10 Même si un contrefacteur essayait de reproduire le procédé décrit ci-dessus, on pourrait en fait identifier la contrefaçon du fait que, si on choisit des paramètres précis pour la formation de la sauce à partir de laquelle on va former le film de NCC, on obtient des caractéristiques optiques d'iridescence très difficilement reproductibles. En effet, lors de la formation de cette sauce, on pourra jouer indépendamment sur au moins six paramètres tout en restant dans les plages indiquées précédemment :

- le facteur de forme du matériau source,
- la charge de surface (liée à la présence de sulfate),
- l'énergie appliquée lors de la dispersion de la suspension par exemple par ultrasons,
- la vitesse de séchage du film,
- l'épaisseur du film.

25 En pratique, il s'avère qu'une ingénierie inverse ne permet pas, à partir d'une analyse des grains de nanocristaux de cellulose et de leurs propriétés optiques, de remonter aux paramètres du procédé utilisé et donc de former des nanocristaux en grain ayant des caractéristiques optiques identiques.

30 De plus, si l'on veut encore complexifier le système, on pourra utiliser plusieurs, au moins deux, catégories de grains de NCC obtenus à partir de films de caractéristiques

différentes. La signature sera encore plus nette et plus facile à identifier.

Le support peut être revêtu du mélange aqueux par un procédé d'enduction ou de pulvérisation.

5 Le mélange aqueux peut être directement introduit lors de la fabrication du support.

RENDICATIONS

1. Procédé de marquage d'un papier comprenant les étapes suivantes :
 - former un film iridescent de nanocristaux de cellulose à partir de nanoparticules de cellulose,
 - 5 broyer par voie sèche le film en grains,
 - incorporer les grains en tant que pigments dans un mélange aqueux contenant un liant,
 - revêtir le papier du mélange aqueux, et
 - sécher,
 - 10 dans lequel, l'étape de formation comprend trois sous-étapes principales :
 - fabrication de nanocristaux de cellulose (NCC),
 - mise en suspension,
 - formation d'un film, et
 - 15 dans lequel, pendant la sous-étape de fabrication de nanocristaux de cellulose (NCC), on part de nanoparticules de cellulose ayant une morphologie allongée, en bâtonnets, avec un facteur de forme compris entre 20 et 70, de préférence entre 40 et 60, et un indice de polydispersité, PDI, inférieur à 0,1.
 - 20 2. Procédé selon la revendication 1, dans lequel les nanoparticules de cellulose sont formées par une forte hydrolyse par de l'acide sulfurique.
 3. Procédé selon la revendication 1 ou 2, dans lequel les nanoparticules de cellulose ont un indice de cristallinité,
 - 25 X_c , supérieur à 80 % et de préférence supérieur à 85 %.
 4. Procédé selon l'une quelconque des revendications 1 à 3, dans lequel, pendant l'étape de formation d'un film, les conditions d'évaporation sont choisies pour que la vitesse d'évaporation soit comprise entre 0,1 mm et 25 mm d'eau évaporée
 - 30 par heure de séchage.
 5. Procédé selon l'une quelconque des revendications 1 à 4, dans lequel, pendant l'étape de formation d'un film, la température de séchage est inférieure à 100°C et de préférence inférieure à 80°C.

6. Procédé selon l'une quelconque des revendications 1 à 5, dans lequel, à l'issue de l'étape de formation d'un film, la teneur finale en eau du film sec est inférieure à 10 %.

7. Procédé selon l'une quelconque des revendications 5 1 à 6, dans lequel, à l'issue de l'étape de formation d'un film, le film a une épaisseur comprise entre 20 et 50 μm .

8. Procédé selon l'une quelconque des revendications 1 à 7, dans lequel, après l'étape de broyage, les grains sont tels que leur plus grande dimension est inférieure à 30 μm .

10 9. Procédé selon l'une quelconque des revendications 1 à 8, dans lequel les nanocristaux de cellulose sont mis dans une solution aqueuse avec une concentration massique comprise entre 10 et 40 grammes par litre.

15 10. Procédé selon l'une quelconque des revendications 1 à 9, dans lequel l'organisation de nanocristaux en suspension aqueuse est modifiée par ajout d'un composé chimique choisi dans le groupe comprenant un sel mono ou divalent, et un poly-électrolyte anionique de faible poids moléculaire.

20 11. Procédé selon la revendication 10, dans lequel, le polyélectrolyte anionique de faible poids moléculaire est un agent choisi parmi la famille comprenant les composés suivants : benzoxazolines, biphényl-stilbènes, coumarins, diazoles, imidazolines, triazoles, triazine-stilbènes.

25 12. Procédé selon l'une quelconque des revendications 1 à 11, dans lequel le liant du mélange aqueux est une suspension de microfibrilles de cellulose.

30 13. Procédé selon l'une quelconque des revendications 1 à 12, dans lequel la proportion de grains iridescents dans le mélange aqueux est comprise entre 0,01 et 10 % et de préférence entre 0,1 et 10 % en poids sec.

14. Procédé selon l'une quelconque des revendications 1 à 13, dans lequel, on choisit de façon précise les paramètres suivants :

- le facteur de forme de la nanocellulose,

- la charge de surface de la nanocellulose, comprise entre 100 et 500 micromoles par gramme avec un taux de sulfate compris entre 0,5 et 1,0 % en poids sec, et de préférence entre 0,6 et 0,8 %,
- 5 - l'énergie dispersive appliquée à la suspension de nanocristaux, dans une plage de 1 à 50 kJ/g,
- la vitesse et la température de séchage du film comprise entre 0,1 et 25 mm d'eau évaporée par heure de séchage, et
- l'épaisseur du film comprise entre 20 et 300 μm et de préférence inférieure à 150 μm .
- 10 15. Papier à cigarette marqué par des grains de nanocristaux de cellulose obtenus par le procédé selon l'une quelconque des revendications 1 à 14.

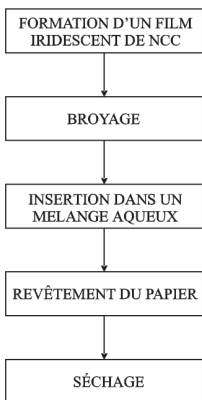


Fig 1

INTERNATIONAL SEARCH REPORT

International application No
PCT/FR2014/050159

A. CLASSIFICATION OF SUBJECT MATTER					
INV.	D21H19/42	A24D1/02	D21H19/52	D21H19/54	D21H19/66
	D21H21/40	D21H21/52	D21H27/00	C09D101/02	C08L101/02
	C08B1/02				
According to International Patent Classification (IPC) or to both national classification and IPC					
B. FIELDS SEARCHED					
Minimum documentation searched (classification system followed by classification symbols)					
D21H A24D C09D C08L C08B					
Documentation searched other than minimum documentation to the extent that such documents are included in the fields searched					
Electronic data base consulted during the international search (name of data base and, where practicable, search terms used)					
EPO-Internal, WPI Data					
C. DOCUMENTS CONSIDERED TO BE RELEVANT					
Category*	Citation of document, with indication, where appropriate, of the relevant passages				Relevant to claim No.
X	WO 2010/124378 A1 (FPINNOVATIONS [CA]; ZOU XUEJUN [CA]; TAN XUEQUAN [CA]; BERRY RICHARD []) 4 November 2010 (2010-11-04)				1-14
Y	claim 1				15
	page 4, line 7 - line 8				
	page 5, line 14 - line 15				
Y	WO 2005/039330 A1 (PHILIP MORRIS PROD [CH]) 6 May 2005 (2005-05-06)				15
	claims 92, 93				
Y	WO 2005/039329 A1 (PHILIP MORRIS PROD [CH]) 6 May 2005 (2005-05-06)				15
	claims 1,2,23,25				
<input type="checkbox"/> Further documents are listed in the continuation of Box C. <input checked="" type="checkbox"/> See patent family annex.					
* Special categories of cited documents : *A* document defining the general state of the art which is not considered to be of particular relevance *E* earlier application or patent but published on or after the international filing date *L* document which may throw doubts on priority claim(s) or which is cited to establish the publication date of another citation or other special reason (as specified) *O* document referring to an oral disclosure, use, exhibition or other means *P* document published prior to the international filing date but later than the priority date claimed *T* later document published after the international filing date or priority date and not in conflict with the application but cited to understand the principle or theory underlying the invention *X* document of particular relevance, the claimed invention cannot be considered novel or cannot be considered to involve an inventive step when the document is taken alone *Y* document of particular relevance, the claimed invention cannot be considered to involve an inventive step when the document is combined with one or more other such documents, such combination being obvious to a person skilled in the art *Z* document member of the same patent family					
Date of the actual completion of the international search			Date of mailing of the international search report		
3 April 2014			28/04/2014		
Name and mailing address of the ISA/ European Patent Office, P.B. 5818 Patentlaan 2 NL - 2280 HV Rijswijk Tel: (+31-70) 340-2040 Fax: (+31-70) 340-3016			Authorized officer Ponsaud, Philippe		

Form PCT/ISA/210 (second sheet) (April 2005)

INTERNATIONAL SEARCH REPORT

Information on patent family members

International application No
PCT/FR2014/050159

Patent document cited in search report	Publication date	Patent family member(s)	Publication date
WO 2010124378 A1	04-11-2010	AU 2010242489 A1	03-11-2011
		CA 2758042 A1	04-11-2010
		CN 102449052 A	09-05-2012
		EP 2424938 A1	07-03-2012
		JP 2012525446 A	22-10-2012
		RU 2011148917 A	10-06-2013
		US 2012237750 A1	20-09-2012
WO 2010124378 A1	04-11-2010		
WO 2005039330 A1	06-05-2005	US 2005211259 A1	29-09-2005
		WO 2005039330 A1	06-05-2005
WO 2005039329 A1	06-05-2005	US 2005121047 A1	09-06-2005
		US 2009139534 A1	04-06-2009
		WO 2005039329 A1	06-05-2005

Form PCT/ISA/210 (patent family annex) (April 2005)

RAPPORT DE RECHERCHE INTERNATIONALE

Demande internationale n°
PCT/FR2014/050159

A. CLASSEMENT DE L'OBJET DE LA DEMANDE					
INV.	D21H19/42	A24D1/02	D21H19/52	D21H19/54	D21H19/66
	D21H21/40	D21H21/52	D21H27/00	C09D101/02	C08L101/02
	C08B1/02				
Selon la classification internationale des brevets (CIB) ou à la fois selon la classification nationale et la CIB					
B. DOMAINES SUR LESQUELS LA RECHERCHE A PORTE					
Documentation minimale consultée (système de classification suivi des symboles de classement)					
D21H A24D C09D C08L C08B					
Documentation consultée autre que la documentation minimale dans la mesure où ces documents relèvent des domaines sur lesquels a porté la recherche					
Base de données électronique consultée au cours de la recherche internationale (nom de la base de données, et si cela est réalisable, termes de recherche utilisés)					
EPO-Internal, WPI Data					
C. DOCUMENTS CONSIDERES COMME PERTINENTS					
Category*	Identification des documents cités, avec, le cas échéant, l'indication des passages pertinents				no. des revendications visées
X	WO 2010/124378 A1 (FPINNOVATIONS [CA]; ZOU XUEJUN [CA]; TAN XUEQUAN [CA]; BERRY RICHARD []) 4 novembre 2010 (2010-11-04)				1-14
Y	revendication 1				15
	page 4, ligne 7 - ligne 8				
	page 5, ligne 14 - ligne 15				
Y	WO 2005/039330 A1 (PHILIP MORRIS PROD [CH]) 6 mai 2005 (2005-05-06)				15
	revendications 92, 93				
Y	WO 2005/039329 A1 (PHILIP MORRIS PROD [CH]) 6 mai 2005 (2005-05-06)				15
	revendications 1,2,23,25				
<input type="checkbox"/> Voir la suite du cadre C pour la fin de la liste des documents <input checked="" type="checkbox"/> Les documents de familles de brevets sont indiqués en annexe					
* Catégories spéciales de documents cités : *A* document définissant l'état général de la technique, non considéré comme particulièrement pertinent *E* document antérieur, mais publié à la date de dépôt international ou après cette date *L* document pouvant jeter un doute sur une revendication de priorité ou cité pour déterminer la date de publication d'une autre citation ou pour une raison spéciale (celle-ci indiquée) *O* document se référant à une divulgation orale, à un usage, à une exposition ou tous autres moyens *P* document publié avant la date de dépôt international, mais postérieurement à la date de priorité revendiquée *T* document ultérieur publié après la date de dépôt international ou la date de priorité et n'appartenant pas à l'état de la technique pertinent, mais cité pour comprendre le principe ou la théorie constituant la base de l'invention *X* document particulièrement pertinent; l'invention revendiquée ne peut être considérée comme nouvelle ou comme impliquant une activité inventive par rapport au document considéré isolément *Y* document particulièrement pertinent; l'invention revendiquée ne peut être considérée comme impliquant une activité inventive lorsque le document est associé à un ou plusieurs autres documents de même nature, cette combinaison étant évidente pour une personne du métier *Z* document qui fait partie de la même famille de brevets					
Date à laquelle la recherche internationale a été effectivement achevée			Date d'expédition du présent rapport de recherche internationale		
3 avril 2014			28/04/2014		
Nom et adresse postale de l'administration chargée de la recherche internationale Office Européen des Brevets, P.B. 5818 Patentlaan 2 NL - 2280 HV Rijswijk Tel: (+31-70) 340-2040 Fax: (+31-70) 340-3016			Fonctionnaire autorisé Ponsaud, Philippe		

Formulaire PCT/ISA/210 (deuxième feuille) (avril 2005)

RAPPORT DE RECHERCHE INTERNATIONALE

Renseignements relatifs aux membres de familles de brevets

Demande internationale n°
PCT/FR2014/050159

Document brevet cité au rapport de recherche	Date de publication	Membre(s) de la famille de brevet(s)	Date de publication		
WO 2010124378 A1	04-11-2010	AU 2010242489 A1	03-11-2011		
		CA 2758042 A1	04-11-2010		
		CN 102449052 A	09-05-2012		
		EP 2424938 A1	07-03-2012		
		JP 2012525446 A	22-10-2012		
		RU 2011148917 A	10-06-2013		
		US 2012237750 A1	20-09-2012		
		WO 2010124378 A1	04-11-2010		

		WO 2005039330 A1	06-05-2005	US 2005211259 A1	29-09-2005
WO 2005039330 A1	06-05-2005				

WO 2005039329 A1	06-05-2005	US 2005121047 A1	09-06-2005		
		US 2009139534 A1	04-06-2009		
		WO 2005039329 A1	06-05-2005		

Appendix 2

Posters

BARRIER PROPERTIES OF SPECIALTY PAPERS COATED WITH MICROFIBRILLATED CELLULOSE: INFLUENCE OF BASE PAPER AND COAT WEIGHT

Raphael Bardet¹, Nathalie Layoine¹, Isabelle Desloges¹, Naceur Belgacem¹, Julien Bras^{1*}

¹GRENOBLE INSTITUTE OF TECHNOLOGY – PAgORA – 461 rue de la Papeterie, 38402 Saint Martin d'Hères, FRANCE

KEY WORDS: MFC, SPECIALTY PAPERS, BARRIER PROPERTIES

Introduction & Background

New packaging materials from sustainable resources, biodegradable and designed for food contact are expected. Since the 2000s, one innovative solution has been more and more studied and consists in using microfibrillated cellulose (MFC) as surface layer onto a substrate.

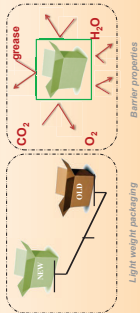


Fig. 1. Main objectives for new packaging materials.

Materials & Methods

- Light weight specialty papers were selected among various kinds of industrial specialty papers in order to study the influence of the substrate (table 1).

Ref.	Application	Basis weight (g/m ²)	Thickness (µm)	Papermaking treatment	Fibres content
A	Specialty	11	16	●●● Surface sized	●●●
B	Coating	23	26	●●●● Surface sized	●●●●
C	Thin printing	25	32	●●●●● Base paper	●●●●●
D	Thin printing	28	28	●●●●●	●●●●●
E	Specialty	42	67	●●●●●	●●●●●

Table 2. Main features of reference base substrates.

- Microfibrillated Cellulose (MFC) The MFC suspension has been produced following process⁸ detailed in table 2 and characterized in table 3.

MFC production

Raw material	Softwood dissolving pulp (Domag Cellulose pulp)
Dimension	Diameter: 20 µm ± 5 µm
Length	> 1 µm
Viscosity	2400 mPa.s (Brookfield viscosity 60 rpm, 25°C)
Dry matter	27%

Table 3. Empty water of the MFC suspension.

MFC production parameters	MFC production parameters
Mechanical Treatment	Cellulose (Monsieur 4760)
	Cons. 3.5%, pH = 6, 1h
	Musko Gildograph
	20 passes at 60°/min/point

Table 4. Main features of reference base substrates.

Table 5. Empty water of the MFC suspension.

Table 6. Main features of reference base substrates.

Table 7. Empty water of the MFC suspension.

Table 8. Main features of reference base substrates.

Table 9. Empty water of the MFC suspension.

Table 10. Main features of reference base substrates.

Table 11. Empty water of the MFC suspension.

Table 12. Main features of reference base substrates.

Table 13. Empty water of the MFC suspension.

Table 14. Main features of reference base substrates.

Table 15. Empty water of the MFC suspension.

Table 16. Main features of reference base substrates.

Table 17. Empty water of the MFC suspension.

Table 18. Main features of reference base substrates.

Table 19. Empty water of the MFC suspension.

Table 20. Main features of reference base substrates.

Table 21. Empty water of the MFC suspension.

Table 22. Main features of reference base substrates.

Table 23. Empty water of the MFC suspension.

Table 24. Main features of reference base substrates.

Table 25. Empty water of the MFC suspension.

Table 26. Main features of reference base substrates.

Table 27. Empty water of the MFC suspension.

Table 28. Main features of reference base substrates.

Table 29. Empty water of the MFC suspension.

Table 30. Main features of reference base substrates.

Table 31. Empty water of the MFC suspension.

Table 32. Main features of reference base substrates.

Table 33. Empty water of the MFC suspension.

Table 34. Main features of reference base substrates.

Table 35. Empty water of the MFC suspension.

Table 36. Main features of reference base substrates.

Table 37. Empty water of the MFC suspension.

Table 38. Main features of reference base substrates.

Table 39. Empty water of the MFC suspension.

Table 40. Main features of reference base substrates.

Strategies & Objectives

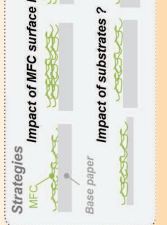


Fig. 2. Strategies and objectives of the study.

Results & Discussions

Part 1: Structure & Morphology of MFC layers



Fig. 7. FE-SEM (left) and AFM (right) pictures of reference ref. C, suspension: 1.6 g/m² of MFC.

Fig. 8. BSE image of reference surface (ref. C) coated with nanotechnology coating weight of MFC.

Fig. 9. Air permeability (cm³/m².Pa.s) as a function of the MFC coated area and water surface sized papers (Ref. A).

Fig. 10. CO₂ Diffusivity as a function of the MFC coat weight (ref. B).

Fig. 11. Relative water absorption gain of MFC coated samples compared to water surface sized samples.

Fig. 12. Pictures showing different water surface sized papers (ref. A) or with MFC coating (ref. A).

Fig. 13. Pictures showing different water surface sized papers (ref. A) or with MFC coating (ref. A).

Fig. 14. Pictures showing different water surface sized papers (ref. A) or with MFC coating (ref. A).

Fig. 15. Pictures showing different water surface sized papers (ref. A) or with MFC coating (ref. A).

Fig. 16. Pictures showing different water surface sized papers (ref. A) or with MFC coating (ref. A).

Fig. 17. Pictures showing different water surface sized papers (ref. A) or with MFC coating (ref. A).

Fig. 18. Pictures showing different water surface sized papers (ref. A) or with MFC coating (ref. A).

Fig. 19. Pictures showing different water surface sized papers (ref. A) or with MFC coating (ref. A).

Fig. 20. Pictures showing different water surface sized papers (ref. A) or with MFC coating (ref. A).

Fig. 21. Pictures showing different water surface sized papers (ref. A) or with MFC coating (ref. A).

Fig. 22. Pictures showing different water surface sized papers (ref. A) or with MFC coating (ref. A).

Fig. 23. Pictures showing different water surface sized papers (ref. A) or with MFC coating (ref. A).

Fig. 24. Pictures showing different water surface sized papers (ref. A) or with MFC coating (ref. A).

Fig. 25. Pictures showing different water surface sized papers (ref. A) or with MFC coating (ref. A).

Fig. 26. Pictures showing different water surface sized papers (ref. A) or with MFC coating (ref. A).

Fig. 27. Pictures showing different water surface sized papers (ref. A) or with MFC coating (ref. A).

Fig. 28. Pictures showing different water surface sized papers (ref. A) or with MFC coating (ref. A).

Fig. 29. Pictures showing different water surface sized papers (ref. A) or with MFC coating (ref. A).

Fig. 30. Pictures showing different water surface sized papers (ref. A) or with MFC coating (ref. A).

Fig. 31. Pictures showing different water surface sized papers (ref. A) or with MFC coating (ref. A).

Fig. 32. Pictures showing different water surface sized papers (ref. A) or with MFC coating (ref. A).

Fig. 33. Pictures showing different water surface sized papers (ref. A) or with MFC coating (ref. A).

Fig. 34. Pictures showing different water surface sized papers (ref. A) or with MFC coating (ref. A).

Fig. 35. Pictures showing different water surface sized papers (ref. A) or with MFC coating (ref. A).

Fig. 36. Pictures showing different water surface sized papers (ref. A) or with MFC coating (ref. A).

Fig. 37. Pictures showing different water surface sized papers (ref. A) or with MFC coating (ref. A).

Fig. 38. Pictures showing different water surface sized papers (ref. A) or with MFC coating (ref. A).

Fig. 39. Pictures showing different water surface sized papers (ref. A) or with MFC coating (ref. A).

Fig. 40. Pictures showing different water surface sized papers (ref. A) or with MFC coating (ref. A).

Fig. 41. Pictures showing different water surface sized papers (ref. A) or with MFC coating (ref. A).

Fig. 42. Pictures showing different water surface sized papers (ref. A) or with MFC coating (ref. A).

Fig. 43. Pictures showing different water surface sized papers (ref. A) or with MFC coating (ref. A).

Fig. 44. Pictures showing different water surface sized papers (ref. A) or with MFC coating (ref. A).

Fig. 45. Pictures showing different water surface sized papers (ref. A) or with MFC coating (ref. A).

Fig. 46. Pictures showing different water surface sized papers (ref. A) or with MFC coating (ref. A).

Fig. 47. Pictures showing different water surface sized papers (ref. A) or with MFC coating (ref. A).

Fig. 48. Pictures showing different water surface sized papers (ref. A) or with MFC coating (ref. A).

Fig. 49. Pictures showing different water surface sized papers (ref. A) or with MFC coating (ref. A).

Fig. 50. Pictures showing different water surface sized papers (ref. A) or with MFC coating (ref. A).

Fig. 51. Pictures showing different water surface sized papers (ref. A) or with MFC coating (ref. A).

Fig. 52. Pictures showing different water surface sized papers (ref. A) or with MFC coating (ref. A).

Fig. 53. Pictures showing different water surface sized papers (ref. A) or with MFC coating (ref. A).

Fig. 54. Pictures showing different water surface sized papers (ref. A) or with MFC coating (ref. A).

Fig. 55. Pictures showing different water surface sized papers (ref. A) or with MFC coating (ref. A).

Conclusions & Perspectives

- A thin MFC layers has an impact on the gas and liquid barrier properties.
- In order to have a homogeneous surface layer, a minimal ratio of 6-8% of MFC is required whatever the basis weight.
- Barrier properties are certainly due to the homogeneous layer and the nanoporous network.
- Some limits are however highlighted: final barrier properties are closely linked to the interactions between water and the base paper.

References

1. Sjö, I. and O. Pääkkö, *Cellulose*, 2010.

2. Andersen, A. et al., *Cellulose*, 2010.

3. Szymanski, K. et al., *Cellulose*, 2010.

4. Hamada, H. et al., *Cellulose*, 2010.

5. Hamada, H. et al., *Cellulose*, 2010.

6. Hamada, H. et al., *Cellulose*, 2010.

7. Hamada, H. et al., *Cellulose*, 2010.

8. Hamada, H. et al., *Cellulose*, 2010.

9. Hamada, H. et al., *Cellulose*, 2010.

10. Hamada, H. et al., *Cellulose*, 2010.

Acknowledgements

The authors gratefully acknowledge the financial partnership of the French National Research Agency (ANR) for the project 'MFC' (ANR-08-0001-01).

Contact

Contact: julien.bras@agora.grenoble-inp.fr

INVESTIGATION OF DIFFERENT POST-TREATMENTS OF NANOCRYSTALLINE CELLULOSE IN ORDER TO OBTAIN NARROWLY DISPersed RODS

R. Bardet, A. Romdhane, V. Perrin, M. Aurousseau, MN. Belgacem, A. Guillet, E. Mauret & J. Bras*

GRENOBLE INSTITUTE OF TECHNOLOGY (INP) – LGP2 - 461 rue de la Papeterie, 38402 Saint Martin d'Hères, France

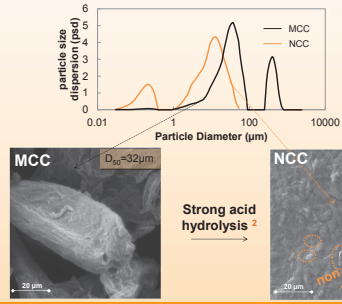
Introduction

The dispersity and the particle average size of a nanocrystalline cellulose (NCC) suspension are **key parameters** that influence the **mechanical properties** of composites or the **nematic organization of rod-like nanoparticle** in an iridescent solid film¹.



Since the 2000s, the process for obtaining NCC through a strong sulphuric acid hydrolysis is well known, however the **size dispersity** of obtained nanoparticles could be **significantly improved using an adapted post treatment**.

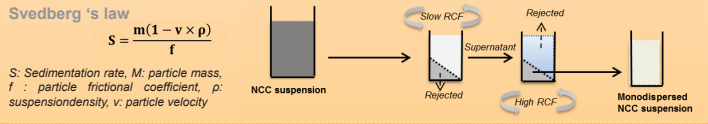
Challenges



- The acid hydrolysis of MCC leads to the obtention of NCC³
- A fraction of NCC in the µm range still remains in the final suspension
- Usually, the solution is to **increase hydrolysis parameters** (Temperature and acid-to-pulp ratio) which lower the production yield²
- However, more effective approaches can be investigated such as :
 - The differential centrifugation^{4,5}
 - The dead-end microfiltration^{6,7}
- Only the first strategy has recently been studied with NCC⁵. Our study will compare the two approaches.

Different post-treatments of nanocrystalline cellulose suspensions

Approach 1 : Differential centrifugation



Svedberg 's law

$$s = \frac{m(1 - v \times \rho)}{f}$$

S: Sedimentation rate, M: particle mass, f: particle frictional coefficient, ρ: suspension density, v: particle velocity

	Low	High
Concentration	0.1%	1.0%
Salt	0	10mM
RCF	3 000	10 000

Two-level factorial design
8 experiments + 3 controls

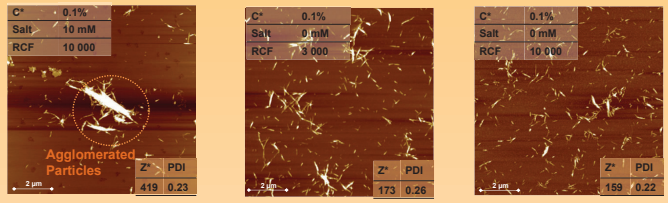
	Reduction of the average length (z*)	Reduction of the polydispersity	maximising the efficiency
Dilution	++	o	++
Salt	---	--	-
Slow speed	+	o	+++

Effect of factors on the main screening properties.
Ex: "+++" strong positive impact or "--" mild negative impact

Optimum parameters for the differential centrifugation are :

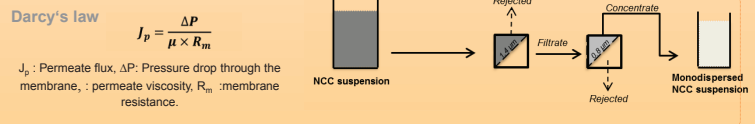
- A low concentration (0.1%)
- A reduced RCF (3000g)
- Salt free suspension

AFM analysis of supernatants by varying centrifugation parameters



- AFM analysis are correlated to DLS analysis.
- Addition of salt results to an agglomeration of NCC. This is because of the screening of the sulphate surface group (SO3H) of NCC by monovalent salt (NaCl).

Approach 2 : Dead-end microfiltration



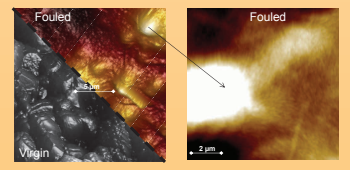
Darcy's law

$$J_p = \frac{\Delta P}{\mu \times R_m}$$

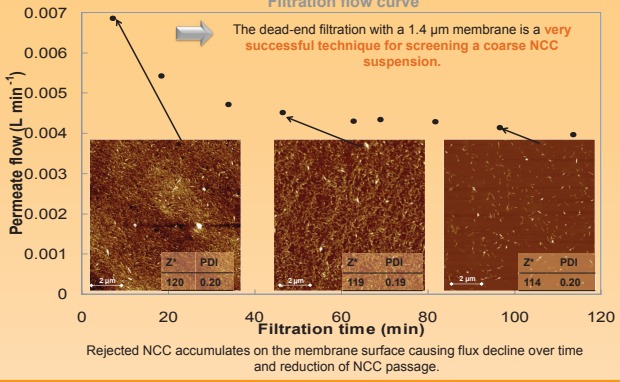
J_p: Permeate flux, ΔP: Pressure drop through the membrane, μ: permeate viscosity, R_m: membrane resistance.



AFM analysis of virgin and fouled 1.4 µm ceramic microfiltration membrane



NCC rods are aligned in the membrane pores direction and fouled the membrane.



Materials & Methods

The NCC suspension has been produced following protocol detailed above :³

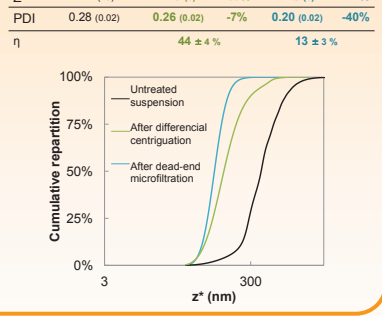
Raw material	Microcrystalline Cellulose – MCC (Avicel®)
Hydrolysis	H ₂ SO ₄ /pulp ratio : 63.5 % Temperature : 45°C Hydrolysis time : 40 minutes
Centrifugation	4 times at 10 000 rpm - until pH=4
Dialysis	5 days – deionized water
Sonication	2000 J/g NCC

- Separation:
- η corresponds to the dry matter yield of the post treatment.
 - The centrifuge sigma 6K-15C was used.
 - Filtration test were done using the SPIRLAB filtration cell from TAMIL Industries with a ceramic disc membrane (Inside Disram, TiO₂, 1.4 µm, 56 cm²).
- Characterization:
- Dynamic Light Scattering (DLS) was used to measure the size of nanoparticles (Vasco® 1, Corduan Technologies, France). Z*, PDI correspond to the hydrothermal diameter and polydispersity index.
 - Suspensions were imaged at 10x10µm² using Atomic Force Microscope, AFM, (Nanoscope III®, Veeco, Canada). Each sample was characterized in tapping mode with a silicon cantilever (OTESPA®, Bruker, USA)

Conclusions & Perspectives

- Post-treatments of coarse NCC suspension leads to a **removing of µ-range particles** and to a **higher homogeneity** of the post-treated suspension .
- The **differential centrifugation** is **very effective** however it is **not suitable for pilot-scale production**.
- The **microfiltration** is **promising** but there are still several drawbacks to overcome :
 - Low efficiency of the separation process .
 - Rapid membrane fouling.
 - Low dry matter of the filtrated suspension
- Cross flow microfiltration combined with sonication** could therefore be considered, with a view to improve the yield and homogeneity of NCC. This filtration can be carried out **after or even during the cellulose hydrolysis**

	Initial NCC Suspension	Optimum differential centrifugation	Dead-end microfiltration
Z*	424 (15)	173 (6) -60%	120 (3) -71%
PDI	0.28 (0.02)	0.26 (0.02) -7%	0.20 (0.02) -40%



Acknowledgments

The authors gratefully acknowledge the **French National Research Agency (ANRT)**, **Papeteries du Léman** and the **Rhône Alpes Region** for the financial and material support for the PhD Thesis.

Contact : Julien.bras@grenoble-inp.fr
Raphael.bardet@gp2.grenoble-inp.fr

Reference

- Dufresne, A., Nanocellulose. From Nature to High Performance Tailored Materials, ed. Series. 2012.
- Marchessault, R.H., F.F. Morehead, and N.M. Walter. Liquid Crystal Systems from Fibrillar Polysaccharides. Nature, 1959. n° 184. p. 632-633.
- Bondeson, D., A. Mathew, and K. Oksman, Optimization of the isolation of nanocrystals from microcrystalline cellulose by acid hydrolysis. Cellulose, 2006. n° 13. 2006. p. 171-180
- Svedberg, T. and K.O. Pedersen, The Ultracentrifuge. 1940
- Bai, W., J. Holbery, and K. Li, A technique for production of nanocrystalline cellulose with a narrow size distribution. Cellulose, 2009. n° 16. p. 455-465.
- Baker, R., et al., Membrane Separation Systems: Recent Developments and Future Directions. Noyes Data Corporation, Park Ridge, NJ, 1991
- Belfort, G., R.H. Davis, and A.L. Zydney, The behavior of suspensions and macromolecular solutions in crossflow microfiltration. Journal of Membrane Science, 1994. n° 96. 1994. p. 1-58.

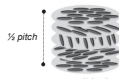
STRUCTURAL COLORED FILMS BASED ON NANOCELLULOSE

R. Bardet, C. Cancé, I. Horvatic, MN. Belgacem, J. Bras*

LGP2/GRENOBLE INP-PAGORA/CNRS - 461 RUE DE LA PAPETERIE, DOMAINE UNIVERSITAIRE, BP 65, 38402 SAINT MARTIN D'HERES CEDEX

Introduction

- One promising properties of NCCs are their **self-assembling property** in a concentrated suspension ¹
- Fingerprint textures are characteristic of **lyotropic liquid crystals** and characterized by the chiral-nematic pitch ². P ~ full 360° rotation of twisted NCCs ³
- A such cholesteric organization in **water** ⁴ or **organic solvents** ⁵ is due to :
 - morphology**: rigid rod-shape
 - surface charge**: negatively charged surface
- Under free evaporation, the self-organization can be preserved ⁶ and if $p \approx n_{\text{visible}}$: **structural colored films** are obtained



- Several physical and chemical factors influence the pitch ¹⁻¹²

	Parameters	Variation range	Pitch	Ref.
Nanoparticles	Aspect ratio	23-31	>	7
	Surface charge	0.14-0.68 e/nm ²	>	8
	Ionic strength	0-600 μM of monovalent salt (NaCl)	>	9
Suspension	Sonication	0-5k J/g	>	10
	Initial concentration	0.2- %wt	>	11
Drying & Evaporation parameters	Contact angle of substrate	20-80°	>	12
	Evaporation rate	2.5-133 μL/h	>	13
	Temperature	4-70°C	>	13

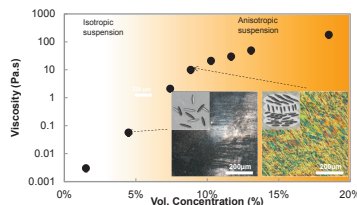
we will investigate the influence of some of these parameters on NCC properties :
 -As a suspension (A)
 -As solid films (B)

Results and discussions

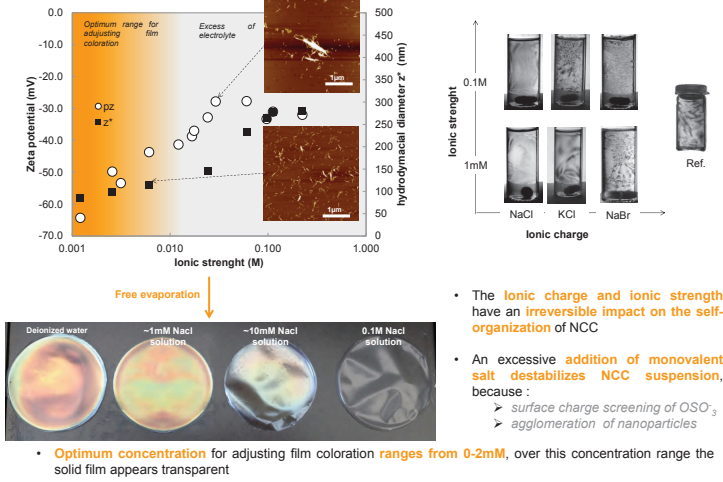
(A) Cholesteric suspension

Influence of NCC concentration

- Minimal volume fraction** for observing a chiral-nematic texture is **5%** (by volume)
- Above this concentration, suspension is colloidal and **nanoparticles are randomly dispersed**.
- From 9-10% (by volume), the suspension is **fully anisotropic and fingerprint textures** are observed on the whole micrograph



Influence of electrolyte: nature of monovalent and concentration

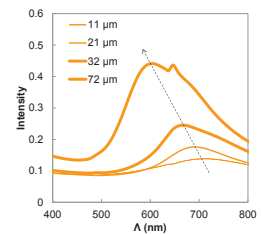


- The **ionic strength** and **ionic strength** have an **irreversible impact on the self-organization** of NCC
- An **excessive addition of monovalent salt destabilizes NCC suspension**, because :
 - surface charge screening of OSO₃
 - agglomeration of nanoparticles

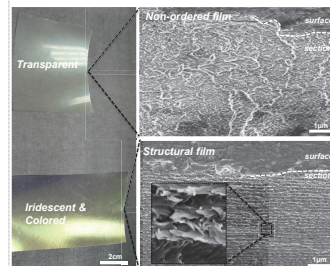
(B) Iridescent solid film

Influence of film thickness

- Film coloration (AMAX) increases with the film thickness
 > because of the increase of number of interference layers
- intense coloration** ~96 g/m², 72 μm
 > 100 ordered layers
- Minimal thickness** ~ 11 g/m², 18 μm
 > 10 ordered layers



Influence of NCC self-assembly onto macroscopic properties



	Non-ordered film	Structural film
Contexture	Thickness μm	71 ± 2
	Grammage g/m ²	103 ± 2
	Density	1.44 ± 0.04
Iridescent	Visual aspect	transparent colored
	λ _{MAX} nm	570 ± 50
Mechanical	Strain at break %	1.1 ± 0.2
	Stress at break MPa	82 ± 16
	Young Modulus GPa	8.4 ± 0.2
Barrier	OTR cm ³ /m ² .day	5.0 ± 0.1
	WVTR g/m ² .day	205 ± 25

Structural film vs non ordered film for the same NCC suspension

- Mechanical properties** : -45% for E_{modulus} and -135% for σ_{break}
 > slippage between stacked layers : facilitate defect propagation
- Barrier properties** : 1/15 for OTR and -16% for WVTR
 > horizontal orientation of rigid nanoparticles : increased tortuosity and diffusion pathway

Materials & Methods

The NCC suspension has been produced following protocol detailed above:

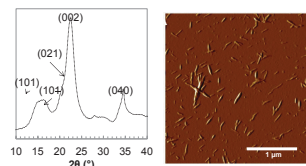
Raw material	Softwood – Bleached kraft pulp
Hydrolysis	H ₂ SO ₄ /pulp ratio : 65 %
	Temperature : 45°C Hydrolysis time : 40 minutes
Centrifugation	4 times at 10 000 rpm - until pH=4
Dialysis	5 days – deionized water
Sonication	2000 J/g NCC

Morphology	Length	AFM	nm	
			174	±3
Thickness	Aspect ratio	EA	8	±3
			~25	
Chemical	Sulfur content	%S	0.72	±0.05
	Potential zeta	mV	-41	±5
	Crystallinity Index	XRD	%	88 ± 2
	Physicochemical	Surface charge density	AFM- EA	e/nm ²

AFM: Atomic Force Microscopy, DLS: Dynamic Light Scattering, EA: Elemental Analysis, CT: Conductometric Titration, XRD: X-Ray Diffraction

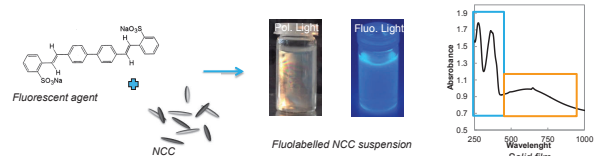
Characterization:

- Dynamic Light Scattering (DLS) was used to measure the size of nanoparticles (Vasco@ I, Corduan Technologies, France)
- The rheological behavior of suspensions was investigated using a controlled stress rheometer (Physica MCR 301, Anton Paar Physica, Austria)
- Suspensions were imaged at 10x10 μm² using Atomic Force Microscope, AFM, (Nanoscope IIIa, Veeco, Canada)
- The structural colored of films were analyzed through UV-Visible spectroscopy (UV 1800, Shimadzu, Japan)



Conclusions & Perspectives

- NCCs isolated from softwood
 - display a **chiral-nematic organization in water beyond 5% in concentration**
 - their self-organization is **strongly influenced by electrolytes** (nature and concentration)
- Color intensity is proportional to the film thickness**
- Self-assembly of NCCs give film structures with a **strong impact on** :
 - Mechanical properties**
 - Barrier properties**
- Further investigation: **NCC labelling with fluorescent agent (anionic polymer) to obtain film with a combination of iridescent and fluorescent properties**



Acknowledgments

The authors gratefully acknowledge the French National Research Agency (ANRT), Papeteries du Léman and the Rhône Alpes Region for the financial and material support for the PhD Thesis.

Contact : Julien.bras@grenoble-inp.fr
 Raphael.bardet@gp2.grenoble-inp.fr

References

- 1.Revol, et al., *Int. J. Biol. Macromolec.*, 1992
- 2.Revol, et al., *Liquid Crystals*, 1994
- 3.Shafiei-Sabet, Hamad, and Hatzikiakos, *Langmuir*, 2012
4. de Vries, *Acta Crystallographica*, 1951
5. Heux, Chauve, and Bonini, *Langmuir*, 2006
6. Revol, et al., WO9521901, 1995
7. Araki and Kuga, *Langmuir*, 2001
8. Elazzouzi-Hafraoui, et al., *J. Phys. Chem. B*, 2009
9. Dong, et al., *Cellulose*, 1998
10. Beck, et al., *Biomacro*, 2011
11. Zhang, et al., *Sens Actuators B Chemical*, 2012
12. Shpopsowitz, et al., *JACS*, 2011
13. Pan, Hamad, and Straus, *Macrom.*, 2010

Short abstract

The original feature of this work is to investigate the contribution of two families of nanocellulose for their application within specialty papers. It exists two families of nanocellulose, i.e. Cellulose Nanocrystals (CNCs) and Cellulose Nanofibers (CNFs). It results in different properties in suspension and solid states. CNFs with their ability to form entangled network are used as dispersive network for particles. In contrast, the self-assembly properties of CNC are used to obtain iridescent films. First, the films based on nanocellulose were considered as model layers. Then, results were implemented at the industrial scale within the papermaking process. It is proposed to use CNF based coating for saving opacifying pigments in lightweight paper, and manufacturing iridescent pigment to impart anti-counterfeiting properties. These sustainable and cost-effective approaches were then validated at pilot scale.

Keywords : nanocellulose, cellulose nanocrystal, cellulose nanofibril, specialty papers

Résumé court

L'originalité de ce travail est d'étudier la contribution des nanocelluloses pour la fonctionnalisation des papiers spéciaux. Il y a deux types de nanocellulose, les nanocristaux de cellulose (NCCs) et les microfibrilles de cellulose (MFCs). Il en résulte des propriétés différentes à l'état de suspension et à l'état sec. La propriété des MFCs de former un réseau d'enchevêtrement est utilisée pour la dispersion des particules. L'auto-assemblage des NCCs a permis d'élaborer des films iridescents. Ces films ont été considérés comme couches modèles puis ensuite mis en œuvre dans le procédé de fabrication des papiers. Il a été proposé avec succès d'utiliser les MFCs dans le couchage pour réduire la quantité de pigments opacifiants pour les papiers minces, et de fabriquer des pigments iridescents pour obtenir des propriétés d'anti-contrefaçon. Ces approches ont été validées à l'échelle laboratoire mais aussi pilote.

Mots clés : *nanocellulose, nanocristaux de cellulose, microfibrilles de cellulose, papiers spéciaux*